Excited Hadronic Matter in a Chiral $SU(3)_L \times SU(3)_R$ Model

Dissertation
zur Erlangung des Doktorgrades
der Naturwissenschaften

vorgelegt beim Fachbereich Physik
der Johann Wolfgang Goethe–Universität
in Frankfurt am Main

von
Detlef Zschiesche
aus Bad Homburg

Frankfurt am Main, Juli 2003
(D F 1)

vom Fachbereich Physik der Johann Wolfgang Goethe–Universit"at
als Dissertation angenommen.

Dekan: Prof. Dr. H. Schmidt-Böcking

Gutachter: Prof. Dr. H. St"ocker, PD. Dr. S. Schramm

Datum der Disputation: 10.10.2003

Zusammenfassung

Allgemeines

In dieser Arbeit werden die Eigenschaften angeregter hadronischer Materie in einem, auf chiraler $SU(3)_L \times SU(3)_R$ Symmetrie basierendem, effektivem Model untersucht. Die theoretische und experimentelle Untersuchung von heißer und dichter hadronischer Materie ist von besonderer Bedeutung für das Verständnis kosmologischer, astrophysikalischer und kernphysikalischer Fragestellungen. Zudem sind die fundamentalen Freiheitsgrade und Symmetrien der derzeit akzeptierten Theorie der starken Wechselwirkung (Quantenchromodynamik bzw. QCD) in "normaler Materie" nicht beobachtbar. Die QCD sagt voraus, dass oberhalb bestimmter kritischer Temperaturen und Dichten die Quarks und Gluonen "befreit" und die fundamentalen Symmetrien restauriert werden. Für eine genaue Untersuchung dieser Phase ist aber die Kenntnis der Eigenschaften angeregter hadronischer Materie unerlässlich. Da hadronische Materie ein Vielteilchensystem gebundener Quarkzustände (Hadronen) mit grossen Kopplungskonstanten darstellt, ist die QCD in diesem Bereich nicht analytisch lösbar. Aus diesem Grunde werden effektive Modelle mit baryonischen und mesonischen Freiheitsgraden konstruiert. Das hier benutzte chirale $SU(3)_L \times SU(3)_R$ σ-ω Modell stellt solch eine effektive hadronische Beschreibung dar. Die Struktur des Modells wird durch die fundamentalen Symmetrien der starken Wechselwirkung, sowie die Phänomenologie der relativistischen Mesonenfeldtheorie bestimmt. In [Pap98a, Pap99] wurde gezeigt, dass dieses Modell die Eigenschaften sowohl unendlicher Kernmaterie als auch endlicher Atomkerne beschreibt. In [Zsc97] wurde das Modell auf die Beschreibung von hadronischer Materie bei endlichen Temperaturen erweitert.

Am Beginn dieser Arbeit steht die Vorstellung des Modells, gefolgt von der systematischen Untersuchung der Eigenschaften heißer und dichter hadronischer Materie. Den Schwerpunkt bilden dann theoretische Berechnungen der Eigenschaften physikalischer Systeme, in denen hadronische Materie auftritt bzw. produziert wird. Diese werden mit experimentellen Daten verglichen, wodurch

zum einen das Modell getestet und verbessert werden kann und zum anderen Rückschlüsse auf die Eigenschaften angeregter hadronischer Materie gezogen werden können. Schließlich wurde die fast durchweg benutzte "Mittlere-Feld-Näherung" zur Beschreibung der Eigenschaften von Vektormesonen im hadronischen Medium durch Einbeziehen der "Dirac-See" auf die relativistische Hartree Näherung erweitert.

Chirales $SU(3)_L \times SU(3)_R$ Modell

Die allgemeine Form der Lagrangedichte des benutzten Modells lautet:

$$\mathcal{L} = \mathcal{L}_{\rm kin} + \sum_{W=X,Y,V,\mathcal{A},u} \mathcal{L}_{\rm BW} + \mathcal{L}_{\rm vec} + \mathcal{L}_0 + \mathcal{L}_{\rm SB}. \tag{1}$$

Hier ist $\mathcal{L}_{\rm kin}$ die kinetische Energie, $\mathcal{L}_{\rm BW}$ beinhaltet die Wechselwirkung der Baryonen mit den Spin-0 und den Spin-1 Mesonen. Der Term $\mathcal{L}_{\rm vec}$ erzeugt die Massen der Vektormesonen durch die Wechselwirkung mit den skalaren Feldern sowie die quartische Selbstwechselwirkung der Vektorfelder. Das mesonische Potential ist durch $\mathcal{L}_0$ gegeben. Dieses induziert die spontane Brechung der chiralen Symmetrie und beinhaltet zudem das logarithmische Potential, das zur Brechung der Skaleninvarianz führt. Schließlich wird durch $\mathcal{L}_{\rm SB}$ eine explizite Brechung der $\mathrm{U}(1)_A$-, der $\mathrm{SU}(3)_V$- und der chiralen Symmetrie erzeugt.
Aus der Lagrangedichte (1) resultieren nichtlineare Quantenfeldgleichungen mit großen Kopplungen, die nicht perturbativ gelöst werden können. Die Gleichungen sind jedoch in der Mittleren-Feld-Näherung lösbar. Hier werden die Mesonen als klassische Felder behandelt. Die resultierende Lagrangedichte des Modells lautet dann:

$$\begin{aligned}
\mathcal{L}_{BX} + \mathcal{L}_{BV} &= -\sum_i \overline{\psi_i}[g_{i\omega}\gamma_0\omega^0 + g_{i\phi}\gamma_0\phi^0 + g_{i\rho}\gamma_0\tau_3\rho^0 + m_i^*]\psi_i \\
\mathcal{L}_{vec} &= \frac{1}{2}m_\omega^2\frac{\chi^2}{\chi_0^2}\omega^2 + \frac{1}{2}m_\phi^2\frac{\chi^2}{\chi_0^2}\phi^2 + g_4^4\left[\omega^4 + 12\frac{Z_\rho}{Z_\omega}\rho^2\omega^2 + \frac{Z_\rho^2}{Z_\omega^2}\rho^4 + 2\frac{Z_\phi^2}{Z_\omega^2}\phi^4\right] \\
\mathcal{L}_0 &= -\frac{1}{2}k_0\chi^2(\sigma^2+\zeta^2) + k_1(\sigma^2+\zeta^2)^2 + k_2(\frac{\sigma^4}{2}+\zeta^4) + k_3\chi\sigma^2\zeta \\
&\quad - k_4\chi^4 - \frac{1}{4}\chi^4\ln\frac{\chi^4}{\chi_0^4} + \frac{\delta}{3}\chi^4\ln\frac{\sigma^2\zeta}{\sigma_0^2\zeta_0} \\
\mathcal{L}_{SB} &= -\left(\frac{\chi}{\chi_0}\right)^2\left[m_\pi^2 f_\pi\sigma + (\sqrt{2}m_K^2 f_K - \frac{1}{\sqrt{2}}m_\pi^2 f_\pi)\zeta\right],
\end{aligned} \tag{2}$$

wobei m_i^* die effektive Masse der Baryonenart i bezeichnet. Die skalaren Kondensate werden mit σ und ζ bezeichnet, ω, ρ, ϕ repräsentieren die verschiedenen Vektorfelder und χ ist das skalare-isoskalare Dilatonfeld. Das thermodynamische

Potential des großkanonischen Ensembles Ω für gegebene chemische Potentiale μ und Temperatur T ergibt sich dann zu

$$\frac{\Omega}{V} = -\mathcal{L}_{vec} - \mathcal{L}_0 - \mathcal{L}_{SB} - \mathcal{V}_{vac} \mp T \sum_i \frac{\gamma_i}{(2\pi)^3} \int d^3k \left[\ln \left(1 \pm e^{-\frac{1}{T}[E_i^*(k) - \mu_i^*]} \right) \right] . \quad (3)$$

Die Summe läuft über alle durch den Impuls $\vec{k}$ charakterisierten Teilchenzustände, alle intrinsischen Quantenzahlen λ und alle betrachteten Mesonen- und Baryonenarten. Die Einteilchenenergien sind $E_i^*(\vec{k}) = \sqrt{\vec{k}_i^2 + m_i^{*2}}$, und die effektiven chemischen Potentiale ergeben sich zu $\mu_i^* = \mu_i - g_{i\omega}\omega - g_{i\phi}\omega - g_{i\rho}\tau_3\rho^0$, mit $\mu_i = (n_q^i - n_{\bar{q}}^i)\mu_q + (n_s^i - n_{\bar{s}}^i)\mu_s$, wobei die chemischen Potentiale der leichten (u,d)-Quarks mit μ_q und die der seltsamen (s)-Quarks mit μ_s bezeichnet werden. Die mesonischen Felder werden so gewählt, dass das großkanonische Potential extremal wird. Sind diese bestimmt, können die thermodynamischen Grössen durch Ableitung des großkanonischen Potentials erhalten werden, z.B.

$$\begin{aligned} p &= -\left[\frac{\partial}{\partial V} \Omega(T, \mu_i) \right]_{T,\mu_i} \\ S &= -\left[\frac{\partial}{\partial T} \Omega(V, \mu_i) \right]_{V,\mu_i} . \end{aligned} \quad (4)$$

Ergebnisse für symmetrische, unendliche hadronische Materie

Die Untersuchung heißer und dichter hadronischer Materie zeigt, dass das vom Modell vorhergesagt Phasendiagramm stark von den Kopplungen der Baryonenresonanzen abhängt. Für kalte hadronische Materie führt die Einbeziehung des Baryonendekupletts, bei entsprechender Wahl der Vektorkopplung, zu einem Phasenübergang erster Ordnung bzw. zu Dichteisomeren (siehe Figur 1). Eine reine σ-Kopplung (C2) der nichtseltsamen Baryonen liefert mögliche Verhältnisse $\mathrm{r_v}$ der Δ-ω zur N-ω Kopplung im Bereich $0.91 < \mathrm{r_v} < 1$. Für eine nichtverschwindende ζ-Kopplung (C1) erhält man $0.68 < \mathrm{r_v} < 1$. Geringere Vektorkopplungen der Resonanzen führen zu verminderter Repulsion und damit zu weicheren Zustandsgleichungen. Insbesondere würden die Dichteisomere absolut stabil werden. Trotzdem erlaubt die Freiheit in den Vektorkopplungen eine sehr große Bandbreite an verschiedenen Zustandsgleichungen, d.h. das Verhalten kalter Kernmaterie kann nicht eindeutig vorhergesagt werden. Für heiße hadronische Materie mit verschwindendem chemischen Potential zeigt sich ebenfalls eine starke Abhängigkeit der Eigenschaften hadronischer Materie von der Ankopplung der baryonischen Resonanzen (siehe Figur 2). Es werden drei verschiedene Arten der Ankopplung der Resonanzen betrachtet, die alle identische Ergebnisse für nichtseltsame kalte hadronische Materie – also z.B. auch

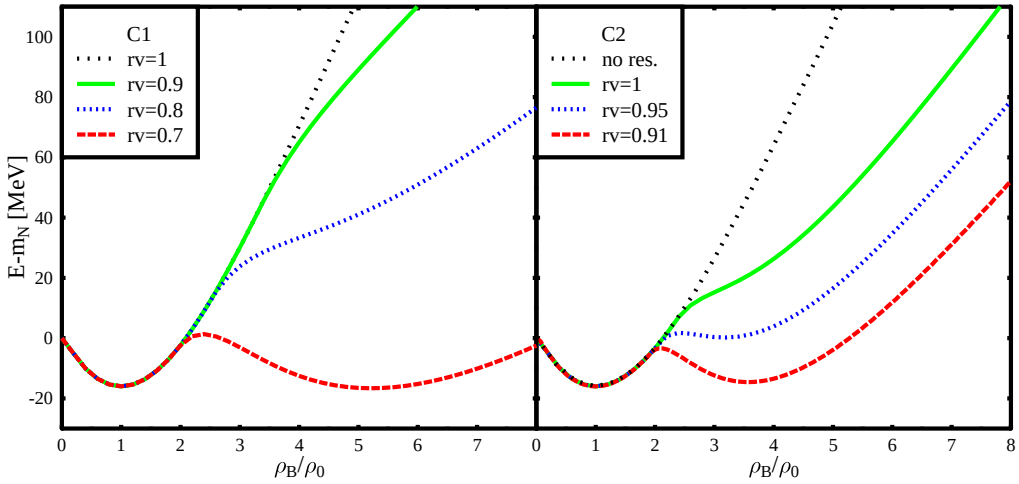

Figur 1: Zustandsgleichung für die Parametersätze C1 und C2 für verschiedene Werte des Quotienten $r_v = \frac{g_{N\omega}}{g_{\Delta\omega}}$ bei $T = 0$.

für den Grundzustand – liefern: CI bezeichnet den Fall ohne Ankopplung des Dekupletts an die Feldgleichungen, in dem mit CII bezeichneten Fall koppeln die Resonanzen an die skalaren Felder, jedoch wird für die seltsamen Dekuplettzustände eine explizite Symmetriebrechung eingeführt. Diese explizite Symmetriebrechung wird in der Parametrisierung CIII weggelassen, so dass die Massen aller Dekuplettzustände ausschließlich durch die skalaren Felder generiert werden. Das resultierende Phasenübergangsverhalten variiert von einem "Crossover" (CI) über einen schwachen Phasenübergang erster Ordnung (CII), zu

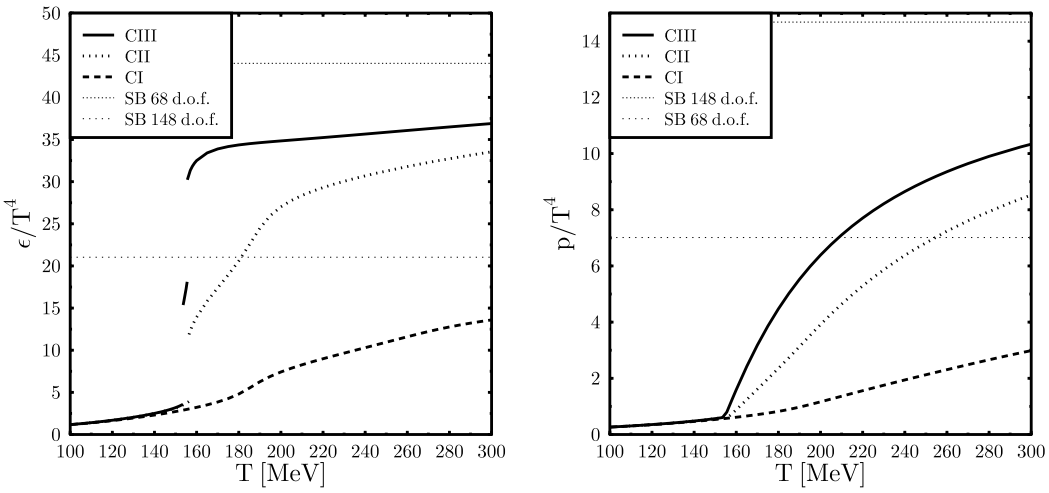

Figur 2: ϵ/T^4 und p/T^4 für die drei verschiedenen Parametersätze CI, CII und CIII für $\mu_q = \mu_s = 0$. Die horizontalen Linien entsprechen dem Stefan-Boltzmann Limes mit und ohne das (anti)-Baryonen Dekuplett.

zwei Phasenübergängen (CIII), die jeweils einer Diskontinuität im nichtseltsamen bzw. im seltsamen Kondensat entsprechen. Man erkennt also, dass obwohl alle drei Parametrisierungen sowohl eine identische Beschreibung des Grundzustands von Kernmaterie als auch von endlichen Kernen liefern, ihre Vorhersagen für das Hochtemperaturverhalten vollkommen verschieden sind. Da ähnliche Resultate auch für kalte aber dichte hadronische Materie gefunden werden, wird deutlich, dass eine bessere Fixierung der Zustandsgleichung hadronischer Materie nur durch Betrachtung physikalischer Systeme möglich ist, in denen angeregte hadronische Materie auftritt, wie z.B. Neutronensterne oder relativistische Schwerionenkollisionen.

Anwendungen des chiralen Modells

Die im chiralen Modell vorhergesagten Eigenschaften von Neutronensternen werden mit Rechnungen im Walecka-Modell verglichen (Figur 3). Dabei zeigte

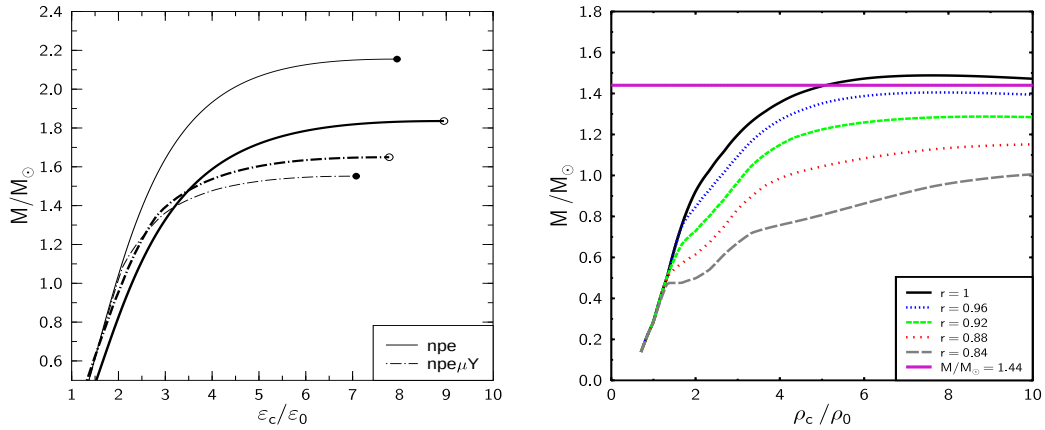

Figur 3: Links: Die Masse von npe- und Hypersternen als Funktion der zentralen Energiedichte $\varepsilon_c/\varepsilon_0$ im chiralen und im Walecka-Modell (TM1). Die Ergebnisse im chiralen Modell sind durch dicke Linien und die TM1 Ergebnisse durch dünne Linien gekennzeichnet. Rechts: Masse von Neutronensternen als Funktion der zentralen Baryonendichte ρ_c für CII bei unterschiedlichen Werten von $\mathrm{r_v}$. Der "kritische" Wert der Vektorkopplung der Resonanzen in dieser statischen Rechnung ist $\mathrm{r_v} \approx 0.97$

sich für den Fall ohne Hyperonen, dass obwohl beide Modelle ähnliche Werte für die effektive Nukleonmasse, die Kompressibilität und Asymmetrieenergie für den Grundzustand von Kernmaterie vorhersagen, die resultierenden maximalen Massen und Radien von Neutronensternen sehr unterschiedlich sind. Werden die hyperonischen Freiheitsgrade miteinbezogen, nähern sich die Ergebnisse in den

beiden Modellen besser an (siehe Figur 3). Die Anteile der Hyperonen sind jedoch im chiralen Modell deutlich niedriger als im Walecka-Modell. Werden zusätzlich die Resonanzen miteinbezogen, zeigt sich, dass die beobachteten Eigenschaften von Neutronensternen die Unbestimmtheit bzgl. der Vektorkopplung des Dekupletts deutlich verringern. Denn, um in statischen Rechnungen eine maximale Neutronensternmasse zu erhalten, die oberhalb des beobachteten Minimalwertes von ca. 1.44 Sonnenmassen liegt, darf sich das Verhältnis $r_v = \frac{g_{\Delta\omega}}{g_{N\omega}}$ für den CII-Fall kaum vom Wert eins unterscheiden. Ansonsten ist die Zustandsgleichung zu weich und die berechneten Werte liegen immer unterhalb des beobachteten Minimalwertes für die Masse von Neutronensternen. Für die Parametrisierung CIII ist dies immer der Fall, zumindest für $r_v \leq 1$. Somit kann die hadronische Zustandsgleichung durch die Eigenschaften von Neutronensternen stark eingeschränkt werden.
Das Raum-Zeit Verhalten relativistischer Schwerionenkollisionen bei SPS- und RHIC-Energien wird mittels einer hydrodynamischen Rechnung studiert. Hierbei werden die durch die Parametrisierungen CI, CII und CIII vorhergesagten Zustandsgleichungen benutzt. Es zeigt sich, dass sich das unterschiedliche

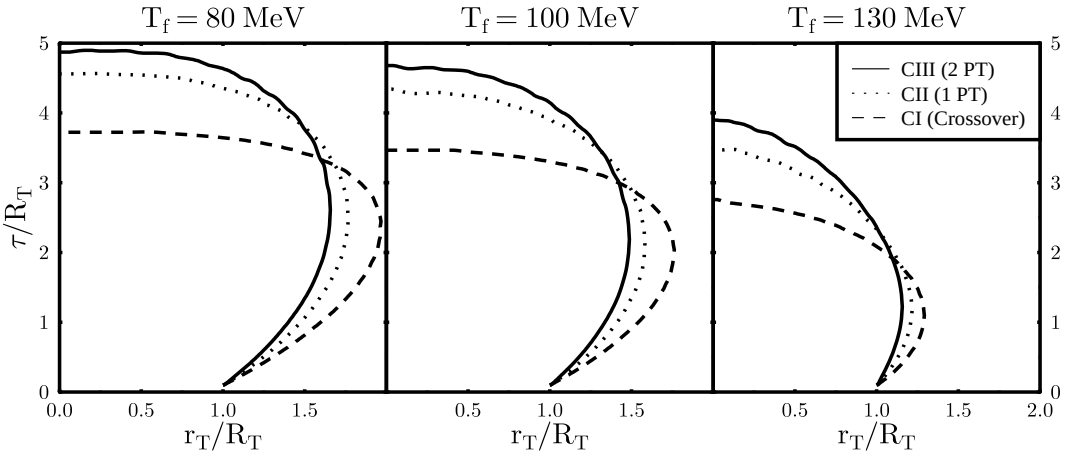

Figur 4: Hyperflächen $T = T_f$ für die drei chiralen Zustandsgleichungen für Au+Au Kollisionen bei RHIC-Energien ($\sqrt{s} = 130$AGeV).

Phasenübergangsverhalten deutlich im Ausfrierverhalten der hadronischen Materie in Schwerionenkollsionen widerspiegelt (siehe Figur 4). Im Crossover Fall (CI) ist die Zeit bis zum Ausfrieren signifikant kürzer als im Fall mit zwei Phasenübergängen (CIII). Dies resultiert aus dem Auftreten gemischter Phasen, in denen die Schallgeschwindigkeit und der Druck verschwinden. Das Verhältnis der HBT-Radiusparamter R_{out}/R_{side} stellt ein Maß für die Lebensdauer des Systems dar. Beim Vergleich der berechneten R_{out}/R_{side} Verhältnisse für die

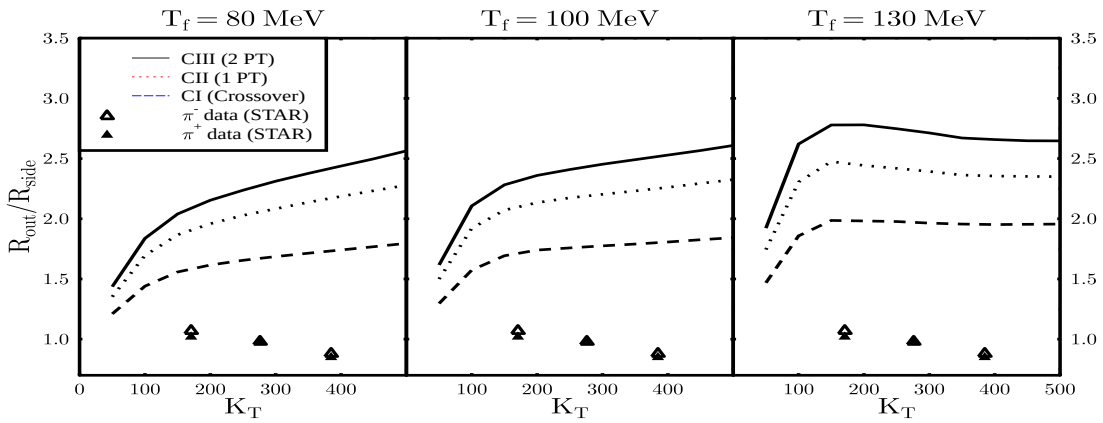

Figur 5: R_{out}/R_{side} als Funktion von K_T bei RHIC.

verschiedenen Zustandsgleichungen des chiralen Modells mit den STAR Daten [Adl01] (siehe Figur 5) zeigt sich, dass die experimentellen Resultate für niedrige T_f nicht reproduziert werden können. Für $T_\mathrm{f} = 130$ MeV ergibt sich zwar ein qualitativ übereinstimmendes Verhalten, aber R_{out}/R_{side} ist hier trotzdem um einen Faktor zwei zu groß. Der Crossover-Fall ist immer am nächsten an den Daten. Dies scheint eine Bestätigung für die Gitter-QCD Ergebnisse zu liefern, welche einen Crossover bzw. maximal einen sehr schwachen Phasenübergang erster Ordnung vorhersagen [Bro90, Iwa96, Lae96]. Da aber auch im Crossover Fall die Abweichungen zum Experiment groß sind, muss die Anwendbarkeit des Ansatzes einer expandierenden idealen Flüssigkeit in Frage gestellt werden. Dies deutet darauf hin, dass ein Nichtgleichgewichtsansatz zur Beschreibung der Expansion hadronischer Materie notwendig ist.

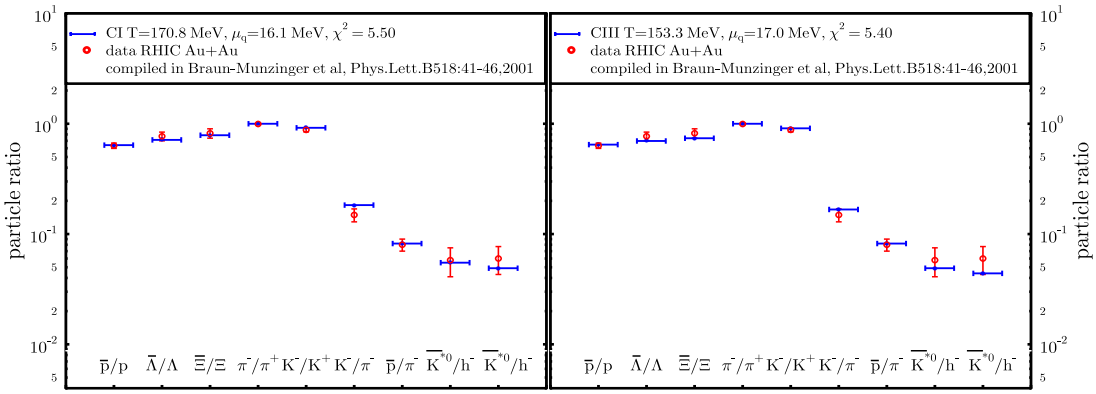

Figur 6: Teilchenzahlverhältnisse für CI (links) und CIII (rechts) im Vergleich zu RHIC Daten [Bra01].

Die im chiralen $SU(3)$ σ-ω Modell berechneten Teilchenzahlverhältnisse werden mit den aus Schwerionenkollisionen von AGS- bis RHIC-Energien erhaltenen experimentellen Daten verglichen (siehe z.B. Figur 6). Dabei zeigt sich, dass sowohl die verschiedenen Parametersätze des chiralen Modells als auch die Rechnungen für ein nichtwechselwirkendes Hadronengas eine ähnlich gute Beschreibung der gemessenen Werte liefern (siehe Figur 8). D.h., in dem gewählten Gleichgewichts-

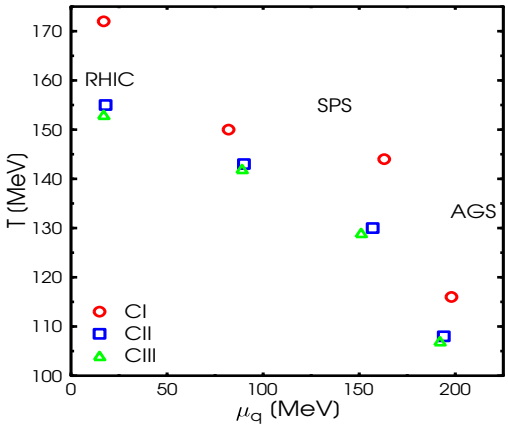

Figur 7: Ausfrierkurve im chiralen Modell (CI, CII, CIII) für relativistische Schwerionenkollisionen von AGS bis RHIC.

ansatz mit globalem chemischen Ausfrieren kann die Untersuchung von Teilchenzahlverhältnissen nicht zwischen unterschiedlichem Phasenübergangsverhalten diskriminieren. Die deduzierten Ausfrierwerte für die Temperatur sind jedoch modellabhängig bzw. sensitiv auf das Phasenübergangsverhalten (siehe Figur 7). Es zeigt sich, dass mit steigender latenter Wärme die erhaltene Ausfriertemperatur sinkt. Die vorhergesagten effektiven Massen am Ausfrierpunkt sind

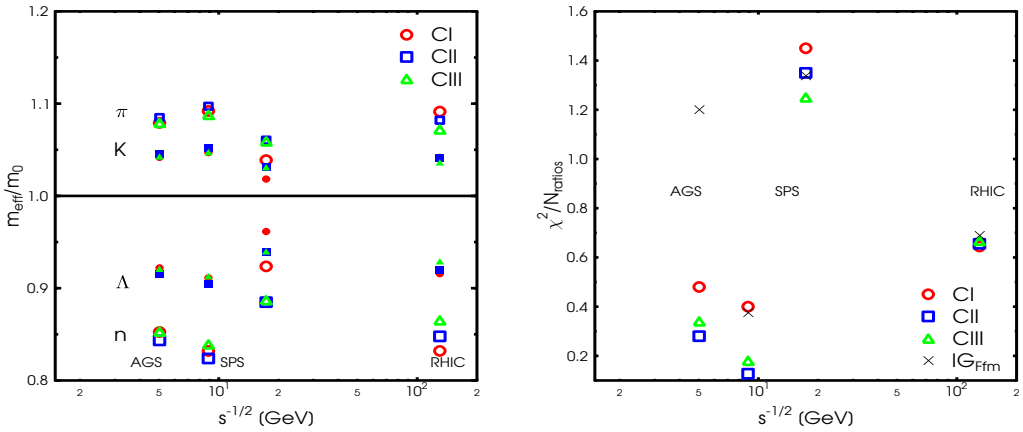

Figur 8: Effektive Massen von N, Λ, π, K (links) und χ^2-Werte (rechts) als Funktion von $\sqrt{s}$ für CI, CII und CIII.

wiederum in allen Parametrisierungen sehr ähnlich, wobei sich jeweils Abweichungen bis zu 15% von den Vakuumwerten ergeben (siehe Figur 8). Zudem zeigt sich, dass die erhaltenen Temperaturen immer unterhalb der jeweiligen kritischen Temperaturen liegen, womit ein direktes Ausfrieren aus der restaurierten Phase in diesem Modell auszuschließen ist.
Die Untersuchung der Eigenschaften von Vektormesonen in dichter hadronischer Materie erfolgte in der Mittleren-Feld- und in der Hartree-Näherung. Hierbei zeigt sich eine signifikante Reduzierung der Teilchenmassen durch Vakuumpolarisationseffekte (siehe Figur 9). Es kann insbesondere nachgewiesen werden,

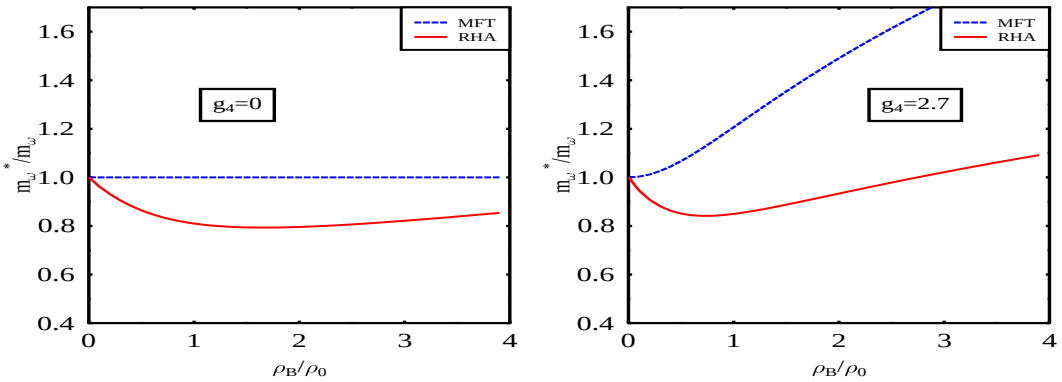

Figur 9: Effektive ω Mesonenmasse in der Mittleren-Feld Näherung und inklusive der Hartree Beiträge. Links: ohne quartische Vektormesonwechselwirkung Rechts: inklusive ω^4 Term.

dass der Beitrag durch die Dirac-See über den aus der Fermi-See resultierenden Beitrag dominiert. Dies zeigt die große Bedeutung der Vakuumpolarisation für die Eigenschaften der Vektormesonen im hadronischen Medium.
Zusammenfassend liefern die in dieser Arbeit erhaltenen Ergebnisse ein verbessertes Verständnis der Verbindung vorhergesagter Eigenschaften angeregter unendlicher hadronischer Materie und dem Verhalten physikalischer Systeme. Zudem konnte die vorhergesagte Zustandsgleichung durch die Untersuchung von Neutronensternen und Schwerionenkollisionen deutlich eingeschränkt werden. Als nächster Schritt wird das Phasenübergangsverhalten mit den kürzlich erhaltenen Gitter-QCD Ergebnissen [Fod02] in Einklang gebracht werden. Dadurch kann die Zustandsgleichung hadronischer Materie noch besser bestimmt werden. Hierdurch würde sich erstmals eine Zustandsgleichung ergeben, die sowohl die Grundzustandseigenschaften von Kernmaterie und die Eigenschaften von Atomkernen als auch das durch Gitter-QCD Rechnungen induzierte Phasenübergangsverhalten bei hohen Dichten und Temperaturen reproduzieren kann. Ein solches Modell hat weitreichende und vielfältige Anwendungen in der Kosmologie, der Astrophysik und der Schwerionenphysik.

Contents

List of Figures

–I–

Introduction

1.1 Aim of this work

In this work the properties of excited hadronic matter are investigated within an effective model based on chiral $SU(3)_L \times SU(3)_R$ symmetry. The theoretical and experimental investigation of hot (approximately 10^{12}K) and dense (several times nuclear density) hadronic and quark matter is essential to understand what happened during the evolution of our universe, how neutron stars are formed, how supernova explosions proceed and whether a quark-gluon plasma (QGP) is formed during relativistic heavy ion collisions. Furthermore, it helps to obtain a deeper understanding of the strong interaction and its ground state as well as of hadronic properties.

1.2 Structure of matter

In order to find out more about the structure of matter, many attemps were made to identify the fundamental building blocks of matter and study the forces between them. The final aim has been the explanation of all the observed phenomena in nature by the fundamental interactions of elementary particles. Many experimental and theoretical efforts were undertaken, which lead to the formulation of a physical theory of the elementary particles and their interactions: The so-called standard model. Up to now this model has turned out to give a good description of the elementary processes in all experiments. The current picture of the structure of matter looks as follows: Matter consists of atoms with a size of approximately 10^{-10} m^3. These atoms are not elementary but are composed of an electron shell and an atomic nucleus. The nucleus is about 10000 times smaller than the entire atom but bears about 99.9% of its mass. It consists of positively

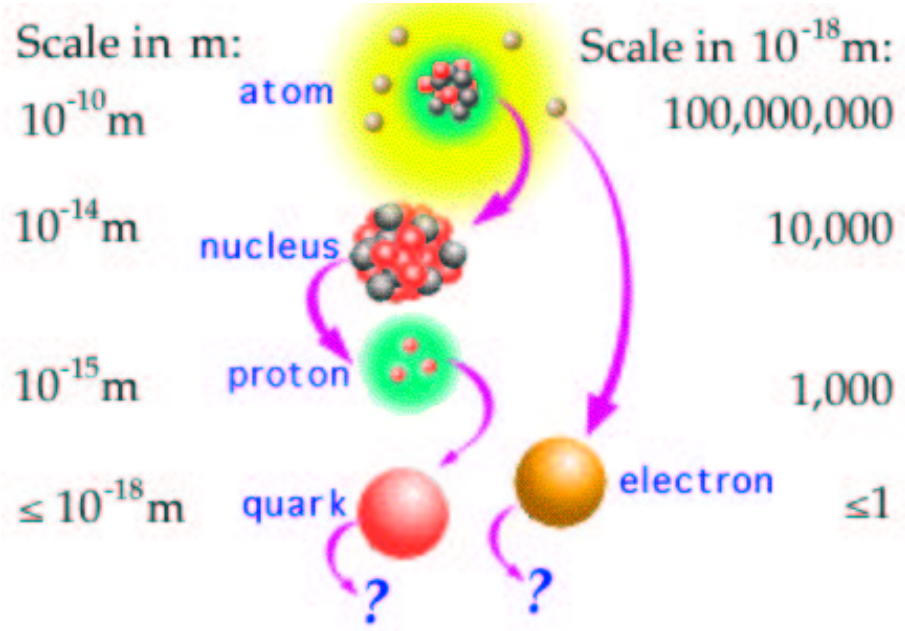

Figure 1.1: The structure of matter: from quarks and electrons to atoms.

charged protons and uncharged neutrons. These building blocks of stable atoms are called nucleons. They are part of a larger family of particles: the hadrons. In the 1960s and 70s it was found that nucleons and all other hadrons also possess an inner structure. They are made up of so-called quarks, which are today viewed as the fundamental building blocks of matter. Experimental and theoretical investi-

Sample Fermionic Hadrons						Sample Bosonic Hadrons					
Baryons qqq and Antibaryons $\bar{q}\bar{q}\bar{q}$						Mesons $q\bar{q}$					
Symbol	Name	Quark content	Electric charge	Mass GeV/c^2	Spin	Symbol	Name	Quark content	Electric charge	Mass GeV/c^2	Spin
p	proton	uud	1	0.938	1/2	π^+	pion	$u\bar{d}$	+1	0.140	0
$\bar{p}$	anti-proton	$\bar{u}\bar{u}\bar{d}$	−1	0.938	1/2	K^-	kaon	$s\bar{u}$	−1	0.494	0
n	neutron	udd	0	0.940	1/2	ρ^+	rho	$u\bar{d}$	+1	0.770	1
Λ	lambda	uds	0	1.116	1/2	D^+	D^+	$c\bar{d}$	+1	1.869	0
Ω^-	omega	sss	−1	1.672	3/2	η_c	eta-c	$c\bar{c}$	0	2.979	0

Figure 1.2: Quark content and characteristic properties of baryons and mesons. Source: [con03]

gations proved the existence of six quarks (u,d,s,c,b,t) which may be grouped in three families. There are also three families of so-called leptons – electrons, muons and taus and the corresponding neutral neutrinos. In addition, four fundamental

FERMIONS matter constituents spin = 1/2, 3/2, 5/2,...

Leptons spin = 1/2

Flavor	Mass GeV/c²	Electric charge
ν_e electron neutrino	$< 7 \times 10^{-9}$	0
e electron	0.000511	−1
ν_μ muon neutrino	< 0.0003	0
μ muon	0.106	−1
ν_τ tau neutrino	< 0.03	0
τ tau	1.7771	−1

Quarks spin = 1/2

Flavor	Approx. Mass GeV/c²	Electric charge
u up	0.005	2/3
d down	0.01	−1/3
c charm	1.5	2/3
s strange	0.2	−1/3
t top (initial evidence)	170	2/3
b bottom	4.7	−1/3

Figure 1.3: Quarks and Leptons: the fundamental building blocks of matter and their properties. Source: [con03]

interactions are known up to today: gravitation, electromagnetic force, strong force and weak interaction. Even though all these forces are in principle present on all scales, they dominate different systems due to their different strength and range. While processes on the macroscopic level are governed by gravitation,

Property \ Interaction	Gravitational	Weak	Electromagnetic	Strong	
		(Electroweak)		Fundamental	Residual
Acts on:	Mass - Energy	Flavor	Electric Charge	Color charge	See Residual Strong Interaction Note
Particles experiencing:	All	Quarks, Leptons	Electrically charged	Quarks, Gluons	Hadrons
Particles mediating:	Graviton (not yet observed)	W^+ W^- Z^0	γ	Gluons	Mesons
Strength for two u quarks at: 10^{-18} m (relative to electromagnetic)	10^{-41}	0.8	1	25	Not applicable to quarks
Strength for two u quarks at: 3×10^{-17} m (relative to electromagnetic)	10^{-41}	10^{-4}	1	60	Not applicable to quarks
Strength for two protons in nucleus	10^{-36}	10^{-7}	1	Not applicable to hadrons	20

Figure 1.4: The properties of the fundamental interactions. Source: [con03]

the prominent force at the atomic level is the electromagnetic attraction between negatively charged electrons and atomic nuclei with positive charge. Atomic nuclei, in turn, are held together by the so-called strong force, which acts between

the quarks within the nucleons and also is responsible for the binding of nucleons in nuclei. In addition, the weak force turns out to be essential for the creation of matter, since, by means of radioactive decay, it allows the transformation of nuclei. The matter in and around us is therefore structured as a hierarchy of various composite systems covering almost 40 orders of magnitude in size, from galaxies and macroscopic matter that we can touch, all the way to the elementary particles - the quarks and electrons. The four known forces hold the systems together in the different scales. Mathematically, the interactions are described by relativistic quantum field theory, which combines quantum mechanics, classical field theory and special relativity. In this context the forces are mediated by the exchange of so-called gauge bosons. Thus, relativistic quantum mechanics turned

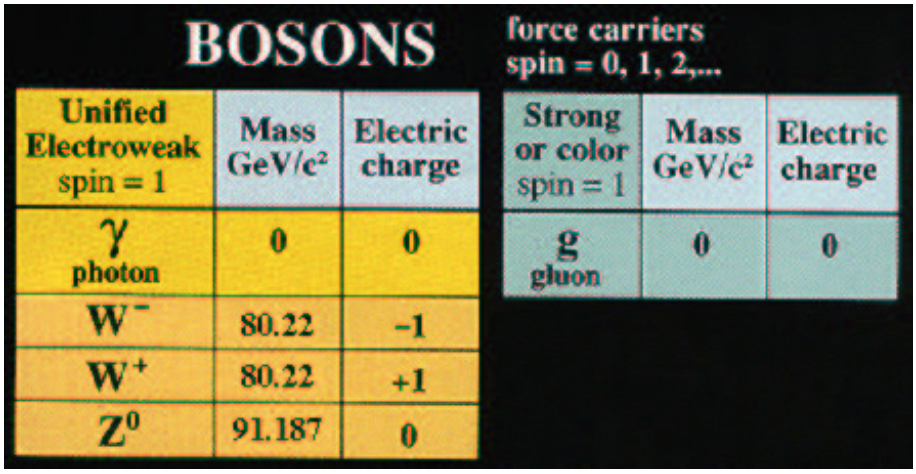

Figure 1.5: The gauge bosons of the electroweak and the strong interaction. Source: [con03]

out to be insufficient for the theoretical description of the elementary particles and their interactions, since particle creation and annihilation processes could not be accounted for. In the electromagnetic interaction the gauge particles are the photons, in the weak interaction these are the so called $W^{\pm}$ and Z bosons and in the strong interaction the color charged gluons bind the quarks together. Up to now it has not been possible to describe gravitation in terms of a quantum field theory.

1.3 Evolution of the universe

In our present picture, the universe originated in the so-called "big bang", then expanded and cooled down from its initial state of extremely high energy densities

and temperatures. At the very beginning of the universe, elementary particles were formed from pure radiation fields. Out of the primordial plasma – consisting of quarks, gluons, photons, and leptons – the building blocks of atomic nuclei – neutrons and protons – were produced only a few fractions of a second after the big bang. Within the first three minutes the lightest atomic nuclei were formed. Neutral atoms appeared 300000 years later. They accumulated into huge gas clouds, from which the first stars were born after about one billion years. Inside the stars the atomic nuclei fused and formed the chemical elements up to iron. The heaviest elements were generated in supernova explosions. Today, 15 billion years after the big bang, these processes still go on and will continue into the distant future.

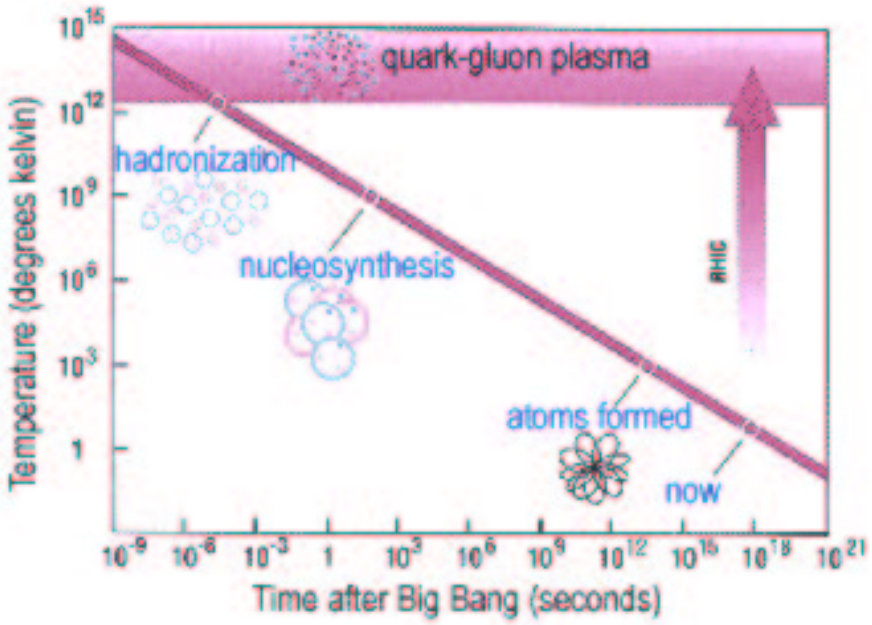

Figure 1.6: Evolution of the universe from the quark gluon plasma to atoms and molecules. Source: [bnl03]

The fundamental symmetries of nature and the laws of physics directly determine the cosmic evolution. Although we know the approximate sequence of events in the cosmic evolution, there are still many unanswered fundamental questions concerning the details. One example is the detailed understanding of the formation of matter. As mentioned above, it is believed that about a millionth of a second after the big bang, all matter existed as a hot, dense primordial plasma consisting of quarks, gluons and other elementary particles. In this so-called quark-gluon plasma, quarks were able to move quasi-freely in contrast to the hadronic phase,

where the quarks are confined to hadrons and where they cannot be observed as isolated degrees of freedom. Similar forms of matter are expected to exist in the interior of neutron stars. The phase of liberated quarks and gluons at the very beginning of the universe was followed, after the hadronization and chiral symmetry breaking, by a phase of hot hadronic matter. The universe cooled down further and further until single hadrons formed nuclei and later atoms and molecules. Relativistic heavy ion collisions are utilized to recreate this state of matter and to study the hadronization and the chiral phase transition. To obtain a full understanding of these processes, knowledge of the properties of hadronic matter under extreme conditions is essential. Furthermore, the dynamics of supernova explosions strongly depends on the nuclear equation of state (EoS). And, since neutron stars are expected to consist of hadronic or quark matter, their properties as well are determined by the characteristic behaviour of these forms of matter. The density in these compact stellar objects is so high that the individual atoms come so close to each other that hadronic matter at several times normal nuclear density is created. The resulting pressure yields the force which prevents the stars from collapsing due to the gravitational force.

1.4 Relativistic heavy ion collisions

As discussed above, excited strongly interacting matter played a major role in the evolution of the universe and is important to understand the structure and dynamics of astrophysical objects and processes, respectively. Furthermore, it constitutes an excited, strongly interacting many body state. Thus, it was tried to create hot and dense strongly interacting matter and learn about its properties. This has been achieved by heavy ion collisions at different energies. The efforts started with the first experiments at Berkeley (Bevalac, $E_{\mathrm{Lab}} = 0.15 - 2$ AGeV), GSI (SIS, $E_{\mathrm{Lab}} = 1$ AGeV) and BNL (AGS, $E_{\mathrm{Lab}} = 10.6 - 14.5$ AGeV). Then, the large program at CERN (SPS, $E_{\mathrm{Lab}} = 40 - 200$ AGeV) followed. About three years ago, the first measurements from the relativistic heavy ion collider (RHIC, $\sqrt{s} = 130, 200$ AGeV) at BNL appeared. Here two gold nuclei are collided with a center of mass energy of $E_{\mathrm{CMS}} = 130$ AGeV. Recently the first 200AGeV data were published. Thus, the center of mass energy is increased by a factor of around 10 compared to the SPS. The next generation facilities are LHC at CERN and the SIS 200 at GSI. These will give further data in the low density high temperature (LHC) and the highest density (SIS200) region.

Excited hadronic matter is produced during the compression stage of relativistic heavy ion collisions. Then eventually a QGP is formed or not. Already at SPS

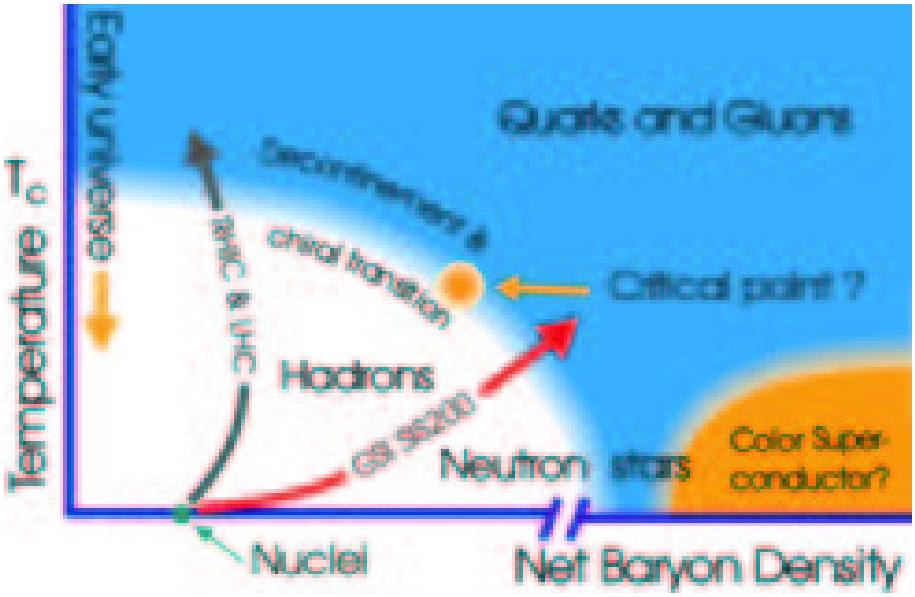

Figure 1.7: Phase structure of nuclear matter in the temeprature-density plane. Furthermore, the (expected) location of physical systems like neutron stars or "fireballs" produced in relativistic heavy ion collisions is depicted. Source: [gsi03]

some hints for the creation of a quark-gluon plasma were obtained. But so far no unambigious signal for its creation could be extracted. However, at RHIC and even more at LHC such a new state of matter is expected to be formed. And for sure, hadronic matter is formed again during the the expansion of the system. Thus, to obtain a full understanding of the entire collision process and to extract the properties of the quark gluon plasma, it is important to know the behaviour of the hadronic matter.

1.5 Theory of excited hadronic matter

Above the importance of the knowledge of the properties of hadronic matter for the understanding of different physical systems was discussed. But how can this be obtained? From an experimental point of view, the observation of neutron stars, supernova explosions, and relativistic heavy ion collisions are most promising. But what about the theoretical side? The theoretical investigation of excited hadronic matter turns out to be a very difficult and challenging task. This is true, even though the underlying theory of strong interaction, Quantum Chromodynamics (QCD), has been known for more than thirty years. However, the ground state of this theory, the QCD-vacuum, already represents a very complicated and dynamical system which is not yet understood. Furthermore, QCD

represents a nonabelian gauge theory and thus is not perturbatively solvable. In particular, on the hadronic scale, the couplings are large and the resulting many body problem is not solvable. Additionally, the degrees of freedom in QCD are quarks and gluons, and thus the hadrons which constitute bound states of these elementary particles cannot be described ab initio. Two main ways out of these problems were followed: On the one hand, it was tried to solve QCD on a discretized lattice. But there several problems arose as well, especially when dense matter was considered. Thus, for a long time calculations were only done for vanishing chemical potentials. Only recently lattice QCD results at finite chemical potential could be obtained. They show for the first time a lattice QCD prediction for the phase diagram of strongly interacting matter. On the other hand, effective models were used, in which baryons and mesons were considered as the relevant degrees of freedom. These models were constructed in the spirit of the idea of Yukawa that the strong force is mediated by the pion. Additional mesons were included and the various couplings were determined from experimental data on the nucleon-nucleon interaction, symmetries of the strong interaction, or the properties of nuclei and nuclear matter. The chiral $SU(3)_L \times SU(3)$ model used in this work represents such an effective hadronic model of the strong interaction. The work is organized as follows: In chaper 2 the theoretical foundations of chiral effective hadronic models are presented. In chapter 3 the chiral $SU(3)_L \times SU(3)_R$ model is discussed in detail. Chapter 4 shows the results for dense and hot hadronic matter. In chapter 5 the properties of neutron stars are investigated. The space-time evolution and HBT analysis of relativistic heavy ion collisions in an ideal-fluid approach using the chiral equation of state is considered in chapter 6. In chapter 7 particle ratios from AGS to RHIC are investigated. The mean-field approach is extended to the Hartree approximation in chapter 8. There also the in-medium properties of vector mesons are calculated. In chapter 9 the main results of this work are summarized and an outlook to future projects is given.

–II–

QCD AND EFFECTIVE MODELS

In this chapter, the basis of our investigation of the properties of excited hadronic matter is presented. The chiral $SU(3) \times SU(3)\, \sigma - \omega$ model we use, is a phenomenological, effective, hadronic Lagrangian. This means, the fundamental interaction of quarks and gluons is described effectively by the interaction of the composite baryonic and mesonic degrees of freedom. The main structure of the model is motivated and constrained on the one hand by the symmetries and properties of QCD [Gro73b, Gro73a, Pol73] and the corresponding phenomenological effective Lagrangians [Wei67, Sch67, Wei68, Col69, Cal69, Gas69] [1] and, on the other hand, by the phenomenology of relativistic meson field theory (see e.g. [Wal95, Ser86, Mac89]).
QCD is, at least up to the energies probed by present accelerators, the accepted underlying theory of the strong interaction. The degrees of freedom in this theory are the fermionic quarks and the bosonic gluons. QCD is a nonabelian theory, with strong couplings and confinement properties at large distances I.e., at low energies there exists no analytical method for the description of QCD. For example, how the observed hadrons, including their rich resonance structure are created from QCD dynamics is still insufficiently understood [Gro99]. Hence, effective models were constructed, which aimed to yield a simplified and solvable description of the underlying theory in the energy domain of interest (see e.g.[Tho84, Hol86, Mei86, Zah86, Got86, Mos89, Vog91, Don92]). In constructing an effective model, the first step is to identify the most important quasi-particles. In the low-energy domain of QCD, these relevant, effective degrees of freedom are the baryons and the mesons. Then rules for the dynamics and interactions of the

[1] Most of these effective Lagrangians were already constructed before QCD was known, just by using symmetries and other properties of the strong interactions known at that time. Since QCD reflects all these characteristics, we will in the following always refer to all these properties as the properties of QCD.

included degrees of freedom have to be set up. This is achieved by constructing an effective Lagrangian, which is based on symmetries, symmetry breaking patterns and other features of the strong interaction [Wei67]. Thus, in the next section, the structure and the important properties of QCD at low energies are reviewed. Then the effective Lagrangian approach for QCD is briefly introduced. As an example, the linear $SU(2) \times SU(2)\,\sigma$ model [Sch57, Pol58, Gel60] is discussed. With this model it can be demonstrated, how symmetries and other properties of QCD may be realized already in a fairly simple Lagrangian. In addition, the nonlinear $SU(2)\,\sigma$ model [Wei68], which cures some shortcomings of the linear approach, is briefly discussed. It also serves as an example of the general framework of nonlinear realizations of chiral symmetry, developed in [Col69, Cal69] (see also appendix B). Despite their close connection to QCD, the pure σ-models do not give a satisfactory description of dense hadronic matter, e.g. the nuclear matter saturation point or the properties of finite nuclei. The understanding of these strongly interacting systems of hadrons is usually called the "nuclear many-body problem". Much work was done to obtain a deeper understanding of the properties of nuclei and nuclear matter. Here, especially scalar and vector mesons turned out to be important. Evidence for the exchange of these particles was found in several investigations of the nucleon-nucleon interaction [Bre37, Bre38, Ros45, Ros48, Erk74, Hol81] and the nuclear many body problem [Due56, Cla73, Cla82]. Due to these findings, large scalar and vector potentials play a key role in the phenomenological relativistic meson field theory [Ser86, Wal95], which turned out to give a very succesful description of hadronic matter and finite nuclei. Section 2.3 gives a brief survey of efforts and results leading to this approach.

As discussed above, the effective description of the strong interaction in terms of (effective) meson fields should account for the constraints given by low energy QCD. Thus, there is a long history of attempts to unite the effective phenomenological meson field theories with QCD symmetries. Some of these efforts are discussed in section 2.4. There, also the construction of the chiral $SU(3)_L \times SU(3)_R\,\sigma$-$\omega$ model is outlined, preparing the detailed description of the corresponding Lagrangian in chapter 3.

2.1 QCD - the gauge theory of quarks and gluons

2.1.1 QCD Lagrangian

QCD is the nonabelian gauge theory of color charge [Gro73b, Gro73a, Pol73]. The Lagrangian is given as

$$\mathcal{L}_{QCD} = -\frac{1}{4} G^{\mu\nu} G_{\mu\nu} + \sum_k \bar{\psi}_k \left(i\gamma^\mu D_\mu - m_k \right) \psi_k, \tag{2.1}$$

where

$$\begin{aligned} G_{\mu\nu} &= \partial_\mu A_\nu - \partial_\nu A_\mu - ig \left[A_\mu, A_\nu \right] && (2.2) \\ D_\mu \psi_k &= \left(\partial_\mu - igA_\mu \right) \psi_k && (2.3) \\ A_\mu &= \sum_{a=1}^{8} A_\mu^a \lambda^a / 2 \,. && (2.4) \end{aligned}$$

ψ_k denote the fermionic quark fields with flavor index $k = u, d, s, ...$, $G_{\mu\nu}$ is the gauge field strength tensor of the bosonic gluon fields A_μ^a, and $\{\lambda^a\}(a = 1, ..., 8)$ are the eight $SU(3)$ Gell-Mann matrices. For each of the N_f quarks flavors there exist $N_c = 3$ colours. The Lagrangian (2.1) is equivalent to the most general renormalizable SU(3) Yang-Mills theory of quarks and gluons [Che94]. The interaction is characterized by a running coupling strength

$$\alpha_s(\mu) = \frac{4\pi}{\beta_0 \ln(\mu^2 / \Lambda_{QCD}^2)}, \tag{2.5}$$

with $\beta_0 = 11 - 2N_f/3$. The parameter μ denotes the energy scale and the QCD scale parameter $\Lambda_{QCD} \simeq 0.2$ GeV.

2.1.2 Symmetries and Currents

As a consequence of gauge invariance, the QCD Lagrangian (2.1) possesses all the symmetries of the strong interaction. The significance of the symmetries is twofold. On the one hand, they create a well defined order in the spectrum of eigenstates of the QCD Hamiltonian. And on the other hand, we know from the Noether theorem [Noe18] that conserved currents exist. These impose constraints on the dynamics of strongly interacting systems, irrespective of whether their relevant degrees of freedom are quarks and gluons or hadrons. In the following we will focus on the light u-, d- and s-quarks, i.e., set $N_f = 3$.

Baryon current

The Lagrangian (2.1) is invariant under $U(1)$ transformations, i.e., multiplication by a global phase factor,

$$\psi(x) \to \exp(i\theta)\psi(x). \tag{2.6}$$

where $\psi(x) = (\psi_1(x), \psi_2(x), \psi_3(x)) = (u(x), d(x), s(x))$. From this invariance results the conserved baryon current $\bar{\psi}\gamma^\mu\psi$ and therefore the conserved baryon number

$$B = \frac{1}{3}\int \mathrm{d}^3x\, \psi^\dagger\psi. \tag{2.7}$$

Chiral Symmetry

The values of the dynamical quark masses at a scale $\mu \sim 1$ GeV are [Gas82, Don89]

$$m_\mathrm{u} = 5 \pm 2 \text{ MeV},\ m_\mathrm{d} = 9 \pm 3 \text{ MeV},\ m_\mathrm{s} = 175 \pm 55 \text{ MeV}. \tag{2.8}$$

These are small compared to typical hadronic masses. In the limit of vanishing u,d and s quark masses, (2.1) is invariant under $SU(3)_L \times SU(3)_R$ flavor transformations on the left- and right-handed components of the quark fields. Rewriting (2.1) as

$$\mathcal{L}_{QCD}|_{m=0} = -\frac{1}{4}G^{\mu\nu}_a G^a_{\mu\nu} + \bar{\psi}_L\gamma_\mu D^\mu\psi_L + \bar{\psi}_R\gamma_\mu D^\mu\psi_R \tag{2.9}$$

shows that the left-handed ψ_L and right-handed ψ_R projections of the quark field have separate invariances. The corresponding chiral symmetry operations are

$$\psi_L \to \exp\left(-i\theta^a_L\lambda_a\right)\psi_L \equiv L\psi_L \tag{2.10}$$

$$\psi_R \to \exp\left(-i\theta^a_R\lambda_a\right)\psi_R \equiv R\psi_R, \tag{2.11}$$

The $SU(3)_L \times SU(3)_R$ transformations can also be written as vector and axialvector transformations

$$\psi \to \exp\left(-i\theta^a_V\lambda_a\right)\psi \tag{2.12}$$

$$\psi \to \exp\left(-i\gamma_5\theta^a_A\lambda_a\right)\psi\,, \tag{2.13}$$

with $\theta_V = (\theta_L + \theta_R)/2$, and $\theta_A = (\theta_L - \theta_R)/2$. The invariance under these transformations is referred to as chiral $SU(3)_L \times SU(3)_R$ or $SU(3)_V \times SU(3)_A$ symmetry. It implies the conserved vector

$$V^\mu_a = \bar{\psi}\gamma^\mu\frac{\lambda_a}{2}\psi, \tag{2.14}$$

and axialvector currents

$$A_a^\mu = \bar{\psi}\gamma^\mu\gamma_5\frac{\lambda_a}{2}\psi. \tag{2.15}$$

The corresponding charges $Q_a^V = \int \mathrm{d}^3x\, V_a^0$ and $Q_a^A = \int \mathrm{d}^3x\, A_a^0$ generate the charge algebra

$$\left[Q_a^V, Q_b^V\right] = if_{abc}Q_c^V \tag{2.16}$$

$$\left[Q_a^V, Q_b^A\right] = if_{abc}Q_c^A \tag{2.17}$$

$$\left[Q_a^A, Q_b^A\right] = if_{abc}Q_c^V. \tag{2.18}$$

Extending (2.16) to the equal time commutation relations of the corresponding currents one obtains the so-called current algebra [Alf73]. These commutation relations are valid even in the presence of symmetry-breaking terms. In addition, the symmetry currents are just the physical currents appearing in electromagnetic and weak interactions. Thus, the symmetries of the strong interaction and the resulting current-algebra relations can directly be tested in electromagnetic or weak interaction processes involving hadrons [Adl68, Alf73].

Spontaneous symmetry breaking

If chiral symmetry were an exact symetry, a degeneracy between states of different parity would be observed, e.g. the ρ meson would be degenerate with the axial a_1 meson or the nucleon (938) should be degenerate with the $N^*(1535)$ resonance. This is not observed in nature. That means: the QCD vacuum state is not symmetric under left and right chiral transformations. Thus, the symmetry must somehow be broken. Since the values of the current quark masses in (2.1) are small compared to hadronic scales, the large mass splitting between the chiral partners cannot result from this contribution. Therefore, one concludes that the chiral symmetry is spontaneously broken. That means, even though the Hamiltonian of the system is chirally symmetric, the ground state is not. Three observations help to understand why the symmetry is "hidden" in the vacuum and which symmetry is spontaneously broken:

- The Goldstone Theorem [Gol61]: Spontaneous breakdown of the symmetry means that the vacuum state is not invariant under the full group of continuous symmetries of the Lagrangian. I.e., if the whole symmetry group has p generators, there will be k operators that respect the symmetries and $(p-k)$ that break the symmetries. Therefore the spectrum of the theory has to include $(p-k)$ massless spinless particles, one for each broken generator.

- The Vafa-Witten thorem [Vaf84] and the mass inequalities for QCD shown by Weingarten [Wei83]: Weingarten has shown that for n-flavor lattice QCD the inequality $m_B \geq m_\pi$ holds. Here m_B denotes the mass of any baryon produced from the vacuum by a three-quark operator. In addition Vafa and Witten have argued that vector like theories (like QCD) cannot spontaneously break vector symmetries (e.g. baryon number and isospin).

- The anomaly matching condition [t'H80]: This powerful condition, formulated by t'Hooft relates fundamental theories with theories in which particles are bound states of the fundamental constituents. It states that a composite particle has to reproduce exactly the anomaly present in the fundamental theory. I.e., the fundamental anomaly and the anomalies in the composite theory must match. Looking at the decay of the pion into two photons, the anomaly matching condition can easily be fulfilled in a world with massless mesons. One only needs to assume that there is a relation between the axial current and the pion, relating the axial current to the decay constant of the pion f_π into muon and neutrino. On the other hand it was shown [Shi91] that a world with massless baryons is not realized in nature.

In summary, the Vafa-Witten argument, the anomaly matching condition and the Goldstone theorem tell us that chiral symmetry is spontaneously broken to its diagonal subgroup in the QCD vacuum. For the $SU(3)_L \times SU(3)_R$ case this means that the vector charges Q_a^V leave the vacuum invariant, while the axialvector charges Q_a^A do not. Thus, the QCD vacuum state is characterized by

$$Q_V^a|0\rangle = |0\rangle \, , \, Q_A^a|0\rangle \neq |0\rangle. \tag{2.19}$$

There are eight axial charges which define a set of physical states $|\phi_a\rangle = Q_a^A|0\rangle$. Since these axial charges commute with the QCD Hamilton operator, they represent an octet of massless pseudoscalars. These can be identified with the eight lightest pseudoscalar mesons. In reality, the pseudoscalar mesons are not massless, but they are light compared to all the other hadrons. The finite mass results from the explicit breaking of the $SU(3)_L \times SU(3)_R$ by the mass term of the QCD Lagrangian. Due to the difference in the current quark masses, i.e., $m_s \gg m_u, m_d$, the mass difference between the nonstrange pseudoscalar mesons, namely the pions and the strange kaons is easily explained. The fact that the pions are Goldstone bosons is of great practical importance. Low energy or temperature hadronic processes are dominated by pions and thus all observables can be expressed as an expansion in pion masses and momenta. This is the basic idea of chiral perturbation theory [Gas84, Gas85, Pic91]. This provides a systematic

method for discussing the consequences of the global flavor symmetries of QCD at low energies by means of an effective field theory [Wei79, Kap95].
Little is known about the mechanism of chiral symmetry breaking from first principles. But, it is largely believed that the spontaneous breakdown of chiral symmetry in the vacuum is followed by a rearrangement of the ground state [Now96]. The vacuum is populated by a condensate of scalar quark-antiquark pairs with a nonvanishing expectation value $\langle 0|\bar{q}q|0\rangle$. The definition of this so-called chiral condensate is given in terms of the quark propagator $S_F(x,y)$ as

$$\langle 0|\bar{\psi}\psi|0\rangle \equiv \langle\bar{\psi}\psi\rangle = \langle\bar{u}u\rangle + \langle\bar{d}d\rangle + \langle\bar{s}s\rangle = -\mathrm{i}\lim_{y\to x_+}\mathrm{Tr}S_F(x,y). \tag{2.20}$$

In the following we will use the expression $\langle\bar{q}q\rangle$ for the the condensates of the light u- and d-quarks. Since the scalar bilinear $\bar{\psi}\psi = \bar{\psi}_R\psi_L + \bar{\psi}_L\psi_R$ mixes right- and left-handed quarks and therefore breaks chiral symmetry, it plays the role of an order parameter for the spontaneous chiral symmetry breaking. If it is nonzero, then the system is not chirally symmetric anymore.
A very interesting nonperturbative feature of QCD in connection with the mechanism of spontaneous chiral symmetry breaking are the so-called instantons. These are exact solutions of the classical Yang-Mills equations in Euclidean space. The assumption that the QCD vacuum is dominated by instanton and antiinstanton fluctuations [t'H76, Cal78] can provide a natural mechanism for the spontaneous breaking of chiral symmetry. This is because instantons and antiinstantons in the vacuum may mix handedness through statistical fluctuations and therefore yield (2.19) [Now96].

2.1.3 Anomalies

Anomalies are symmetries of classical Lagrangians that are broken at the quantum level [Col85]. QCD shows two anomalies: the abelian axial ($U_A(1)$) anomaly and the trace anomaly.

Axial $U(1)$ anomaly

The QCD Lagrangian (2.1) is invariant under a global axial $U(1)$ transformation

$$\psi(x) \to \exp(\mathrm{i}\theta\gamma_5)\psi(x), \tag{2.21}$$

in addition to its $SU(3)_L \times SU(3)_R$ flavour symmetry. According to the Noether theorem, this implies the existence of a ninth conserved current

$$A_0^\mu = \bar{\psi}\gamma^\mu\gamma_5\psi, \tag{2.22}$$

with $\partial_\mu A_0^\mu = 0$. However, this symmetry is broken in the full quantum field theory [Adl69, Fuj79]. If quantum corrections are taken into account, the divergence of the axial singlet current, c.f. Eq. (2.22), does not vanish but is proportional to the gluon fields:

$$\partial_\mu A_0^\mu = \frac{\alpha_s}{4\pi} N_f G_{\mu\nu} \tilde{G}^{\mu\nu}, \tag{2.23}$$

where $\tilde{G}^{\mu\nu}$ is the adjoint gluon field tensor. Thus, the $U(3)_L \times U(3)_R$ ($SU(3)_L \times SU(3)_R \times U(1)_V \times U_(1)_A$) symmetry of the QCD Lagrangian is reduced to $SU(3)_L \times SU(3)_R \times U(1)_V$, which is spontaneously broken to $SU(3)_V \times U(1)_V$. The axial anomaly explains why there are only eight light pseudoscalar mesons or why the η' has a much larger mass than the other members of the multiplet, respectively.
At the quark level, the $U(1)_A$ breaking can be generated by the instanton-induced effective interaction

$$\delta\mathcal{L} \sim G_{inst} \left[det J_{ij}^+ + det J_{ij}^- \right], \tag{2.24}$$

with $J_{ij}^\pm = \bar{\psi}_i (1 \pm \gamma_5) \psi_j$ and $i = u, d, s$. This interaction involves all combinations of quarks such as $(\bar{u}u)(\bar{d}d)(\bar{s}s)$ simultaneously.

Trace anomaly

In the limit of vanishing quark masses, the QCD-Lagrangian (2.1) contains no dimensional parameters and therefore exhibits a classical scale invariance. I.e., the theory is invariant under the transformations

$$\psi(x) \to \lambda^{\frac{3}{2}} \psi(\lambda x),\ A_\mu^a(x) \to \lambda A_\mu(\lambda x), \tag{2.25}$$

with λ arbitrary. This leads to a traceless energy momentum tensor $\Theta^{\mu\nu}$, with conserved dilaton current J_{scale}^μ

$$J_{scale}^\mu = x_\nu \Theta^{\mu\nu},\ \partial J_{scale}^\mu = \Theta_\nu^\nu = 0. \tag{2.26}$$

The scale invariance is also broken by quantum effects. This results from the necessary introduction of a scale if loop diagrams are considered. That means, to fully specify QCD one needs to specify not only the Lagrangian but also a scale parameter. Thus, the full quantum theory is not scale invariant and the dilatational currents are not conserved. In other words, it turns out that the trace of the energy momentum tensor has an anomaly [Cre72, Cha73, Col77]. If the quantum effects are taken into account, the trace of the energy momentum tensor does not vanish anymore but has contributions from the gluons. If furthermore

the finite quark masses are taken into account, the trace of the energy-momentum tensor is given as [Now96]

$$\theta^{\mu}_{\mu} = \frac{\beta_{QCD}}{2g} G^{a}_{\mu\nu} G^{\mu\nu}_{a} + \sum_{k} m_k \bar{\psi}_k \psi_k. \tag{2.27}$$

Here, $\beta_{QCD} \equiv -R\frac{\partial e(R)}{\partial R}$, with e and R denoting the running charge and the distance, respectively. It characterizes the rate at which the charge runs with respect to the change in the scale. Evaluating β_{QCD} to lowest order (one loop level), with N_c colors and N_f flavors, yields for the trace of the energy momentum tensor

$$\begin{aligned} \theta^{\mu}_{\mu} &= \frac{\beta_{QCD}}{2g} G^{a}_{\mu\nu} G^{\mu\nu}_{a} \\ &= \left[-\frac{11 N_c g^3}{48\pi^2} \left(1 - \frac{2N_f}{11N_c}\right) + \mathcal{O}(g^5) \right] G^{a}_{\mu\nu} G^{\mu\nu}_{a}. \end{aligned} \tag{2.28}$$

2.1.4 Hadronic spectrum

As discussed in the previous section, the QCD vacuum spontaneously breaks chiral symmetry. This is due to the finite expectation value of the quark condensate, which mixes left- an right-handed spinor components. The result of this dynamical symmetry breaking can directly be seen in the hadronic mass spectrum, the excitations of the nonperturbative QCD vacuum, which shows a characteristic gap

$$\Delta_{mass} \approx m_N \approx m_\rho. \tag{2.29}$$

While the masses of all baryon states and most of the meson states are well separated from the ground state by the gap Δ, the masses of the pseudoscalar octet members lie right in the gap. I.e., the finite ground state expectation value of the quark condensate introduces a spontaneous symmetry breaking scale of approximately 1 GeV in the spectrum of excited states built on this nonperturbative vacuum. Within this gap one finds collective low-mass excitations, the Goldstone bosons of the dynamically broken symmetries. Thus, the quark condensate strongly determines the properties of the baryons and mesons. At very high temperatures or densities the chiral symmetry is expected to be restored. This restoration will again be visble in the hadronic mass spectrum, if hadrons still exist. Thus, a temperature and density dependence of the quark condensate and thereby of the hadron masses can be expected.

2.2 Effective Lagrangians

Introduction

In the last section some properties of QCD, the underlying theory of strong interactions, were presented. It turned out that already the QCD vacuum is a very complicated object. This is because the gluons are massless, and their strong interaction is not damped by a small parameter. Thus, the QCD vacuum polarization effect is extremely strong, and the empty space is not empty at all but contains a soup of appearing, interacting, and disappearing gluons. Furthermore, there must also be pairs of virtual quark-antiquark pairs that are also color-charged, and emit and absorb virtual gluons. At present it is not possible to find the vacuum wave function analytically. Some hints of what the strong interaction vacuum looks like are given by QCD lattice calculations. Other solutions of the QCD fields are not any simpler. Solutions corresponding to isolated quarks do not exist at all, this is what is called confinement. Solutions for quark-antiquark pairs and for three-quark states exist, the mesons and baryons, respectively. But these are even more complicated to obtain than those for the vacuum, even within QCD lattice calculations. There is no hope to describe composite objects like mesons or baryons from quarks and gluons. That means, if we want to describe the properties of hadronic matter, the degrees of freedeom we have to use are baryons and mesons. This corresponds to isolating and considering the most important or most relevant degrees of freedom. The crucial idea in constructing the effective theory is to incorporate the general properties of the underlying or more fundamental theory. Hereby, symmetries play the essential role in the construction of the effective theory or model, respectively. Historically, effective (phenomenological) Lagrangians were formulated so as to reproduce the results of current algebra and PCAC at tree level [Wei67, Wei73, Das69]. In these formulations analycity, unitarity and symmetries were easier to achieve. The scope of the effective Lagrangian approach was greatly extended by Weinberg in 1979 [Wei79], by postulating that the effective Lagrangians can be used beyond current algebra. As a very instructive example of an effective Lagrangian for QCD, the linear $SU(2) \times SU(2)\sigma$ model will be presented in the next section.

2.2.1 Linear $SU(2) \times SU(2)\,\sigma$ model

The linear σ model [Sch57, Gel60] already contains many properties of QCD, especially the basic ingredients of chiral symmetry. It is the simplest, but also one of the most instructive examples of a linear effective chiral Lagrangian. Including

explicitly the nucleons, the model reads for the $SU(2) \times SU(2)$ case

$$\begin{aligned} \mathcal{L} &= \bar{N}\left[i\gamma_\mu \partial^\mu - g\left(\sigma + i\vec{\tau}\cdot\vec{\pi}\gamma_5\right)\right] N \\ &+ \frac{1}{2}\left(\partial_\mu \sigma\right)^2 + \frac{1}{2}\left(\partial_\mu \vec{\pi}\right)^2 + \frac{\mu^2}{2}\left(\sigma^2 + \vec{\pi}^2\right) - \frac{\lambda}{4}\left(\sigma^2 + \vec{\pi}^2\right)^2 . \end{aligned} \tag{2.30}$$

The Lagrangian is invariant under the $SU(2)_V$ transformations

$$\begin{aligned} \sigma &\rightarrow \sigma' = \sigma \\ \vec{\pi} &\rightarrow \vec{\pi}' = \vec{\pi} + \vec{\alpha} \times \vec{\pi} \\ N &\rightarrow N' = N + \mathrm{i}\vec{\alpha}\cdot\frac{\vec{\tau}}{2} N \end{aligned} \tag{2.31}$$

and the $SU(2)_A$ transformations given by

$$\begin{aligned} \sigma &\rightarrow \sigma' = \sigma + \vec{\beta}\cdot\vec{\pi} \\ \vec{\pi} &\rightarrow \vec{\pi}' = \vec{\pi} + \vec{\beta}\sigma \\ N &\rightarrow N' = N + \mathrm{i}\vec{\beta}\cdot\frac{\vec{\tau}}{2}\gamma_5 N. \end{aligned} \tag{2.32}$$

The conserved Noether currents read

$$V_\mu^a = \bar{N}\gamma_\mu \frac{\tau^a}{2} N + \epsilon^{abc}\pi^b \partial_\mu \pi^c \tag{2.33}$$

$$A_\mu^a = \bar{N}\gamma_\mu\gamma_5 \frac{\tau^a}{2} N + \left(\partial_\mu \sigma\right)\pi^a - \left(\partial_\mu \pi^a\right)\sigma \tag{2.34}$$

and satisfy the Gell-Mann current algebra. Without an explicit symmetry breaking term, both, the vector as well as the axialvector currents are conserved, i.e.,

$$\partial^\mu V_\mu^a = 0, \quad \partial^\mu A_\mu^a = 0. \tag{2.35}$$

The charges

$$T^a = \int \mathrm{d}^3 x V_0^a(x), \; X^a = \int \mathrm{d}^3 x A_0^a(x) \tag{2.36}$$

are the generators of the $SU(2)_V \times SU(2)_A$ algebra. With $\mu^2 < 0$, the potential has a minimum at the unique configuration $\sigma = \vec{\pi} = 0$, i.e., the full symmetry is present. Hence, the meson masses are degenerate and read

$$m_\sigma^2 = m_\pi^2 = -\mu^2. \tag{2.37}$$

Spontaneous symmetry breaking occurs for $\mu^2 > 0$, generating degenerate ground states ("chiral circle") with

$$\sigma^2 + \vec{\pi}^2 = v^2 \text{ with } v = \sqrt{\frac{\mu^2}{\lambda}}. \tag{2.38}$$

One can choose

$$\langle 0|\vec{\pi}|0\rangle = 0,\ \langle 0|\vec{\sigma}|0\rangle = \sqrt{\frac{\mu^2}{\lambda}} \equiv v. \tag{2.39}$$

Other ground states yield the same physics, but require relabelling of the fields. For the choice (2.39), pionic fluctuations do not require any energy, i.e., the pions are Goldstone bosons. After redefining the scalar field through $\sigma \to \sigma + v$, the Lagrangian reads

$$\begin{aligned} \mathcal{L} &= \bar{N}\left(\mathrm{i}\gamma_\mu\partial^\mu - gv\right)N - g\bar{N}\left(\sigma + \mathrm{i}\vec{\tau}\cdot\vec{\pi}\gamma_5\right)N. \\ &+ \frac{1}{2}\left[(\partial_\mu\sigma)^2 - 2\mu^2\sigma^2\right] + \frac{1}{2}\left(\partial_\mu\vec{\pi}\right)^2 - \frac{\lambda}{4}\left(\sigma^2 + \vec{\pi}^2 - v^2\right)^2 \end{aligned} \tag{2.40}$$

The Lagrangian (2.40) directly shows the results of the dynamical symmetry breaking. The pions are massless, while the σ and nucleon fields are massive. I.e., the mass degeneracy $m_\sigma = m_{\vec{\pi}}$ is not present anymore. However, the full set of symmetry currents remain conserved. For a normal symmetry, particles fall into mass-degenerate multiplets and have couplings which are related by the symmetry. In a certain sense, the hidden (spontaneously broken) symmetry gives rise to degenerate states whose couplings are related by the symmetry. The degeneracy consistes of a state taken alone or accompanied by an arbitrary number of Goldstone bosons. E.g., here it can be a nucleon and the same nucleon accompanied by a zero-energy massless pion which are degenerate. Moreover, the couplings of such configurations are restricted by the symmetry. One can e.g. derive identities like

$$\lim_{q_\mu\to 0}\langle\pi^k(q)N'|O|N\rangle = -\frac{\mathrm{i}}{F_\pi}\langle N'|\left[Q_5^k, O\right]|N\rangle, \tag{2.41}$$

where O is some local operator and N, N' are nucleons or other states. Such "soft-pion theorems" relate the couplings of the N states to those of the degenerate πN states. This is the analogue for hidden symmetry of coupling constant relations for a normal symmetry. Thus, chiral symmetry, despite being spontaneously broken, still has a great deal of importance in restricting particle behaviour, e.g. by yielding information about the excitation or annihilation of particles.
The nucleon mass is generated through the ground state expectation value of the scalar field which plays the role of the quark condensate or the order parameter of the spontaneuos symmetry breaking, respectively. A nucleon mass term of the form $m_N\bar{N}N$ would not be invariant under the axial transformations [2].

[2] A nucleon mass term is possible if the chiral partner of the nucleon, which is believed to be the $N^*(1535)$, is included [DeT89].

Furthermore the nucleon mass is too large to be the result of the explicit chiral symmetry breaking as reflected in the PCAC relation. Thus, the dynamical nucleon mass generation through the scalar field is in agreement with the QCD properties discussed in section 2.1.2. Including an explicit symmetry breaking term of the form

$$\mathcal{L}_{esb} = m_\pi^2 f_\pi \sigma \,, \tag{2.42}$$

corresponds to the explicit chiral symmetry breaking due to the finite quark masses in the QCD Lagrangian (2.1). It yields the correct finite pion mass, preserves the conservation of the vector current but breaks the conservation of the axial current, in agreement with the PCAC hypothesis [Che94].

2.2.2 Nonlinear σ model

The linear σ model in several aspects represents an effective Lagrangian for the theory of strong interactions. However, it shows two main shortcomings:

- The direct S-wave coupling of the π-field to the nucleon
- Heavy particles do not themselves exist in chiral multiplets, thus it would be more appropriate to include them on the basis of vectorial flavor invariance.

The "nonlinear realization" of (2.30) is an example of a model which 'cures' these shortcomings. It naturally yields a pseudovector π-N-coupling in accordance with scattering data and gives a scheme for the introduction of heavy degrees of freedom in the chiral symmetric model.
If one rewrites the fields used in the linear σ model as

$$\Sigma = \sigma + \mathrm{i}\vec{\tau}\cdot\vec{\pi} \equiv (v+S)U,\ U = \exp\left(\mathrm{i}\vec{\tau}\cdot\vec{\pi}'/v\right). \tag{2.43}$$

then the Lagrangian reads

$$\begin{aligned}
\mathcal{L} &= \bar{\psi} i\gamma_\mu \partial^\mu \psi - g(v+S)\left(\bar{\psi}_L U \psi_R + \bar{\psi}_R U \psi_L\right) \\
&+ \frac{1}{2}\left[(\partial_\mu S)^2 - 2\mu^2 S^2\right] + \frac{(v+S)^2}{4}\left(\partial_\mu U \partial_\mu U^\dagger\right)^2 \\
&- \lambda v S^3 - \frac{\lambda}{4} S^4 - m_\pi^2 f_\pi \sigma
\end{aligned} \tag{2.44}$$

Here v is the expectation value of the scalar field and S denotes the corresponding fluctuations. If we now also perform redefinitions on the fermion fields

$$N_L \equiv \xi^\dagger \psi_L,\ N_R \equiv \xi \psi_R,\ , U = \xi\xi \tag{2.45}$$

where $\xi = \exp(\mathrm{i}\vec{\tau}\cdot\vec{\pi}/2F_\pi)$, one obtains

$$\begin{aligned}
\mathcal{L} &= \bar{N} i\gamma_\mu D^\mu N - g(v+S)\bar{N}N \\
&+ \frac{1}{2}\left[(\partial_\mu S)^2 - 2\mu^2 S^2\right] + \frac{(v+S)^2}{4}\left(\partial_\mu U \partial_\mu U^\dagger\right)^2 \\
&- \lambda v S^3 - \frac{\lambda}{4}S^4 - m_\pi^2 f_\pi \sigma \\
D_\mu &= \partial_\mu + i\bar{V}_\mu, \\
\bar{V}_\mu &= -\frac{i}{2}\left(\xi^\dagger\partial_\mu\xi + \xi^\dagger\partial_\mu\xi\right), \\
\bar{A}_\mu &= -\frac{i}{2}\left(\xi^\dagger\partial_\mu\xi - \xi^\dagger\partial_\mu\xi\right),
\end{aligned} \tag{2.46}$$

where now the nucleon only has pseudovector couplings to the pions. The new fields transform as

$$\xi \to L\xi V^\dagger,\ N_L \to V N_L,\ N_R \to V N_R \quad . \tag{2.47}$$

For pure vector transformations one has $L = R = V$. For $L \neq R$ the property of V is more complicated, and Eq. (2.47) implies that it cannot be a simple global transformation, but must be a function of $\vec{\pi}(x)$ and hence is a function of x. At first sight, the need to express an $SU(2)$ transformation matrix like V as a function of $\vec{\pi}(x)$ appears unnatural. However, it is in fact consistent with physical expectations. Recall from the general discussion of dynamical symmetry breaking in section 2.1.2 that in the symmetry limit, axial transformations mix the proton not with the neutron (as in isospin transformations), but rather with states consisting of nucleons plus zero momentum pions. Mathematically, the important point is that N_L and N_R transform in an identical fashion. This corresponds to the fact that heavy fields do not transform chirally, but have a common vectorial $SU(2)$ transformation. The Lagrangian is invariant under the transformations (2.47). Thus, we have obtained the expected result that the baryons can have a vectorial $SU(2)$ invariance, while maintaining a chiral invariance for pion couplings. We see in the above example the ingredients of a general procedure for adding heavy fields to effective Lagrangians. The heavy fields are assumed to have an $SU(n)$ transformation described by the matrix V. A derivative ∂_μ acting on the heavy field must be incorporated as part of covariant derivative $\mathcal{D}$ in order to maintain this invariance. Couplings to pions are described by the matrices ξ and U, with ξ having the same transfomations as in (2.47). It is usually straightforward to combine factors of ξ and U in such a way that the overall Lagrangian is invariant. In the general case, each invariant term will have an unknown coefficient, which must be determined phenomenologically.

2.3 Meson field theory and the nuclear many body problem

Excited hadronic matter, the object of our investigation, constitutes a relativistic interacting many-body system. The only consistent theoretical framework for describing such a system is a relativistic quantum field theory based on a local Lagrangian [Wal95]. Thus, the model used in this work represents such a local Lagrangian of baryons and mesons. The meson theory of the strong interaction has a very long tradition. In the beginning, meson theory was thought of as the fundamental theory with the mesons being the field quanta in analogy to the photon in QED. This is reflected in the pioneering work of Yukawa, who was able to explain in particular the short range of the strong force compared to the electromagnetic interaction by the exchange of particles with intermediate mass, the mesons [Yuk35]. Even though today QCD is believed to be the fundamental theory of strong interactions, meson "theory" is still important, since it can be understood as an effective description of quark-gluon dynamics in the low energy regime. Thus, the meson-theory approach beginning with the investigation of the nuclear forces and their application to nuclear matter or finite nuclei up to the present relativistic meson field theory shall be briefly reviewed here. For a more detailed description see for example [Mac89, Ser86, Wal95].

2.3.1 Nuclear forces

Based on Yukawa's idea, much work was done to describe the strong force in terms of the exchange of massive mesons, even long before the pion was found (see e.g. [Pau46, Wen49]). Breit [Bre37, Bre38] and Rosenfeld [Ros45, Ros48] already recognized that vector and scalar fields create a spin-orbit force, for which empirical evidence was seen in the spectra of light nuclei. As the pion was found experimentally in 1947 [Lat47a, Lat47b, Gar48], a lot of theoretical efforts were made to build a theory of the strong interaction, with the pion being the exchange quantum of the force, in analogy to the photon in QED. Of utmost theoretical and practical importance was the identification of three regions in the nuclear force [Tak51]: the long range (classical, $r \geq 2$ fm) part, the intermediate range (dynamical, 1 fm $\leq r \leq$ 2 fm) and the short-range (core, $r \leq 2$ fm) region. This subdivision is still physically most meaningful, and is interpreted in the following way: In the long range part one pion exchange is dominant, while in the intermediate range two-pion exchange is most important, although heavier mesons also become relevant. Finally, in the core region many different processes play a role: multipion exchanges, different kinds of heavy mesons and - as known

today - genuine quark-gluon exchanges. This classification for the different regions of the nuclear force permitted a different derivation for different parts of the force [Mac89]. Here, the one pion exchange was well established as the long range part of the nuclear force already in the 1950s. In contrast, the two pion exchange was difficult to evaluate and did not describe the data well and many discrepancies appeared (for reviews see [Mor51, Phi59, Hul57, Bet55, Sup56, Sup67]). Thus, the field-theoretic program based on single and multipion exchanges only, failed in describing the N-N force.

In a different line of research in that time, Attempts were made to give a simple phenomenological description of the nuclear potential. The reasons for constructing such a potential of the two-nucleon interaction are twofold: First, it provides an economical summary of the data for comparison with potential-like results from theory (e.g. meson theory). Second, it serves as an input for nuclear calculations. Much work was done in this area over the years, up to e.g. the hard- and soft-core potentials developed by Reid [Rei68] which were very often applied in nuclear structure physics in the 70's. Though very successful, the disadvantage of these approaches is that about 30-50 fit parameters are necessary to give a satisfactory description of the N-N potential.

The failure of the interpretation of the strong interaction in terms of the pion exchange only and the rich phenomenological experience with the N-N interaction (e.g. short range interaction and spin-orbit force) that occured, revived the idea of vector meson exchange, which predicts both features. These ideas were additionally supported by the explanation of the nuclear form factor through vector meson dominace [Nam57, Sak60a, Sak60b, Sak60c, Fra59, Fra60] and the detection of the ω and the ρ meson. Thus, so-called one boson exchange (OBE) models were constructed (for a review see [Mor72, Sup67, Gre67]). These approaches assume that uncorrelated multipion exchange is negligible – in contrast to the ideas of the 1950s, where only uncorrelated multipion exchange was considered – and the correlated mulipion exchanges may be described effectively by the exchange of single mesons. The immediate practical advantages of these approaches were: One particle exchanges are straigtforward to calculate in contrast to multimeson exchanges and much fewer parameters (on the order of 10) were necessary compared to the phenomenolgical models. All the OBE models show large contributions from one or two isoscalar scalar bosons with their masses in the range $400-800$ MeV. This particle provides the necessary intermediate-range attraction of the nuclear force. This may be understood as an indication that uncorrelated and correlated 2π exchange is in part well simulated by scalar particle exchange [Mac89].

Looking at the empirical properties of the nuclear force it turns out that with

each of the most important features, one can associate at least one boson field [Mac89]. This manifests the basic reason why meson exchange is appropriate and successful for the description of nuclear forces. The most important empirical features of the nuclear force are [Bla52, Sha74, Seg77, Mor51, Wil63]:

- short range
- attractive in intermediate range
- repulsive core
- tensor force
- spin orbit force

It turns out that only three types of meson fields are necessary to effectively describe these properties:

$$\begin{array}{rl} \text{pseudoscalar} & \pi \\ \text{scalar} & \sigma \\ \text{vector} & V_\mu \end{array} \quad .$$

In a modern view, these are the effective, nonfundamental fields. From symmetry, simplicity and physical intuition the interactions of these fields with the nucleons are commonly written as

$$\begin{aligned} \mathcal{L}_{ps} &= -g_{ps}\bar{\psi}\mathrm{i}\gamma_5\psi\pi \\ \mathcal{L}_s &= g_s\bar{\psi}\psi\sigma \\ \mathcal{L}_v &= -g_v\bar{\psi}\mathrm{i}\gamma^\mu\psi V_\mu - \frac{f_v}{4M}\bar{\psi}\sigma^{\mu\nu}\psi\left(\partial_\mu V_\nu - \partial_\nu V_\mu\right) \end{aligned} \tag{2.48}$$

Alternatively, as induced by chiral symmetry [Wei67], there exists a pseudovector coupling for the pseudoscaler mesons

$$\mathcal{L}_{pv} = -\frac{f_{ps}}{m_{ps}}\bar{\psi}\gamma^5\gamma^\mu\psi\partial_\mu\pi. \tag{2.49}$$

Now the contribution to the N-N interaction from the exchange of the different mesons can be evaluated [Mac89]. Then one finds that the pion as the lightest particle provides the long range part and the tensor force. This tensor force is reduced at short ranges by the ρ (vector-isovector) meson to a realistic size. The ω (vector-isoscalar) creates the short range repulsion and the (short-ranged) spin-orbit force. The intermeditae range attraction is explained by a scalar meson with a mass of 500-700 MeV. Thus, the four bosons $\pi, \sigma, \rho, \omega$ build up the characteristic properties of the nuclear potential [Mac89].

2.3.2 Nuclear matter and finite nuclei

The nucleus is a unique form of matter, since it consists of many baryons interacting through strong, weak and electromagnetic forces. Thus, the nucleus provides a unique microscopic laboratory to test the structure of the fundamental interactions. It manifests remarkable properties as a strongly interacting quantum mechanical many-body system. If nuclear matter, the hypothetical infinite uniform system of nucleons interacting via the strong force is considered, substantial mathematical simplifications arise due to the translational invariance. Symmetric nuclear matter denotes such a system with an equal number of neutrons and protons. Nuclear matter at $T = 0$ is characterized by its energy per particle as a function of the particle density, the nuclear equation of state. The minimum of that curve, i.e., the saturation point is deduced by extrapolation from the properties of finite nuclei. Taking only the volume term of the Bethe-Weizsäcker mass formula [Wei35, Bet36] gives $E/A - m_N \approx -16$ MeV. The saturation density can be deduced from the charge density of finite nuclei, accounting for corrections due to Coulomb interaction and surface tension [Bra64], giving $\rho_0 \approx 0.16$ fm^{-3}. Furthermore the incompressibility or compression modulus of saturated nuclear matter is defined as

$$K = k_F^2 \frac{\partial^2 \left[E/A(k_F)\right]}{\partial k_F^2}\Big|_{k_F = k_F^0} \quad . \tag{2.50}$$

From the nonrelativistic systematics of the isoscalar monopole vibrations in nuclei [You77, Bla76, Bla80] one obtains

$$K = 210 \pm 30 \text{ MeV}. \tag{2.51}$$

The pressure is

$$p = \rho^2 \frac{\partial (E/A)}{\partial \rho}\Big|_{S=const, \rho=\rho_0} , \tag{2.52}$$

where E/A denotes the energy per particle.
In the conventional approach to the nuclear many-body problem, the nucleus was treated as a collection of nucleons, obeying the nonrelativistic Schrödinger equation and interacting through two-body potentials [Rin80]. This potential was either calculated from the N-N interaction with the Hartree-Fock method or phenomenological potentials (e.g. Woods-Saxon) were used. But the very repulsive core in the N-N interaction made conventional perturbation theory inadequate, since a corresponding hard-core potential would give an infinite contribution in each order. The problem was solved by replacing the bare N-N interaction by the so-called Brückner G-Matrix [Brü54, Gol57]. This ansatz solves the hard core

problem by a consistent resummation of certain classes of linked diagrams up to infinite order. However, this approach could not predict the correct saturation density and binding energy. It turned out that there are substantial differences in the predictions both for the saturation energy and the saturation density for different realistic potentials fitting two-nucleon data accurately. But none of the different potentials could describe both quantities correctly. The points lie on the so called "Coester-band" [Coe70]. After extensive efforts, it was clear that there was a fundamental problem in obtaining a good fit to nuclear properties in a model with two-body forces obtained from the study of N-N scattering in free space. Thus, the so-called "Density-Dependent Hartree-Fock" (DDHF) theory was introduced, which contained a phenomenological, density dependent force in the medium (see e.g.[Sky59, Mig67]). This was included either ad hoc (see e.g. [Bar82]) or oriented towards a Brueckner G matrix originally obtained from a free potential (e.g. [Neg70]). These interactions were then adjusted to reproduce the properties of nuclear matter or finite nuclei. The ground state properties of spherical nuclei are reproduced very well. Calculations of the single-particle structure in nuclei give the correct ordering of the single-particle levels. However, discrepanices remained between calculated and empirical results, since DDHF calculations put too much shell structure in the interior nuclear charge distribution and have difficulty in explaining the single-particle spin-orbit interaction, which forms the basis of the nuclear periodic system [Rin80, Ser86].

Due to the success of the OBE potentials in describing the nuclear force, as discussed in section 2.3.1, these potentials were also used to calculate the properties of nuclear matter. But again one encountered the standard problem: if the binding energy of the system was correct, the saturation density was too large, and if the density was correct, the system was underbound. The density dependence of the OBE-potentials again turned out to be such that the saturation point moves along the Coester band [Mac86]. Thus, although the nonrelativistic many-body formalism based on two body interactions had many successes, it turned out to be inadequate for a detailed understanding of nuclei and nuclear matter. However, it was shown e.g in [Gra89, Lej00] that the introduction of three-body forces yields a better description of nuclear matter saturation properties. In addition, in [Pud97] the authors found that nonrelativistic Hamiltonians containing two- and three-nucleon interactions based on the Argonne v_{18} potential [Wir95] can reproduce the energies of all the bound and narrow states of up to eight nucleons with an rms error $\leq 1\%$. Here, the three-nucleon interactions give a significant fraction of nuclear binding energies.

The ultimate change in the understanding of the nuclear many problem resulted from the description of the motion of the nucleons in the nuclei by the Dirac

equation with scalar and vector potentials, i.e., the application of a relativistic ansatz in combination with one-boson exchange (see [phy85] for a historical survey). The early work in this direction was done by Schiff [Sch51], who already considered relativistic field theory of the nuclear many body problem based on baryons and a classical neutral scalar meson field. This approach was improved by Johnson and Teller [Joh55] and Duerr[Due56], who showed that many properties of finite nuclei, including spin-orbit interaction and the energy dependence of the real part of the optical potential could be obtained from a scalar and vector theory. Duerr also observed that nuclear saturation arises naturally in such a model.

These ideas were revived in the approach of Clark et al [Cla73], who solved a Dirac equation with strong scalar and vector potentials to describe proton-nucleus scattering (Dirac phenomenology). It turned out that a quanitative fit of spin observables was possible. These are only poorly described by the Schrödinger equation. In a Dirac-Hartree model for nuclei a successful description of single-particle energy levels, particularly spin orbit splittings, were obtained [Mil72]. A similar phenomenology was introduced by Walecka [Wal74], for the study of "highly condensed matter". Here a relativistic model based on a local Lagrangian of baryons and mesons was considered. The free parameters were fitted to experimental data on nuclear matter saturation properties.

Inspired by these successes and "in an attempt to understand the phenomenological success of these models" [Cel86], a relativistic extension of Brueckner theory has been suggested by Shakin et al [Ana83], the so-called Relativistic Brueckner-Hartree-Fock theory. In analogy to the new ideas in scattering, the essential point was to use the Dirac equation for the single particle motion in nuclear matter with an attractive scalar and a repulsive vector potential. The fields are in the order of several hundred MeV and strongly density dependent. It turned out that this approach can describe both, nuclear matter saturation properties and finite nuclei. In addition, the spin-orbit splitting is described naturally. The RBHF theory is characterized by having no free parameters other than those introduced in fitting free-space nucleon-nucleon scattering data (for a review on the RBHF or Dirac-Brueckner approach, respectively, see [Bro96]).

The Dirac-Brueckner approach is time-consuming and does not account for a possible change of the N-N interaction in the medium due to a change in the hadron properties. In addition, the phenomenological relativistic models based on the work by Walecka [Wal74] turned out to be very successful in the description of nuclear matter, finite nuclei and neutron star matter and are widely applied and extended up to today. As stated above, this approach includes the essential features of the RBHF theory, in particular the interaction of nucleons with a

scalar and a vector meson field. These were the only mesons considered in the first version of this model. The pions average essentially to zero in the description of the bulk properties of nuclear matter or nuclei and can thus be omitted. In addition, if symmetric nuclear matter is considered, the ρ does not contribute as well. The resulting relativistic quantum field theory based on the local, Lorentz invariant hadronic Lagrangian density, given as

$$\begin{aligned} \mathcal{L} &= \bar{\psi}\left[\gamma_\mu\left(i\partial^\mu - g_v V^\mu\right) - \left(M - g_s\phi\right)\right]\psi \\ &+ \frac{1}{2}\left(\partial_\mu\phi\partial^\mu\phi - m_s^2\phi^2\right) - \frac{1}{4}F_{\mu\nu}F^{\mu\nu} + \frac{1}{2}m_v^2 V_\mu V^\mu \quad , \end{aligned} \tag{2.53}$$

was called quantum hadrodynamics (QHD) [Ser86]. Here V^μ, ϕ denote the scalar and vector fields, respectively and $F_{\mu\nu} \equiv \partial_\mu V_\nu - \partial_\nu V_\mu$. In the static limit of infinitely heavy baryon sources, the scalar and vector meson exchanges give rise to an effective potential of the form [Wal95]

$$V_{static} = \frac{g_v^2}{4\pi}\frac{\exp(-m_v r)}{r} - \frac{g_s^2}{4\pi}\frac{\exp(-m_s r)}{r} \quad . \tag{2.54}$$

Spin- and isospin-dependent interactions tend to average out in nuclear matter [Wal95]. With appropriate choices of coupling constants and masses, the potential (2.54) describes the important features of the N-N interaction in bulk nuclear matter: a short-range repulsion between baryons coming from ω exchange and a midrange attraction coming from σ-exchange. Many extensions of the basic Lagrangian (2.53) exist, e.g. introducing additional fields or taking into account nonlinear scalar or vector couplings. For a review see [Ser86, Wal95, Ser97].
The resulting field equations are nonlinear quantum field equations, and thus not directly solvable. Due to the large couplings g_v and g_s, perturbative approaches are also not applicable. Thus, certain approximations are necessary. One of those, which should become increasingly valid as the density increases and which turned out to be very successful in the description of nuclear matter, finite nuclei and neutron star matter, is the so called mean-field approximation. Here, the fermions are treated as single particle operators and the bosons as classical fields. The corresponding models are the so-called relativistic mean-field (RMF) models. For a review and a detailed description of this approximation and several applications see [Ser86, Wal95, Ser97, Hor81, Rei86, Rei89, Gam90, Ser92, Sha93]. The modern perspectives and progress in this approach are discussed in [Fur00c, Ser97, Wal95]. Here one should especially mention the importance of effective field theory [Kap95, Fur00d, Ste00, Fur00c] and density functional theory [Dre90, Sch95] for understanding the success of QHD. In addition, these modern perspectives yield a consistent, controlled expansion and approximation that allows computing reliable results for bulk nuclear properties [Fur00a, Fur00b, Fur00d, Fur00c]. These

treatments are out of the scope of this work, but on the one hand show possible refinements and extensions of the approach used in this work and, on the other hand, they yield additional support for the scalar-vector-type models.

2.4 Effective chiral Lagrangians for nuclei and nuclear matter

There have been many attempts to unite the successful relativistic mean-field (RMF) phenomenology and QCD properties. In particular, the construction of so-called "chiral σ-ω models" which are based on the linear σ model, and where the light scalar meson plays a dual role as the chiral partner of the pion and the mediator of the intermediate range N-N attraction were performed by several authors [Lee74, Ker74, Nym76b, Nym76a, Mat82, Bog83b, Bog83a, Jac83, Sar85, Kun86, Kun87, Bog89, Fom95]. In [Fur93] it was shown that a broad class of these chiral hadronic models fail to reproduce basic properties of finite nuclei at the Hartree level. The authors showed that chiral models built upon the conventional linear sigma model cannot reproduce observed properties of finite nuclei in the Hartree approximation. As stated in [Fur96b], the main problems in these linear sigma models arise from the nonlinear terms in the "Mexican hat " potential, which serves to precipitate spontaneous symmetry breaking, and from the large pion coupling. The consequences are a scalar meson mass that is too large and density dependent forces with the wrong systematics. However, there exist examples of successful approaches, i.e., chiral models which satisfactorily describe nuclear matter saturation and finite nuclei. Some examples are mentioned in the following:

The nonlinear chiral model of Furnstahl et al [Fur95, Fur96b]

This model exhibits a nonlinear realization of chiral symmetry and the effective Lagrangian is chosen such that the model satisfies the low energy theorems of broken scale invariance. By working with a nonlinear representation of chiral symmetry, the problematic constraints of the linear approach can be removed, because the chiral scalar singlet (called σ' by Weinberg [Wei67]) can be decoupled from the other fields. Then a *new* chiral scalar can be introduced to incorporate the dynamics in the scalar-isoscalar sector. The Lagrangian given in [Fur95] reads

$$\begin{aligned}\mathcal{L}(x) &= \overline{N}\Big(i\gamma^\mu\mathcal{D}_\mu + g_A\gamma^\mu\gamma_5 a_\mu - M + g_s\phi + \cdots\Big)N - \frac{1}{4}(\partial_\mu V_\nu - \partial_\nu V_\mu)^2 \\ &\quad + \frac{1}{2}\Big[1 + \eta\frac{\phi}{S_0} + \cdots\Big]\Big[\frac{1}{2}f_\pi^2\,\mathrm{tr}\,(\partial_\mu U\partial^\mu U^\dagger) + m_v^2 V_\mu V^\mu\Big]\end{aligned}$$

$$+\frac{1}{4!}\zeta(g_v^2 V_\mu V^\mu)^2+\frac{1}{2}\partial_\mu\phi\partial^\mu\phi-H_{\rm q}\Big(\frac{S^2}{S_0^2}\Big)^{2/d}\Big(\frac{1}{2d}\ln\frac{S^2}{S_0^2}-\frac{1}{4}\Big)+\cdots\ , \tag{2.55}$$

where $g_A\approx 1.26$ is the axial coupling constant, $\mathcal{D}_\mu=\partial_\mu+iv_\mu+ig_vV_\mu$ is a chirally covariant derivative, and U, v_μ, and a_μ depend on the pion field [Fur95]. The nonlinearly transforming nucleon field is denoted as N and the new scalar field as $S(x)$. The scalar fluctuation field ϕ is related to S by $S(x)\equiv S_0-\phi(x)$.

The linear chiral model of Heide et al [Hei94]

This model is based on a generalization of the linear σ model that incorporates the broken chiral and scale symmetries of QCD. This Lagrangian contains two scalar fields: the σ field, treated as the chiral partner of the pion, and the glueball field Φ. Bulk properties of finite nuclei favor a ω-mass generation by the glueball field, i.e., a mass term of the form $\omega_\mu\omega^\mu\Phi^2$. The Lagrangian is given in terms of the chiral invariant combination of sigma and pion fields, σ and $\vec{\pi}$, the glueball field ϕ, the field of the omega vector meson ω_μ and, since the authors considered finite nuclei, the vector-isovector field $\vec{b}_\mu$ and the Maxwell field A_μ. The Lagrangian reads [Hei94]

$$\begin{aligned}\mathcal{L}_0=&\frac{1}{2}\partial_\mu\sigma\partial^\mu\sigma+\frac{1}{2}\partial_\mu\vec{\pi}\cdot\partial^\mu\vec{\pi}+\frac{1}{2}\partial_\mu\phi\partial^\mu\phi-\tfrac{1}{4}F_{\mu\nu}F^{\mu\nu}-\tfrac{1}{4}\vec{B}_{\mu\nu}\cdot\vec{B}^{\mu\nu}\\&-\tfrac{1}{4}f_{\mu\nu}f^{\mu\nu}+\tfrac{1}{2}\omega_\mu\omega^\mu[G_{\omega\sigma}(\sigma^2+\vec{\pi}^2)+G_{\omega\phi}\phi^2]+\tfrac{1}{2}G_\rho\phi^2\vec{b}_\mu\cdot\vec{b}^\mu\\&+\bar{N}[\gamma^\mu(i\partial_\mu-g_\omega\omega_\mu-\frac{1}{2}g_\rho\vec{b}_\mu\cdot\vec{\tau}-\frac{1}{2}e(1+\tau_3)A_\mu)-g(\sigma+i\vec{\pi}\cdot\vec{\tau}\gamma_5)]N\ .\end{aligned} \tag{2.56}$$

Here $F_{\mu\nu}=\partial_\mu\omega_\nu-\partial_\nu\omega_\mu$, $\vec{B}_{\mu\nu}=\partial_\mu\vec{b}_\nu-\partial_\nu\vec{b}_\mu$ and $f_{\mu\nu}=\partial_\mu A_\nu-\partial_\nu A_\mu$ denote the different field strength tensors. In addition, the scale breaking term

$$\begin{aligned}V_G(\phi,\sigma,\vec{\pi})\ &=\ B\phi^4\left(\ln\frac{\phi}{\phi_0}-\frac{1}{4}\right)-\frac{1}{2}B\delta\phi^4\ln\frac{\sigma^2+\vec{\pi}^2}{\sigma_0^2}\\&\quad+\frac{1}{2}B\delta\zeta^2\phi^2\left(\sigma^2+\vec{\pi}^2-\frac{1}{2}\frac{\phi^2}{\zeta^2}\right)\ ,\end{aligned} \tag{2.57}$$

was used to reproduce the effective trace anomaly.

The gauge invariant model of Fomenko et al [Fom97]

In this approach, all vector fields are treated as Yang-Mills fields, the pion being the only Goldstone particle. The model contains altogether three scalar-isosclar

fields: One (S_π) which simulates the intermediate-range attraction of the N-N force, one (Σ), which is the chiral partner of the pion and a third (σ) playing the role of a Higgs field for the ω. The detailed Lagrangian is given in [Fom95, Fom97].

The chiral $SU(3) \times SU(3)$ model used in this work [Pap99]

This model will be discussed in detail in chapter 3. The Lagrangian exhibits a nonlinear realization of chiral $SU(3)$ symmetry, and incorporates broken scale invariance similar as in [Hei94] and as already proposed in [Sch80]. The SU(3) multiplets for baryons, spin scalar, pseudoscalar, vector and axialvector mesons are included (see appendix A).

–III–

Chiral $SU(3)_L \times SU(3)_R$ model

3.1 The model

We consider a relativistic field theoretical model of baryons and mesons[1] built on chiral $SU(3)_L \times SU(3)_R$ symmetry and broken scale invariance [Pap99, Zsc00b]. A nonlinear realization (see [Wei68, Cal69] and appendix B) of chiral symmetry is adopted that has been successful in a simultaneous description of finite nuclei and hyperon potentials [Pap99]. The general form of the Lagrangian is as follows:

$$\mathcal{L} = \mathcal{L}_{\text{kin}} + \sum_{W=X,Y,V,\mathcal{A},u} \mathcal{L}_{\text{BW}} + \mathcal{L}_{\text{vec}} + \mathcal{L}_0 + \mathcal{L}_{\text{SB}}. \tag{3.1}$$

$\mathcal{L}_{\text{kin}}$ is the kinetic energy term, $\mathcal{L}_{\text{BW}}$ includes the interaction terms of the baryons with the spin-0 and spin-1 mesons, the former generating the baryon masses. $\mathcal{L}_{\text{vec}}$ generates the masses of the spin-1 mesons through interactions with spin-0 fields and contains quartic self-interactions of the vector fields. $\mathcal{L}_0$ gives the meson-meson interaction terms which induce the spontaneous breaking of chiral symmetry. It also includes a scale-invariance breaking logarithmic potential. Finally, $\mathcal{L}_{\text{SB}}$ introduces an explicit symmetry breaking of the $\text{U}(1)_A$, $\text{SU}(3)_V$ and chiral symmetry.

3.1.1 Kinetic energy terms

Since the vector transformation $h(\pi(x))$ (Eq. B.16) of the hadrons depends in general on the pseudoscalar mesons and thus is local (appendix B), covariant derivatives have to be used for the kinetic terms in order to preserve chiral invariance. Then for example the covariant derivative for the baryons B (A.5)

[1] The corresponding multiplets are described in appendix A

reads

$$D_\mu B = \partial_\mu B + i[\Gamma_\mu, B], \tag{3.2}$$

where

$$\Gamma_\mu = -\frac{\mathrm{i}}{2}\left[u^\dagger(\partial_\mu + ig_v l_\mu)u + u(\partial_\mu + ig_v r_\mu)u^\dagger\right] \quad , \tag{3.3}$$

with the unitary transformation operator (appendix B,[Pap99]).

$$u = \exp\left[\frac{\mathrm{i}}{2\sigma_0}\pi^a\lambda_a\gamma_5\right]. \tag{3.4}$$

Γ_μ is a composite vector-type field, which transforms according to

$$\Gamma'_\mu \;=\; h\Gamma_\mu h^\dagger - ih\partial_\mu h^\dagger. \tag{3.5}$$

The external fields l_μ and r_μ can be any gauge field of the weak or the electromagnetic interactions. In [Pap99, Sch02] the photon gauge field, $l_\mu = r_\mu = QA_\mu$, with $Q = T_3 + Y/2$, and the electrical charge, $g_v = e$, was incorporated to study finite nuclei. In this work, nuclear and neutron star matter are considered, hence the electromagnetic interactions can be neglected. The spin-1 nonet of the strong interactions are here introduced as massive, homogeneously transforming fields, following the approach [Bor96, Bir96], in order to avoid complications arising from the mixing of the axial with the pseudoscalar mesons.
The pseudoscalar mesons are given as parameters of the symmetry transformation (appendix B). Their kinetic energy term is introduced by defining (in analogy to Eq. (3.3))

$$u_\mu = -\frac{i}{2}\left[u^\dagger(\partial_\mu + ig_v l_\mu)u - u(\partial_\mu + ig_v r_\mu)u^\dagger\right], \tag{3.6}$$

where the axialvector u_μ transforms under chiral rotations as $u'_\mu = hu_\mu h^\dagger$. The standard form for the kinetic energy of the pseudoscalar mesons is $\mathrm{Tr}(u_\mu u^\mu)$. However, the approximate validity of $g_{N\sigma} \approx m_N/f_\pi$, where $f_\pi = -\sigma_0$, in the Walecka-type models [Fur87, Fur96a] and results obtained in [Pap98b, Hei94] indicate that the constraints of the linear σ model on the scalar condensates in the vacuum are also applicable to the description of hadronic matter and nuclei. In order to incorporate those constraints in the nonlinear realization we modify the standard kinetic energy term to include a coupling of the scalar and pseudoscalar mesons, denoted as X and Y, respectively (see appendix B). The resulting kinetic term reads

$$\mathrm{Tr}(u_\mu X u^\mu X + X u_\mu u^\mu X). \tag{3.7}$$

This term contains, besides higher order self-interactions, the kinetic energy term for the pseudoscalar mesons. The pseudoscalar matrix in the exponential of

Eq. (3.4) is defined as ([Bar69], appendix B)

$$\frac{1}{\sqrt{2}}\pi_a\lambda^a = \begin{pmatrix} \frac{1}{\sqrt{2}}\left(\pi^0 + \frac{\eta^8}{\sqrt{1+2\,w^2}}\right) & \pi^+ & 2\,\frac{K^+}{w+1} \\ \pi^- & \frac{1}{\sqrt{2}}\left(-\pi^0 + \frac{\eta^8}{\sqrt{1+2\,w^2}}\right) & 2\,\frac{K^0}{w+1} \\ 2\,\frac{K^-}{w+1} & 2\,\frac{\overline{K}^0}{w+1} & -\frac{\eta^8\sqrt{2}}{\sqrt{1+2\,w^2}} \end{pmatrix}. \qquad (3.8)$$

The renormalization factors containing $w = \sqrt{2}\zeta_0/\sigma_0$ are included to obtain the canonical form of the kinetic energy terms for pseudoscalar mesons[2] from (3.7). For $w = 1$, one has an $SU(3)_V$ symmetric vacuum and the matrix (3.8) reduces to the matrix normally used e.g. in chiral perturbation theory [Don92]. The advantage of (3.8) is that $SU(3)_V$ breaking effects (such as $f_\pi \neq f_K$) are accounted for even at lowest order.

After computing the axial current for pions and kaons from Eq. (3.7), one obtains the same relations

$$\sigma_0 = -f_\pi \qquad \zeta_0 = -\frac{1}{\sqrt{2}}(2f_K - f_\pi) \qquad , \qquad (3.9)$$

for the VEV of the scalar condensates found in the linear σ model [Pap98b].

In summary, the kinetic energy terms read

$$\begin{aligned} \mathcal{L}_{kin} &= i\mathrm{Tr}\overline{B}\gamma_\mu D^\mu B + \frac{1}{2}\mathrm{Tr}D_\mu X D^\mu X + \mathrm{Tr}(u_\mu X u^\mu X + X u_\mu u^\mu X) \\ &+ \frac{1}{2}\mathrm{Tr}D_\mu Y D^\mu Y + \frac{1}{2}D_\mu\chi D^\mu\chi - \frac{1}{4}\mathrm{Tr}\left(\tilde{V}_{\mu\nu}\tilde{V}^{\mu\nu}\right) - \frac{1}{4}\mathrm{Tr}\left(\mathcal{A}_{\mu\nu}\mathcal{A}^{\mu\nu}\right) \qquad (3.10) \end{aligned}$$

Here B is the baryon octet, X is the scalar multiplet, Y is the pseudoscalar chiral singlet, $\tilde{V}^\mu$ is the vector meson multiplet (A.4) with field tensor $\tilde{V}_{\mu\nu} = D^\nu\tilde{V}^\mu - D^\mu\tilde{V}^\nu$ [3], $A_{\mu\nu} = D^\nu A^\mu - D^\mu A^\nu$ is the axialvector field tensor and χ is the scalar, iso-scalar glueball-field (for its discussion see Sec.3.1.3 and appendix D). The pseudoscalar singlet is independent of the octet and thus has a kinetic term of its own. For the dilaton field χ , which is also a chiral singlet, it makes no difference if the normal derivative is replaced with the covariant derivative because the additional commutator term vanishes.

[2]The same normalization of the pseudoscalar matrix has to be taken if the kinetic energy term $\frac{1}{2}\mathrm{Tr}(\partial_\mu M^\dagger \partial^\mu M)$ is used with $M = u(X + iY)u$ and $M^\dagger = u^\dagger(X - iY)u^\dagger$.

[3]As described in section 3.1.3, the vector mesons need to be renormalized. The physical fields will be denoted as V_μ and $\rho_\mu, \omega_\mu, \phi_\mu$ respectively and the unrenormalized, mathematical fields as $\tilde{V}_\mu$ and $\tilde{\rho}_\mu, \tilde{\omega}_\mu, \tilde{\phi}_\mu$.

3.1.2 Baryon-meson interaction

The $SU(3)$ structure of the the baryon-meson interaction terms are the same for all mesons, except for the difference in Lorentz space. For a general meson field W they read

$$\mathcal{L}_{BW} = -\sqrt{2}g_8^W \left(\alpha_W[\overline{B}\mathcal{O}BW]_F + (1-\alpha_W)[\overline{B}\mathcal{O}BW]_D\right) - g_1^W \frac{1}{\sqrt{3}}\mathrm{Tr}(\overline{B}\mathcal{O}B)\mathrm{Tr}W\,, \tag{3.11}$$

with $[\overline{B}\mathcal{O}BW]_F := \mathrm{Tr}(\overline{B}\mathcal{O}WB - \overline{B}\mathcal{O}BW)$ and $[\overline{B}\mathcal{O}BW]_D := \mathrm{Tr}(\overline{B}\mathcal{O}WB + \overline{B}\mathcal{O}BW) - \frac{2}{3}\mathrm{Tr}(\overline{B}\mathcal{O}B)\mathrm{Tr}W$. The different terms to be considered are those for the interaction of baryons with scalar mesons ($W = X, \mathcal{O} = 1$), with vector mesons ($W = \tilde{V}_\mu, \mathcal{O} = \gamma_\mu$ for the vector and $W = \tilde{V}_{\mu\nu}, \mathcal{O} = \sigma^{\mu\nu}$ for the tensor interaction), with axial vector mesons ($W = \mathcal{A}_\mu, \mathcal{O} = \gamma_\mu\gamma_5$) and with pseudoscalar mesons ($W = u_\mu, \mathcal{O} = \gamma_\mu\gamma_5$), respectively. For the spin-$\frac{3}{2}$ baryons (D^μ) one can construct a coupling term similar to (3.11)

$$\mathcal{L}_{\mathrm{DW}} = -\sqrt{2}g_{D8}^W[\overline{D^\mu}\mathcal{O}D_\mu W] - g_{D1}^W[\overline{D^\mu}\mathcal{O}D_\mu]TrW\,, \tag{3.12}$$

where $[\overline{D^\mu}\mathcal{O}D_\mu W]$ and $[\overline{D^\mu}\mathcal{O}D_\mu]$ are obtained from coupling $[1\bar{0}] \times [10] \times [8] = [1] + [8] + [27] + [64]$ and $[1\bar{0}] \times [10] \times [1]$ to an SU(3) singlet, respectively. In the following we discuss the relevant couplings for the current investigation.

Baryon-scalar meson interaction

The baryons and the scalar mesons transform equally in the left and right subspaces. Therefore, in contrast to the linear realization of chiral symmetry, an f-type coupling is allowed for the baryon meson interaction. In addition, it is possible to construct mass terms for baryons and to couple them to chiral singlets. After insertion of the vacuum expectation value for the scalar multiplet matrix $\langle X\rangle_0$, one obtains the baryon masses as generated by the VEV of the nonstrange $\sigma \sim \langle\bar{u}u + \bar{d}d\rangle$ and the strange $\zeta \sim \langle\bar{s}s\rangle$ scalar fields [Pap99]

$$\begin{aligned}
m_N &= m_0 - \frac{1}{3}g_8^S(4\alpha_S - 1)(\sqrt{2}\zeta_0 - \sigma_0)\\
m_\Lambda &= m_0 - \frac{2}{3}g_8^S(\alpha_S - 1)(\sqrt{2}\zeta_0 - \sigma_0)\\
m_\Sigma &= m_0 + \frac{2}{3}g_8^S(\alpha_S - 1)(\sqrt{2}\zeta_0 - \sigma_0)\\
m_\Xi &= m_0 + \frac{1}{3}g_8^S(2\alpha_S + 1)(\sqrt{2}\zeta_0 - \sigma_0),
\end{aligned} \tag{3.13}$$

with $m_0 = g_1^S(\sqrt{2}\sigma + \zeta)/\sqrt{3}$. The three parameters g_1^S, g_8^S and α_S can be used to fit the baryon masses to their experimental values. Then, besides the current

quark mass terms discussed in section 3.1.4, no additional explicit symmetry breaking term is needed. In the following we will refer to this case as C1. Note that the nucleon mass depends on the *strange condensate* ζ! For $\zeta = \sigma/\sqrt{2}$ (i.e., $f_\pi = f_K$), the masses are degenerate, and the vacuum is $SU(3)_V$-invariant. For the baryon decuplet the procedure is similar, the members are treated as spin-$\frac{1}{2}$ particles with spin-$\frac{3}{2}$ degeneracy. If the vacuum matrix for the scalar condensates is inserted, one obtains the dynamically generated vacuum masses of the baryon decuplet

$$\begin{aligned} m_\Delta &= g_D^S \left[(3-\alpha_{DS})\sigma + \alpha_{DS}\sqrt{2}\zeta\right] \\ m_{\Sigma^*} &= g_D^S \left[2\sigma + \sqrt{2}\zeta\right] \\ m_{\Xi^*} &= g_D^S \left[(1+\alpha_{DS})\sigma + (2-\alpha_{DS})\sqrt{2}\zeta\right] \\ m_\Omega &= g_D^S \left[2\alpha_{DS}\sigma + (3-\alpha_{DS})\sqrt{2}\zeta\right] \quad . \end{aligned} \tag{3.14}$$

The new parameters are connected to the parameters in (3.12) by $g_{D8}^W = -\sqrt{120}(1-\alpha_{DS})g_D^S$ and $g_{D1}^W = \sqrt{90}g_D^S$. They can now be adjusted to reproduce the masses of the baryon decuplet. As in the case of the nucleon, the coupling of the Δ to the strange condensate is nonzero. This type of mass generation is denoted as C_1 in the following.

We will also consider the limit where the nonstrange baryons, n and Δ, do not couple to the strange condensate ζ. This case will be denoted as C_2 and is obtained by choosing $\alpha_S = 1$ and $g_1^S = \sqrt{6}g_8^S$ in the octet sector and $\alpha_{DS} = 0$ for the decuplet. Then the coupling constants between the baryons and the two scalar condensates are related to the additive quark model. This leaves only one coupling constant free, which is adjusted to give the correct nucleon mass. For a fine tuning of the remaining masses, it is necessary to introduce an explicit symmetry breaking term, which breaks the SU(3) symmetry along the hypercharge direction. For the octet a possible term already discussed in [Pap98b, Sch69], which respects the Gell-Mann-Okubo mass relation, is

$$\mathcal{L}_{\Delta m} = -m_1 \mathrm{Tr}(\overline{B}B - \overline{B}BS) - m_2 \mathrm{Tr}(\overline{B}SB), \tag{3.15}$$

where $S_b^a = -\frac{1}{3}[\sqrt{3}(\lambda_8)_b^a - \delta_b^a]$. The three coupling constants $g_{N\sigma} \equiv 3g_8^S$, m_1 and m_2 are sufficient to satisfactorily reproduce the experimentally known baryon masses. The resulting baryon octet masses read:

$$\begin{aligned} m_N &= -g_{N\sigma}\sigma_0 \\ m_\Lambda &= -g_{N\sigma}\left(\frac{2}{3}\sigma_0 + \frac{1}{3}\sqrt{2}\zeta_0\right) + \frac{m_1+2m_2}{3} \\ m_\Sigma &= -g_{N\sigma}\left(\frac{2}{3}\sigma_0 + \frac{1}{3}\sqrt{2}\zeta_0\right) + m_1 \end{aligned}$$

$$m_\Xi = -g_{N\sigma}\left(\frac{1}{3}\sigma_0 + \frac{2}{3}\sqrt{2}\zeta_0\right) + m_1 + m_2. \tag{3.16}$$

For the baryon decuplet the explicit symmetry breaking terms are proportional to the number of strange quarks for a given baryon species. The additional parameter is denoted as m_{Ds}. Thus, the mass terms of the baryon decuplet read

$$\begin{aligned} m_\Delta &= g_{\Delta\sigma}\left[3\sigma\right] \\ m_{\Sigma^*} &= g_{\Delta\sigma}\left[2\sigma + \sqrt{2}\zeta\right] + m_{Ds} \\ m_{\Xi^*} &= g_{\Delta\sigma}\left[1\sigma + 2\sqrt{2}\zeta\right] + 2m_{Ds} \\ m_\Omega &= g_{\Delta\sigma}\left[0\sigma + 3\sqrt{2}\zeta\right] + 3m_{Ds} \quad . \end{aligned} \tag{3.17}$$

Baryon-vector meson interaction

Two independent interaction terms of baryons with spin-1 mesons can be constructed in analogy with the baryon-spin-0-meson interaction. They correspond to the antisymmetric (f-type) and symmetric (d-type) couplings, respectively. As for the case with scalar mesons (section 3.1.2), for $g_1^V = \sqrt{6}g_8^V$, the strange vector field $\phi_\mu \sim \overline{s}\gamma_\mu s$ does not couple to the nucleon. The remaining couplings to the baryons are then determined by symmetry relations

$$\begin{aligned} g_{N\tilde{\omega}} &= (4\alpha_V - 1)g_8^V \qquad g_{N\tilde{\phi}} = 0 \\ g_{\Lambda\tilde{\omega}} &= \frac{2}{3}(5\alpha_V - 2)g_8^V \qquad g_{\Lambda\tilde{\phi}} = -\frac{\sqrt{2}}{3}(2\alpha_V + 1)g_8^V \\ g_{\Sigma\tilde{\omega}} &= 2\alpha_V g_8^V \qquad g_{\Sigma\tilde{\phi}} = -\sqrt{2}(2\alpha_V - 1)g_8^V \\ g_{\Xi\tilde{\omega}} &= (2\alpha_V - 1)g_8^V \qquad g_{\Xi\tilde{\phi}} = -2\sqrt{2}\alpha_V g_8^V \quad . \end{aligned} \tag{3.18}$$

From the universality principle [Sak69] and the vector meson dominance model one may conclude that the d-type coupling should be small. Here we will use pure f-type coupling, i.e., $\alpha_V = 1$ for all fits, even though a small admixture of d-type coupling allows for some fine-tuning of the single particle energy levels of nucleons in nuclei (see [Pap99, Sch02]). The resulting Lagrangian reads:

$$\mathcal{L}_{BV} = -\sqrt{2}g_8^V\left([\overline{B}\gamma_\mu B\tilde{V}^\mu]_F + \mathrm{Tr}(\overline{B}\gamma_\mu B)\mathrm{Tr}\tilde{V}^\mu\right), \tag{3.19}$$

and the resulting couplings of the unrenormalized fields may all be expressed in terms of the N-$\tilde{\omega}$-coupling $g_{N\tilde{\omega}}$ (table 3.1). Thus, in this limit all coupling constants are fixed once $g_{N\tilde{\omega}}$ or equivalently $g_{N\omega} \equiv \sqrt{Z_\omega}g_{N\tilde{\omega}}$, is specified. This is done by fitting it to the energy density at nuclear matter saturation ($E/A = -16$ MeV). Since the axial vector mesons have a vanishing expectation

$g_{N\tilde{\omega}} = 3g_8^V$	$g_{N\tilde{\phi}} = 0$	$g_{N\tilde{\rho}} = g_8^V = \frac{1}{3}g_{N\tilde{\omega}}$
$g_{\Lambda\tilde{\omega}} = 2g_8^V = \frac{2}{3}g_{N\tilde{\omega}}$	$g_{\Lambda\tilde{\phi}} = -\sqrt{2}g_8^V = -\frac{\sqrt{2}}{3}g_{N\tilde{\omega}}$	$g_{\Lambda\tilde{\rho}} = 0$
$g_{\Sigma\tilde{\omega}} = 2g_8^V = \frac{2}{3}g_{N\tilde{\omega}}$	$g_{\Sigma\tilde{\phi}} = -\sqrt{2}g_8^V = -\frac{\sqrt{2}}{3}g_{N\tilde{\omega}}$	$g_{\Sigma\tilde{\rho}} = 2g_8^V = \frac{2}{3}g_{N\tilde{\omega}}$
$g_{\Xi\tilde{\omega}} = 1g_8^V = \frac{1}{3}g_{N\tilde{\omega}}$	$g_{\Xi\tilde{\phi}} = -2\sqrt{2}g_8^V = -\frac{2\sqrt{2}}{3}g_{N\tilde{\omega}}$	$g_{\Xi\tilde{\rho}} = g_8^V = \frac{1}{3}g_{N\tilde{\omega}}$

Table 3.1: Baryon-vector meson couplings in the limit $\alpha_V = 1$

value at the mean-field level, their coupling constants to the baryons will not be discussed here. For the coupling of the baryon resonances to the vector mesons we obtain the same Clebsch-Gordan coefficients as for the coupling to the scalar mesons. This leads to the following relations between the coupling constants

$$\begin{aligned} g_{\Delta\tilde{\omega}} &= (3-\alpha_{DV})g_{DV} & g_{\Delta\tilde{\phi}} &= \sqrt{2}\alpha_{DV}g_{DV} \\ g_{\Sigma^*\tilde{\omega}} &= 2g_{DV} & g_{\Sigma^*\tilde{\phi}} &= \sqrt{2}g_{DV} \\ g_{\Xi^*\tilde{\omega}} &= (1+\alpha_{DV})g_{DV} & g_{\Xi^*\tilde{\phi}} &= \sqrt{2}(2-\alpha_{DV})g_{DV} \\ g_{\Omega\tilde{\omega}} &= \alpha_{DV}g_{DV} & g_{\Omega\tilde{\phi}} &= \sqrt{2}(3-\alpha_{DV})g_{DV} \quad . \end{aligned} \tag{3.20}$$

In analogy to the octet case we set $\alpha_{DV} = 0$, so that the strange vector meson ϕ does not couple to the Δ baryon. The resulting coupling constants obey the additive quark model constraints (see table 3.2). Hence, all coupling constants

$g_{\Delta\tilde{\omega}} = 3g_8^V$	$g_{\Delta\tilde{\phi}} = 0$	$g_{\Delta\tilde{\rho}} = 3g_8^V = g_{\Delta\tilde{\omega}}$
$g_{\Sigma^*\tilde{\omega}} = 2g_8^V = \frac{2}{3}g_{\Delta\tilde{\omega}}$	$g_{\Sigma^*\tilde{\phi}} = -\sqrt{2}g_8^V = -\frac{\sqrt{2}}{3}g_{\Delta\tilde{\omega}}$	$g_{\Sigma^*\tilde{\rho}} = 2g_8^V = \frac{2}{3}g_{\Delta\tilde{\omega}}$
$g_{\Xi^*\tilde{\omega}} = g_8^V = \frac{1}{3}g_{\Delta\tilde{\omega}}$	$g_{\Xi^*\tilde{\phi}} = -2\sqrt{2}g_8^V = -\frac{2\sqrt{2}}{3}g_{\Delta\tilde{\omega}}$	$g_{\Xi^*\tilde{\rho}} = g_8^V = \frac{1}{3}g_{\Delta\tilde{\omega}}$
$g_{\Omega\tilde{\omega}} = 0$	$g_{\Omega\tilde{\phi}} = -3\sqrt{2}g_8^V = -\sqrt{2}g_{\Delta\tilde{\omega}}$	$g_{\Omega\tilde{\rho}} = 0$

Table 3.2: Baryon resonance-vector meson couplings in the limit $\alpha_{DV} = 0$

of the baryon decuplet are again fixed if one overall coupling g_{DV} is specified. Since there is no vacuum restriction on the Δ-ω coupling, like in the case of the scalar mesons, we have to consider different constraints. This will be discussed in section 4.1.

3.1.3 Meson-meson interaction

Vector mesons

The vector meson-meson interactions contain the mass terms of the vector mesons and higher order vector meson self-interactions. The simplest scale invariant mass

term is

$$\mathcal{L}_{vec}^{(1)} = \frac{1}{2} m_V^2 \frac{\chi^2}{\chi_0^2} \mathrm{Tr} \tilde{V}_\mu \tilde{V}^\mu. \tag{3.21}$$

It implies a mass degeneracy for the vector meson nonet. The scale invariance is assured by the square of the glueball field χ (see below and appendix D for details). In (3.21) the vector meson masses do only couple to the glueball field. As has been shown in [Pap98a, Hei94], a coupling to the scalar meson does not give a satisfactory description of finite nuclei. To split the masses, one can add the chiral invariants [Gas69, Mit68]

$$\mathcal{L}_{vec}^{(2)} = \frac{1}{4} \mu \mathrm{Tr} \left[\tilde{V}_{\mu\nu} \tilde{V}^{\mu\nu} X^2 \right] \tag{3.22}$$

and

$$\mathcal{L}_{vec}^{(3)} = \frac{1}{12} \lambda_V \left(\mathrm{Tr} \left[\tilde{V}_{\mu\nu} \right] \right)^2. \tag{3.23}$$

Combining the contributions (3.22) and (3.23) with the kinetic energy term (3.10), one obtains the following kinetic terms for the vector mesons in the vacuum

$$\mathcal{L}_{\tilde{V}} = -\frac{1}{4} Z_\rho^{-1} \left(\tilde{V}_{\tilde{\rho}}^{\mu\nu} \right)^2 - \frac{1}{4} Z_\omega^{-1} \left(\tilde{V}_{\tilde{\omega}}^{\mu\nu} \right)^2 - \frac{1}{4} Z_\phi^{-1} \left(\tilde{V}_{\tilde{\phi}}^{\mu\nu} \right)^2, \tag{3.24}$$

with e.g. $\tilde{V}_{\tilde{\rho}}^{\mu\nu} = \partial^\mu \tilde{\rho}^\nu - \partial^\nu \tilde{\rho}^\mu$. The new, renormalized vector meson fields are defined as $\rho = Z_\rho^{-1/2} \tilde{\rho}$, $\omega = Z_\omega^{-1/2} \tilde{\omega}$, $\phi = Z_\phi^{-1/2} \tilde{\phi}$. Explicitly the renormalization constants are given as

$$Z_\rho^{-1} = \left(1 - \mu \frac{\sigma_0^2}{2} \right); \quad Z_{\omega,\phi}^{-1} = \left[\left(1 - \frac{\mu(\sigma_0^2 + 2\xi_0^2) - 2\lambda_V}{4} \right) \pm \frac{1}{2} D^{1/2} \right] \tag{3.25}$$

where

$$D = \frac{\mu^2}{4} (\sigma_0^2 - 2\xi_0^2)^2 + \lambda_V^2 - \frac{\lambda_V}{3} \mu (\sigma_0^2 - 2\xi_0^2). \tag{3.26}$$

Then the Lagrangian for the renormalized vector fields in the vacuum reads

$$\mathcal{L}_V^{vac} = -\frac{1}{4} \left(\left(V_\rho^{\mu\nu} \right)^2 + (V_\omega^{\mu\nu})^2 + \left(V_\phi^{\mu\nu} \right)^2 \right) + \frac{1}{2} \frac{\chi^2}{\chi_0^2} \left(m_\rho^2 \rho^2 + m_\omega^2 \omega^2 + m_\phi^2 \phi^2 \right) \tag{3.27}$$

where

$$m_\rho^2 = Z_\rho m_V^2 \quad , \quad m_\omega^2 = Z_\omega m_V^2 \quad , \quad m_\phi^2 = Z_\phi m_V^2 \tag{3.28}$$

denote the vector meson masses in the vacuum. Using $m_V = 687.33\mathrm{MeV}$, $\mu\sigma_0^2 = 0.41$ and $\lambda_V = -0.041$, the correct ω-, ρ- and ϕ-masses are obtained. The vector meson self-interactions [Sug94] read

$$\mathcal{L}_{vec}^{(4)} = 2(\tilde{g}_4)^4 \, \mathrm{Tr}(\tilde{V}_\mu \tilde{V}^\mu)^2. \tag{3.29}$$

The coupling of this self-interaction term is also modified by the redefinition of the fields. The redefined couplings of the quartic interaction of the vector fields can be expressed in terms of the coupling $\tilde{g}_4$ of the term (3.29). Furthermore, the quartic vector meson interaction gives a contribution to the vector meson masses in the medium, i.e., for finite values of the vector fields. The resulting expressions for the vector meson masses in the medium (isospin symmetric) read

$$m_\omega^{*2} = Z_\omega m_V^2 + 12 g_4^4 \omega^2 \tag{3.30}$$

$$m_\rho^{*2} = Z_\rho m_V^2 + 12 g_4^4 \frac{Z_\rho}{Z_\omega} \omega^2 \tag{3.31}$$

$$m_\phi^{*2} = Z_\phi m_V^2 + 24 g_4^4 \frac{Z_\phi^2}{Z_\omega^2} \phi^2, \tag{3.32}$$

with $g_4 = \sqrt{Z_\omega}\tilde{g}_4$ denoting the renormalized coupling for the quartic vector meson interaction. Since this quartic self-interaction contributes only in the medium, the coupling g_4 cannot unambigiously be fixed. It is fitted, so that in the mean-field approximation (section 3.2) the compressibility is in the desired region between 200-300 MeV.

Spin-0 Potential

In the nonlinear realization of chiral symmetry the couplings of the scalar mesons X with each other are only governed by $\mathrm{SU}(3)_V$-symmetry. However, only three kinds of independent invariants exist, namely

$$I_1 = \mathrm{Tr}(X), \quad I_2 = \mathrm{Tr}(X)^2, \quad I_3 = \det(X). \tag{3.33}$$

All other invariants, $\mathrm{Tr}(X)^n$, with $n \geq 3$, can be expressed as a function of the invariants (see [Sch71], appendix C). The invariants of (3.33) are considered as building blocks, from which different forms of the meson-meson interaction are constructed. In this work we will use the same form of the potential as in the linear σ model with $U(1)_A$ breaking (see [Pap99]). It reads

$$\mathcal{L}_0 = -\frac{1}{2} k_0 \chi^2 I_2 + k_1 (I_2)^2 + k_2 I_4 + 2 k_3 \chi I_3, \tag{3.34}$$

χ denotes a scalar color-singlet gluon field. It is introduced to construct the model to satisfy the QCD trace anomaly (appendix D), i.e., the nonvanishing of the trace of the energy-momentum tensor $\theta_\mu^\mu = \frac{\beta_{QCD}}{2g} \mathcal{G}_{\mu\nu}^a \mathcal{G}^{\mu\nu a}$ (2.1.3). Here, $\mathcal{G}_{\mu\nu}^a$ is the gluon field strength tensor of QCD.
All the terms in the Lagrangian are multiplied by appropriate powers of the glueball field to obtain a dimension [Mass]^4 in the fields. Then all coupling

constants are dimensionless and therefore the model is scale invariant [Sch80]. Then, a scale breaking potential

$$\mathcal{L}_{\text{scalebreak}} = -\frac{1}{4}\chi^4 \ln\frac{\chi^4}{\chi_0^4} + \frac{\delta}{3}\chi^4 \ln\frac{I_3}{\det\langle X\rangle_0} \tag{3.35}$$

is introduced. This yields $\theta_\mu^\mu = (1-\delta)\chi^4$. By identifying the χ-field with the gluon condensate and the choice $\delta = 6/33$ for three flavors and three colors with β_{QCD} as given by the one loop level, the correct trace anomaly is obtained. The first term in (3.35) corresponds to the contribution of the gluons and the second term describes the contribution from the quarks to the trace anomaly. Finally, the term

$$\mathcal{L}_\chi = -k_4\chi^4 \tag{3.36}$$

generates a phenomenologically consistent finite vacuum expectation value.

The parameters k_0,k_2 and k_4, are used to ensure an extremum in the vacuum for the σ-, ζ- and χ-field equations, respectively. As for the remaining constants, k_3 is constrained by the η and η' masses and k_1 is fixed such that in the mean-field fit with quartic vector meson interaction the effective nucleon mass at saturation density is around $0.65\, m_N$ and the σ-mass is of the order of 500 MeV. Note that in this work we will set $\chi = \chi_0$. We will refer to this case as the "frozen glueball limit". The VEV of the gluon condensate, χ_0, is fixed to fit the pressure $p = 0$ at the saturation density $\rho_0 = 0.15\,\text{fm}^{-3}$.

3.1.4 Explicitly broken chiral symmetry

In order to eliminate the Goldstone modes from a chiral effective theory, explicit symmetry breaking terms have to be introduced. Here, we again take the corresponding term of the linear σ-model

$$\mathcal{L}_{SB} = \frac{1}{2}\text{Tr}A_p(M + M^\dagger) = \text{Tr}A_p\left(u(X+iY)u + u^\dagger(X-iY)u^\dagger\right), \tag{3.37}$$

with $A_p = 1/\sqrt{2}\text{diag}(m_\pi^2 f_\pi, m_\pi^2 f_\pi, 2m_K^2 f_K - m_\pi^2 f_\pi)$ and $m_\pi = 139$ MeV, $m_K = 498$ MeV. This choice for A_p together with the constraints (3.9) on the VEV on the scalar condensates assure that the PCAC-relations of the pion and kaon are fulfilled. With $f_\pi = 93.3$ MeV and $f_K = 122$ MeV we obtain $\sigma_0 = 93.3$ MeV and $\zeta_0 = 106.56$ MeV.

3.2 Mean-field approximation

3.2.1 Lagrangian

From the Lagrangian (3.1) nonlinear quantum field equations with large couplings result. Therefore, perturbative approaches are not applicable. To overcome this problem approximations must be found, which make the problem solvable. First, the mean-field approximation [Ser97], which will be used nearly in all the following investigations is introduced. In section 8.2 the relativistic Hartree approximation will be presented, which in addition takes into account the contribution of the negative-energy Dirac sea.

In the mean-field approximation the mesons are treated as classical fields. I.e., the meson field operators are replaced by their expectation values, which are classical fields. These quantities are independent of x_μ for a static uniform system. If furthermore rotational invariance holds, the expectation value of the three-vector part of the vector meson field vanishes, i.e., $\langle \vec{V} \rangle = 0$. Then the Lagrangian (3.1) becomes

$$\begin{aligned}
\mathcal{L}_{BX} + \mathcal{L}_{BV} &= -\sum_i \overline{\psi_i}[g_{i\omega}\gamma_0\omega^0 + g_{i\phi}\gamma_0\phi^0 + g_{i\rho}\gamma_0\tau_3\rho^0 + m_i^*]\psi_i \\
\mathcal{L}_{vec} &= \frac{1}{2}m_\omega^2\frac{\chi^2}{\chi_0^2}\omega^2 + \frac{1}{2}m_\phi^2\frac{\chi^2}{\chi_0^2}\phi^2 + g_4^4\left(\omega^4 + 12\frac{Z_\rho}{Z_\omega}\rho^2\omega^2 + \frac{Z_\rho^2}{Z_\omega^2}\rho^4 + 2\frac{Z_\phi^2}{Z_\omega^2}\phi^4\right) \\
\mathcal{V}_0 &= \frac{1}{2}k_0\chi^2(\sigma^2+\zeta^2) - k_1(\sigma^2+\zeta^2)^2 - k_2(\frac{\sigma^4}{2}+\zeta^4) - k_3\chi\sigma^2\zeta \\
&\quad + k_4\chi^4 + \frac{1}{4}\chi^4\ln\frac{\chi^4}{\chi_0^4} - \frac{\delta}{3}\chi^4\ln\frac{\sigma^2\zeta}{\sigma_0^2\zeta_0} \\
\mathcal{V}_{SB} &= \left(\frac{\chi}{\chi_0}\right)^2\left[m_\pi^2 f_\pi\sigma + (\sqrt{2}m_K^2 f_K - \frac{1}{\sqrt{2}}m_\pi^2 f_\pi)\zeta\right] \qquad , \qquad (3.38)
\end{aligned}$$

where m_i^* is the effective mass of the hadron species i. σ and ζ correspond to the scalar condensates, ω, ρ, ϕ represent the nonstrange-isoscalar, nonstrange-isovector and the strange-isoscalar vector fields, respectively, and χ is the scalar-isoscalar dilaton field. In the mean-field approximation only the scalar ($\mathcal{L}_{BX}$) and the vector meson terms ($\mathcal{L}_{BV}$) contribute to the baryon-meson interaction, since for all other mesons the expectation value vanishes.

3.2.2 Hamiltonian

From the Lagrangian (3.38) the conserved baryon four-current and the energy momentum tensor can directly be derived [Bjo64, Itz80]

$$\rho_B \equiv \mathcal{B}_0 = \sum_i \bar{\psi}_i \gamma_0 \psi_i \quad , \tag{3.39}$$

$$\begin{aligned} \mathcal{T}^{MFT}_{\mu\nu} &= -\mathrm{g}_{\mu\nu}\mathcal{L}_{MFT} + \sum_i \frac{\partial\psi_i}{\partial x^\nu}\frac{\partial\mathcal{L}_{MFT}}{\partial(\partial\psi_i/\partial x_\mu)} \\ &= \mathrm{i}\sum_i \bar{\psi}_i\gamma_\mu\partial_\nu\psi_i - \mathrm{g}_{\mu\nu}\left(\mathcal{L}_{\mathrm{vec}} + \mathcal{L}_0 + \mathcal{L}_{\mathrm{SB}}\right) \quad . \end{aligned} \tag{3.40}$$

Since the mesons are treated as classical fields, only the fermions need to be quantized. The Dirac field equations follow from $\mathcal{L}_{MFT}$ using the Euler-Lagrange equations. This yields

$$\left[\mathrm{i}\gamma_\mu\partial^\mu - g_{i\omega}\gamma_0\omega^0 - g_{i\phi}\gamma_0\phi^0 - g_{i\rho}\gamma_0\tau_3\rho^0 - m_i^*\right]\psi_i(\vec{x},t) = 0 \quad . \tag{3.41}$$

These equations are linear and therefore can be solved exactly. The chosen stationary solutions for a uniform system are

$$\psi_i = \psi_i(\vec{k},\lambda)\exp(\mathrm{i}\vec{k}\cdot\vec{x} - \mathrm{i}\epsilon(\vec{k})t), \tag{3.42}$$

where $\psi_i(\vec{k},\lambda) = (U(\vec{k},\lambda), V(\vec{k},\lambda))$ is a four-component Dirac spinor, and λ denotes the spin index. Then the spinors $U(\vec{k},\lambda)$ and $V(\vec{k},\lambda)$ obey the equations

$$\begin{aligned} \left[\epsilon^+(\vec{k}) - g_{i\omega}\omega^0 - g_{i\phi}\phi^0 - g_{i\rho}\tau_3\rho^0\right]U(\vec{k},\lambda) &= \left[\vec{\alpha}\cdot\vec{k} + \beta m_i^*\right]U(\vec{k},\lambda) \\ \left[\epsilon^-(-\vec{k}) - g_{i\omega}\omega^0 - g_{i\phi}\phi^0 - g_{i\rho}\tau_3\rho^0\right]V(\vec{k},\lambda) &= \left[\vec{\alpha}\cdot(-\vec{k}) + \beta m_i^*\right]V(\vec{k},\lambda) \end{aligned} \tag{3.43}$$

where $\vec{\alpha}$ and β denote the Dirac matrices [Bjo64]. Using these conventions, the resulting single-particle spectrum reads

$$\epsilon(k) \equiv \epsilon^{\pm}(k) = g_{i\omega}\omega^0 + g_{i\phi}\phi^0 + g_{i\rho}\tau_3\rho^0 \pm \sqrt{\vec{k}^2 + (m_i^*)^2} \tag{3.44}$$

$$\equiv g_{i\omega}\omega^0 + g_{i\phi}\phi^0 + g_{i\rho}\tau_3\rho^0 \pm E_i^*(\vec{k}) \quad . \tag{3.45}$$

The baryon field operator is then given by

$$\begin{aligned} \psi_i(\vec{x},t) = \frac{1}{\sqrt{V}}\sum_{\vec{k}\lambda}\Big[&A_{\vec{k}\lambda}U(\vec{k},\lambda)\exp(\mathrm{i}\vec{k}\cdot\vec{x} - \mathrm{i}\epsilon^+(\vec{k})t) \\ &+ B^\dagger_{\vec{k}\lambda}V(\vec{k},\lambda)\exp(-\mathrm{i}\vec{k}\cdot\vec{x} - \mathrm{i}\epsilon^-(\vec{k})t)\Big], \end{aligned} \tag{3.46}$$

where V is the volume of the system and the spinors have the normalization

$$U^\dagger(\vec{k},\lambda)U(\vec{k},\lambda') = V^\dagger(\vec{k},\lambda)V(\vec{k},\lambda') = \delta_{\lambda,\lambda'}. \tag{3.47}$$

Substituting the baryon field operator (3.46) into the baryon number operator (3.39) gives (neglecting the index i for the particle species)

$$\mathcal{B}_0 = \int_V d^3x\, \hat{\psi}^\dagger \hat{\psi} = \sum_{\vec{k}\lambda} \left(A^\dagger_{\vec{k}\lambda} A_{\vec{k}\lambda} + B_{\vec{k}\lambda} B^\dagger_{\vec{k}\lambda} \right). \tag{3.48}$$

Normal ordering of this expression yields

$$\mathcal{B}_0 = \sum_{\vec{k}\lambda} \left(A^\dagger_{\vec{k}\lambda} A_{\vec{k}\lambda} - B^\dagger_{\vec{k}\lambda} B_{\vec{k}\lambda} \right) + \sum_{\vec{k}\lambda} 1. \tag{3.49}$$

The last term represents the sum over all the occupied states in the negative-energy Dirac sea. Since the argument in the sum is just the "1", it is constant and independent of the dynamics. Therefore the expression for the observed or physical baryon density is obtained by subtracting this constant, i.e., the vacuum expectation value of $\mathcal{B}_0$. Thus, the physical baryon number is given as

$$\mathcal{B}_0 \equiv \int_V d^3x \left[\hat{\psi}^\dagger \hat{\psi} - \langle 0|\hat{\psi}^\dagger \hat{\psi}|0\rangle \right] = \sum_{\vec{k}\lambda} \left(A^\dagger_{\vec{k}\lambda} A_{\vec{k}\lambda} - B^\dagger_{\vec{k}\lambda} B_{\vec{k}\lambda} \right). \tag{3.50}$$

This definition assures that the baryon number operator has the intuitive interpretation of counting the number of baryons minus the number of antibaryons. Substituting the baryon field operator (3.46) in the energy-momentum tensor (3.39) yields

$$\begin{aligned} \mathcal{H} &= \int_V d^3x\, \mathcal{T}_{00} \\ &= \sum_{\vec{k}\lambda} \sqrt{\vec{k}^2 + m_i^{*2}} \left(A^\dagger_{\vec{k}\lambda} A_{\vec{k}\lambda} - B_{\vec{k}\lambda} B^\dagger_{\vec{k}\lambda} \right) - \mathcal{L}_{\rm vec} - \mathcal{L}_0 - \mathcal{L}_{\rm SB}. \end{aligned} \tag{3.51}$$

Normal ordering of this expression gives

$$\mathcal{H} = \sum_{\vec{k}\lambda} \sqrt{\vec{k}^2 + m_i^{*2}} \left(A^\dagger_{\vec{k}\lambda} A_{\vec{k}\lambda} + B^\dagger_{\vec{k}\lambda} B_{\vec{k}\lambda} \right) - \sum_{\vec{k}\lambda} \sqrt{\vec{k}^2 + m_i^{*2}} - \mathcal{L}_{\rm vec} - \mathcal{L}_0 - \mathcal{L}_{\rm SB}. \tag{3.52}$$

Here the sum over the occupied negative energy states is weighted by the effective energy and therefore depends on the effective baryon mass. Thus, the contribution of the Dirac sea to the energy is a dynamical quantity, i.e., it is density dependent. Therefore, this term is not cancelled by the vacuum expectation value of the Hamilton operator. In the mean-field approach this problem is "solved" by just neglecting the complete contribution of the negative energy states to the energy. I.e., the total Hamiltonian is a sum of the mean-field Hamiltonian $\mathcal{H}_{MFT}$, the contribution from the Dirac sea $\delta\mathcal{H}$ and the vacuum expectation value of $\mathcal{H}$.

$$\mathcal{H} = \mathcal{H}_{MFT} + \delta\mathcal{H} - \langle 0|\mathcal{H}|0\rangle \tag{3.53}$$

with

$$\mathcal{H}_{MFT} = \sum_{\vec{k}\lambda} \sqrt{\vec{k}^2 + m_i^{*2}} \left(A^\dagger_{\vec{k}\lambda} A_{\vec{k}\lambda} + B^\dagger_{\vec{k}\lambda} B_{\vec{k}\lambda} \right) - \mathcal{L}_{\text{vec}} - \mathcal{L}_0 - \mathcal{L}_{\text{SB}} \tag{3.54}$$

$$\delta\mathcal{H} = -\sum_{\vec{k}\lambda} \left[\sqrt{\vec{k}^2 + m_i^{*2}} - \sqrt{\vec{k}^2 + m_i^2} \right] \tag{3.55}$$

$$\langle 0|\mathcal{H}|0\rangle = \sum_{\vec{k}\lambda} \sqrt{\vec{k}^2 + m_i^{*2}} \tag{3.56}$$

The effects of the negative-energy states can be taken into account in the relativistic Hartree approximation (see section 8.2). The remaining Hamiltonian $\mathcal{H}_{MFT}$ defines the mean-field theory of the chiral $SU(3)_L \times SU(3)_R$ model. Since it is diagonal, the problem can be solved exactly. The physical interpretation of the approximation is that of baryons and antibaryons propagating in constant, condensed scalar and vector fields. This approximation should become increasingly valid with higher density, since the source terms for the scalar and vector mesons increase with density and thus the neglected fluctuations of the fields should then be of less importance.

3.2.3 Grand canonical potential

The grand canonical ensemble describes a system which may exchange energy as well as particles with a thermodynamic reservoir [Gre93] und hence is a natural choice for the description of a relativistic quantum system. The temperature T, the Volume V and the chemical potentials μ then define the macroscopic state of the system. Starting from the first law of thermodynamics

$$dE = TdS - pdV + \mu dN, \tag{3.57}$$

the grand canonical potential Ω is obtained by a Legendre transformation as [Gre93]

$$\Omega\,(T, V, \mu) = -pV = E - TS - \mu N. \tag{3.58}$$

with the total differential

$$d\Omega = -SdT - pdV - Nd\mu \tag{3.59}$$

Here, S denotes the entropy and N the particle number. The grand canonical partition function of the strongly interacting hadronic system reads [Zsc97]

$$Z = Sp\,\hat{\rho} = \sum_i \sum_{N_i, \bar{N}_i = 0}^{1} \langle N| \exp[-\beta(\mathcal{H} - \mu_i \mathcal{N}_i)]|N\rangle, \tag{3.60}$$

where $|N\rangle = |n_N, n_\Lambda, ...\rangle$ runs over all possible states. The thermodynamic potential of the grand canonical ensemble, Ω per volume V, at a given chemical potential μ and temperature T is then given by

$$\Omega\,(T, V, \mu) = -T \ln Z. \tag{3.61}$$

Inserting the mean-field Hamiltonian of the chiral $SU(3)_L \times SU(3)_R$ model (3.54) and also taking into account thermal meson production (appendix E), we obtain

$$\frac{\Omega}{V} = -\mathcal{L}_{vec} - \mathcal{L}_0 - \mathcal{L}_{SB} - \mathcal{V}_{vac} \mp T \sum_i \frac{\gamma_i}{(2\pi)^3} \int d^3k \left[\ln\left(1 \pm e^{-\frac{1}{T}[E_i^*(k) - \mu_i^*]}\right)\right], \tag{3.62}$$

where the sum runs over all single-particle states denoted by $\vec{k}$, all intrinsic quantum numbers λ and all considered baryon and meson species i. The vacuum energy $\mathcal{V}_{vac}$ (the potential at $\rho = 0$) has been subtracted in order to get a vanishing vacuum energy. The single particle energies are $E_i^*(\vec{k}) = \sqrt{\vec{k}_i^2 + m_i^{*2}}$, and the effective chemical potentials read $\mu_i^* = \mu_i - g_{i\omega}\omega - g_{i\phi}\omega - g_{i\rho}\tau_3\rho^0$, with $\mu_i = (n_q^i - n_{\bar{q}}^i)\mu_q + (n_s^i - n_{\bar{s}}^i)\mu_s$[4].

Equations of motion

From the grand canonical potential the equations determining the meson fields can be derived. For a system in equilibrium, these should be chosen such that the grand canonical potential Ω is stationary [Fur90]. Since we use the frozen glueball approximation (i.e $\chi = \chi_0$), we have coupled equations for the fields σ, ζ, ω, ϕ and ρ in the selfconsistent calculation:

$$\begin{aligned} \frac{\partial(\Omega/V)}{\partial\sigma} &= k_0\chi^2\sigma - 4k_1(\sigma^2 + \zeta^2)\sigma - 2k_2\sigma^3 - 2k_3\chi\sigma\zeta - 2\frac{\delta\chi^4}{3\sigma} + \\ &+ \left(\frac{\chi}{\chi_0}\right)^2 m_\pi^2 f_\pi + \sum_i \frac{\partial m_i^*}{\partial\sigma}\rho_i^s = 0 \end{aligned} \tag{3.63}$$

$$\begin{aligned} \frac{\partial(\Omega/V)}{\partial\zeta} &= k_0\chi^2\zeta - 4k_1(\sigma^2 + \zeta^2)\zeta - 4k_2\zeta^3 - k_3\chi\sigma^2 - \frac{\delta\chi^4}{3\zeta} + \\ &+ \left(\frac{\chi}{\chi_0}\right)^2 \left[\sqrt{2}m_K^2 f_K - \frac{1}{\sqrt{2}}m_\pi^2 f_\pi\right] + \sum_i \frac{\partial m_i^*}{\partial\zeta}\rho_i^s = 0 \end{aligned} \tag{3.64}$$

[4]For the case of strongly interacting matter two conserved charges exist, namely the baryon number and the strangeness number. Thus, two chemical potentials have to be introduced. Here we use the parametrization in terms of the light and strange quark chemical potentials denoted as μ_q and μ_s, respectively. As shown in [Zsc97], this is equivalent to the choice μ_B and μ_S for the baryon and strangeness chemical potential.

$$\frac{\partial(\Omega/V)}{\partial\omega} = -\left(\frac{\chi}{\chi_0}\right) m_\omega^2 \omega - 4g_4^4 \left(\omega^3 + 6\frac{Z_\rho}{Z_\omega}\rho^2\omega\right) + \sum_i g_{i\omega}\rho_i = 0 \tag{3.65}$$

$$\frac{\partial(\Omega/V)}{\partial\phi} = -\left(\frac{\chi}{\chi_0}\right) m_\phi^2 \phi - 8g_4^4 \frac{Z_\phi^2}{Z_\omega^2}\phi^3 + \sum_i g_{i\phi}\rho_i = 0 \tag{3.66}$$

$$\frac{\partial(\Omega/V)}{\partial\rho} = -\left(\frac{\chi}{\chi_0}\right) m_\rho^2 \rho - 4g_4^4 \left(\frac{Z_\rho^2}{Z_\omega^2}\rho^3 + 6\frac{Z_\rho}{Z_\omega}\rho\omega^2\right) + \sum_i g_{i\omega}\tau_3\rho_i = 0 \tag{3.67}$$

The scalar and vector densities are given as

$$\rho_i = \frac{\gamma_i}{(2\pi)^3}\int d^3k\,(n_{k,i} - \bar{n}_{k,i}) \tag{3.68}$$

$$\rho_i^s = \frac{\gamma_i}{(2\pi)^3}\int d^3k \frac{m_i^*}{E_i^*}\,(n_{k,i} - \bar{n}_{k,i})\,, \tag{3.69}$$

where the particle and antiparticle distribution functions read

$$n_{k,i} \equiv n_{k,i}(T,\mu_i^*) = \frac{1}{e^{\frac{1}{T}[E_i^* - \mu_i^*]} \pm 1} \tag{3.70}$$

$$\bar{n}_{k,i} \equiv \bar{n}_{k,i}(T,\mu_i^*) = \frac{1}{e^{\frac{1}{T}[E_i^* + \mu_i^*]} \pm 1}. \tag{3.71}$$

Once the meson fields are determined, the thermodynamical quantities which are given as partial differentials of the grand canonical potential (3.59) are also determined:

$$p = -\left[\frac{\partial}{\partial V}\Omega(T,\mu_i)\right]_{T,\mu_i} \tag{3.72}$$

$$S = -\left[\frac{\partial}{\partial T}\Omega(V,\mu_i)\right]_{V,\mu_i}. \tag{3.73}$$

The energy of the system may now be calculated using the energy-momentum tensor (3.39) or the Euler equation $E = TS - pV + \sum_i \mu_i N_i$. Both results must be identical to assure thermodynamical consistency.

T=0

For the case $T = 0$ the particle and antiparticle distribution functions read

$$n_{k,i} = \begin{cases} 1 & \text{for } k \le k_{F,i} \\ 0 & \text{for } k > k_{F,i} \end{cases} \tag{3.74}$$

$$\bar{n}_{k,i} = 0, \tag{3.75}$$

All states up to the Fermi level are filled and no antiparticles appear. Then the grand canonical potential reads

$$\frac{\Omega}{V} = -\mathcal{L}_{vec} - \mathcal{L}_0 - \mathcal{L}_{SB} - \mathcal{V}_{vac} - \sum_i \frac{\gamma_i}{(2\pi)^3} \int_0^{k_{F,i}} d^3k [E_i^*(k) - \mu_i^*]. \tag{3.76}$$

The scalar densities ρ_i^s and the vector densities ρ_i can now be calculated analytically, yielding

$$\rho_i^s = \gamma_i \int \frac{d^3k}{(2\pi)^3} \frac{m_i^*}{E_i^*} = \frac{\gamma_i m_i^*}{4\pi^2} \left[k_{Fi} E_{Fi}^* - m_i^{*2} \ln \left(\frac{k_{Fi} + E_{Fi}^*}{m_i^*} \right) \right] \tag{3.77}$$

$$\rho_i = \gamma_i \int_0^{k_{Fi}} \frac{d^3k}{(2\pi)^3} = \frac{\gamma_i k_{Fi}^3}{6\pi^2} \,. \tag{3.78}$$

3.2.4 Fitting of parameters

As already discussed in this chapter, the parameters of the model are constrained by symmetry relations, characteristics of the vacuum, and nuclear matter properties. Table 3.3 summarizes the fixing of the parameters in the mean-field approach. In table 3.4 the parameters and observables for the two different ways of baryon mass generation, C1 and C2, are summarized. The resulting hadron masses in the vacuum for the different parameter sets are shown in table 3.5. The values of the condensates and nuclear matter properties at nuclear matter saturation density ρ_0 are summarized in table 3.6. The binding energy per particle and the pressure as a function of baryon density are shown in figure 3.1. With the choice of the parameter sets discussed above, the chiral model is found to produce unrealistically large hyperon potential depths in nuclear matter in comparison to the experimental value of $U_\Lambda^N \approx -28$ MeV for the Λ particle (see [Pap99, Pap98a] for details). Parameter sets that reproduce reasonable values of U_Λ^N are, however, found to yield unsatisfactory nuclear properties [Pap99]. Fortunately, explicit symmetry breaking can be introduced in the nonlinear realization without affecting, e.g., the partially conserved axial-vector currents relations (see appendix B). This allows for the inclusion of additional terms for the hyperon-scalar meson coupling [Pap99]:

$$\mathcal{L}_{\rm hyp} = m_3 \mathrm{Tr} \left(\overline{\psi}\psi + \overline{\psi} [\psi, S] \right) \mathrm{Tr} \left(X - X_0 \right) \,, \tag{3.79}$$

where X represents a scalar and $S_b^a = -[\sqrt{3}(\lambda_8)_b^a - \delta_b^a]/3$ with λ's are the usual Gell-Mann matrices. In the mean-field approximation this leads to the following additional mass term

$$\widetilde{m}_i^* = m_i^* + a\, m_3 \left[\sqrt{2}(\delta - \delta_0) + (\zeta - \zeta_0) \right], \tag{3.80}$$

Parameter	Interaction	Lagrange-term	Observable/Constraint
g_1^S		$g_1^S \frac{1}{\sqrt{3}}\mathrm{Tr}(\overline{B}B)\mathrm{Tr}X$	
g_8^S	$\mathcal{L}_{BM}$	$\sqrt{2}g_8^S\left(\alpha_S[\overline{B}BX]_F\right.$	$m_N, m_\Lambda, m_\Sigma, m_\Xi$
α_s		$\left.+(1-\alpha_S)[\overline{B}BX]_D\right)$	
g_1^V		$g_1^V \frac{1}{\sqrt{3}}\mathrm{Tr}(\overline{B}\gamma_\mu B)\mathrm{Tr}V^\mu$	$g_{N\phi}=0 \Rightarrow g_1^V=\sqrt{6}g_8^V$
g_8^V	$\mathcal{L}_{BV}$	$\sqrt{2}g_8^V\left(\alpha_V[\overline{B}\gamma_\mu BV^\mu]_F\right.$	$E/A(\rho_0)=-16$ MeV
α_V		$\left.+(1-\alpha_V)[\overline{B}\gamma_\mu BV^\mu]_D\right)$	F-D mixing (VMD)
m_V	$\mathcal{L}_{vec}^{(1)}$	$\frac{1}{2}m_V^2\frac{\chi^2}{\chi_0^2}\mathrm{Tr}V_\mu V^\mu$	
μ	$\mathcal{L}_{vec}^{(2)}$	$\frac{1}{4}\mu\mathrm{Tr}\left[V_{\mu\nu}V^{\mu\nu}X^2\right]$	m_ω, m_ρ, m_ϕ
λ_V	$\mathcal{L}_{vec}^{(3)}$	$\frac{1}{4}\lambda_V\left(\mathrm{Tr}\left[V_{\mu\nu}\right]\right)^2$	
g_4	$\mathcal{L}_{vec}^{(4)}$	$2g_4^4\mathrm{Tr}V_\mu V^\mu$	$K\approx 200-300$ MeV
k_0		$-\frac{1}{2}k_0\chi^2 I_2$	$\frac{\partial\Omega}{\partial\sigma}\vert_{vac}=0$
k_1		$k_1(I_2)^2$	$m_\sigma\approx 500$ MeV
k_2	scalar	$k_2 I_4$	$\frac{\partial\Omega}{\partial\zeta}\vert_{vac}=0$
k_3	potential	$2k_3\chi I_3$	η,η' splitting
k_4		$-k_4\chi^4$	$\frac{\partial\Omega}{\partial\chi}\vert_{vac}=0$
δ		$\frac{\delta}{3}\chi^4\ln\frac{\mathrm{I_3}}{\mathrm{detX}}$	β_{QCD}
χ_0			$p(\rho_0)$=0

Table 3.3: Parameters of the model, the corresponding terms in the Lagrangian and constraints for fixing them.

	g_1^S	g_8^S	α_S	m_1	m_2	$g_{N\omega}$	$g_4/g_{N\omega}$
C1	-8.39	-2.36	1.45	0.00	0.00	13.61	0.21
C2	-8.22	-3.35	1.00	64.44	-57.06	12.82	0.21
	k_0	k_1	k_2	k_3	k_4	33δ	χ_0
C1	2.37	1.40	-5.55	-2.65	-0.23	2	401.93
C2	2.36	1.40	-5.55	-2.64	-0.23	2	402.66

Table 3.4: Parameters of the two different ways of mass generation, C1 and C2.

The resulting hyperon potentials for the choices $a=1$ and $a=2$ are shown in table 3.7.

	Spin-0 particle masses			
	$m_\pi(139)$	$m_K(495)$	$m_\eta(547)$	$m_{\eta'}(958)$
C1	139.0	498.0	574.5	969.2
C2	139.0	498.0	574.5	969.2
	$m_{a_0}(980)$	m_κ (900)	m_σ	$m_{f_0}(980)$
C1	953.5	995.7	473.32	1039.1
C2	953.5	995.7	475.55	1039.1
	Spin-1 particle masses			
	$m_\omega(783)$	$m_{K^*}(892)$	$m_\rho(770)$	$m_\phi(1020)$
C1	783.0	863.7	770.0	1019.0
C2	783.0	863.7	770.0	1019.0
	Spin-$\frac{1}{2}$ particle masses			
	$m_N(939)$	$m_\Lambda(1115)$	$m_\Sigma(1193)$	$m_\Xi(1315)$
C1	939.0	1115.0	1196.0	1331.5
C2	939.0	1115.3	1196.0	1331.5
	Spin-$\frac{3}{2}$ particle masses			
	$m_\Delta(1232)$	$m_{\Sigma^*}(1385)$	$m_{\Xi^*}(1530)$	$m_\Omega(1672)$
C1	1232.0	1385.0	1538.0	1691.0
C2	1232.0	1380.2	1528.4	1676.6

Table 3.5: Hadron masses (in MeV) for the fits C1 and C2.

	m_N^*/m_N	σ/σ_0	ζ/ζ_0	K [MeV]	a_4 [MeV]
C1	.61	.63	.92	276.34	30.3
C2	.64	.64	.91	266.08	29.0

Table 3.6: Condensates and properties of nuclear matter at ρ_0.

	U_N	U_Λ	U_Σ	U_Ξ
C1 $a=1$	-71.0	-28.2	3.2	-42.1
C1 $a=2$	-71.0	-28.2	3.2	30.3
C2 $a=1$	-68.8	-32.6	-32.6	-52.9
C2 $a=2$	-68.8	-32.6	-32.6	3.5

Table 3.7: Baryonic potential depths in nuclear matter.

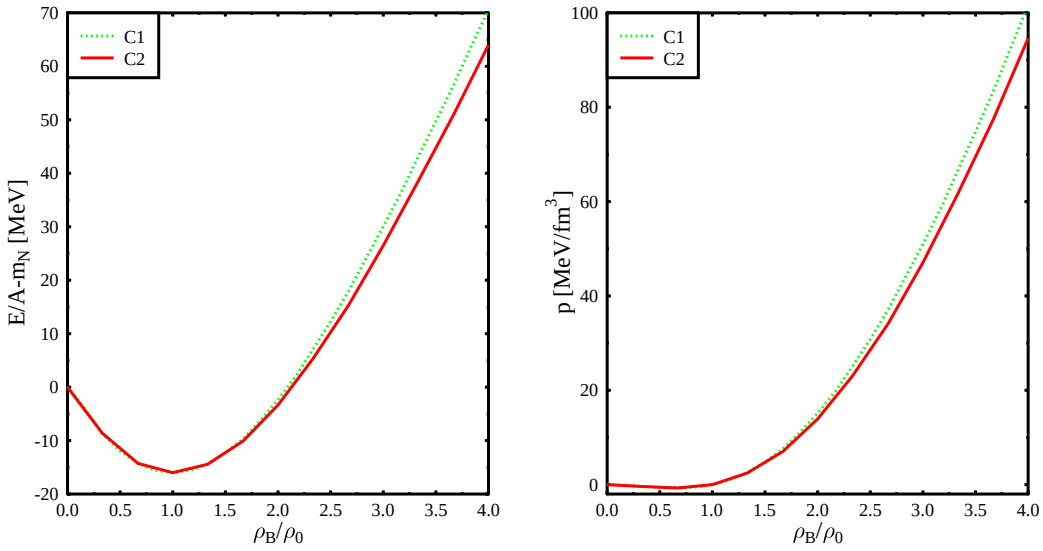

Figure 3.1: Binding energy per particle (left) and pressure (right) as a function of density for symmetric nuclear matter for parameter sets C1 and C2.

–IV–

Excited hadronic matter

4.1 Cold and dense hadronic matter

Fixing of the parameters to vacuum and nuclear matter ground state properties was discussed in detail in section 3.2. It has been shown that the obtained parameter sets describe the nuclear matter saturation point, hadronic vacuum masses, and properties of finite nuclei [Pap98a, Pap99, Sch02] reasonably well.

Once the parameters have been fixed to nuclear matter at ρ_0, the condensates and hadron masses at high baryon densities can be investigated, assuming that the change of the parameters of the effective theory with density are small. The behaviour of the fields and the masses of the baryon octet have been investigated in [Pap99, Pap98a]. It is found that the gluon condensate χ stays nearly constant when the density increases. This implies that the approximation of a frozen glueball is reasonable. The resulting scalar and vector fields for this approximation are depicted in figure 4.1. The strange condensate ζ is only reduced by about 10 percent from its vacuum expectation value. This is not surprising, since there are only nucleons in the system and the nucleon–ζ coupling is fairly weak. The main effect occurs for the nonstrange condensate σ: This field drops to 30 percent of its vacuum expectation value at four times normal nuclear density, at even higher densities the σ field saturates. The behaviour of the condensates is also reflected in the behaviour of the baryon masses, c.f. figure 4.1. The change of the scalar fields causes a change of the baryon masses in the dense medium. Furthermore, the change of the baryon masses depends on the strange quark content of the baryon. This is due to the different coupling of the baryons to the nonstrange and strange condensate and the explicit symmetry breaking for the hyperons. The behaviour of the fields and the effective baryon masses is similar in the two parameter sets C1 and C2.

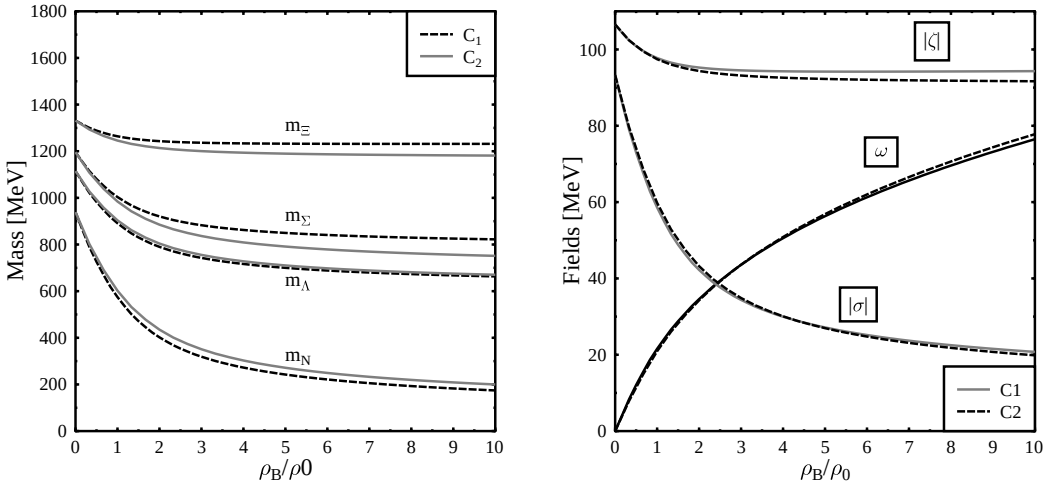

Figure 4.1: Baryon octet masses (left) and scalar condensates (right) as function of baryon density ρ_B for $T = 0$.

Now we discuss the effects of the inclusion of baryonic spin-$\frac{3}{2}$ resonances [Zsc01b]. How do they affect the behaviour of dense hadronic matter? We consider the two parameter sets C1 and C2 which satisfactorily describe finite nuclei [Pap99]. As stated above, the main difference between the two parameter sets is the coupling of the strange condensate to the nucleon and to the Δ. In C2 this coupling is set to zero, while the nucleon and the Δ couple to the ζ field in the case of C1. Fig. 4.2 shows how the strength of the coupling of the strange condensate to the nucleon and the Δ depends on the vacuum expectation value of the strange condensate ζ_0. The field ζ_0 in turn is a function of the kaon decay constant ($\zeta_0 = \frac{1}{\sqrt{2}}(f_\pi - f_K)$). The results are obtained by changing the value of f_K, starting from parameter set C1. f_K is expected to be in the range of 105 to 125 MeV [Jin95a]. For infinite nuclear matter one obtains good fits for the whole range of expected values. But when these parameter sets are used to describe finite nuclei, satisfactory results are only obtained for a small range of values for f_K, as can be seen for the proton single particle levels in Fig. 4.3: with decreasing f_K the gap between the single-particle levels $1h_{\frac{9}{2}}$ and $3s_{\frac{1}{2}}$ in ^{208}Pb decreases such that e.g. for $f_K = 112$ MeV the experimentally observed shell closure cannot be reproduced in the calculation. This result is not very surprising, because the smaller value of f_K leads to a stronger coupling of the nucleon to the strange field, with a mass of $m_\zeta \approx 1$ GeV. But it has been shown [Fur96a] that for a reasonable description of finite nuclei the nucleon must mainly couple to a scalar field with a mass of approximately 500-600 MeV. The equation of state of dense hadronic matter for vanishing strangeness is shown in Fig. 4.4. Here two C1 fits are

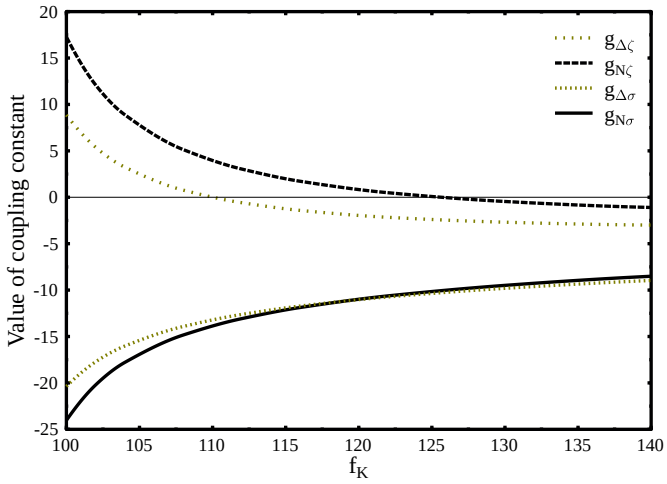

Figure 4.2: Coupling of the nucleon and the Δ to the nonstrange (σ) and strange (ζ) scalar condensates as a function of the kaon decay constant f_K. For $f_K \approx 115-125$ MeV the coupling of the nucleon and the Δ to the nonstrange scalar field σ are nearly equal. The coupling strength to the strange scalar field are different in sign. This results in the mass difference of $\Delta m \approx 300$MeV in the vacuum.

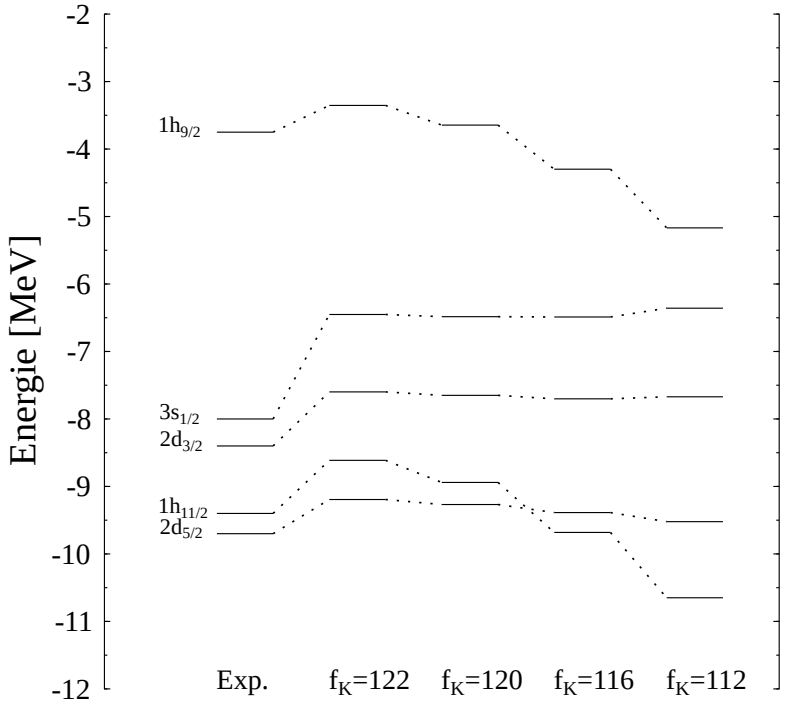

Figure 4.3: Single particle energie levels for protons in Pb^{208} for parameter sets with different values of the kaon decay constant f_k (in MeV). The smaller the decay constant is chosen, the more the gap between the levels $1h_{\frac{9}{2}}$ and $3s_{\frac{1}{2}}$ decreases. The parameter sets were obtained by just variing f_k in C1.

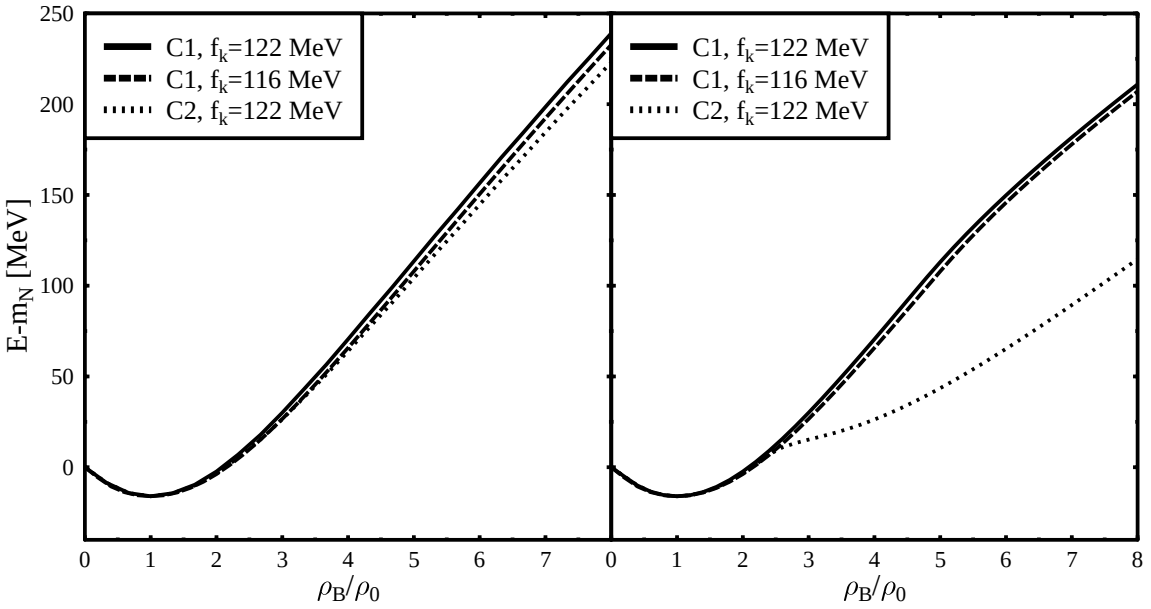

Figure 4.4: Equation of state for infinite nuclear matter for the parameter sets C1 ($m_N = m_N(\sigma, \zeta)$) and C2 ($m_N = m_N(\sigma)$). In the left picture resonances are neglected while they are included in the right picture. If the strange condensates couples to the nucleon the influence of the Δ resonances on the equation of state is much weaker.

compared, one with $f_k = 122$, which corresponds to the fit that has been tested to describe finite nuclei satisfactory in [Pap99], and a C1-type fit with $f_k = 116$, as the minimum acceptable value extracted from Fig. 4.3. The resulting values of coupling constants to the nucleon are $g_{N\zeta} \approx 0.49$ for $f_K = 122$ MeV and $g_{N\zeta} \approx 1.72$ for $f_K = 116$ MeV. For the Δ-baryon $g_{\Delta\zeta} \approx -2.2$ and $g_{\Delta\zeta} \approx -0.59$, respectively. If these values are compared to the couplings to the nonstrange condensate – which is around -10 for the nucleon and the Δ in both cases – one observes that the mass difference between nucleon and Δ is due to the different coupling to the strange condensate.

Furthermore, the resulting equation of state for parameter set C2 is plotted. Here the nucleon and Δ mass do not depend on the strange condensate. Fig. 4.4 shows two main results: First, the resulting EoS does not change significantly if f_K in the C1-fits is varied within the reasonable range discussed above. Thus, in the following we refer to the C1-fit of [Pap99] with $f_K = 122$ MeV.

Second, the different ways of nucleon and Δ mass generation lead to drastic differences in the resulting equations of state:

A pure σ dependence of the masses of the nonstrange baryons (C2) leads to an equation of state which is strongly influenced by the production of resonances at high densities. This is not the case when both masses are partially generated by the strange condensate (C1), Fig. 4.4. In both fits the coupling of the Δ to

the ω-meson ($g_{\Delta\omega}$) has been set equal to $g_{N\omega}$. The very different behaviour of the EoS can be understood from the ratio of the effective Δ mass to the effective nucleon mass, Fig. 4.5. If the coupling of the nucleon to the ζ field is set to zero

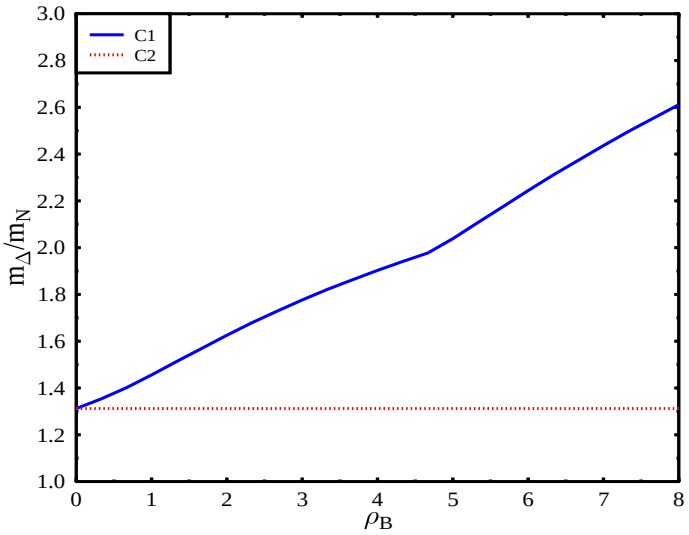

Figure 4.5: Ratio of Δ mass to nucleon mass as a function of density for the two parameter sets C1 and C2.

(C2), the mass ratio stays at the constant value $\frac{m_\Delta}{m_N} = \frac{g_{\Delta\sigma}}{g_{N\sigma}} \approx 1.31$. However, if the nucleon couples to the strange condensate (C1), the mass ratio $\frac{m_\Delta}{m_N}$ increases with density due to the different coupling of the nucleon and the Δ to the strange condensate ζ. The Δ does not feel less scalar attraction since the coupling to the σ field is the same for the nonstrange baryons. However, the mass of the Δ does not drop as fast as in the case of pure σ-couplings, and hence the production of baryon resonances is less favorable at high densities, Fig. 4.6.

Variation of the vector coupling

Both coupling constants of the Δ baryon are freely adjustable in the models discussed in [Ser86, Bog83b, Kos98, Wal87]. Contrary, the chiral model incorporates dynamical mass generation, and therefore the scalar couplings have to be chosen such that the corresponding hadronic vacuum masses can be reproduced. As was pointed out before, different couplings in the scalar sector are still possible, depending on the inclusion of an explicit symmetry breaking term. We want to address this case first. If small explicitly symmetry breaking terms $m1$ and $m2$ are used, and the coupling of the nucleon to the strange scalar field ζ is set to zero (C2), the chiral model behaves similarly to the models [Ser86, Bog83b, Kos98, Wal87] with $r = \frac{g_{\Delta\sigma}}{g_{N\sigma}} = \frac{m_\Delta}{m_N}$. That means, there is already

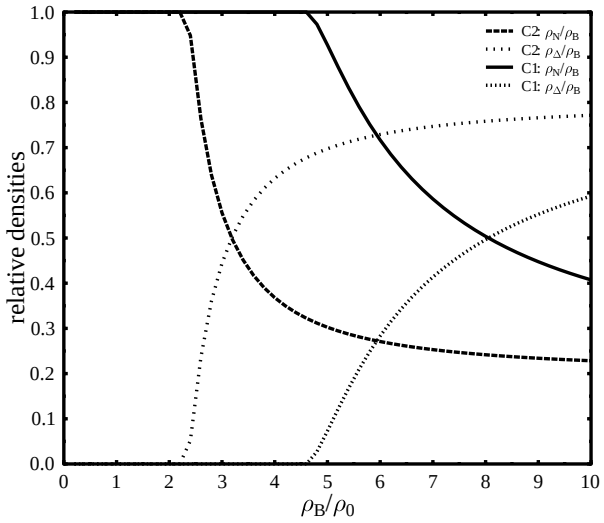

Figure 4.6: Relative densities of nucleons and Δs for various parameter sets. The production rate of Δs depends strongly on the parameter set, i.e., on the strength of the nucleon-ζ and the Δ-ζ coupling.

a strong softening of the equation of state at high density for equal coupling strength of the nucleon and the Δ, $g_{\Delta\omega} = g_{N\omega}$ (Figure 4.4). Furthermore, if the coupling of the Δ to the ω-field is only slightly reduced, density isomers are predicted in the chiral model and in models like [Ser86, Bog83b, Kos98, Wal87]. However, the chiral model shows a different dependence on the Δ-vector meson couplings when no explicit symmetry breaking for the baryon mass generation is included (C1). Then the scalar couplings are completely fixed by the fit to the hadronic masses in the vacuum. This necessarily leads to a coupling of the strange condensate to both, the nucleon and the Δ (Figure 4.2). As the strange condensate is not as strong modified with increasing density, the Δs have a much smaller influence on the EoS for $g_{\Delta\omega} = g_{N\omega}$ than in the first case discussed. This leads to a much lesser influence of the Δs on the equation of state for $g_{\Delta\omega} = g_{N\omega}$ compared to the first case. The behaviour is more similar to the models [Ser86, Bog83b, Kos98, Wal87] with a scalar coupling of the Δ that is smaller than $\frac{m_\Delta}{m_N} g_{N\sigma}$. This can be seen in Figure 4.4 and is due to the different density dependence of the Δ-mass, as was stated before. However, since in contrast to the models in [Ser86, Bog83b, Kos98, Wal87] the nucleon and the Δ both couple to two scalar fields with different coupling constants, the mass ratio m_Δ/m_N is not a constant anymore (Figure 4.5) which leads to a supression of the production of Δs as a function of density, c.f. Eq. (4.6). For the models with only one scalar field the mass ratio m_Δ/m_N stays constant as a function of density. If the Δ-ω coupling is reduced the equation of state is softened again and density isomers appear. In general, the second minimum in the equation of

state appears at higher densities. This is similar to the behaviour of the models [Ser86, Bog83b, Kos98, Wal87] with the scalar coupling of the Δ set to smaller values. The analysis above shows that the fixing of the coupling of the resonances to the vector mesons is of great importance. Even though in the chiral model the freedom in the choice of the scalar coupling can be reduced, due to the spontaneous mass generation in the scalar sector, the equation of state can still show very different behaviour due to the unknown vector coupling. Therefore, one has to find ways to restrict the values of these coupling constants. Two requirements, as proposed e.g. in [Kos98], are: Resonances are absent in the ground state of normal nuclear matter, and possible secondary minima in the nuclear equation of state should lie above the saturation energy of normal nuclear matter. Furthermore, QCD sum-rule calculations suggest [Jin95a] that the net attraction for Δs in nuclear matter is larger than that of the nucleon. From these constraints a "window" of possible parameter sets $g_{\Delta\sigma}, g_{\Delta\omega}$ has been extracted in [Kos98]. In the chiral model one obtains for the different types of mass generation only a small region of possible values for $g_{\Delta\omega}$ (Fig. 4.7). Pure σ coupling (C2) of

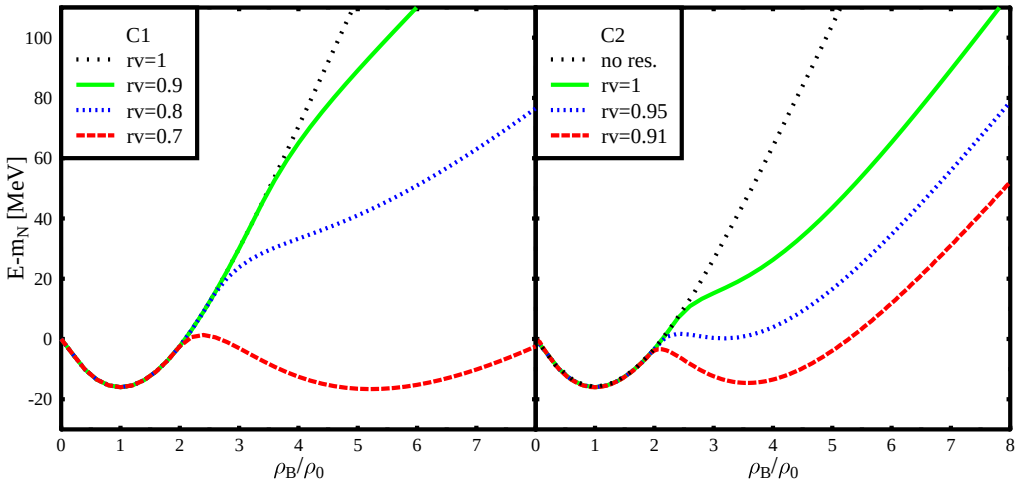

Figure 4.7: Equation of state for parameter sets C1 and C2 for different values of the quotient $r_v = \frac{g_{N\omega}}{g_{\Delta\omega}}$. For the C2-fit the value of r_v should not be less than 0.91 to avoid the density isomer being absolutely stable. For C2, r_v must be larger than 0.68.

the nonstrange baryons yields a range of coupling constants $r_v = \frac{g_{\Delta\omega}}{g_{N\omega}}$ between $0.91 < r_v < 1$. For a nonvanishing ζ-coupling (C1) one obtains $0.68 < r_v < 1$. A smaller value of the ratio r_v (less repulsion) leads to higher Δ contributions and to softer equations of state. However, due to the freedom in the coupling of the resonances to the vector mesons, the equation of state cannot be predicted unambigiously from the chiral model. Here additional input from experiments and theory are necessary. As will be shown in chapter 5, the investigation of neutron

stars puts stronger constraints on the vector coupling of the baryon resonances.

4.2 Strange hadronic matter

In figure 4.8 the binding energy per particle of hadronic matter with different netto strangeness f_s is depicted. Six different parametrizations are considered: For each of the two ways of mass generation already discussed in 3.1.2, C1 and C2, three different ways of coupling the resonances are used. Since the different scenarios for C1 and C2 show similar qualitative behaviour, we will focus in the following on C1 and denote the corresponding three different resonance couplings as CI, CII and CIII. In parameter set CI, the baryon decuplet is neglected, and the only degrees of freedom in the system are the members of the (anti)baryon octet, the pseudoscalar meson nonet and the vector meson nonet. In parameter set CII and CIII we include the (anti)-baryon decuplet. This increases the number of degrees of freedom by 80. The parameter sets CII and CIII differ in the treatment of the strange spin-$\frac{3}{2}$ resonances. In parameter set CII an additional explicit symmetry breaking for the baryon resonances along the hypercharge direction, as described in [Pap99] for the baryon octet, is included. This is neglected in parameter set CIII. For CI and CII nonstrange matter shows the largest binding up to about very high ($> 9\rho_0$) densities. Only for CIII, matter with a nonzero strangeness content becomes favorable at lower densities ($6 - 7\rho_0$). Thus, the masses of the octet hyperons and also the strange decuplet baryons in the CII case do not sufficiently drop to make strange matter energetically favorable. This only happens if strange particle species without large symmetry breaking terms, like the strange members of the baryon decuplet in CIII, are included. The very different behaviour of the baryon masses can be seen in figures 4.9. The scalar and vector fields for the different paramter sets are depicted in figure 4.10

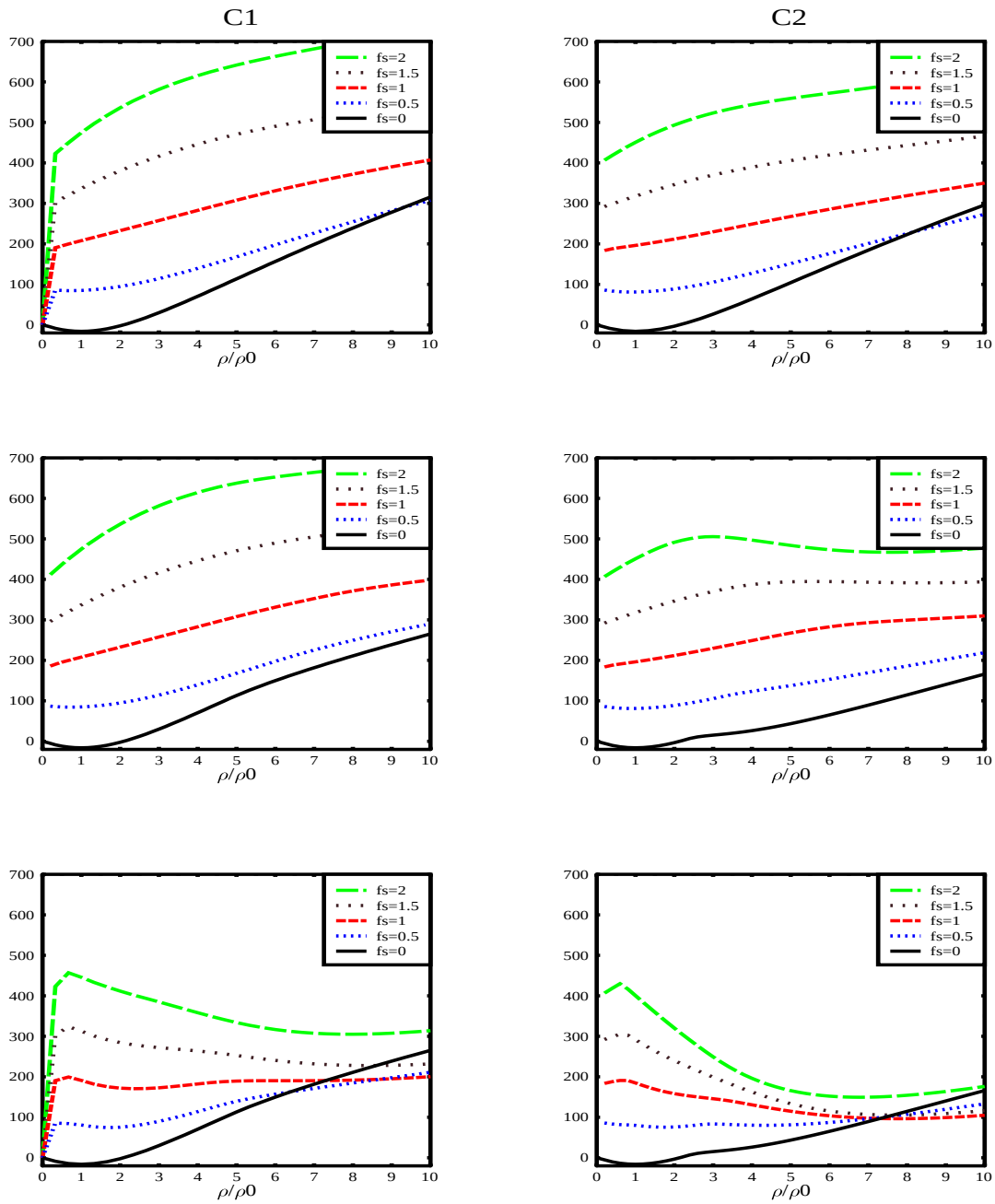

Figure 4.8: Binding energy per particle as a function of baryon density for hadronic matter with different netto strangeness f_s for C1 (left) and C2 (right). Top: no baryon resonances. Middle: inclusion of baryon resonances and additional symmetry breaking in the strange sector. Bottom: inclusion of baryon resonances without additional symmetry breaking in the strange sector.

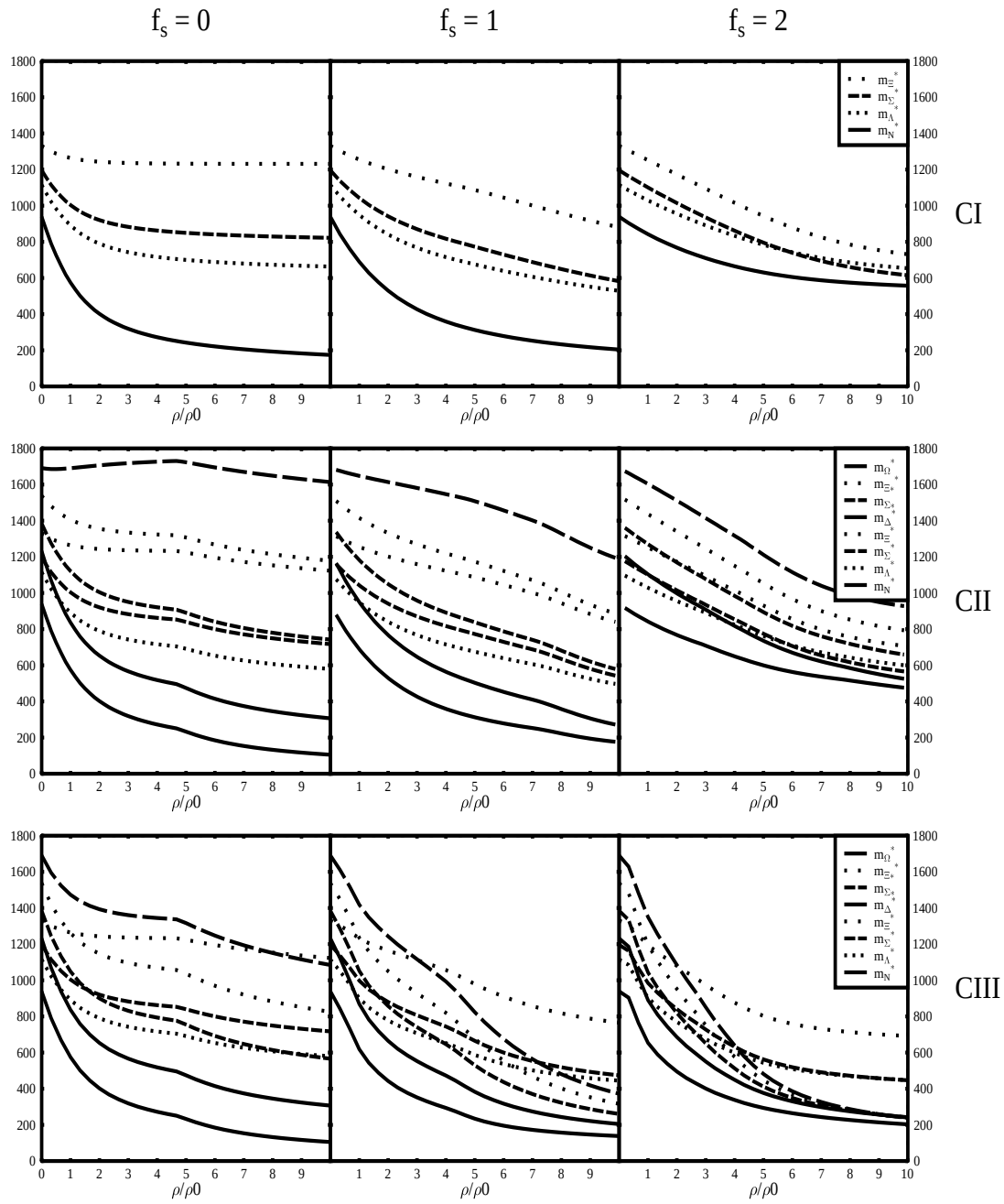

Figure 4.9: Baryon masses for $f_s = 0$ (left), $f_s = 1$ (middle) and $f_s = 2$ (right) as a function of density for C1 and three different ways of treating the baryon resonances: no coupling of the baryon resonances (CI, top), inclusion of baryon resonances and additional symmetry breaking in the strange sector (CII, middle), and inclusion of baryon resonances without additional symmetry breaking in the strange sector (CIII, bottom).

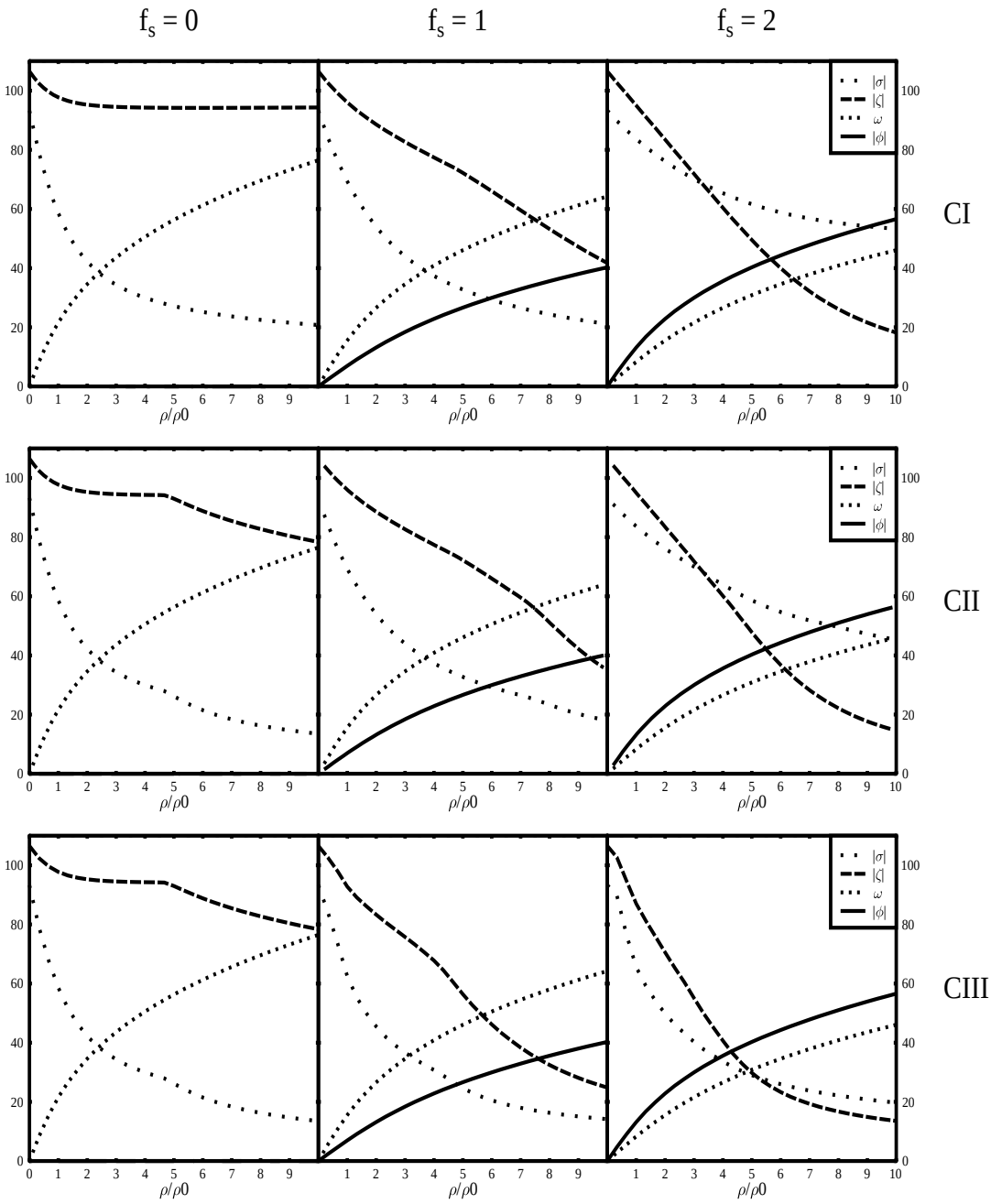

Figure 4.10: Scalar and vector fields for $f_s = 0$ (left), $f_s = 1$ (middle) and $f_s = 2$ (right) as a function of baryon density. Three different ways of treating the baryon resonances are considered: no baryon resonances (top), inclusion of baryon resonances and additional symmetry breaking in the strange sector (middle) and, inclusion of baryon resonances without additional symmetry breaking in the strange sector (bottom).

4.3 Hot hadronic matter

The model shows a phase transition or a crossover around $T_c = 150$ MeV. Since there are only hadronic degrees of freedom in the model, this phase transition is of purely hadronic nature, i.e., the strong increase of the scalar density reduces the masses of the baryons which in turn again increases the scalar density (compare e.g. to [The83]).
The characteristics (e.g. the order, the latent heat) of the various phase transitions depend on the chosen parameters and on the considered degrees of freedom. We will again use the three different parameter sets CI, CII and CIII which differ in their treatment of the baryon resonances. This leads to different predictions concerning the behaviour of hot hadronic matter. In figure 4.11 the resulting

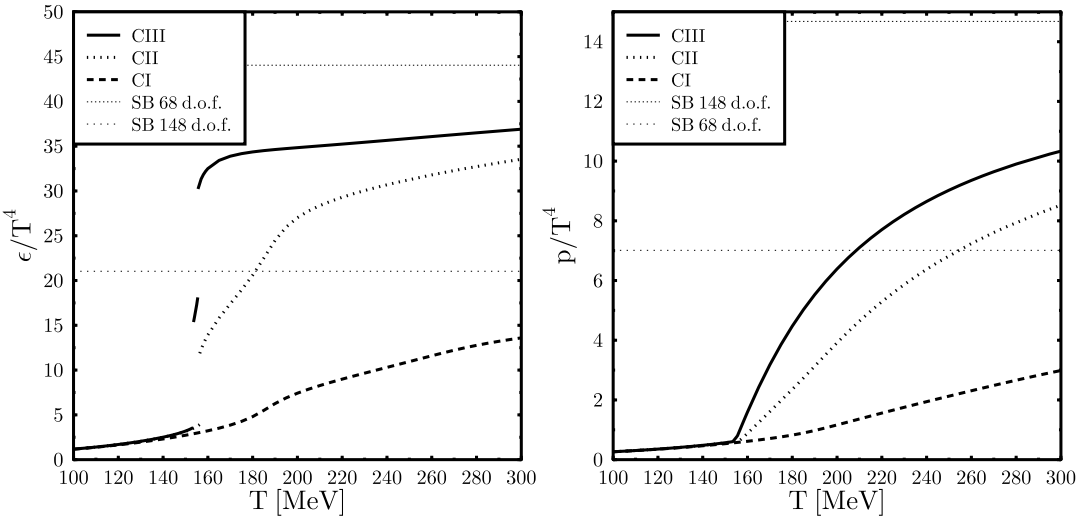

Figure 4.11: ϵ/T^4 and p/T^4 for the three different parameter sets CI, CII, CIII at $\mu_q = \mu_s = 0$. Depending on the chosen parameters we observe a different phase transition behavior. For CI a smooth crossover occurs. In contrast CII leads to a jump in ϵ/T^4 at $T \approx 150$MeV and a discontinuity in the rise of P/T^4 with T. Finally, CIII even shows two discontinuities in ϵ/T^4. The horizontal lines correspond to the Stefan-Boltzmann limit with and without the (anti)-baryon decuplet.

pressure and energy density are plotted as a function of temperature for vanishing chemical potential. Parameter set CI exhibits a smooth crossover, while a first order phase transition is observed for parameter set CII. Two first order phase transitions are found for parameter set CIII. This behavior is due to separate jumps in the nonstrange and the strange condensate. The latent heat for CII is $\Delta E_{II} \approx 600\text{MeV/fm}^3$, while it is $\Delta E_{III} \approx 850\text{MeV/fm}^3 + 920\text{MeV/fm}^3 = 1770\text{MeV/fm}^3$ for CIII (Both values are for $\mu_q = \mu_s = 0$). The jumps of the con-

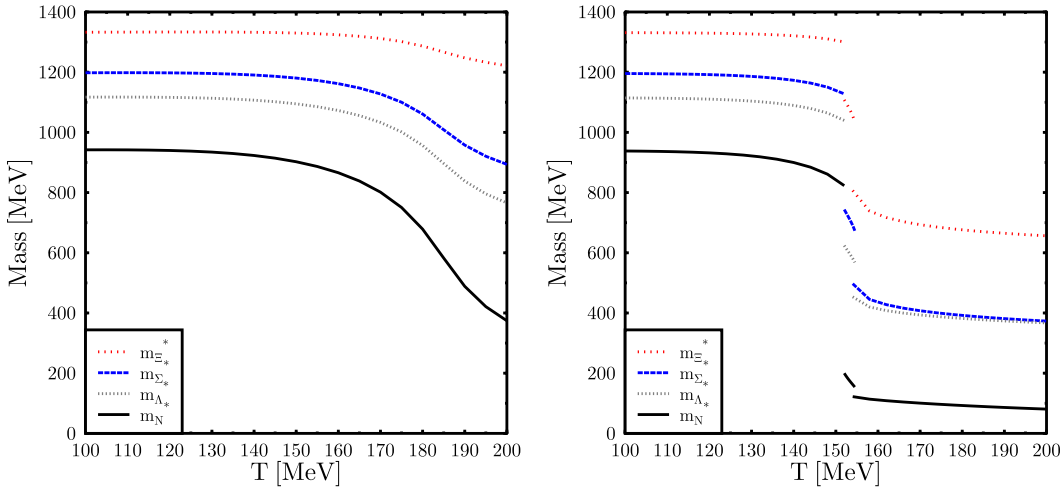

Figure 4.12: Baryon octet masses as function of temperature for vanishing chemical potential. Left CI, right CIII. Note the continuous change of the masses starting around $T = 150$ MeV. In contrast, for CIII two phase-transitions occur around $T_c \approx 155$ MeV. These result from the separate jumps in the nonstrange (σ) and the strange (ζ) condensate.

densates are reflected in the behaviour of the baryon masses, c.f. figure 4.12. As can be seen from Fig 4.13, the occurence of a first order phase transition depends on the chemical potential. For small chemical potential, $\mu_q < 100$ MeV, CIII shows two phase transitions due to the jump in the σ and the ζ field while CII exhibits one phase transition due to the jump in the σ field. At higher chemical potentials, 100 MeV $< \mu_q <$ 370 MeV, CIII shows a phase transition due to the jump in the ζ field only. Furthermore, since in the $SU(3)$-approach two chemical potentials (μ_q, μ_s) have to be considered, the condition $f_s \equiv \rho_s/\rho_B = 0$ does not hold for each phase in the mixed-phase region, but only for the total strangeness fraction. This leads to a slight change of the temperature in the mixed phase. For chemical potential $\mu_q > 370$MeV there is no phase transition for $f_s = 0$. The energy densities and entropy densities in the phase transition regions are specified in table 4.1.

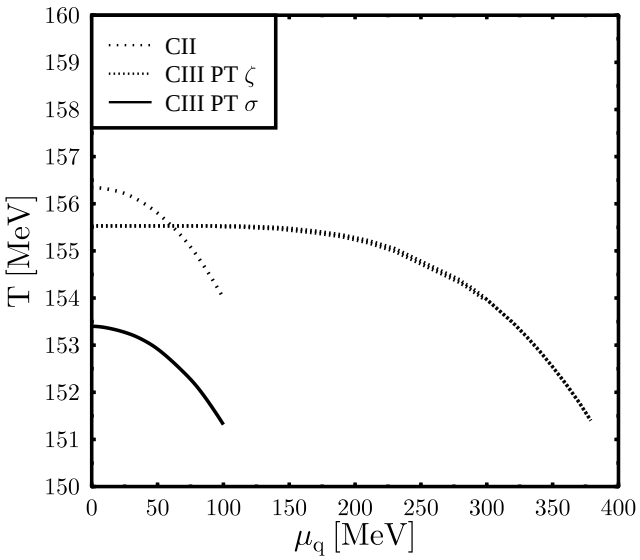

Figure 4.13: Phase diagram for the parameter sets CII and CIII for $f_s \equiv \rho_s/\rho_B = 0$. The two chemical potentials (μ_q, μ_s) of the system lead to a slight change of the temperature in the phase transition region.

	ϵ^-/ϵ_0	ϵ^+/ϵ_0	$s^-[fm^{-3}]$	$s^+[fm^{-3}]$	T_c[MeV]
CII	2.1	6.3	2.3	6.2	156.3
CIII - 1st PT	1.7	7.6	2.0	7.5	153.4
CIII - 2nd PT	9.4	15.7	9.3	15.2	155.5

Table 4.1: Energy density and entropy density in the phase transition regions for CII,CIII, $\mu_q = \mu_s = 0$. The $(-),(+)$ signs stand for values below and above the phase transition, respectively. T_c denotes the phase transition temperature. $\epsilon_0 = 138.45$ MeV/fm^3 denotes the energy density of nuclear matter in the ground state.

4.4 Hot and dense hadronic matter

In the following figures different properties of nonstrange, hot and dense hadronic matter for the two parameter sets CI and CIII are shown. The figures 4.14, 4.15, and 4.16 show the effective nucleon, Λ and Ξ mass as a function of temperature T and q-quark chemical potential μ_q. For CI one observes a smooth decrease of

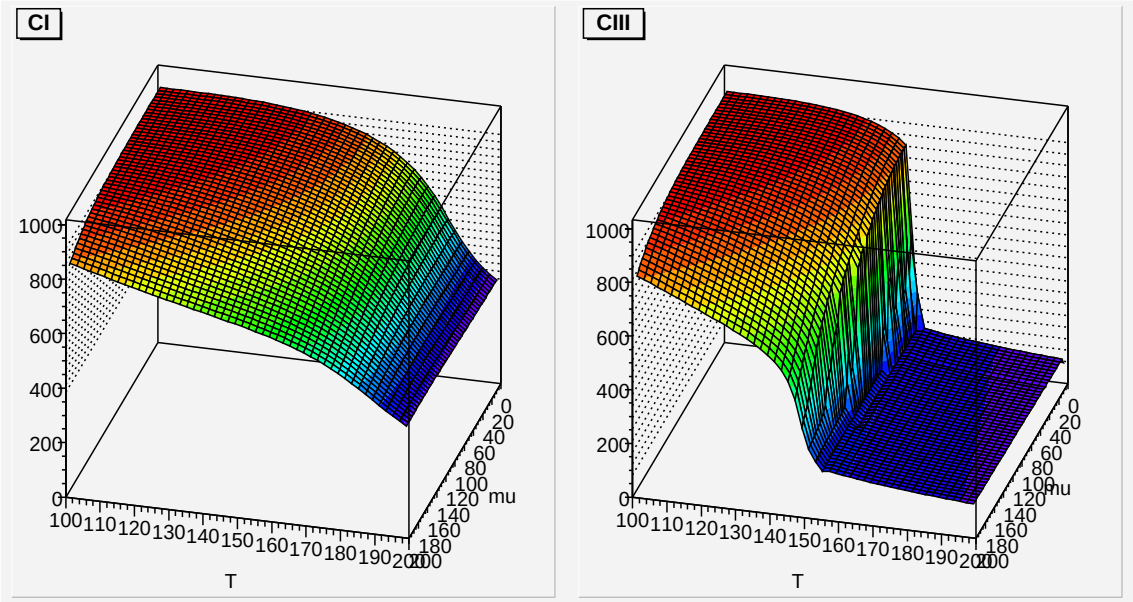

Figure 4.14: Effective nucleon mass in MeV as a function of T and μ_q

the baryon masses with increasing temperature. In contrast, for CIII a jump in the masses occurs, which results from the discontinuity in the scalar fields (see figures 4.17 and 4.18).

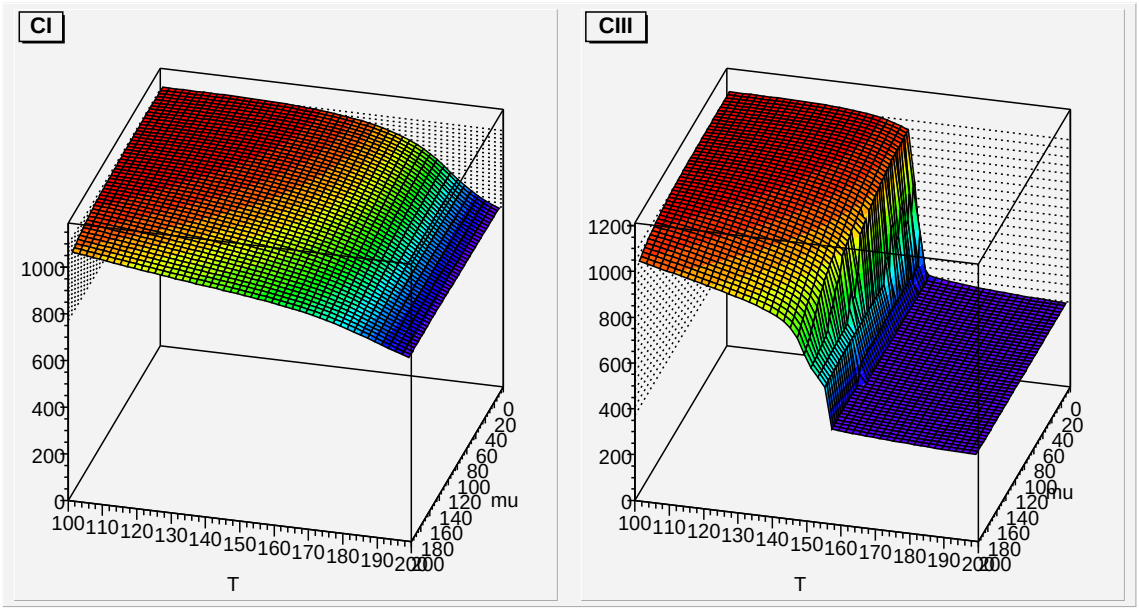

Figure 4.15: Effective Λ mass in MeV as a function of T and μ_q

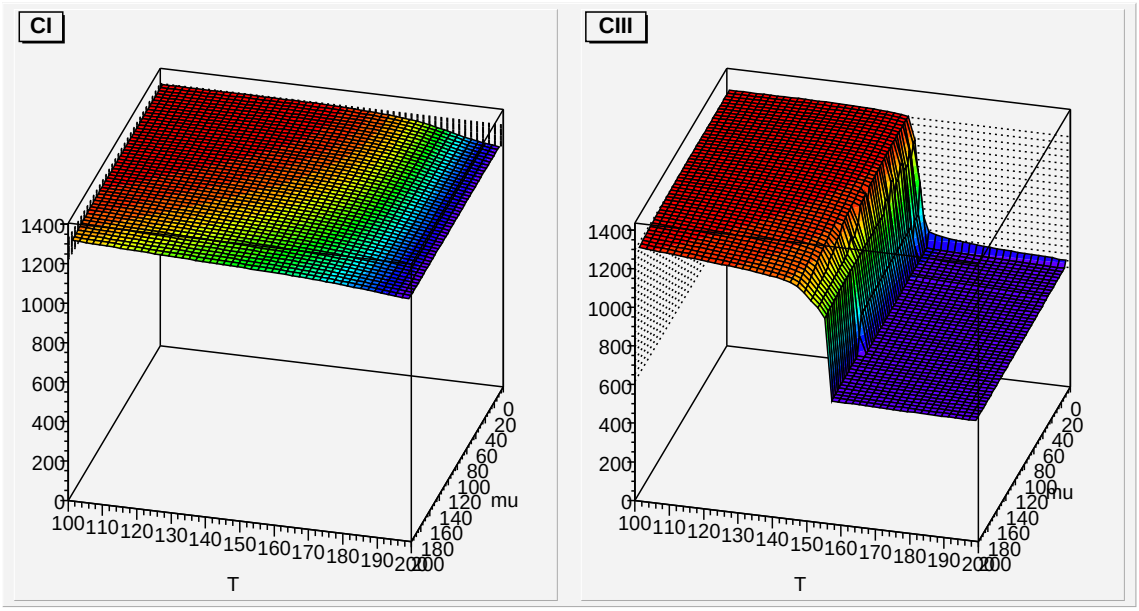

Figure 4.16: Effective Ξ mass in MeV as a function of T and μ_q

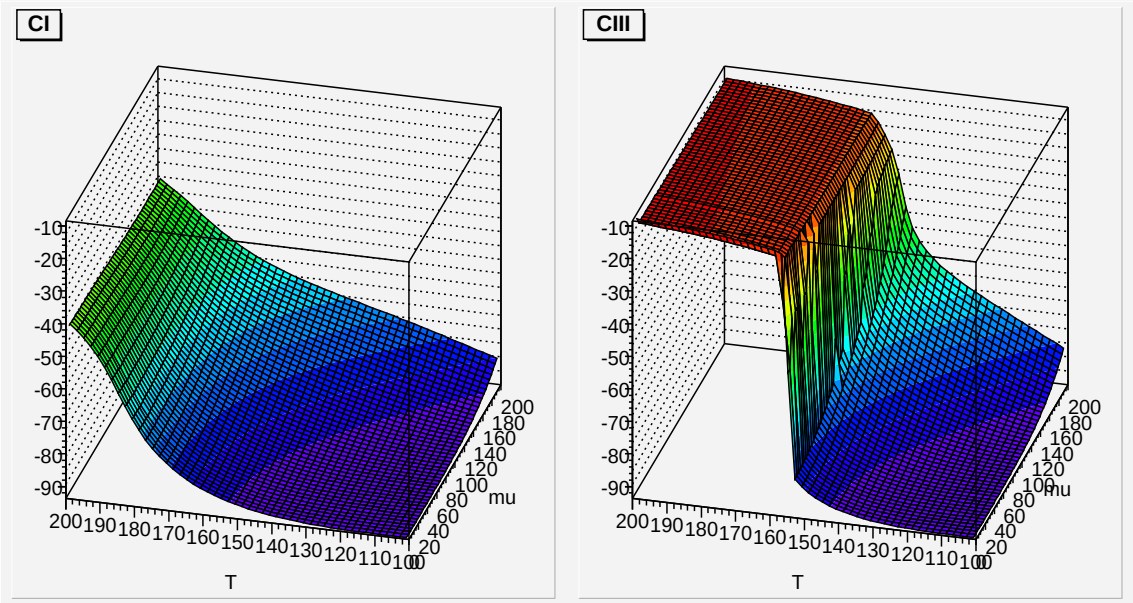

Figure 4.17: Nonstrange condensate σ in MeV as a function of T and μ_q

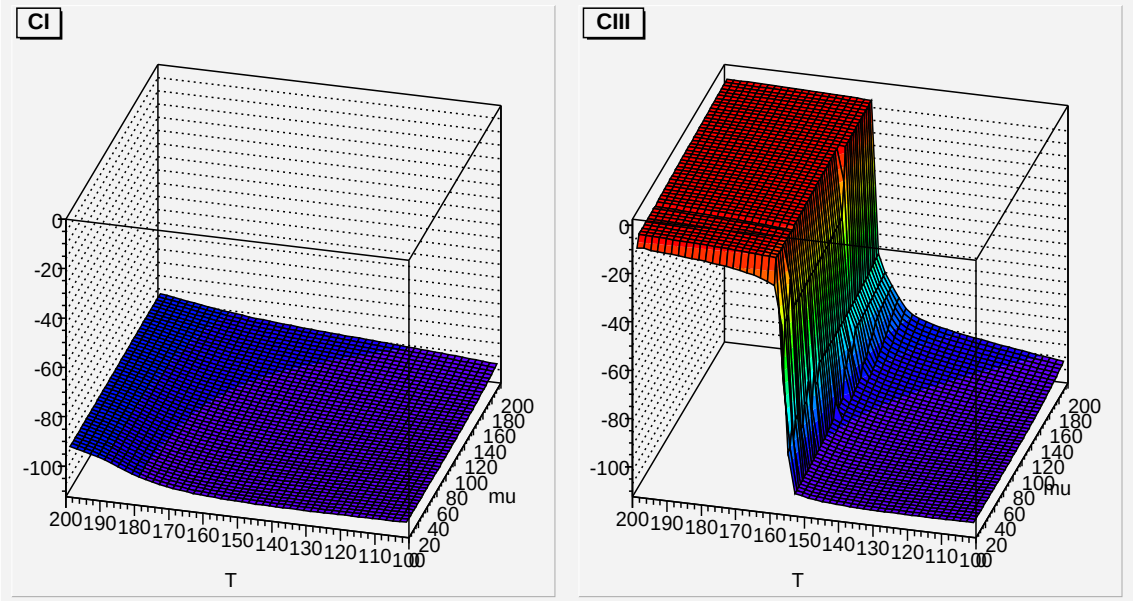

Figure 4.18: Strange condensate ζ in MeV as a function of T and μ_q

Furthermore, the change of the strange condensate with increasing temperature or density is much smaller than for the nonstrange condensate. This behaviour is again reflected in the effective masses: the decrease of the hyperon masses is much smaller than for the nucleons. In contrast, the effective π-mass shows a

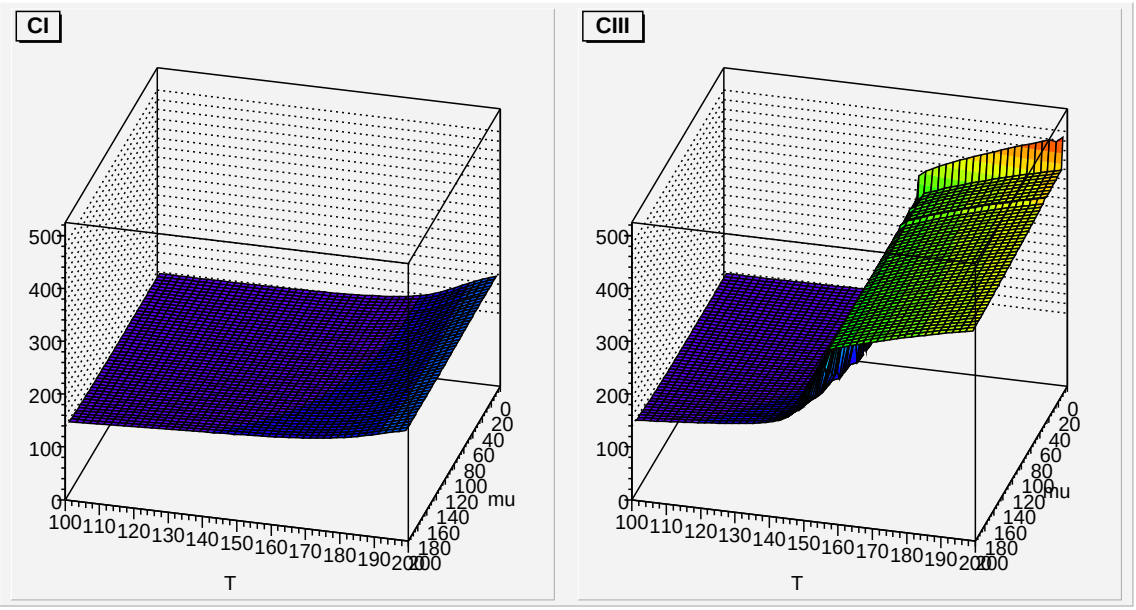

Figure 4.19: Effective π mass as a function of T and μ_q

moderate increase for high temperatures or densities for CI and a much stronger increase around T_c for CIII. Looking at the thermodynamical quantities, one first observes that the qualitative behaviour of the baryon density is similar in the two parametrizations, but the values are higher for CI than for CIII for a given T-μ_q pair. This results from the lower baryon masses in the CIII case compared to CI, which give much higher antibaryon densities and therefore a reduced vector density even though the density of each baryon and antibaryon species is enhanced. The pressure, the energy density, and the entropy density are shown in figures 4.21, 4.22, and 4.22, respectively. For all these thermodynamic quantities the values are higher for CIII than for CI for a given T-μ_q pair. This results from the higher number of degrees of freedom in the CIII-case. Furthermore, for CIII the jump in the energy density and the entropy density around $T \approx 150$ MeV arising from the first order phase transition can be observed.

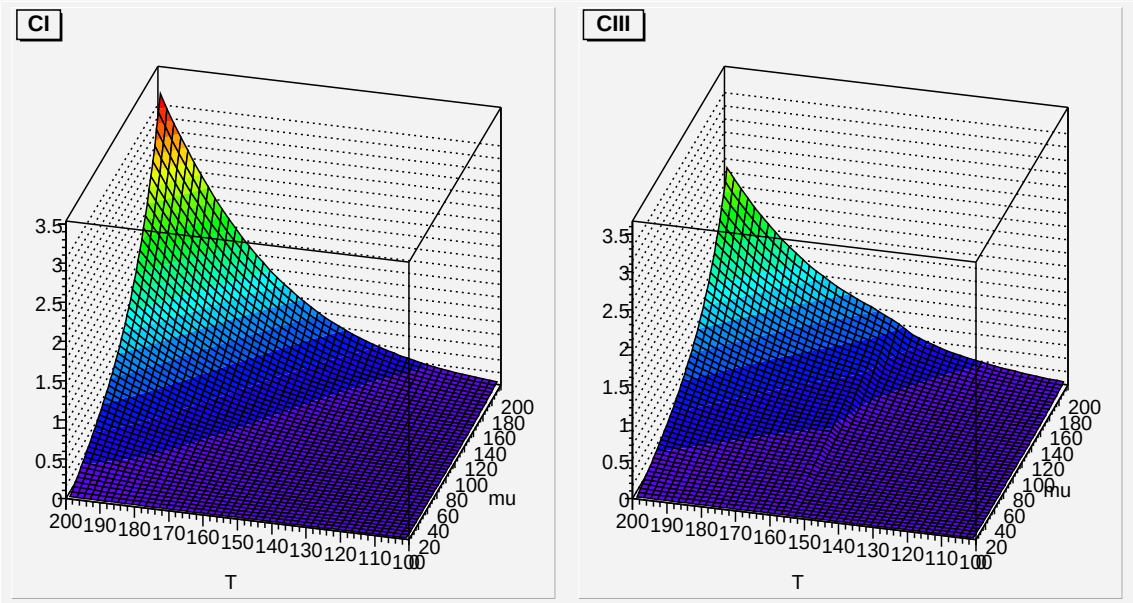

Figure 4.20: Baryon density ρ_B in fm^{-3} as a function of T and μ_q

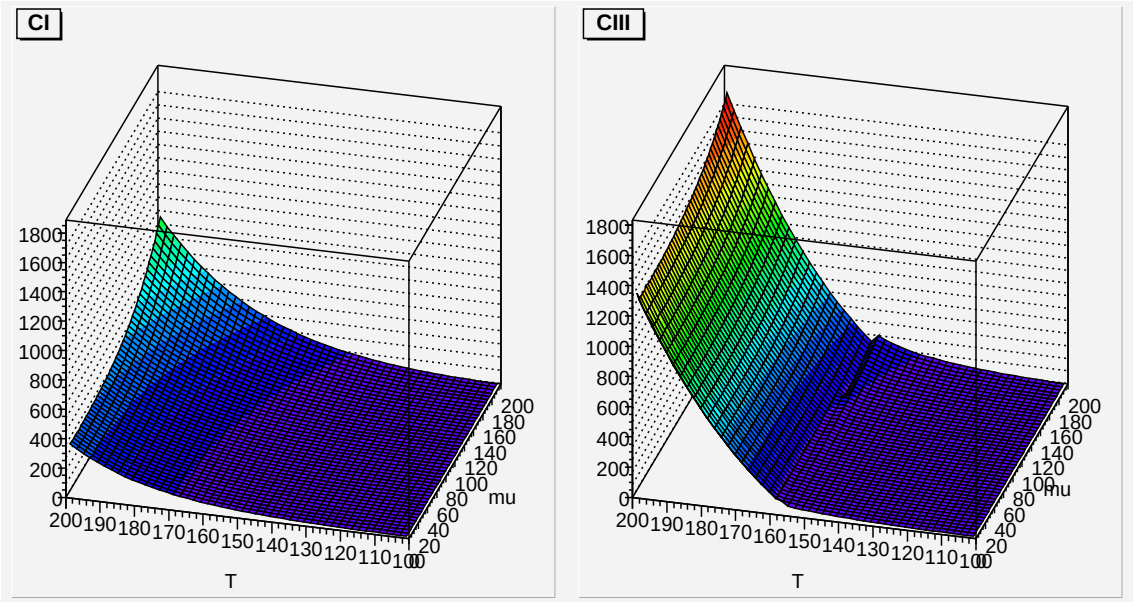

Figure 4.21: Pressure in MeV/fm^3 as a function of T and μ_q

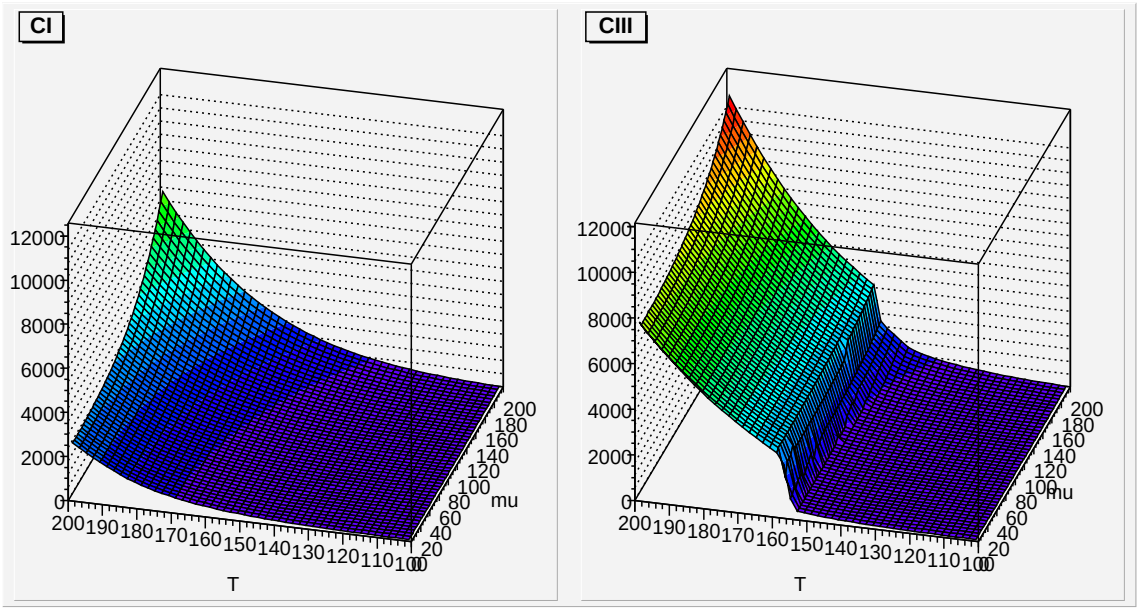

Figure 4.22: Energy density ϵ in MeV/fm^3 as a function of T and μ_q

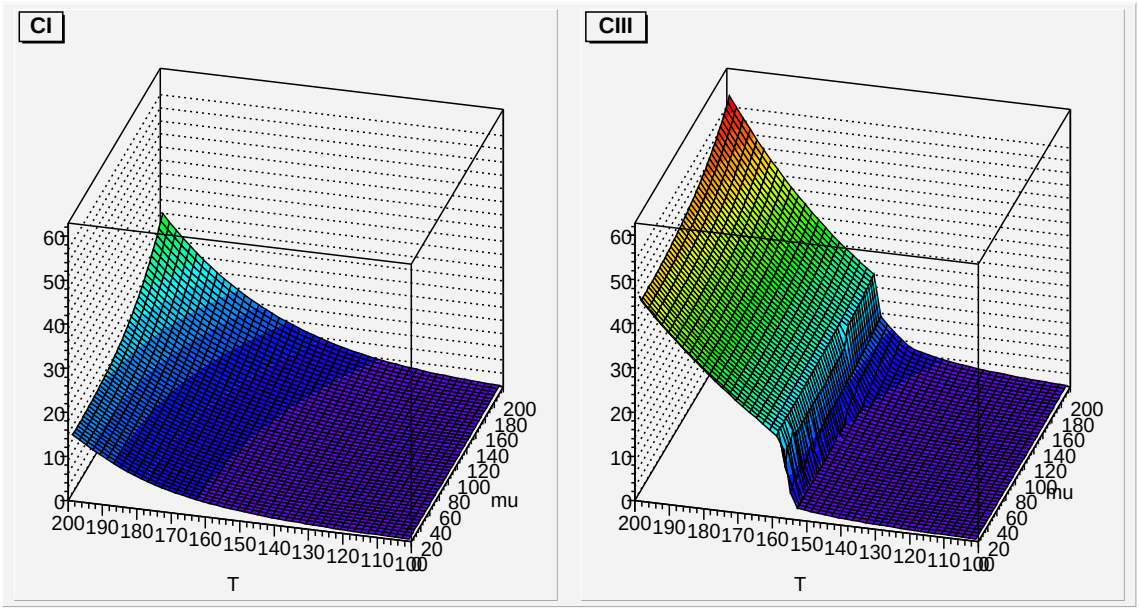

Figure 4.23: Entropy density s in fm^{-3} as a function of T and μ_q

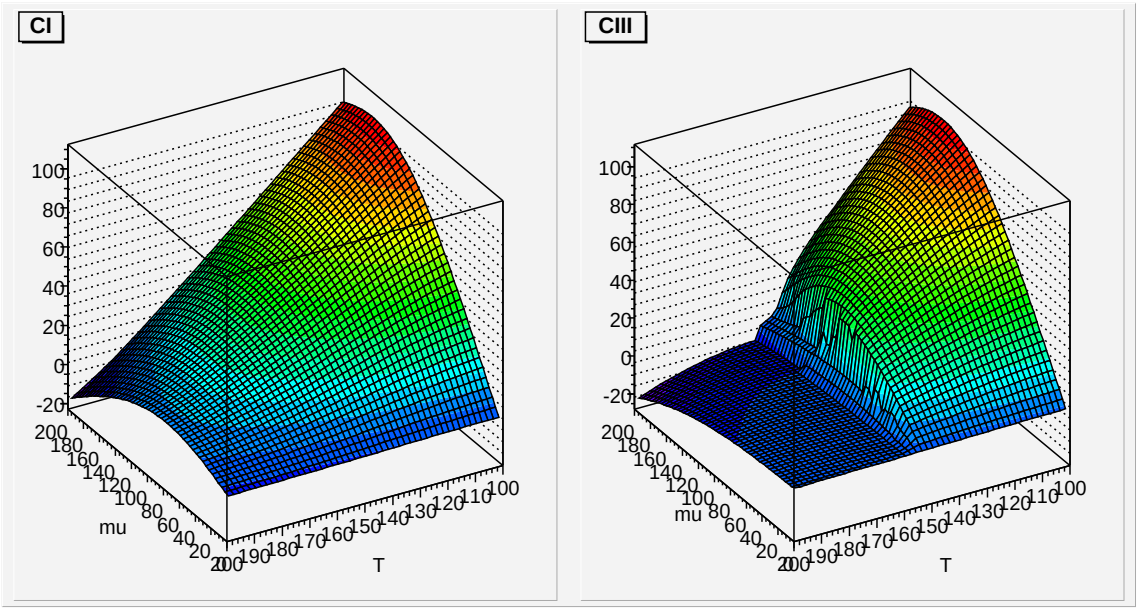

Figure 4.24: Strange quark chemical potential μ_s in MeV as a function of T and μ_q

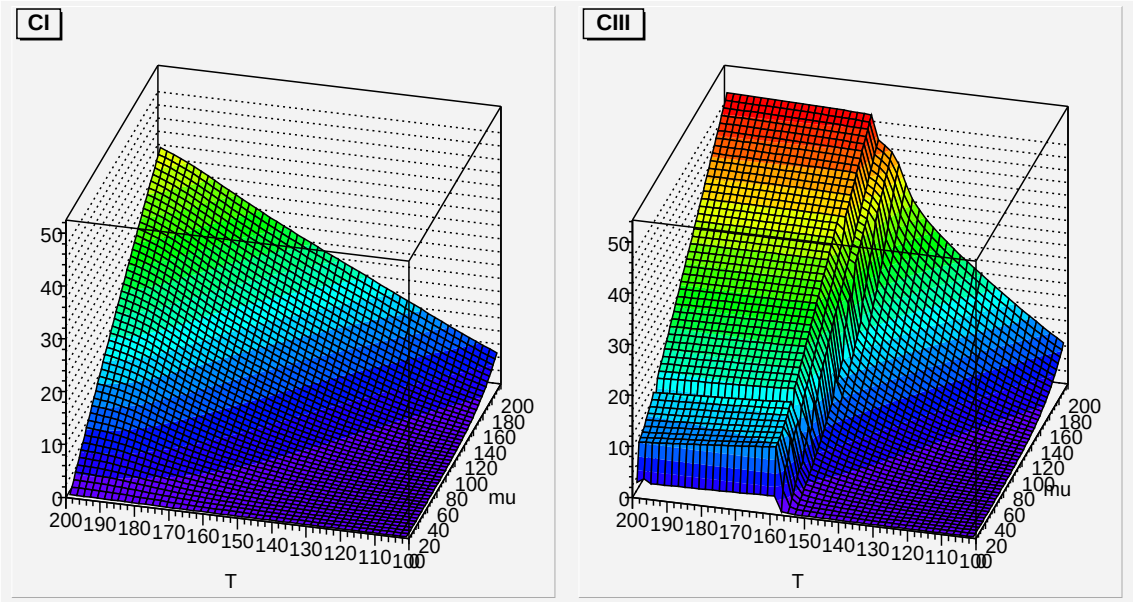

Figure 4.25: Vector field ω in MeV as a function of T and μ_q

Figur 4.24 shows the strange quark chemical μ_s for the excited nuclear matter, and in figur 4.25 the ω field is depicted.

–V–

Neutron stars

5.1 General description of neutron stars

Neutron stars are the densest and smallest stars known. They are made of baryons but probably also contain cores of quark matter [Gle96, Han01]. However, the neutron stars are not bound by the short range nuclear force but by the long range gravitational force. Estimating the binding energy per nucleon due to gravity one finds a gravitational energy of about 160 MeV/A [Gle96], compared to the binding energy of nuclear matter of about 16 MeV/A. In addition, gravity compresses the matter of neutron stars to densities far above the nuclear saturation density. Only the Fermi pressure, and the short range repulsion of the nuclear force prevent the star from the gravitational collapse. Due to these properties, neutron stars belong to the most important physical systems where the strong interaction at extreme dense conditions is "tested" (for a review see [Gle96, Web99]). Furthermore, in contrast to (ultra)relativistic heavy-ion collisions, where also high baryonic densities might be obtained by choosing the appropriate bombarding energy, neutron star matter exists at practically zero temperature – at least on a hadronic scale. Thus, the investigation of neutron stars is the complementary task of what lattice gauge calculations can achieve for high-temperature, zero-density matter. Even though nuclear matter or nuclei and neutron star matter are made of baryons and the considered densities lie in the same order of magnitude, the two systems show important differences: First, since neutron stars are bound

by gravitation, the much stronger and repulsive Coulomb force must vanish in a stable star, i.e., the net charge in a star must be essentially zero [Gle96]. This charge neutrality drives the stellar matter away from isospin-symmetric nuclear matter and so the study of neutron stars can give important clues for understanding the isospin-dependence of nuclear forces. A related regime of strong interactions can be experimentally investigated using secondary beams of nuclei going towards the neutron drip-line of nuclei. Second, since the weak interaction time scale is $\tau_{\text{weak}} \approx 10^{-10}$ seconds, strangeness is not conserved in astrophysical objects. I.e., at the high densities found in neutron stars, it is energetically favorable and possible for nucleons at the top of the Fermi sea to convert into other baryons, including hyperons [Gle96]. Thus, when going to central densities of a few times nuclear matter saturation density the inclusion of hyperon degrees become essential, and matter with a finite strangeness content is expected to exist. In summary, neutron star matter is cold, charge-neutral, hadronic matter in its lowest energy state (β-equilibrium). That means, at a given density, all baryons are populated such that the state of lowest possible energy as allowed by baryon conservation and charge neutrality is obtained.

As it always will be difficult to get clear and unambiguous information on the stellar interior from the relatively limited observational data it is important to relate star properties with other observables like neutron distribution radii in neutron-rich nuclei or multi-fragmentation in heavy ion collisions with different N/Z nuclei. It is therefore very useful to implement the chiral $SU(3)_L \times SU(3)_R$ model, which has a broader applicability including nuclear matter, finite nuclei, and chiral symmetry restoration. Thus, we are able to simultaneously study different observables within a unified approach using the same set of parameters for all calculations.

5.2 Field equations and chemical equilibrium

From the above, two main differences to nuclear matter arise, if neutron star matter is discussed in the chiral $SU(3)_L \times SU(3)_R$ model: First, we have to add the leptonic contributions to the Lagrangian (3.1), and second, instead of strangeness conservation, one has to account for charge neutrality since the matter is in β-

equilibrium [Gle96]. The total Lagrangian of the chiral $SU(3)_L \times SU(3)_R$ model for neutron star matter in the mean-field approximation then reads [1]

$$\mathcal{L} = \mathcal{L}_{\rm kin} + \mathcal{L}_{\rm BM} + \mathcal{L}_{\rm BV} + \mathcal{L}_{\rm vec} + \mathcal{L}_0 + \mathcal{L}_{\rm SB} + \mathcal{L}_{\rm lep} \ , \tag{5.1}$$

where

$$\begin{aligned}
\mathcal{L}_{\rm BM} + \mathcal{L}_{\rm BV} &= -\sum_i \overline{\psi}_i \left[m_i^* + g_{i\omega}\gamma_0\omega^0 + g_{i\phi}\gamma_0\phi^0 + g_{N\rho}\gamma_0\tau_3\rho_0 \right] \psi_i \ , \\
\mathcal{L}_{\rm vec} &= \frac{1}{2}m_\omega^2\frac{\chi^2}{\chi_0^2}\omega^2 + \frac{1}{2}m_\phi^2\frac{\chi^2}{\chi_0^2}\phi^2 + \frac{1}{2}\frac{\chi^2}{\chi_0^2}m_\rho^2\rho^2 + g_4^4(\omega^4 + 2\phi^4 + 6\omega^2\rho^2 + \rho^4) \ , \\
\mathcal{L}_0 &= -\frac{1}{2}k_0\chi^2(\sigma^2+\zeta^2) + k_1(\sigma^2+\zeta^2)^2 + k_2(\frac{\sigma^4}{2} + \zeta^4) + k_3\chi\sigma^2\zeta \\
&\quad -k_4\chi^4 - \frac{1}{4}\chi^4\ln\frac{\chi^4}{\chi_0^4} + \frac{\delta}{3}\ln\frac{\sigma^2\zeta}{\sigma_0^2\zeta_0} \ , \\
\mathcal{L}_{\rm SB} &= -\left(\frac{\chi}{\chi_0}\right)^2 \left[m_\pi^2 f_\pi \sigma + (\sqrt{2}m_K^2 f_K - \frac{1}{\sqrt{2}}m_\pi^2 f_\pi)\zeta \right] , \\
\mathcal{L}_{\rm lep} &= \sum_{l=e,\mu} \overline{\psi}_l [i\gamma_\mu\partial^\mu - m_l]\psi_l \ .
\end{aligned} \tag{5.2}$$

The corresponding thermodynamic potential of the grand canonical ensemble per unit volume at zero temperature for the neutron star matter can be written as

$$\Omega/V = -\mathcal{L}_{\rm vec} - \mathcal{L}_0 - \mathcal{L}_{\rm SB} - \mathcal{V}_{\rm vac} - \sum_i \frac{\gamma_i}{(2\pi)^3}\int d^3k\,[E_i^*(k) - \mu_i^*] - \frac{1}{3}\sum_l \frac{1}{\pi^2}\int \frac{dk\,k^4}{\sqrt{k^2+m_l^2}}. \tag{5.3}$$

with $E_i^*(k) = \sqrt{k_i^2 + m_i^{*2}}$. As mentioned above, there are only two conserved charges with their corresponding chemical potentials in a neutron star: the baryon and the electric charge number. Thus, the chemical potentials of all other constituents can be written in terms of these two. I.e., for a given baryon species i the chemical potential μ_i reads

$$\mu_i = b_i\mu_B - q_i\mu_Q, \tag{5.4}$$

[1] In the neutron star calculations the couplings of the vector mesons were chosen as without the renormalization factors discussed in section 3. This corresponds to abandonning the addtional constraint of pure f-type coupling and neglecting the extra factor to the ϕ in the quartic term which, however, gives only a very small contribution

where b_i and q_i denote the baryon number and charge of the ith species. The effective chemical potentials read

$$\mu_i^* = \mu_i - g_{i\omega}\omega_0 - g_{i\phi}\phi_0 - g_{i\rho}I_{3i}\rho_0 \ , \tag{5.5}$$

with $\mu_i^* \equiv E_i^*(k = k_{F_i})$. The energy density and pressure follow from the Gibbs-Duhem relation, $\varepsilon = \Omega/V + \sum_{k=i,l} \mu_k \rho_k$ and $P = -\Omega/V$. At a given baryon density ρ_B, the field equations as obtained by extremizing Ω/V are solved self-consistently in conjunction with the equation for the baryon density $\rho_B = \sum_i \rho_i$ and the charge neutrality condition $\sum_{k=i,l} Q_k \rho_k = 0$, with Q_k denoting the charge of particle species k.

5.3 Properties of neutron star matter

Figure 5.1 shows the energy per baryon neglecting the Coulomb interaction as a function of baryonic density ρ_B for varying neutron-proton asymmetries, $\delta = (\rho_n - \rho_p)/\rho_B$, calculated in the chiral model. The curve $\delta = 0$ describes infinite

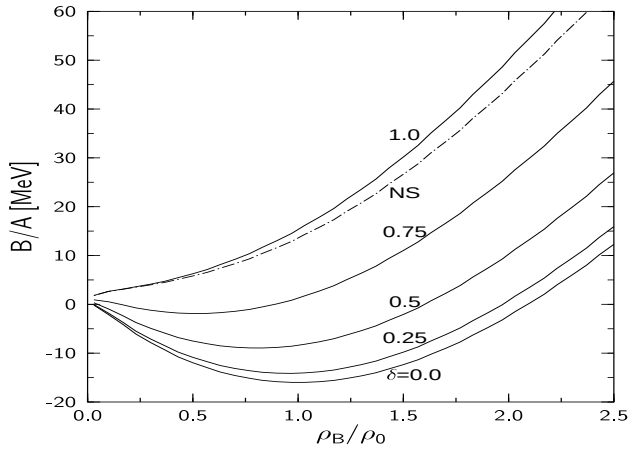

Figure 5.1: Binding energy per nucleon B/A versus the baryonic density ρ_B/ρ_0 for different values of neutron-proton asymmetries $\delta = (\rho_n - \rho_p)/\rho_B$ in the chiral model. The normal nuclear matter density is $\rho_0 = 0.15$ fm^{-3}. The curve labeled NS describes a neutron star matter consisting of nucleons and electrons.

symmetric nuclear matter with a minimum at ρ_0. With increasing asymmetry,

($\delta > 0$) the binding energy decreases and the saturation density is shifted to lower values. The binding in nuclear matter for small values of δ stems from the isospin symmetric nuclear forces. At asymmetries $\delta \geq 0.84$ (i.e., a neutron to proton ratio > 11), the system starts to become unbound even at the low density regimes. The stiffest equation of state is obtained for pure neutron matter with $\delta = 1$. Due to the β-equilibrium conditions, the EoS for neutron star matter (labeled NS) composed of neutrons, protons and electrons (npe) is softer as compared to pure neutron matter. The gravitational attraction provides the necessary binding of neutron stars. The present results from the chiral model corroborate those obtained in Walecka-like models [Gle96, Web99] and in the relativistic Brueckner-Hartree-Fock calculations [Eng94].

As already mentioned, the inclusion of hyperons is essential for the discussion of neutron stars. In the chiral $SU(3)_L \times SU(3)_R$ model, the hyperons are included naturally as members of the baryon octet (see section 3.2.4). We use the parameter set CI (no baryon resonances) and choose $a = 2$ for the explicit symmetry breaking in the hyperon sector. This corresponds to an explicit symmetry breaking weighted with the strangeness content of the corresponding particle[2]. The obtained results are compared with those of a Walecka-type model with cubic and quartic meson self-interactions. These nonlinear interactions read $U(\sigma) = g_2\sigma^3/3 + g_3\sigma^4/4$ for the σ field , and $\mathcal{L}_v = g_4(\omega^\mu\omega_\mu)^2$ for the vector field ω. The inclusion of these terms gives a reasonable nuclear matter compressibility [Bog77, Bog83c] and lead to a good reproduction of the Dirac-Brueckner calculation [Sug94]. We have used the parameter set TM1 of Ref. [Sug94] which gives a saturation density and binding energy of $\rho_0 = 0.145$ fm^{-3} and $B/A = -16.3$ MeV. Note that in the TM1 set, the values of $m_N^*/m_N = 0.63$, $K = 281$ MeV, and $a_{\rm sym} = 36.9$ MeV which primarily influence the bulk properties of neutron star matter are very similar to those in the chiral model (see section 3.2.4). The hyperon couplings σ-Y are obtained from a depth of $U_Y^N = -28$ MeV, while the ω-Y couplings are obtained from SU(6) symmetry relations (6). Two additional strange mesons, ζ and ϕ, are introduced which couple only to the hyperons. The ζ-Y couplings are fixed by the condition $U_\Xi^\Xi \approx 2U_\Lambda^\Lambda \approx -40$ MeV [Sch94, Sch96a].

[2]As can be seen in figure 5.3, the two cases $a = 1$ and $a = 2$ discussed in section 3.3 yield nearly identical equations of state. The only difference may be visible in the particle composition of neutron star matter, where the choice $a = 1$ leads to a decrease of the Ξ threshold density.

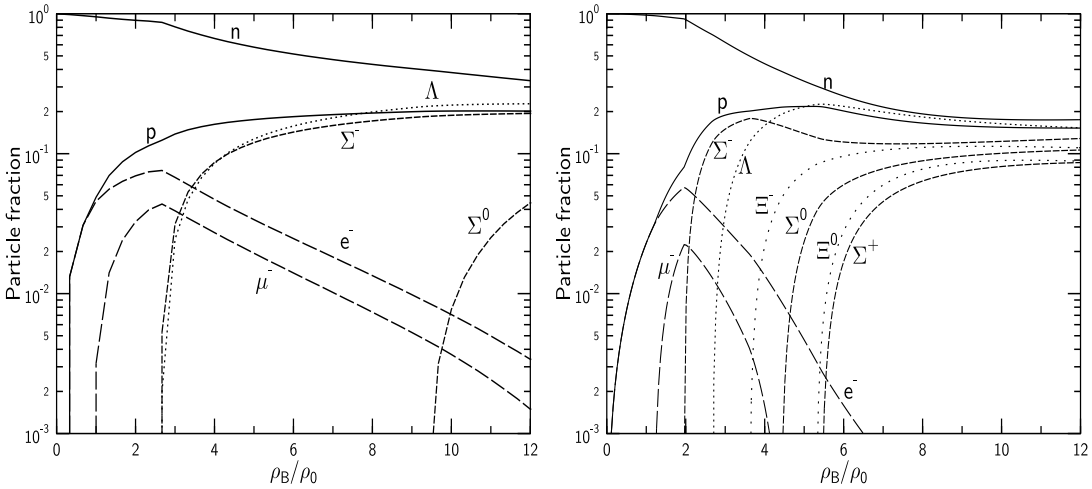

Figure 5.2: Composition of neutron star matter with hyperons in the chiral (left) and in the TM1 (right) model.

Figure 5.2 shows the particle fractions versus the baryonic density in β-equilibrated matter in the chiral model (left side) and the Walecka-type model, TM1 (right side).

In both models it is energetically favorable at high densities for nucleons at the top of the Fermi sea to convert into other baryons. The sequence of appearance of the hyperon species is the same in both cases. The first strange particle to appear is the Σ^- (in the chiral model together with the Λ) since its somewhat higher mass (as compared to the Λ) is compensated by the electro-chemical potential in the chemical equilibrium condition (5.5). Because of its negative charge, charge neutrality can be achieved more economically. This causes a drop in the lepton fraction. More massive and positively charged particles than these appear at higher densities. These are in fact generic features found in neutron star calculations with hyperons [Gle96, Web99, Pra97, Pal99]. Because of the equilibrium condition (5.5) and the dependence of the effective masses on the scalar fields, the threshold densities of the different hyperon species are, however, strongly dependent on the strength of their coupling to the scalar and vector fields as well as the magnitude of meson fields. The relatively smaller attractive scalar fields and additional symmetry breakings in the hyperon sector cause a significant shift of the density at which the hyperons ($\Sigma^0, \Sigma^+, \Xi^0$) appear in the

chiral model calculation. This enhances the fractions of both the neutrons and protons at high densities (at a level of $\sim 30\%$) in the chiral model. Consequently, the cores of massive stars in the TM1 model – and also in other Walecka-type models [Sch96a] – are in general predicted to be very ($> 50\%$) hyperon-rich. The chiral model, on the other hand, predicts neutron stars with considerable smaller hyperon fractions in the core.
The most profound implication of the constitution of neutron star matter on its bulk properties are manifested in the equation of state (EoS).

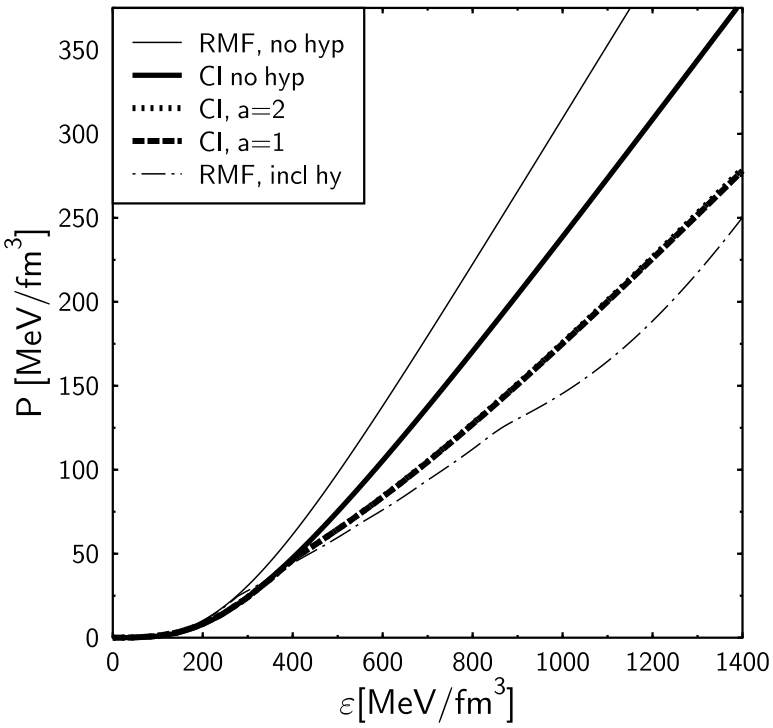

Figure 5.3: Pressure P versus the energy density ε. The results are for *npe* stars (solid lines), and for stars with further inclusion of hyperons and muons (dash-dotted lines). The calculations are in the chiral model (thick lines) and in the TM1 model (thin lines).

Figure 5.3 shows the pressure as a function of energy density ε for the chiral (thick lines) and TM1 (thin lines) model. For *npe* stars (solid lines), although the incompressibility K and the effective nucleon mass m_N^* at the normal nuclear

matter density are similar in the two models, the EoS at large densities is found to be considerably softer for the chiral model as compared to the EoS for TM1. In the latter model, the m_N^* rapidly decreases with density. Consequently, the EoS passes quickly to one that is dominated by the repulsive vector mesons (ω and ρ) leading to a stiffer EoS. This has a strong bearing on the mass and radius of such stars discussed below.

When the hyperon degrees of freedom are included, the EoS (represented by dash-dotted lines in Fig. 5.3) for both of the models are appreciably softer as compared to *npe* stars. This is caused by the opening of the hyperon degrees of freedom which relieves some of the Fermi pressure of the nucleons. Also the decrease of the pressure exerted by the leptons (they are replaced by negatively charged hyperons to maintain charge neutrality) contributes to softening of the EoS. Since the threshold density for the appearance of the hyperons, especially $(\Sigma^0, \Sigma^+, \Xi^0)$ (see Fig. 5.2), are smaller in TM1 model, these stars contain more baryon species. This leads to a considerably enhanced softening as compared to that in the chiral model. In fact, both models with hyperons predict quite similar values of pressure up to moderate densities, but the TM1 EoS exhibits a smaller pressure at higher densities. These structures observed in the EoS (Fig. 5.3) result from the population of different hyperon species and should reflect both in the masses and radii of the neutron stars.

The results of section 4.1 suggest that the inclusion of the baryon decuplet will lead to a further softening of the equation of state. We will consider the two parameter sets already introduced in section 4.1, CII and CIII. Figure 5.4 shows the equations of state for neutron star matter for these two paramter sets with $\mathrm{r_v} = 1$ compared to the EoS without baryon resonances (CI). In both cases the EoS is softened by the additional degrees of freedom. In section 4.2 and in figure 5.6 it is shown that CIII predicts much lower values for the masses of the strange members of the baryon decuplet in symmetric nuclear matter. Thus, these degrees of freedom become energetically favorable at lower densities than for CII. Hence CIII shows a much stronger softening of the EoS than CII and even a first order phase transition. Figure 5.5 shows the change of the composition of the neutron star matter when different ways of including the baryon decuplet are used. Note that the Δ baryons (especially the Δ^-) significantly contribute to the particle composition. The Λ and the Σ^- are strongly suppressed compared

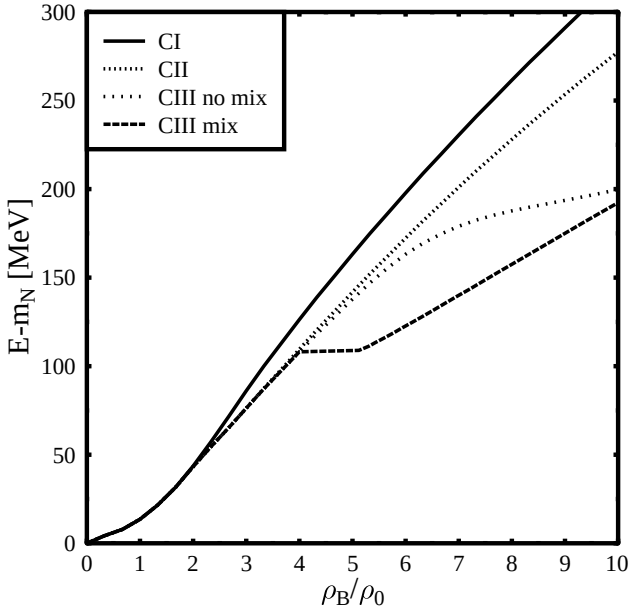

Figure 5.4: Binding energy per particle as a function of baryon density for the three parameter sets CI, CII and CIII. The inclusion of the resonances leads to a softening of the EoS. For CIII a first order phase transition appears.

to the CI case. For CIII the strange baryon resonances completely dominate the particle composition, the only octet hyperons appearing are Λs. This behaviour is explained by the different dependence of the effective masses on baryon density (Fig. 5.6). The mass of the Δ falls below the masses of the octet hyperons around normal nuclear matter density in accordance with the earlier results for symmetric nuclear matter. For CII the masses of the Σ, Σ^* and the Ξ, Ξ^*,respectively, approach each other with increasing density. For CIII the masses of the decuplet members fall below the masses of the corresponding octet members around $\rho_B \approx 1.5\rho_0$.

In section 4.1 it was discussed that the modification of the equation of state by the baryon resonances strongly depends on the choice of the parameter $r_v = \frac{g_{\Delta\omega}}{g_{N\omega}}$, i.e., the ratio of the vector couplings of the Δ and the nucleon. This is also true for the equation of state for neutron star matter. In figure 5.7 the energy per particle and the pressure as a function of baryon density for the cases CII and CIII for different values of r_v are depicted. The resulting equations of state show

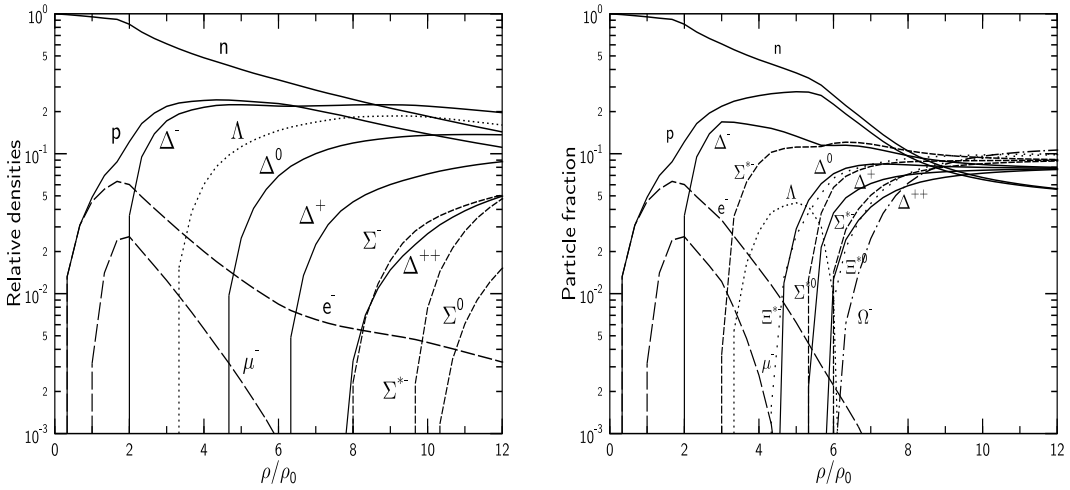

Figure 5.5: Particle composition of neutron star matter for CII (left) and CIII (right) for $r_v = 1$. In both cases the resonacnes (especially the Δs) dominate over the octet hyperons. For CIII the Λ is the only octet Hyperon contributing.

the possibility of a first order phase transition. This happens in the CIII case already for $r_v = 1$ and in the CII case for $r_v < 0.84$. The dotted lines in Fig. 5.7 correspond to the states unstable with respect to the decomposition of matter into two coexisting phases with different baryon and charge densities. The Gibbs condition for phase equilibrium at fixed T when there are two conserved charges is

$$\begin{aligned} \mu_B^{(1)} &= \mu_B^{(2)} \\ \mu_Q^{(1)} &= \mu_Q^{(2)} \\ T^{(1)} &= T^{(2)} \\ p^{(1)} &= p^{(2)}. \end{aligned} \tag{5.6}$$

In the mixed phase the charge conservation condition does not need to hold in each single phase, but only the overall charge neutrality must be assured [Gle92], i.e.,

$$\lambda\rho_Q^{(1)} + (1-\lambda)\rho_Q^{(2)} = 0, \tag{5.7}$$

must hold. Here λ denotes the fraction of phase 1 in the mixed phase. By using these equations, the resulting pressure and energy in the mixed phase can be

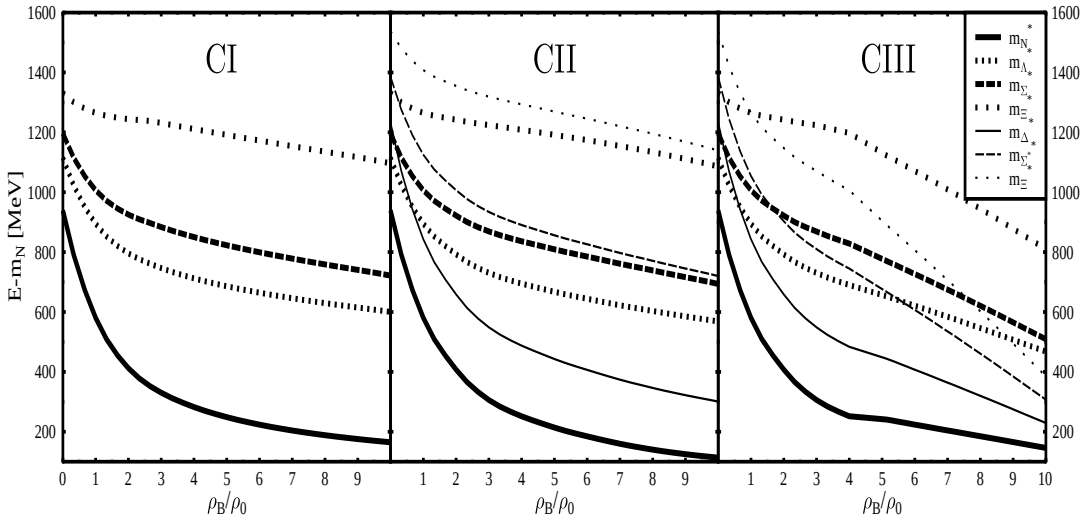

Figure 5.6: Baryon masses as a function of baryon density in neutron star matter for CI (left), CII (middle), and CIII (right). The masses of the octet baryons behave similar in all three cases. However, CII and CIII predict very distinct effective masses for the strange decuplet members. While for CII the effective mass of a certain decuplet particle approaches the effective mass of the corresponding octet hyperon from above, for CIII the masses of the strange decuplet members fall below those of the octet hyperons at $\rho_B \approx 1.5\rho_0$.

calculated as a function of density. The dashed curves in Fig. 5.7 represent these equlibrium values for CIII. Note that this procedure is very different from the Maxwell construction adopted for the case of just one conserved charge implying a constant pressure in the mixed phase region. Fig. 5.7 verifies that this does not hold anymore if two conserved charges exist.

Both, the pressure and the energy per particle show a significant softening with decreasing r_v in agreement with the corresponding results for symmetric nuclear matter. The effect is considerably larger for CIII than for CII. One can further see that both cases, CII and CIII, are similar at low densities ($\rho_B < 0.2\text{fm}^{-3}$) for all chosen values of r_v, where the resonances do not contribute. But at higher densities the equation of state for CIII is always considerably softer and exhibits the above discussed first order phase transition. This behaviour for the CIII case is again due to the strong decrease of the masses of the strange members of the baryon decuplet (Fig. 5.6).

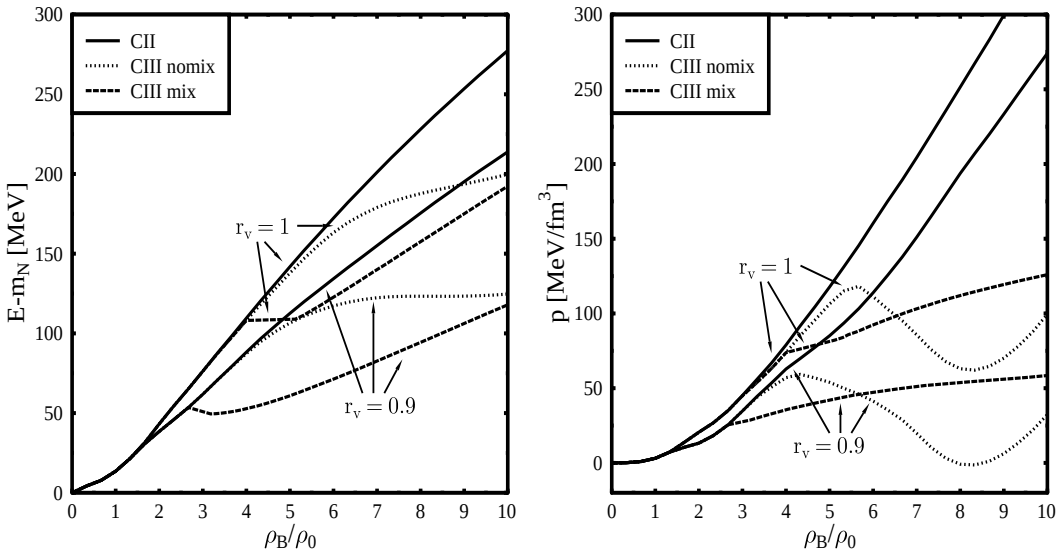

Figure 5.7: Binding energy per particle (left) and pressure (right) as a function of baryon density for $r_v = 1$ and $r_v = 0.9$. The solid lines correspond to CII, the dotted lines to CIII without a mixed phase (see text), and the dashed lines correspond to CIII with accounting for an equilibrium mixed phase.

Looking at the composition of the neutron star matter for CII with $r_v = 0.9$ (Fig. 5.8), the contribution of the baryon resonances is even more dominant than in the $r_v = 1$ case. This results of course from the decreased vector coupling of the baryon decuplet and the corresponding lowered repulsion in the dense matter for these particles. The threshold density for the octet hyperons is further increased. Especially the Σ (octet) is now replaced by the Σ^* (decuplet) since the decuplet members feel less repulsion at high densities and their effective masses are lower (see Fig. 5.6).

5.4 Neutron star properties

The structure of static neutron stars can be determined by solving the Tolman-Oppenheimer-Volkoff equations [Tol39, Opp39] (for the investigation of rotating neutron stars in the chiral model see [Sch03]). We use the results of Baym, Pethick and Sutherland [Bay71] to describe the crust consisting of leptons and nuclei at the low-density ($\rho_B < 0.001$ fm^{-3}) EoS. For the mid-density regime ($0.001 < \rho_B <$

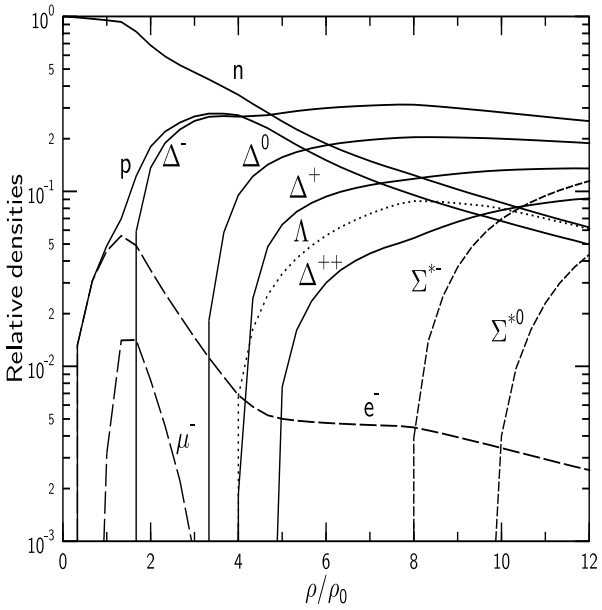

Figure 5.8: Particle composition of neutron star matter for CII with $r_v = 0.9$. As expected, the decuplet members dominate even more than for the $r_v = 1$ case.

0.08 fm^{-3}) the results of Negele and Vautherin [Neg73] are employed. Above this density, the EoS for the relativistic models have been adopted. The masses M of the nonrotating neutron star sequence is shown in Fig. 5.9 as a function of central energy density ε_c for the CI parameter set of the chiral model and for the Walecka model (TM1).

It is observed that the stiffer EoS for a *npe* star in the TM1 model can support a larger maximum mass of $M_{\max} = 2.16 M_\odot$ with a corresponding radius of $R_{M_{\max}} = 11.98$ km at a central baryonic density of $\rho_c = 6.08\rho_0$. The corresponding values obtained in the chiral model are $M_{\max} = 1.84 M_\odot$, $R_{M_{\max}} = 11.10$ km, and $\rho_c = 6.98\rho_0$. The large difference in the $M_{\max}$ values obtained in the two models, with nearly identical K and m_N^* values at ρ_0, clearly demonstrates that measurements of maximum masses of neutron (*npe*) stars at high densities cannot be used to constrain the incompressibility and the effective nucleon mass around the nuclear matter densities. Constraints on K and m_N^* from radius measurements of massive stars will be even more uncertain, since about 40% of these stars' radius originates from the low density EoS. In fact, no precise radius measurements currently exist.

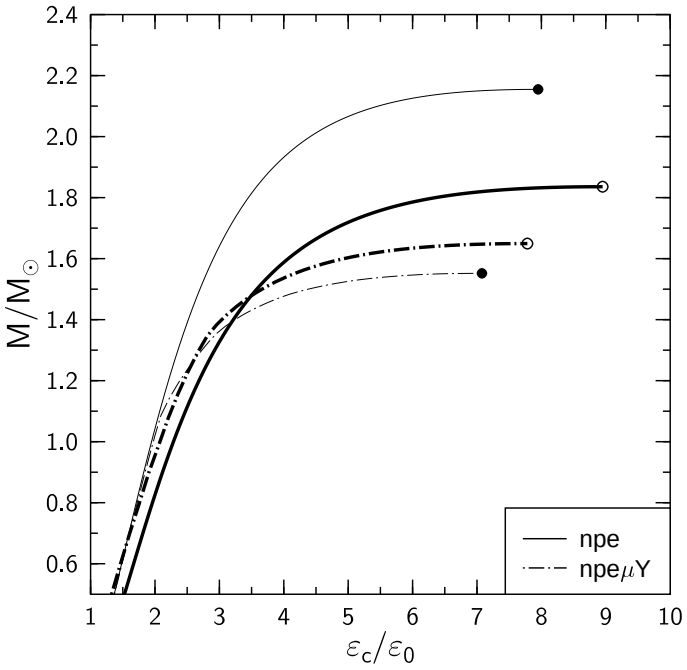

Figure 5.9: Mass as a function of central energy density $\varepsilon_c/\varepsilon_0$ for *npe* stars and for stars with further inclusion of hyperons and muons in the chiral and TM1 models. The chiral model results are represented by thick lines, and the TM1 results are given by the thin lines. The circles correspond to the respective maximum masses. The central energy density at normal nuclear matter value is $\varepsilon_0 = 138.45$ and 137.0 MeV/fm^3 in the chiral and in the TM1 model, respectively.

The maximum masses and corresponding radii of stars with hyperons (no baryon resonances) in the two models are $M_{\max} = 1.65 M_\odot$, $R_{M_{\max}} = 11.84$ km, and $\rho_c = 6.44\rho_0$ (CI), and $M_{\max} = 1.55 M_\odot$, $R_{M_{\max}} = 12.14$ km, and $\rho_c = 5.97\rho_0$ (TM1). The magnitude of the central densities indicates that the hyperons $(\Sigma^0, \Sigma^+, \Xi^0)$ are entirely precluded in stars for the chiral model whereas all hyperon species appear with comparable abundances in the TM1 model for the maximum-mass star. The strangeness fraction, $f_S = \sum_i |S_i| \rho_i/\rho_B$, are vastly different at the center of the maximum-mass stars: 0.33 vs. 0.75 in the chiral and in the TM1 model, respectively. Thus, models with similar nuclear matter incompressibilities and effective nucleon masses, leading to similar maximum star masses and corresponding similar radii can still have a widely different baryonic

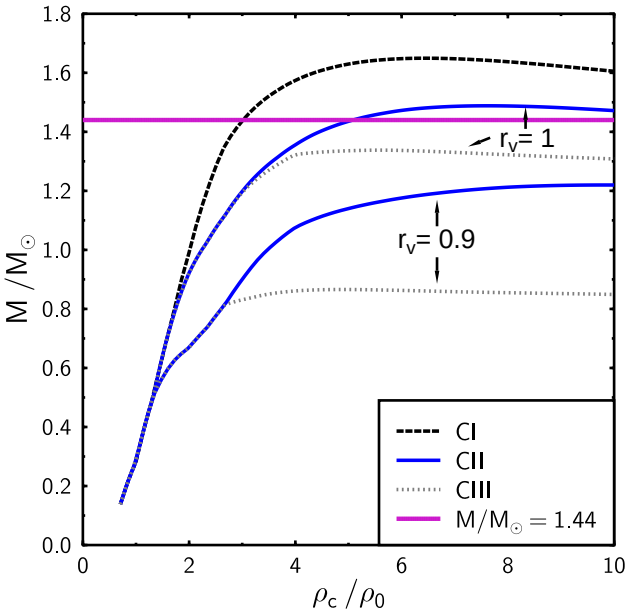

Figure 5.10: Mass of a neutron star as a function of central baryon density ρ_c. For $r_v = 1$ CII predicts a maximum mass above the lower observational minimum. For CIII the maximum mass is always below this limit.

constitution!

For progressively smaller central densities, the masses of the stars with hyperons are larger in the TM1 model (see Fig. 5.9), although the pressure at a given density is smaller than in the chiral model. This is because the masses of stars are determined by the overall EoS, and the TM1 model possess a distinctively stiffer EoS at moderate densities (see Fig. 5.3). In both models, stars of mass $1.44 M_\odot$ (corresponding to the lower limit imposed by the larger mass of the binary pulsar PSR 1913+16 [Wei84]) also contain many hyperon species with sizeable concentration.

If the baryon decuplet is taken into account, one can investigate, how much the parameter r_v may be decreased, i.e., the equation of state may be softened, until the predicted maximum mass for the neutron stars falls below the observerd lower mass limit. By only considering symmetric nuclear matter, this coupling can hardly be constrained, thus predicting a wide variety of possible equations of

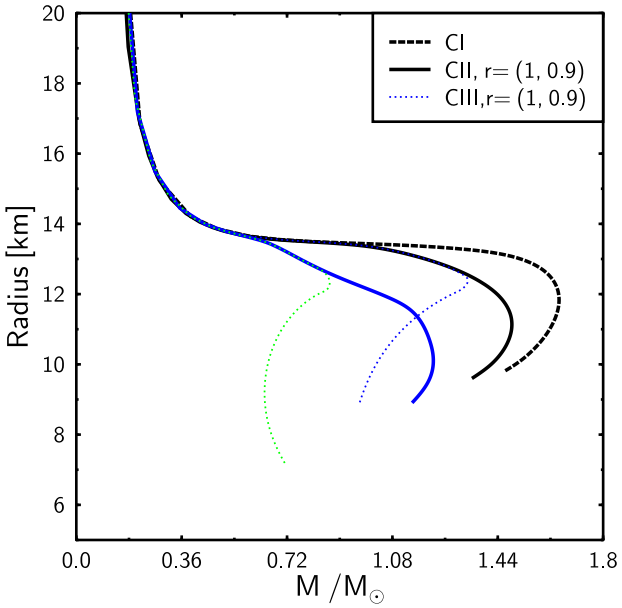

Figure 5.11: Radius as a function of neutron star mass.

state (see section 4).

Figure 5.10 shows the mass of the neutron star as a function of the central baryon density for CII and CIII and different values of r_v. First, it can be seen that for CIII the maximum mass of the neutron star is always below the observed minimum value of $M/M_\odot = 1.44$. E.g. for $r_v = 1$ the maximum mass is $M/M_\odot = 1.34$. Thus, static neutron star calculations exclude this paramter set. In contrast, for CII a realistic description of neutron stars is obtained. In Figure 5.12 (left) the neutron star mass as a function of central density for different values of r_v for the CII case is depicted. The maximum neutron star masses decrease with a decreasing value of r_v. As shown in figure 5.12, for the CII case the minimum value for r_v is $r_v \approx 0.97$. The resulting Radius-Mass dependencies are shown in figure 5.13. Thus, it turned out that the neutron star properties yield far stronger constraints on the vector coupling of the resonances than the symmetric nuclear matter case. However, especially the very different particle composition for the applied parrameter sets shows that further investigations are necessary. Hereby the main focus should be put on the treatment of the octet and the decuplet

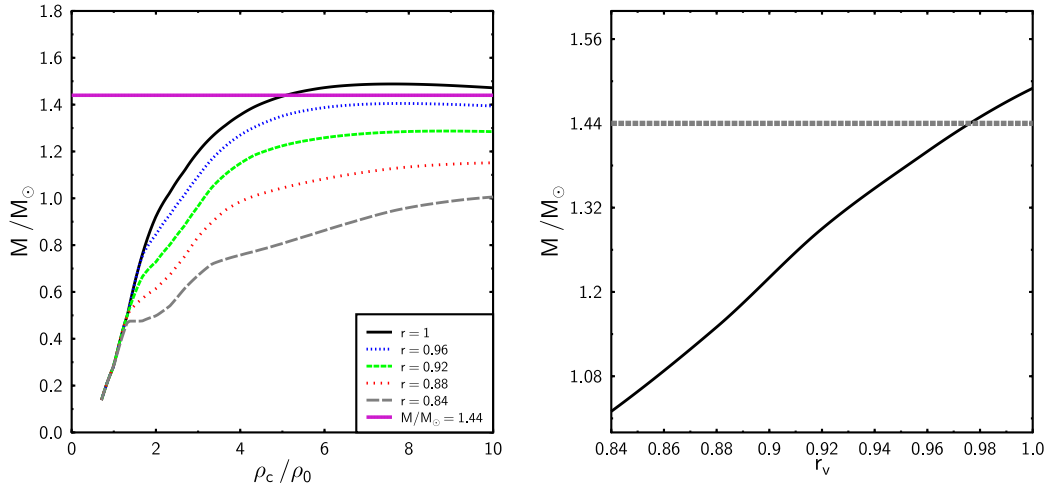

Figure 5.12: Left: Mass of a neutron star as a function of central baryon density ρ_c for CII and different values of r_v. Right: Mass of a neutron star as a function of the parameter $r_v = g_{\Delta\omega}/g_{N\omega}$ for CII. The "critical" value in this static calculation is $r_v \approx 0.97$.

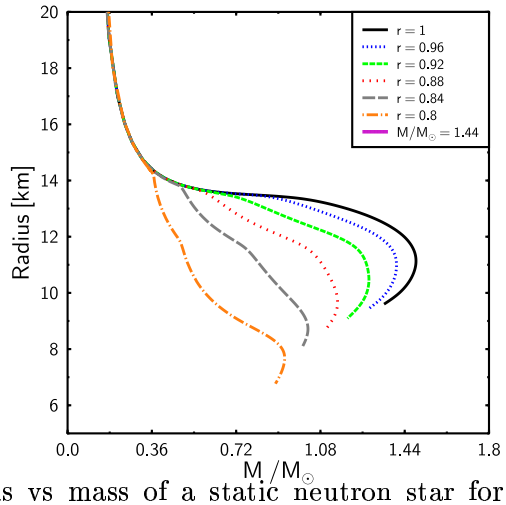

Figure 5.13: Radius vs mass of a static neutron star for the CII paramter set of the chiral model. For maximum masses above the minimum observational limit, the corresponding radius is $R \approx 12$ km.

hyperons. In addition, as already discussed in section 4.3, the scalar coupling of the Δ baryons should be investigated in more detail also in connection with the predictions of the model for finite temperature and vanishing chemical potential.

This will be discussed in more detail in section 9.

–VI–

Space-time evolution and HBT analysis of relativistic heavy ion collisions

6.1 General remarks

General theoretical arguments [Pis84] and lattice QCD simulations [Bro90, Iwa96] predict the occurrence of a transition of strongly interacting matter to a state where chiral symmetry is (approximately) restored. Since Bose-Einstein correlations in multiparticle production processes [Gol60] due to the Hanbury Brown-Twiss effect [Han56, Kop74] provide valuable information on the space-time dynamics of fundamental interactions [Shu73, Gyu79, Mak88, Ham88], correlations of identical pions produced in high energy collisions of heavy ions may provide information on the characteristics of that phase transition[1].

In particular, a first order phase transition leads to a prolonged hadronization time as compared to a cross-over or a hadron gas with no symmetry restoration, and has been related to unusually large Hanbury-Brown–Twiss (HBT) radii [Pra86, Ber88, Ber89, Sch92, Bol93b, Bol93a, Ris96b]. The coexistence of hadrons and QGP reduces the "explosivity" of the high-density matter before

[1]For recent reviews on HBT interferometry in heavy ion collisions see [Wei00, Cso02, Wie99, Hei99].

hadronization, prolonging the emission duration of pions [Pra86, Ber88, Ber89, Sch92, Bol93b, Bol93a, Ris96b]. This phenomenon should then depend on the critical temperature T_c and the latent heat of the transition. Typically, calculations assuming a first order phase transition are carried out with an equation of state derived from matching the bag model with an ideal hadron gas model, for which the latent heat of the transition is large [Sch92, Bol93b, Bol93a, Ris96b]. Consequently, the predicted HBT radii were large. As has been shown in section 4.3, the different parametrizations of the chiral model show a strong (CIII) and a weak (CII) first order phase transition as well as a smooth crossover (CI). By using these different models, we can study the influence of the EoS and the phase transition on the space time characteristics of the expansion and on the HBT radii [Zsc02b]. A smooth transition (crossover) at high temperatures was also considered in [Ris96b], however without explicit reference to chiral symmetry restoration and dynamical hadron masses. The equations of fluid dynamics describe the collective evolution of the system, while the chiral $SU(3) \times SU(3)$ model yields the underlying equation of state. Thus, as the hot and dense central region expands both in the longitudinal and transverse directions, the hadrons approach their vacuum masses. The initial excitation energy is converted into both, collective flow *and* massive hadrons. Using the various equations of state in a hydrodynamic simulation should discriminate between the different phase transition scenarios. Since the model only contains hadronic degrees of freedom, we only test the influence of the chiral phase transition but not of the deconfinement phase transition. In any case, the main effect as far as collective expansion is concerned, is due to the difference in the latent heat for the transition, irrespective of its microscopic origin.

6.2 Scaling hydrodynamics

Ideal Hydrodynamics is defined by (local) energy-momentum and net charge conservation [Lan59],

$$\partial_\mu T^{\mu\nu} = 0 \quad , \quad \partial_\mu N_i^\mu = 0 \quad . \tag{6.1}$$

$T^{\mu\nu}$ denotes the energy-momentum tensor, and N_i^μ the four-current of the ith conserved charge. We will explicitly consider only one such conserved charge, the

net baryon number. We implicitly assume that the local densities of all other charges which are conserved on strong-interaction time scales, e.g. strangeness, charm, and electric charge, vanish. The corresponding four-currents are therefore identically zero, cf. eq. (6.2), and the conservation equations are trivial.
For ideal fluids, the energy-momentum tensor and the net baryon current assume the simple form [Lan59]

$$T^{\mu\nu} = (\epsilon + p)\, u^\mu u^\nu - p g^{\mu\nu} \quad , \quad N_B^\mu = \rho_B u^\mu \quad , \tag{6.2}$$

where ϵ, p, ρ_B are energy density, pressure, and net baryon density in the local rest frame of the fluid, which is defined by $N_B^\mu = (\rho_B, \vec{0})$. $g^{\mu\nu} = \mathrm{diag}(+,-,-,-)$ is the metric tensor, and $u^\mu = \gamma(1, \vec{v})$ the four-velocity of the fluid ($\vec{v}$ is the three-velocity and $\gamma = (1 - \vec{v}^2)^{-1/2}$ the Lorentz factor). The system of partial differential equations (6.1) is closed by choosing an equation of state (EoS) in the form $p = p(\epsilon, \rho_B)$, cf. below.
For central collisions at high energy (such as at CERN-SPS and BNL-RHIC energies) around midrapidity, the assumpion of boost-invariant, cylindrically symmetric transverse expansion should be reasonable [Kaj83a, Kaj82, Bjo83, Bay83, Kaj83b]. This leads to an (approximately) rapidity independent energy density and a longitudinal scaling flow profile, $v_z = z/t$.
A quantitative comparison to experimental data, which we postpone to a future publication, should however analyze the effects due to coupling of longitudinal and transverse flows around midrapidity. At least up to CERN-SPS energies, $\sqrt{s} \sim 20A$ GeV, such a coupling was shown to exist [Stö82, Stö94, Ven94, Dum95, Sch96b, Bra00, Mor00].
The hydrodynamic equations of motion are solved on a discretized space-time grid ($\Delta r_\mathrm{T} = R_\mathrm{T}/100 = 0.06$ fm, $\Delta\tau = 0.99\Delta r_\mathrm{T}$) by employing the RHLLE algorithm as described and tested in [Ris96b, Ris95]. We have checked that the algorithm accurately conserves total energy and baryon number, and that profiles of rarefaction and shock waves are reproduced accurately for various initial conditions [Dum99, Ris95, Ris96a].
As already mentioned above, eqs. (6.2), we assume a perfect, i.e., nondissipative, relativistic fluid. In principle, it is possible to calculate the transport coefficients from the Lagrangean of our model [Pap99, Zsc00b]. (For example, various transport coefficients have been computed in the symmetry broken phase

based on the assumption of an ideal gas of hadrons [Wel92, Pra93, Hag94].) Also, dynamical simulations indicate that dissipation strongly affects the pion correlation functions at small relative momentum, and thus the deduced HBT radii [Sof01, Bas99a, Tea03]. Quantitative comparisons to experimental data should therefore account for dissipative effects. On the other hand, the purpose of this work is to explore the effects from varying the latent heat and the order of the phase transition. In that vein, we can leave aside the great technical and principal difficulties related to a treatment of dissipation in dynamical simulations [Mur02], and give an impression of the largest possible effects of varying the phase transition parameters that can be expected. This will also allow for a comparison to previous results for the pion HBT correlation functions, which employed ideal fluid dynamics with an EoS derived from the bag model [Sch92, Bol93b, Bol93a, Ris96b].

6.3 Chiral EoS for hydrodynamics

To close the system of coupled equations of hydrodynamics, an equation of state (EoS) has to be specified. Lattice QCD predicts chiral symmetry restoration at a critical temperature of $T_c = 140 - 170$ MeV [Bro90, Iwa96, Lae96] (for $\rho_B = 0$). We use the equation of state from the chiral $SU(3) \times SU(3)\sigma$-ω model that was discussed in detail in section 4.3. As already mentioned in section 6.2, the thermodynamic quantities like the pressure or the entropy must be given in terms of the energy density and the baryon density. Since this is difficult to obtain in a direct selfconsistent calculation, the thermodynamic functions are stored in a table and obtained by interpolation during the hydrodynamical calculation. The obtained pressure as a function of baryon density and energy density for the different scenarios is plotted in figures 6.1,6.2, and 6.3. As can be seen, for CI no phase transition occurs, but the pressure continously increases as a function of baryon density and energy density. In contrast, for CII the pressure stays nearly constant as a function of density in the phase transition region, corresponding to the mixed phase[2]. In addition, the values of the pressure are always lower

[2]Strangeness neutrality is a global constraint, only [Gre87, Gre88, Gre91, Spi98]. Within a mixed phase, however, the individual phases may adopt nonzero values for f_s. This may lead

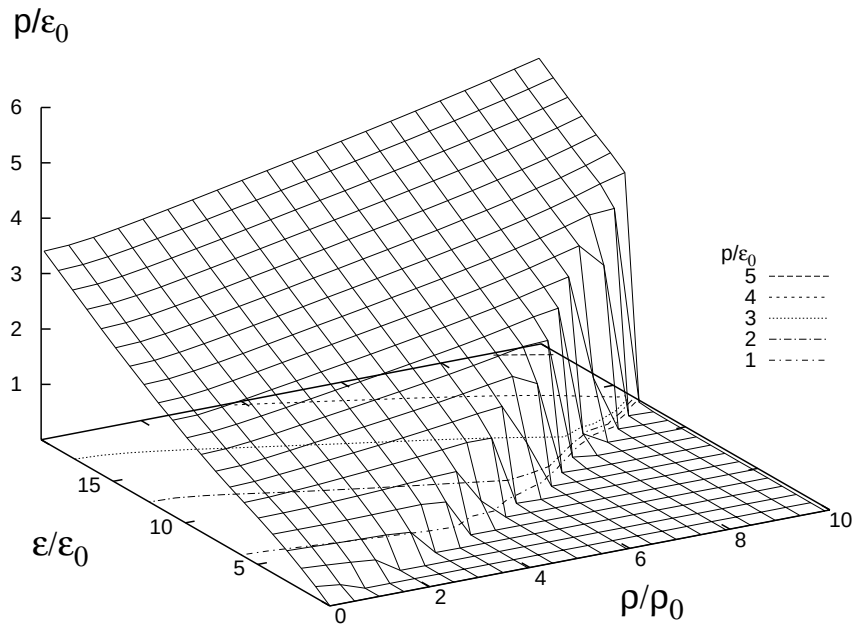

Figure 6.1: Pressure as a function of baryon density ρ and energy density ϵ for CI.

than for CI if the same energy density and baryon density are considered. These observations are even more obvious for parameter set CIII. In this case the two phase transitions lead to two areas of nearly constant pressure corresponding to the two domains where mixed phase exists. Furthermore, the pressure for CIII is considerably lower than for CI and CII for a given baryon and energy density.
The different phase transition behaviour of the three models is also reflected in the velocities of sound (figure 6.4). The crossover EoS shows a decrease of c_s^2 around $\epsilon = 1\text{GeV/fm}^3$. This is due to the strong reduction of the baryonic masses around the phase transition region. However, because the latent heat is zero in the crossover case, c_s^2 remains finite. In contrast c_s^2 vanishes in the phase transition regions for CII and CIII (however, it is nonzero if $\mu_q, \mu_s > 0$). The latent heat for

to a slight change of the pressure in the mixed phase.

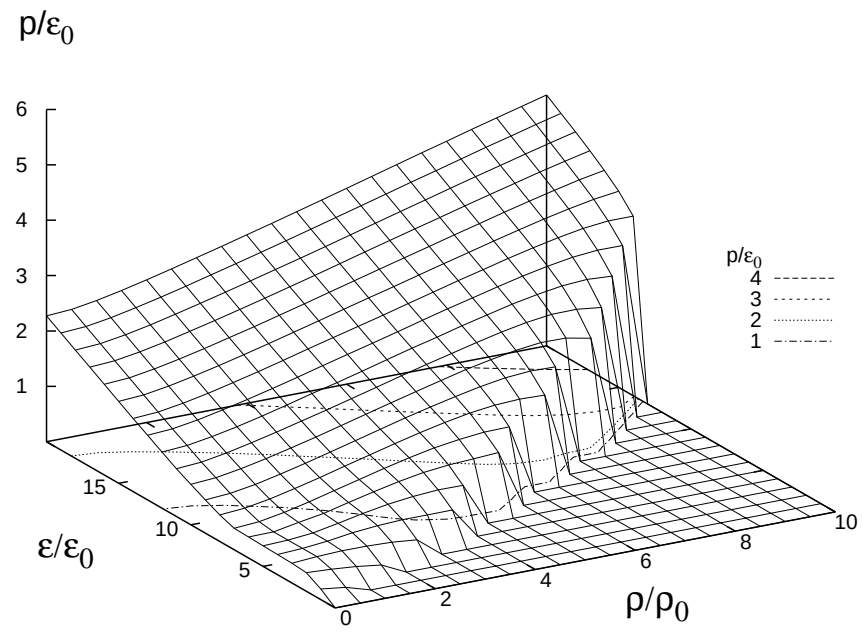

Figure 6.2: Pressure as a function of baryon density ρ and energy density ϵ for CII.

CII is $\Delta E_{II} \approx 600\text{MeV/fm}^3$, while it is $\Delta E_{III} \approx 850\text{MeV/fm}^3 + 920\text{MeV/fm}^3 = 1770\text{MeV/fm}^3$ for CIII (Both values are for $\mu_q = \mu_s = 0$). Between the two distinct first order transitions in model CIII, c_s^2 is nonzero again. However, this happens in a very narrow interval of energy density, and plays no significant role in our analysis.

As already discussed in section 4.3 (Fig 4.13), the occurence of a first order phase transition depends on the chemical potential. The energy densities and entropy densities in the phase transition regions have already been specified in table 4.1. The effective thermodynamic potential for parameter set CII around the phase transition temperature T_c is depicted on the r.h.s of figure 6.4. We observe that the effective thermodynamic potential varies very rapidly around T_c. The spinodal points, i.e., the temperatures at which the inflection points for the two minima

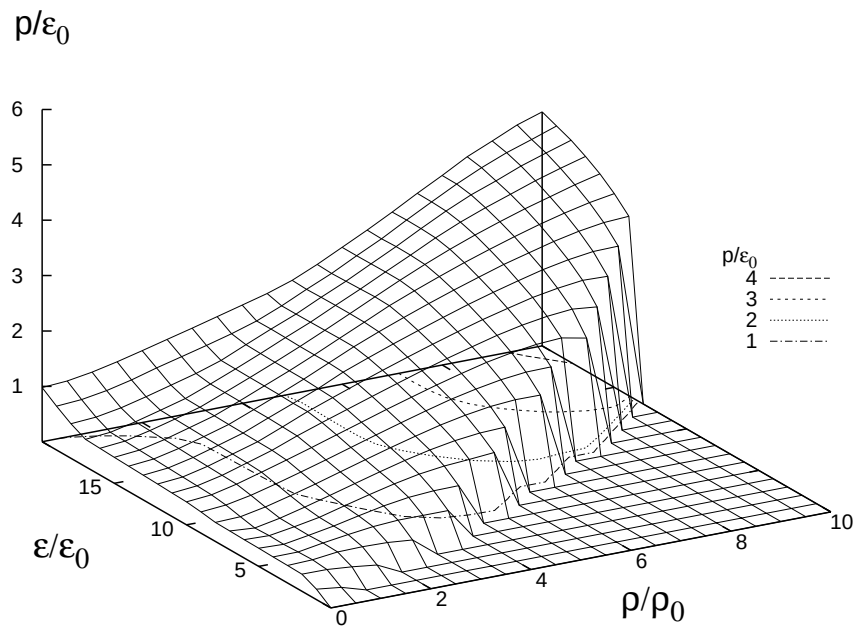

Figure 6.3: Pressure as a function of baryon density ρ and energy density ϵ for CIII.

appear, are only $2-3\%$ off T_c. This potential therefore varies substantially faster than that from the Gross-Neveu model or from the $SU(2)$ linear sigma model investigated in [Cho01, Sca01a]. However, the variation of the potential around T_c obtained from our model is in the same range as for the model used in [Dum01, Sca01b], where the authors showed that such a fast variation of the effective potential around T_c might lead to explosive behavior via rapid spinodal decomposition with supercooling (as opposed to an adiabatic phase transition). This questions the applicability of our approach of equilibrium hydrodynamics. In principle, one should study the real-time, nonequilibrium dynamics of the long wavelength modes of the chiral fields,i.e., the order parameters, coupled to the expansion of the matter fields [Pae03b]. However, as a first approximation, we study the effects dynamically, assuming that local equilibrium does hold, i.e. that

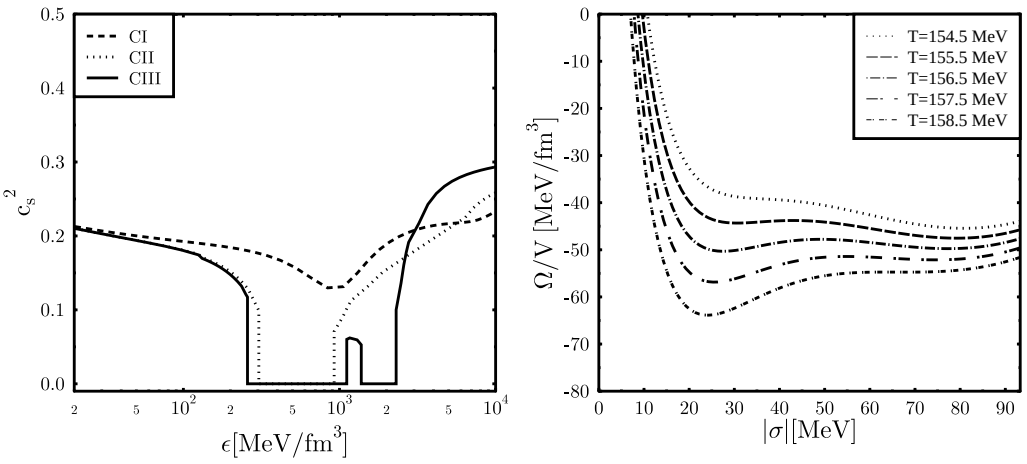

Figure 6.4: Left: $c_s^2 \equiv \partial p/\partial\epsilon$ for three different equations of state at $\mu_q = \mu_s = 0$. Right: Effective Potential $\Omega/V \equiv -p$ as a function of the scalar condensate σ around T_c. For parameter set CII and $\mu_q = \mu_s = 0$ (ζ has been chosen such as to maximize the pressure for given σ).

the mean-fields in fact assume the value of the global minimum of the potential, and that at the critical temperature two phases (corresponding to the two minima of the effective potential) coexist.

6.3.1 Initial Conditions

The initial conditions in scaling hydrodynamics are specified on a proper-time hyperbola $\tau = \tau_i$. On that space-like hypersurface one has to specify the entropy per net baryon and the net baryon rapidity density at midrapidity, dN_B/dy. A model with an MIT bag model equation of state [Cho74] for the high temperature phase and an ideal hadron gas in the low-temperature region can reproduce both [Dum99], the measured transverse energy at midrapidity, and the p_{T}-spectra of a variety of hadrons at $\sqrt{s} = 17.4A$ GeV (CERN-SPS energy), assuming the standard thermalization (proper) time $\tau_i = 1$ fm/c, and a specific entropy of $s/\rho_B = 45$ and a net baryon rapidity density $dN_B/dy = 80$. This value for s/ρ_B is also in good agreement with the measured relative abundances

of hadrons [Let93, Bra99, Zsc00a]. The initial net baryon density follows as $\rho_B = 4.5\rho_0$. The corresponding values of ϵ_i, T, μ_q and μ_s (q- and s-quark chemical potential respectively) for the various chiral EoS are listed in table 6.1.

		ϵ/ϵ_0	p/ϵ_0	T[MeV]	μ_q[MeV]	μ_s[MeV]
SPS	CI	49.2	10.5	256.0	236.2	133.0
	CII	40.2	6.6	197.0	241.3	58.6
	CIII	37.3	5.9	180.6	246.6	36.4
RHIC	CI	127.9	29.3	313.3	138.4	95.8
	CII	100.4	21.4	242.0	151.6	60.9
	CIII	93.7	22.0	230.0	154.6	53.0

Table 6.1: Initial conditions for the three chiral EoS, corresponding to $s/\rho_B = 45$ and $dN_B/dy = 80$ for CERN-SPS energy and $s/\rho_B = 200$ and $dN_B/dy = 25$ for BNL-RHIC energy. $\epsilon_0 = 138.45$ MeV/fm^3 is the energy density of nuclear matter in the ground state. Here, ϵ and s/ρ_B denote the average values at midrapidity at the initial time τ_i, i.e. the mean of the respective transverse distribution. The other quantities have been computed from those average values for ϵ and s/ρ_B, using the corresponding EoS.

The initial net baryon density is independent of the underlying EoS because the continuity equation for the net baryon current in (6.1) does not involve the pressure p explicitly.

Due to the higher density at midrapidity, thermalization may be faster at BNL-RHIC energies – following [Ris96b] we assume $\tau_i = 0.6$ fm/c. Various microscopic models, e.g. PCM [Gei93], RQMD [Sch93], FRITIOF 7.02 [Ger95], and HIJING/B [Van98], predict a net baryon rapidity density of $dN_B/dy \approx 20 - 35$ and specific entropy of $s/\rho_B \approx 150 - 250$ in central Au+Au at $\sqrt{s} = 130$AGeV at midrapidity. We will employ $s/\rho_B = 200$ and dN_B/dy=25. The resulting baryon density at midrapidity is $\rho_i = 2.3\rho_0$. Hadron multiplicity ratios at midrapidity can be described with these initial conditions [Xu02, Bra01]. The energy density and baryon density are initially distributed in the transverse plane according to a so-called "wounded nucleon" distribution with transverse radius $R_\mathrm{T} = 6$ fm. For further details, we refer to refs. [Dum99, Sof01, Bas99a, Tea03]. As seen from table 6.1, the initial energy density more than doubles when going

from CERN-SPS energy to BNL-RHIC energy. The initial temperature increases by about 50 MeV, while the initial chemical potential for u and d quarks decreases by about 100 MeV, in all cases. Note that for a bag model EoS the chemical potential for s quarks vanishes because of strangeness neutrality in the QGP phase, see e.g. [Dum99]. Strangeness neutrality is a global constraint, only [Gre87, Gre88, Gre91, Spi98]. Within a mixed phase, however, the individual phases may adopt nonzero values for f_s. In a hadronic model, the hyperons contain nonstrange quarks and adopt a finite chemical potential if $\mu_q \neq 0$. Therefore, the hyperon vector density is positive at finite temperature. This surplus of strange quarks contained in the hyperons is balanced by the strange antiquarks in strange mesons. This leads to a finite strangeness chemical potential μ_s, which is adjusted to yield $n_s = n_{\bar{s}}$. Here $n_s, n_{\bar{s}}$ denote the total number of strange and strange antiquarks in the system, respectively. As already discussed in [Gre87, Gre88, Gre91, Spi98], in the mixed phase only the total strangeness fraction f_s vanishes, while each of the two coexisting phases does, in general, carry net strangeness. Furthermore, for the case of a strong first order phase transition the evaporation of pions and kaons and strangeness distillation [Gre87, Gre88, Gre91, Spi98] should be studied, since these influence the unlike particle correlations (e.g. K^+/K^-, see [Sof97, Ard99]).

6.4 Results

6.4.1 Hypersurfaces

Before presenting results on pion correlations, in this section we shall discuss the effects from varying the latent heat in the EoS on the space-time evolution of the hadronic fluid. Qualitatively, the same effects are observed for both sets of initial conditions, and we therefore show only the results corresponding to the BNL-RHIC case. Figure 6.5 shows the calculated hypersurfaces at fixed temperature, $T = T_{\rm f}$, in the transverse plane at rapidity $\eta = 0$ for the three chiral EoS.
Comparing the freeze-out curves for the different equations of state one finds that the phase-transition behavior of the three parameter sets is reflected in the space-time evolution of the system. In case I (crossover) the time until freeze-out is shorter than in case III (two first order phase transitions). This is not surprising,

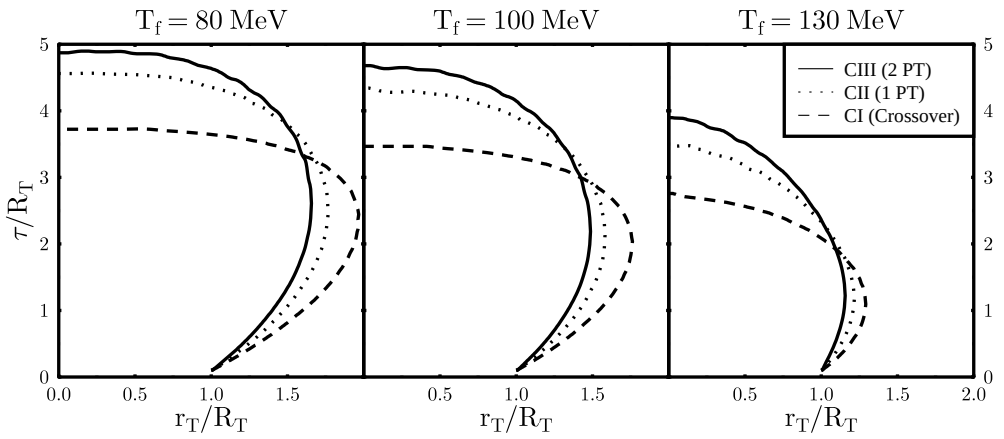

Figure 6.5: Hypersurfaces $T = T_{\rm f}$ for the three chiral EoS. This figure corresponds to initial conditions as appropriate for central Au+Au collisions at BNL-RHIC energy ($\sqrt{s} = 130$AGeV).

since the occurence of a mixed phase prolongs the expansion time. This is due to the above-mentioned drop of the speed of sound, c_s. The fastest expansion is obtained for a crossover with no latent heat and, accordingly, no discontinuity in the entropy density.

The different space-time evolutions for the three EoS are most obvious for $T_{\rm f} = 80$ MeV and $T_{\rm f} = 100$ MeV but can also be seen for $T_{\rm f} = 130$ MeV. For CERN-SPS energies we obtained similar results, with only slightly smaller lifetimes and radial extensions.

6.4.2 Two particle correlations

The correlation function $C_2(\mathbf{p}_1, \mathbf{p}_2)$ of two identical particles of momenta $\mathbf{p}_1$ and $\mathbf{p}_2$ is defined as

$$\begin{aligned} C_2(\mathbf{p}_1, \mathbf{p}_2) &= \frac{P_2(\mathbf{p}_1, \mathbf{p}_2)}{P_1(\mathbf{p}_1) \cdot P_1(\mathbf{p}_2)} \\ &= \frac{\mathrm{Tr}\left(\hat{\rho} a^\dagger(\mathbf{p}_1) a^\dagger(\mathbf{p}_2) a(\mathbf{p}_2) a(\mathbf{p}_1)\right)}{\mathrm{Tr}\left(\hat{\rho} a^\dagger(\mathbf{p}_1) a(\mathbf{p}_1)\right) \cdot \mathrm{Tr}\left(\hat{\rho} a^\dagger(\mathbf{p}_2) a(\mathbf{p}_2)\right)}, \end{aligned} \tag{6.3}$$

where $P_1(\mathbf{p})$ and $P_2(\mathbf{p}_1, \mathbf{p}_2)$ are the single and double inclusive cross sections, respectively. The density matrix of the multiparticle system is denoted as $\hat{\rho}$ and $a^\dagger(\mathbf{p})$, $a(\mathbf{p})$ are the creation and annihilation operators for momenttum $\mathbf{p}$, respectively. To calculate the two particle correlation function we use the method developed in [Shu73, Gyu79, Mak88, Ham88, Pra86, Ber88, Ber89, Sch92]. The higher order matrix elements can be expressed in terms of two-point functions $< a^\dagger(\mathbf{p_i})a(\mathbf{p_j}) >$ for a purely chaotic pion source, giving [Sch92]

$$C_2(\mathbf{p}_1, \mathbf{p}_2) = \frac{< a^\dagger(\mathbf{p_1})a(\mathbf{p_2}) >< a^\dagger(\mathbf{p_2})a(\mathbf{p_1}) >}{< a^\dagger(\mathbf{p_1})a(\mathbf{p_1}) >< a^\dagger(\mathbf{p_2})a(\mathbf{p_2}) >}. \tag{6.4}$$

This factorization is possible for bosons, if no single particle mode p_i is macroscopically occupied, i.e., all $< n_i >$ are $\ll 1$. Since the pions undergo considerable rescattering in the excited matter produced in relativistic heavy ion collisions, the phase correlations among them are destroyed and the factorization (6.4) is expected to hold [Bay98]. The two-point functions can be written in terms of the Wigner-function, $g(x_\mu, p^\mu)$, as follows:

$$< a^\dagger(\mathbf{p_i})a(\mathbf{p_j}) >= \int \mathrm{d}^4x \exp\left[\mathrm{i}x_\mu(p_i^\mu - p_j^\mu)\right] g\left(x_\mu, \frac{1}{2}(p_i^\mu + p_j^\mu)\right). \tag{6.5}$$

The analogy between the Wigner function and the classical phase space distribution can be used to obtain an expression for $g(x_\mu, p^\mu)$ for a hydrodynamically expanding source [Pra84, Sch92]. It is assumed that the pion correlation function is determined on a hypersurface of given temperature T_f, where the pion mean free path supposedly becomes too large to maintain local equilibrium. On this $T = T_\mathrm{f}$ hypersurface, the two-particle correlation function is then given by [Sch92, Bol93b, Bol93a, Ris96b]

$$C_2(\mathbf{p}_1, \mathbf{p}_2) = 1 + \frac{1}{\mathcal{N}} \left| \int \mathrm{d}\sigma \cdot K e^{i\sigma\cdot q} f\left(u \cdot K/T\right) \right|^2. \tag{6.6}$$

The normalization factor $\mathcal{N}$ is given by the product of the invariant single-particle inclusive distributions of the pions evaluated at momenta $\mathbf{p}_1$ and $\mathbf{p}_2$, respectively. u^μ denotes the four-velocity of the fluid on the $T = T_\mathrm{f}$ surface, σ^μ; $K^\mu = (p_1^\mu + p_2^\mu)/2$, $q^\mu = p_1^\mu - p_2^\mu$ are the average four-momentum and the relative four-momentum of the pion pair, respectively. As already mentioned above, at

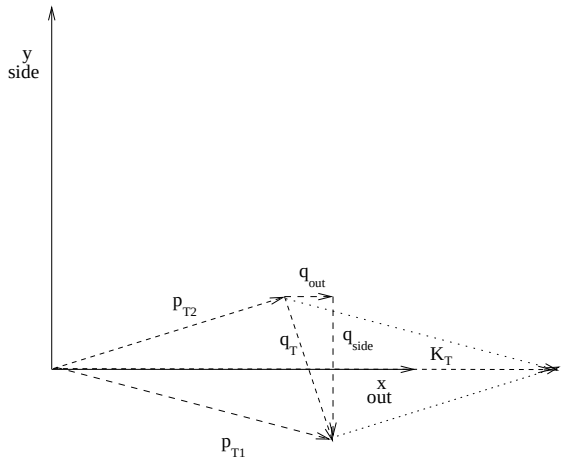

Figure 6.6: Different momenta in the "long-side-out" coordinate system

present we refrain from a detailed study of transport coefficients of our model. Rather, our approach shall be more pragmatic, and we shall consider T_f as a free parameter. The correlation function in general depends both on the relative momentum, q^μ, and on the mean momentum, K^μ, of the pion pair, cf. equation (6.6). Let q_long and K_long denote the components of $\mathbf{q}, \mathbf{K}$ in beam direction and $\mathbf{q}_\mathrm{T}, \mathbf{K}_\mathrm{T}$ the components transverse to that direction A three-dimensional coordinate system is chosen, where the *longitudinal* direction is along the beam axis, the *outward* axis (the x-direction) is along the transverse component of $\mathbf{K}$ and the y, or *side* axis, is in the direction perpendicular to K_T and the beam axis. Furthermore, q_out be the projection of the transverse momentum difference on the transverse momentum of the pair and q_side the component perpendicular to $\mathbf{K}_\mathrm{T}$. Then the correlation function depends on the five quantities $q_\mathrm{out}, q_\mathrm{side}, q_\mathrm{long}, K_\mathrm{T}, K_\mathrm{long}$.
To analyse HBT data, the most straightforward way is to parametrize the correlation function C_2 as a Gaussian in the momentum variables [Bay98]. By this, one can relate the inverse widths of the correlation functions to radius parameters. The chosen coordinate system suggests a parametrization of the correlation function in terms of four radii [Cha95]

$$\begin{aligned} &C_2(q_\mathrm{out}, q_\mathrm{side}, q_\mathrm{long}, K_\mathrm{T}, K_\mathrm{long}) = \\ &1 + \exp\left[-q_\mathrm{out}^2 R_\mathrm{out}^2 - q_\mathrm{side}^2 R_\mathrm{side}^2 - q_\mathrm{long}^2 R_\mathrm{long}^2 - q_\mathrm{long} q_\mathrm{out} R_\mathrm{long} R_\mathrm{out}\right]. \end{aligned} \quad (6.7)$$

The inverse width of the correlation function in out-direction ($R_{\rm out}$) increases with the duration of the particle emission, i.e. the lifetime of the source [Pra84, Pra94, Pra86, Ber88, Ber89]. Analogously, the inverse width of the correlation function in side-direction ($R_{\rm side}$) is a measure for the (transverse) size of the source. It was pointed out in [Ris96b] that both for model calculation as well as for experimental data it is tedious, if not impossible, to relate $R_{\rm side}$ and $R_{\rm out}$ to the real source size and lifetime. However, the ratio $R_{\rm out}/R_{\rm side}$ can be used as a measure for the lifetime of the system.

The HBT radii shown below are obtained as follows. In (6.6), f denotes the local distribution function of pions in momentum space, at a temperature $T_{\rm f}$. For simplicity, we shall assume a thermal distribution function and neglect the interaction energy of the pions, which amounts to only a $\sim 5\%$ correction relative to the vacuum mass of the pion. For midrapidity pions, $K_{\rm long} = q_{\rm long} = 0$. Thus, for the cylindrical geometry, the correlation function depends on three variables only; that is, the *out* and *side* components of q, and the transverse momentum of the pion pair, $K_{\rm T}$. Hence, for a given value of $K_{\rm T}$ we define side- and out- correlation functions as $C_{2,side}(q_{\rm side}) \equiv C_2(K_{\rm T}, 0, q_{\rm side})$ and $C_{2,out}(q_{\rm out}) \equiv C_2(K_{\rm T}, q_{\rm out}, 0)$, respectively. The corresponding inverse widths or HBT radii for a given $K_{\rm T}$ are determined as $R_{\rm out} = \sqrt{\ln 2}/q^*_{\rm out}$ and $R_{\rm side} = \sqrt{\ln 2}/q^*_{\rm side}$, where $q^*_{\rm out}$, $q^*_{\rm side}$ are defined by $C_{2,out}(q^*_{\rm out}) = C_{2,side}(q^*_{\rm side}) = 3/2$. The determination of the width is sufficient for the extraction of the radius parameters, since the Gaussian gives a very good approximation of the correlation function, cf. figure 6.7.

In Fig. 6.8 we show the resulting HBT-radii $R_{\rm side}$ and $R_{\rm out}$ for central Pb+Pb collisions at SPS energy ($\sqrt{s}/A = 17.4$ GeV), and compare to recent preliminary data obtained by the NA49 collaboration [Afa02a]. Of course, in view of the approximations mentioned above such a comparison should be interpreted with care. At $T_{\rm f} = 130$ MeV, $R_{\rm out}$ is reproduced reasonably well. In particular, it appears that the EoS with the largest latent heat overestimates $R_{\rm out}$. This is rather similar to the bag model EoS [Ris96b, Sof01, Bas99a, Tea03]. Note that $R_{\rm out}$ describes the size of the source folded with the mean emission duration [Wie99, Pra86, Ber88, Ber89, Sch92, Bol93b, Bol93a, Ris96b, Sof01, Bas99a, Tea03, Pra84, Pra94]. The average radius of the pion source decreases with increasing latent heat, but the emission duration increases. Integrating over the emission surface, Fig. 6.8 shows that for $K_{\rm T} \geq 50$ MeV the latter dominates in

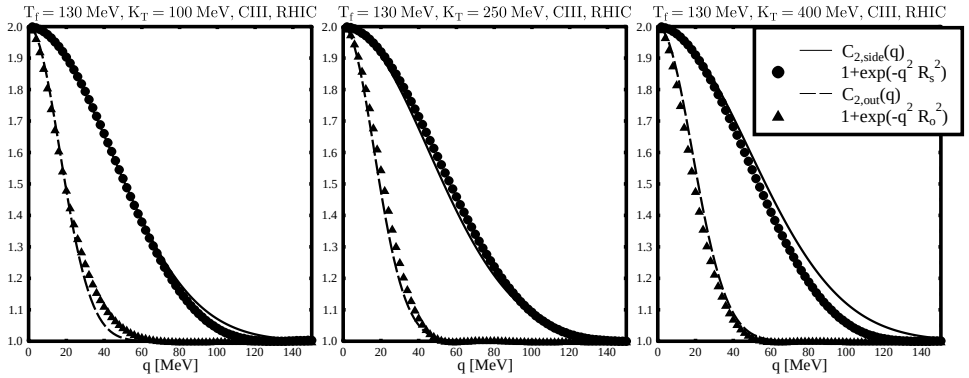

Figure 6.7: Comparison of calculated correlation functions $C_{2,side}(q_{\rm side})$ and $C_{2,out}(q_{\rm out})$ for $T_{\rm f}$ = 130MeV with the Gaussians determined by the extracted radius paramters $R_{\rm out}$ and $R_{\rm side}$, respectively.

case of longitudinal scaling expansion, and $R_{\rm out}$ increases with the latent heat of the chiral transition. The EoS with vanishing or small latent heat is closest to the data.

At $T_{\rm f}$ = 80 MeV and $T_{\rm f}$ = 100 MeV, the pion source has expanded further and hence $R_{\rm out}$ is larger. At large $K_{\rm T}$, the EoS with first order phase transition predicts too large values for $R_{\rm out}$ for both values of $T_{\rm f}$. At small transverse momenta, on the other hand, all three EoS describe the data better than for the high freeze out temperature. This observation is in agreement with the results of ref. [Sof01, Bas99a, Tea03], which shows that due to dissipative effects particles which suffer soft hadronic rescatterings freeze out at much later times than particles subject to harder interactions. We can not account for that effect within our ideal-fluid model, but it can be mimicked by choosing a lower $T_{\rm f}$ at smaller $K_{\rm T}$. In any case, our main focus is on effects from the chiral phase transition. Our results suggest that a weakly first order transition, or a smooth crossover, can give a better description of $R_{\rm out}$ than a phase transition with large latent heat (as in the bag model).

$R_{\rm side}$ measures the geometric size of the pion source in the transverse plane [3], and does not depend on the emission duration [Wie99, Pra86, Ber88, Ber89, Sch92, Bol93b, Bol93a, Ris96b, Sof01, Bas99a, Tea03, Pra84, Pra94]. First, we

[3] More precisely, it corresponds to the scale of spatial homogeneity [Mak88, Ham88].

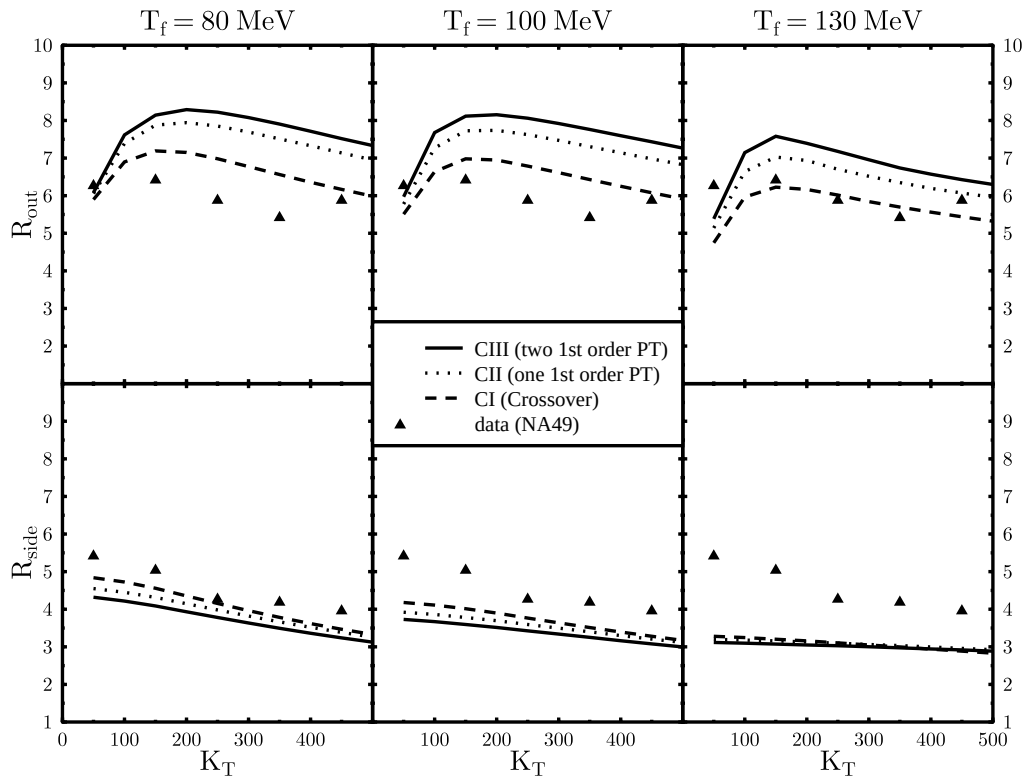

Figure 6.8: $R_{\rm side}$ and $R_{\rm out}$ as a function of $K_{\rm T}$ at SPS. $T_{\rm f} = 80, 100, 130$MeV.

note that the effective source radius depends only very weakly on the latent heat for the transition, in particular for large $T_{\rm f}$. This is in accord with the space-time evolution as described in 6.4.1. At small $K_{\rm T}$, $R_{\rm side}$ decreases slightly with the latent heat. However, for all three EoS, $R_{\rm side}$ comes out too small. Only for $T_{\rm f} = 80$ MeV a reasonable description is obtained. This could be partly due to the neglect of resonance decays, which form a "halo" surrounding the direct pion source [Gyu89, Sch92, Bol93b, Bol93a, Wie99, Cso96], and increase its effective size. On the other hand, the resonance decays would also tend to increase $R_{\rm out}$. As discussed in [Ris96b], a reasonable measure for the emission duration of pions therefore is the ratio $R_{\rm out}/R_{\rm side}$, which is also less affected by resonance decays. In Fig. 6.9 we show the results for initial conditions appropriate for BNL-RHIC energies. Both radii increase as compared to the lower SPS energy. That is

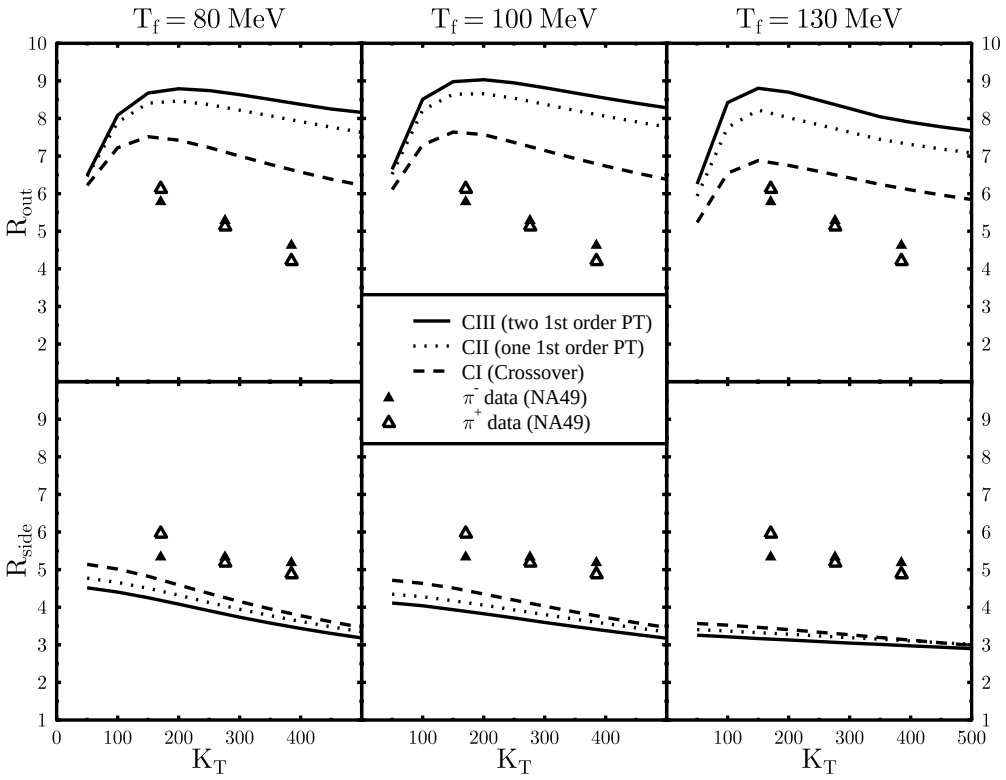

Figure 6.9: $R_{\rm side}$ and $R_{\rm out}$ as a function of $K_{\rm T}$ at RHIC. $T_{\rm f} = 80, 100, 130$MeV.

because the initial entropy density is significantly larger. Thus, the system takes longer to cool down to $T_{\rm f}$, and has more time to expand in the transverse direction. For example, at $K_{\rm T} = 500$ MeV, $R_{\rm out}$ increases by about 1 fm for the EoS with a strongly first order phase transition. $R_{\rm side}$ increases even less. This is in contrast to an EoS with only pions in the hadronic phase [Pra84, Pra94, Pra86, Ber88, Ber89, Ris96b], where the ratio of entropies of the two thermodynamic phases is very large at T_c. The very moderate increase of the radii from SPS to RHIC energy is in qualitative agreement with the results from STAR for Au+Au collisions at RHIC [Adl01]. On the other hand, as already discussed above, the "geometric size" of the source, $R_{\rm side}$, is too small. As at SPS energy, this could be due to decays of resonances. We shall therefore discuss next the behavior of the ratio $R_{\rm out}/R_{\rm side}$ with $K_{\rm T}$, which is less affected by decays [Ris96b], and which is a good

measure for the lifetime of the pion source.

Figures 6.10 and 6.11 show the experimentally measured ratio $R_{\rm out}/R_{\rm side}$ as a function of $K_{\rm T}$ for the three different equations of state for SPS and RHIC energies. One observes that at both energies the shortest lifetime of the sys-

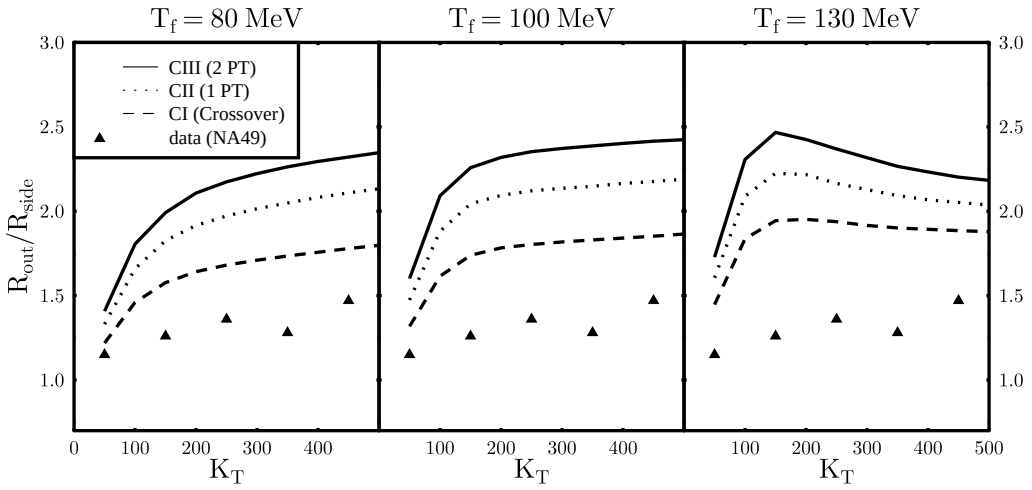

Figure 6.10: $R_{\rm out}/R_{\rm side}$ as a function of $K_{\rm T}$ at SPS.

tem emerges from the EoS featuring a crossover (CI), while the slowest expansion results from the EoS with largest latent heat (CIII). At SPS energy, the data [Afa02a] yield a slowly rising $R_{\rm out}/R_{\rm side}$ ratio. This is obtained for all three EoS, if the freeze-out temperature is low, $T_{\rm f} = 80, 100$ MeV. However, the absolute value of $R_{\rm out}$ is too large, while $R_{\rm side}$ is too small, and so the ratio comes out way too large. As is obvious from the figures, we are not able to reproduce the data for $R_{\rm out}/R_{\rm side}$, though a small or even vanishing latent heat and a smaller freeze-out temperature improve the picture. Turning to RHIC, we see that the predicted general behavior of $R_{\rm out}/R_{\rm side}$ is similar as at the SPS, except for a slight overall increase of that ratio. That is because the larger initial entropy per baryon, which is deduced from the larger π/p and $\bar{p}/p$ ratios, increases the lifetime of the system slightly. On the other hand, the STAR data [Adl01] show $R_{\rm out}/R_{\rm side} \simeq 1$, and a decrease with $K_{\rm T}$. This behavior can evidently not be reproduced for low $T_{\rm f}$. Larger freeze-out temperatures, $T_{\rm f} = 130$ MeV, lead to

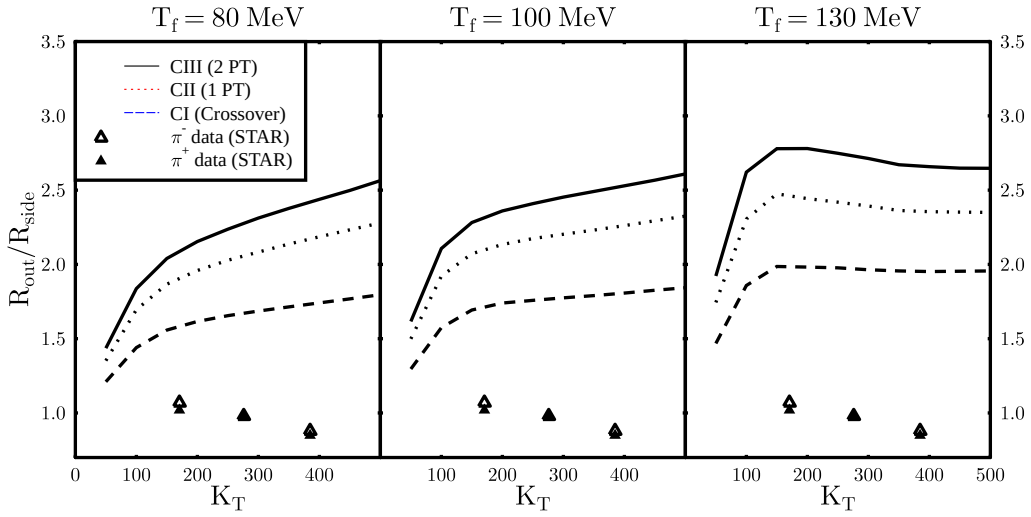

Figure 6.11: $R_{\rm out}/R_{\rm side}$ as a function of $K_{\rm T}$ at RHIC.

flat, or even slightly decreasing $R_{\rm out}/R_{\rm side}$. Nevertheless, $R_{\rm out}/R_{\rm side}$ is about a factor of 2 higher for $K_{\rm T} \geq 100$ MeV than seen in the STAR data.

In summary, a small latent heat, i.e. a weak first order chiral phase transition or even a smooth crossover, leads to larger emission regions and smaller emission duration, as well as to larger $R_{\rm side}$ and smaller $R_{\rm out}$ HBT radii than a strong first order transition, as for example assumed in the bag model.

In almost all cases, we observe that the results obtained with a crossover EoS are closest to the experimental data. However, a quantitative description of the data, both at SPS energy as well as at RHIC energy, is not possible within our present ideal-fluid approach with longitudinal scaling flow, employing the various SU(3) chiral EoS.

Apparently, conclusions can only be drawn after considerable improvements on various aspects of the description of high-energy heavy-ion collisions.

In particular, the effective chiral SU(3) potential is rather rapidly varying around T_c. Therefore, a nonequilibrium description, accounting for the coupling of the order parameters to the expanding fluid, supercooling effects and/or rapid spinodal decomposition, might be in order [Cho01, Sca01a, Dum01, Sca01b]. In fact, it has been argued that the decay of a droplet of chirally symmetric matter from

a region of negative pressure may yield smaller values for the HBT radii, as well as a smaller ratio $R_{\rm out}/R_{\rm side}$ [Cso94][4]. Such considerations are out of the scope of the current work but will be studied in detail in the future. More realistic freeze-out descriptions [Sof01, Bas99a, Tea03, Bug96, Mag99, And99] may improve the results. However, as dissipative effects are expected to prolong the lifetime of the pion source even more, it appears very likely that a quasi-adiabatic first order phase transition with large latent heat, for which a hydrodynamic description should be adequate, can not describe the pion HBT data from CERN-SPS and from BNL-RHIC. This observation may be viewed as an experimental confirmation of the predictions from lattice QCD [Bro90, Iwa96, Lae96], which do not show a large latent heat for the chiral transition at high T and moderate μ_B.

[4] Note, however, that within our effective theory for chiral symmetry restoration the spinodal instability occurs before negative pressure is reached, see Fig. 6.4 (left).

–VII–

Particle ratios from AGS to RHIC

7.1 General remarks

Thermodynamical equilibrium calculations of particle production in high energy particle and nuclear collisions have been carried out for a long time [Fer50, Lan53, Wes76, Stö78, Cse86, Hah86, Bra96, Let00, Raf01, Bec01, Bra01]. The hadron abundances and particle ratios have been measured in heavy ion collisions from SIS, AGS, SPS to RHIC energies. These data have revived the interest in the extraction of temperatures and chemical potentials from thermal equilibrium "chemical" model analyses. The experimentally determined hadron ratios can be fitted well with straightforward noninteracting gas model calculations [Bra96, Let00, Bra98, Cle99, Raf01, Bec01, Bra01], if a sudden breakup of a thermalized source is assumed and once the subsequent feeding of the various channels by the strongly decaying resonances is taken into account (for a detailed description of this approach see [Mic01, Bra03]). From the χ^2 freeze-out fits one has constructed a rather narrow band of freeze-out values in the T-μ_B plane (see e.g.[Bra98, Cle99]). The extracted freeze-out parameters are fairly close to the phase transition curve for SPS and RHIC energies. However, when these extracted freeze-out values are indeed so close to the phase transition or to a crossover, one should not neglect the in-medium effects which are the ob-

ject of investigation and which, after all, do produce the phase transition. Thus, since noninteracting gas models neglect any kind of possible in-medium modifications, they can not yield information about the phase transition. Contrary, the chiral $SU(3)_L \times SU(3)_R$ model embodies the restoration of chiral symmetry at high temperatures or densities and predicts temperature and density dependent hadronic masses and effective chemical potentials. Furthermore, three different phase transition scenarios are given by the three diffrent parametrizations CI, CII and CIII (section 4.3). Thus, using different versions of the chiral $SU(3)$ model we can investigate whether the freeze-out in fact takes place close to the phase transition boundary (if it exists) and if the extracted T-μ_B parameters are strongly model dependent.

7.2 Particle ratios in the chiral $SU(3) \times SU(3)$ model

Since the chiral $SU(3)$ model predicts density and temperature dependent hadronic masses and effective potentials, in contrast to noninteracting models, the resulting particle ratios and therefore the deduced freeze-out temperatures and baryon chemical potentials are expected to change [Zsc01a, Zsc02a]. Hence we identify combinations of temperatures and chemical potentials that fit the observed particle ratios in the chiral model. In all calculations the value of the strange chemical potential μ_S is chosen such that the net strangeness $f_s = 0$. We are looking for minima of χ^2 with

$$\chi^2 = \sum_i \frac{\left(r_i^{\text{exp}} - r_i^{\text{model}}\right)^2}{\sigma_i^2}. \tag{7.1}$$

Here r_i^{exp} is the experimental ratio, r_i^{model} is the ratio calculated in the model and σ_i represents the error in the experimental data points. At RHIC we use the same ratios as in [Bra01]:
$\bar{p}/p$, $\bar{\Lambda}/\Lambda$, $\bar{\Xi}/\Xi$, π^-/π^+, K^-/K^+, K^-/π^-, K_0^*/h^-, $\bar{K_0^*}/h^-$.
For SPS 158 AGeV the following ratios were used:
$K^+/K^-, K^+/(\pi^+ + \pi^-), \bar{\Lambda}/\Lambda, \Xi/\bar{\Xi}, \bar{\Omega}/\Omega, \bar{\Xi}/\Lambda, \Omega/\bar{\Xi}^-, \Lambda/(\pi^+ + \pi^-)$ [Afa02b, Bac99, Afa02c, Fri02, Afa02d].

For SPS 40 AGeV:
$K^+/K^-, K^+/(\pi^+ + \pi^-), \bar{\Lambda}/\Lambda, \Lambda/(\pi^+ + \pi^-)$ [Afa02b, Afa02c].
And for AGS 11.6 AGeV the considered ratios are:
$K^+/\pi^+, K^+/K^-, \Lambda/\pi^+, p/\pi^+, \bar{p}/p$,
taken from [Bec01].
Even though the only parameters in a thermal and chemical equilibrium approach on first sight are the temperature and the baryon chemical potential, there exist further unknowns: On the one hand, some decays of high mass resonances are not well known and on the other hand the effect of weak decays in the experiments strongly depends on the detector geometry and on the reconstruction efficiency of the experiments. The feeding correction from the strong and electromagnetic decays of the hadronic resonances used here employs the procedure used in the UrQMD model [Bas99b, urq] without isospin dependence. Weak decays are not considered here. We rather focus on the principal question whether an interacting chiral SU(3) approach with $m^* \neq m_{vac}$ can at all describe the particle yields from AGS to RHIC. Fine tuning of the χ^2 by adjustment of the weak decay scheme is not our intention. Even though it has been shown [Mic01] that χ^2 values may be improved by adjusting the treatment of the weak decays.
To compare the quality of the fits obtained in the chiral model with those obtained from the noninteracting gas approach, we set all masses and chemical potentials contained in the chiral model to their vacuum values and again use the same UrQMD feeding procedure as for the interacting model. This yields the ideal hadron gas model denoted $\mathrm{ig_{FFM}}$. We find that the resulting ratios are not identical but comparable to those obtained in the literature [Zsc01a, Mic01, Bra01, Flo02]. The differences should only result from a different treatment of weak interactions and from the uncertainty in the decay scheme of high mass resonances.

7.3 Results for Au+Au Collisions at RHIC

First, we find that a reasonable fit of the measured particle ratios at RHIC is possible in all three phase transition scenarios of the chiral model and the ideal gas case with comparable quality.

Second, the resulting freeze-out values depend significantly on the model employed, i.e., crossover, weak first order, strong first order or free thermal gas.
Third, a reasonable description of the data is impossible above T_c in the models showing a first order phase transition. This suggests that the system at RHIC emerges after the chiral phase transition. This of course is only true if a first order phase transition does actually occur in QCD at small chemical potentials and high T. "Freezing" of the relative abundances of various hadrons in the symmetric phase (at $T > T_c$) is thus excluded.
Figure 7.1 shows the value of χ^2 in the T-μ_B plane for the crossover case (CI) and for the strong first order phase transition (CIII). One observes that the best fit T-μ_B values differ in both models. Furthermore, in the crossover case χ^2 is well behaved as a function of T and μ_B. In contrast, the model with a strong first order phase transition shows a very steep increase of χ^2 at the phase transition boundary: The quality of the fit decreases drastically due to the jump of the effective masses at the phase transition boundary. Above T_c the χ^2 values are inacceptable, $\chi^2 > 500$. The resulting best-fit particle ratios, χ^2-values and thermodynamic quantities are shown in table 7.1 and figure 7.2, respectively. The χ^2 values for the chiral model are: $\chi^2_{\mathrm{CI}} = 5.5$, $\chi^2_{\mathrm{CII}} = 5.7$ and $\chi^2_{\mathrm{CIII}} = 5.4$. Thus, all three parameter sets describe the data equally well. Furthermore, the agreement is as good as in the noninteracting gas calculation ($\chi^2_{\mathrm{BMRS}} = 5.7$ [Bra01], $\chi^2_{\mathrm{FFM}} = 5.7$). The best fit T-μ_B parameters vary quite considerably between the different models. Our noninteracting gas calculation yields $T = 187.6$ MeV and $\mu_B = 44.1$ MeV. These freeze-out values can be compared to those obtained in other ideal gas calculations: $T = 174$ MeV, $\mu_B = 46$ MeV in [Bra01], $T = 165$ MeV, $\mu_B = 41$ MeV in [Flo02] and $T = 190$ MeV, $\mu_B = 45$ MeV in [Xu02]. The crossover case in the interacting chiral model (CI) yields $T = 170.8$ MeV, $\mu_B = 48.3$ MeV. Very strong deviations are found for the models with a first order phase transition (CII, CIII): The freeze-out temperatures are $T = 155$ MeV (CII) and $T = 153.3$ MeV (CIII), more than 30 MeV lower than for ig$_{\mathrm{FFM}}$. The fitted baryon chemical potentials μ_B increase by about 7-10 MeV. These T-μ_B pairs are very close to the phase boundary (CII) or even right on it (CIII) and are about 10 MeV higher than the values obtained at SPS energies [Zsc03]. Mainly due to the different freeze-out temperatures the values of the corresponding thermodynamic quantities vary between the different approaches.

Au+Au	Experiment	CI	CII	CIII	$\mathrm{ig}_{\mathrm{FFM}}$	BMRS
T_{chem} [MeV]		**170.8**	**155.0**	**153.3**	**187.6**	**174.0**
μ^B_{chem} [MeV]		**48.3**	**54.6**	**51.0**	**44.1**	**46.0**
μ^s_{chem} [MeV]		**11.1**	**9.8**	**9.4**	**13.5**	**13.6**
χ^2		**5.5**	**5.7**	**5.4**	**5.7**	**5.7**
ρ_{had} [fm^{-3}]		**0.66**	**0.38**	**0.35**	**1.12**	
$\rho_B + \rho_{\bar{B}}$ [fm^{-3}]		**0.15**	**0.08**	**0.07**	**0.28**	
p [MeV/fm^3]		**108**	**55**	**51**	**207**	
ϵ [MeV/fm^3]		**695**	**356**	**326**	**1324**	
E/A [MeV]		**1053**	**937**	**931**	**1182**	$\approx$ **1100**
S/A		**157**	**164**	**177**	**142**	
$\overline{p}/p$	0.65(7) [STAR] 0.64(8) [PHENIX] 0.60(7) [PHOBOS] 0.61(6) [BRAHMS]	0.640	0.648	0.652	0.629	0.629
$\overline{\Lambda}/\Lambda$	0.77(7) [STAR]	0.714	0.695	0.702	0.721	0.753
$\overline{\Xi}/\Xi$	0.82(8) [STAR]	0.787	0.731	0.743	0.834	0.894
π^-/π^+	1.00(2) [PHOBOS] 0.95(6)[BRAHMS]	1.000	1.000	1.000	1.000	1.007
K^-/K^+	0.88(5) [STAR] 0.78(13) [PHENIX] 0.91(9) [PHOBOS] 0.89(7) [BRAHMS]	0.919	0.914	0.915	0.916	0.894
K^-/π^-	0.15(2) [STAR]	0.183	0.168	0.168	0.179	0.145
$\overline{p}/\pi^-$	0.08(1) [STAR]	0.082	0.084	0.078	0.083	0.078
$\overline{K^*_0}/h^-$	0.058(17) [STAR]	0.055	0.049	0.049	0.046	0.032
K^*_0/h^-	0.060(17) [STAR]	0.049	0.044	0.044	0.041	0.037

Table 7.1: Chiral fit of the particle ratios measured at RHIC at $\sqrt{s} = 130$ GeV compared to ideal gas results. Data and BMRS-fit taken from [Bra01].

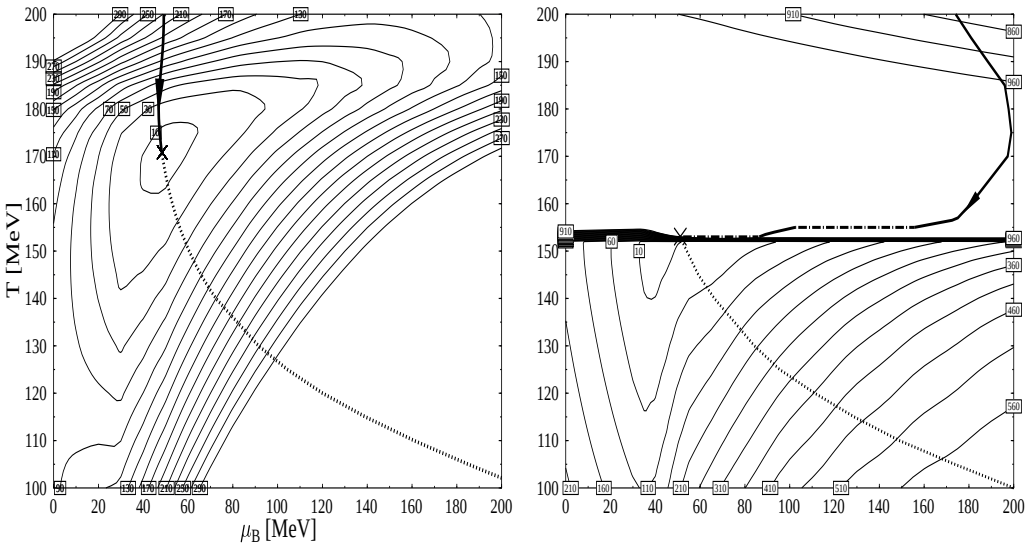

Figure 7.1: χ^2 contours in the T-μ_B plane for CI (left) and CIII (right). The deduced freeze-out values are marked with a cross ($\times$). Ratio data are taken from [Bra01]. On the left, the adiabatic path (constant entropy per net baryon S/A), corresponding to expansive cooling of an ideal fluid, is also shown. μ_S is chosen such that $f_s = 0$.

However, the energy per particle E/A is approximately 1 GeV in all cases. This "unified freeze-out" condition' has already been proposed in [Cle98].

The fact that the freeze-out appears right at the phase boundary or at crossover implies that there are large in-medium corrections, in particular for the effective masses, a phenomenon observed already in [The83]. The effective masses shown in figure 7.3 are shifted up to 15% from their vacuum values. However, all the interacting models show similar values for the effective mass of a given hadron. The strongest in-medium modifications are observed for the nonstrange baryons ($\Delta m_i^*/m_i \approx 15\%$). Mesons and strange baryons show smaller changes of the effective masses, e.g. about 10% for Λ, π, K^*, about 5% for the Kaons, and nearly no change for the Ξs.

These results, together with the steep χ^2 contours from fig. 7.1, suggest that the relative particle abundances "freeze" shortly after the spontaneous breaking of chiral symmetry. The success of our fit suggests extremely rapid chemical equilibration (through abundance-changing reactions) in the state with broken

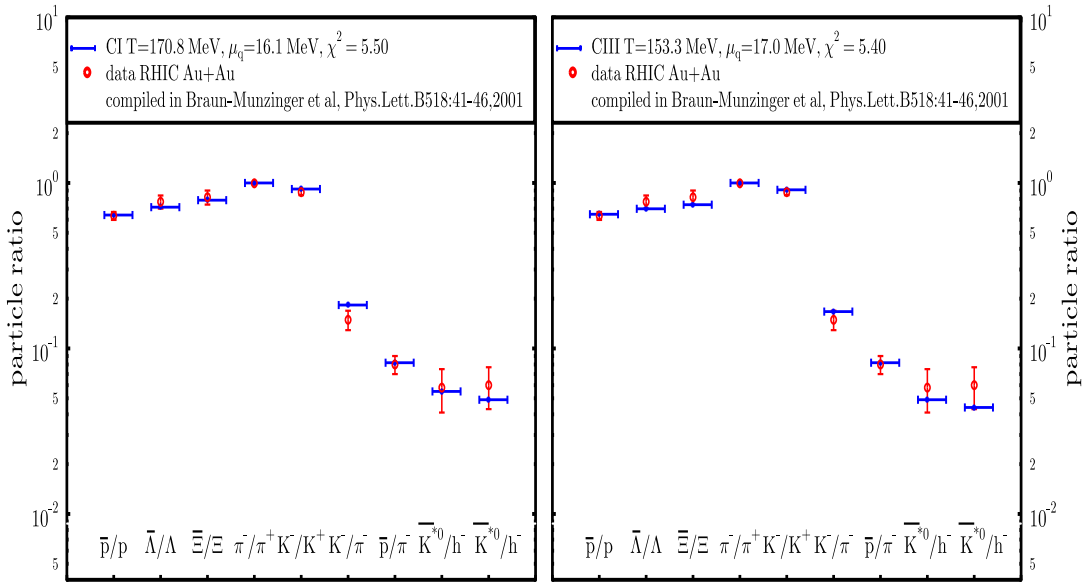

Figure 7.2: Particle ratios calculated with CI (left) and CIII (right) compared to RHIC data as compiled in [Bra01].

symmetry. Fig. 7.1 shows that the chemical composition of the hadronic system has to change substantially within a small temperature interval, just before freeze-out. This is even the case for the crossover transition (CI); for reference, we have indicated the dynamical path in the T-μ_B plane corresponding to the expansion of a perfect fluid, i.e., with constant entropy per net baryon [Sub86]). While $2 \to n$ reactions are perhaps too slow to explain such rapid chemical equilibration [Bas01, Bas00], $m \to n$ processes with several particles in the initial state may be important as well [Rap01, Gre01, Gre02b, Gre02a].
Alternatively, the appearence of chemical equilibrium right after the phase transition (or the crossover) to the state of broken chiral symmetry might just be the outcome of the dynamical symmetry breaking process itself [Sca02], with statistical occupation of the various hadronic channels according to phase space [Bec97, Bec98, Sto99b, Sto99a]. If so, number-changing reactions in the broken phase need not proceed at a high rate. To test this picture experimentally, it might be useful to consider central collisions of small ions like protons

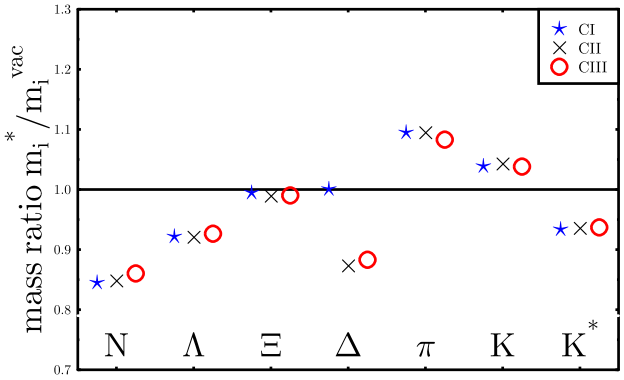

Figure 7.3: Effective masses for the different interacting chiral models and the ideal gas (vacuum values) case. The differences among the interacting approaches are less than 2%.

or deuterons, at similar energy and particle densities in the central region as for central Au+Au. For systems of transverse extent comparable to the correlation lengths of the chiral condensates, the dynamical symmetry breaking process should be different from that in large systems (for example, the mean-field approximation should not apply). The correlation lengths $\xi_{\sigma,\zeta}$ are given by

$$\xi_\sigma^{-2} = \frac{\partial^2 (\Omega/V)}{\partial \sigma^2} \,, \tag{7.2}$$

and accordingly for ξ_ζ. We evaluate the curvature of the thermodynamical potential at the global minimum for T, μ_B, μ_S at the freeze-out point. For parameter sets CI, CII, CIII we obtain $\xi_\sigma = 0.37$ fm, 0.41 fm, 0.40 fm, respectively. For the correlation length of the strange condensate we obtain $\xi_\zeta = 0.20$ fm in all three cases. The correlation lengths are not very much smaller than, say, the radius of a proton. Thus, even if the freeze-out point for high-energy p+p collisions happens to be close to that for Au+Au collisions at RHIC energies, the transition from the symmetry restored to the broken phase might be different. Finally, we also note that the correlation lengths obtained from our effective potential are not larger than the thermal correlation length $1/T$ at freeze-out, and so corrections beyond the mean-field approximation employed here should be analyzed in the future.

7.4 Particle ratios from AGS to RHIC

To obtain the so-called "freeze-out" curve in the T-μ plane, the best fits from AGS to RHIC energies are determined. Fig. 7.4 shows the deduced temperatures and chemical potentials for the different systems and energies[1]. First, one

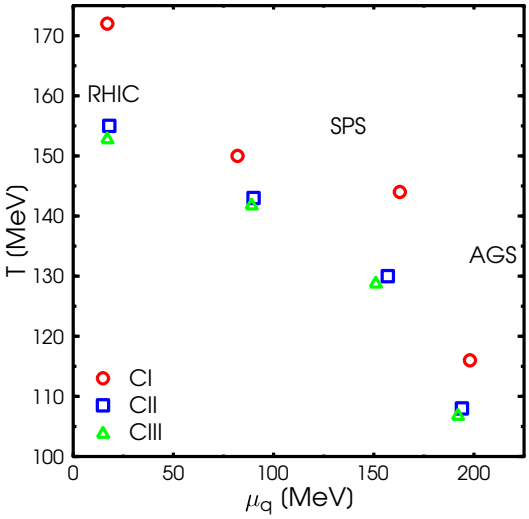

Figure 7.4: Freeze-out curve in the chiral model (CI, CII, CIII) for relativistic heavy ion collisions from AGS to RHIC.

observes that the freeze-out values are never above the phase transition line or its generalization for the crossover case, respectively. As already discussed above, for RHIC the deduced freeze-out occurs right at the phase transition border. For SPS 160 AGeV the freeze-out is slightly below the phase-transition or crossover, respectively and for lower energies further below. Thus, the chemically equilibrated hadron gas phase disappears with increasing energy. As already observed for RHIC, the deduced temperatures for the crossover case (CI) are always considerably above the values obtained in the two scenarios with a first order phase-transition (CII, CIII), while the μ_q values are nearly identical in all cases. This is also illustrated in figure 7.5, showing the temperature (left) and the chemical

[1]The investigation for 80 AGeV at SPS is not presented here since not enough data for a reasonable fitting procedure was available.

potential (right) as a function of center of mass energy $\sqrt{s}$. Furthermore, one ob-

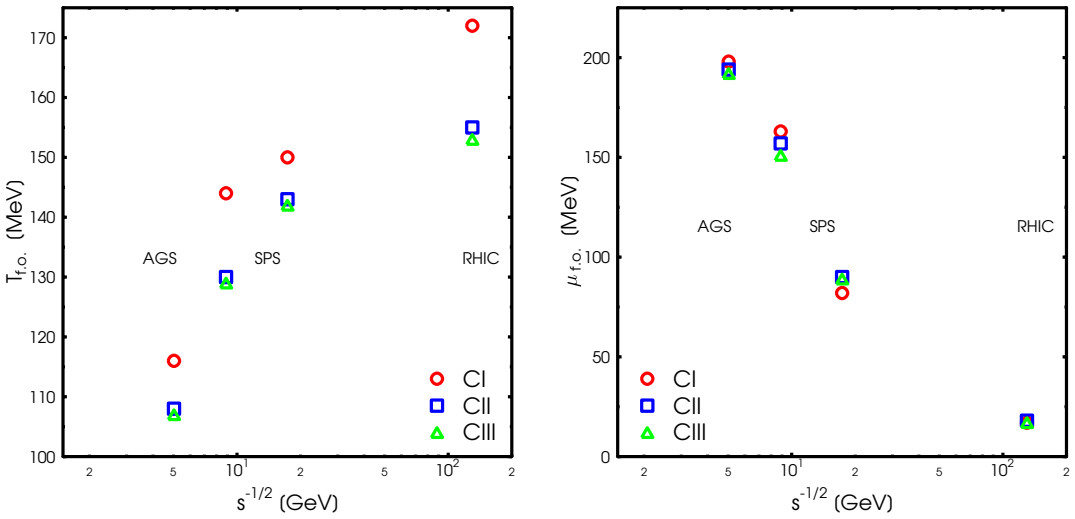

Figure 7.5: Freeze-out temperature (left) and chemical potential (right) as a function of $\sqrt{s}$ for CI, CII and CIII.

serves that with decreasing energy the freeze-out temperature decreases, and the freeze-out chemical potential increases, in accordance with the results from ideal gas calculations. Comparing the interacting and the noninteracting case (i.e., the freeze-out curve shown in [Bra03]), it turns out that the freeze out values for CI are close to those obtained in the ideal gas case. In contrast for CII and CIII considerably lower temperatures are extracted. This shows the uncertainty and the model dependence in the determination of the assumed freeze-out conditions. In general on can state that the stronger the phase transition for $\mu = 0$ in the chiral model is, the more the freeze-out temperature is lower compared to the ideal gas.

In figure 7.6 the predicted "freeze-out masses" are depicted as a function of $\sqrt{s}$. They differ by up to about 15% from their vacuum values. The biggest effect is observed for the nonstrange particles, in particular the nucleon and the pion. However, no simple functional dependence on the center of mass energy $\sqrt{s}$ is observed. Here again further studies are necessary to understand this behaviour, which might also result from the different sets of data available. Figure 7.6 (right)

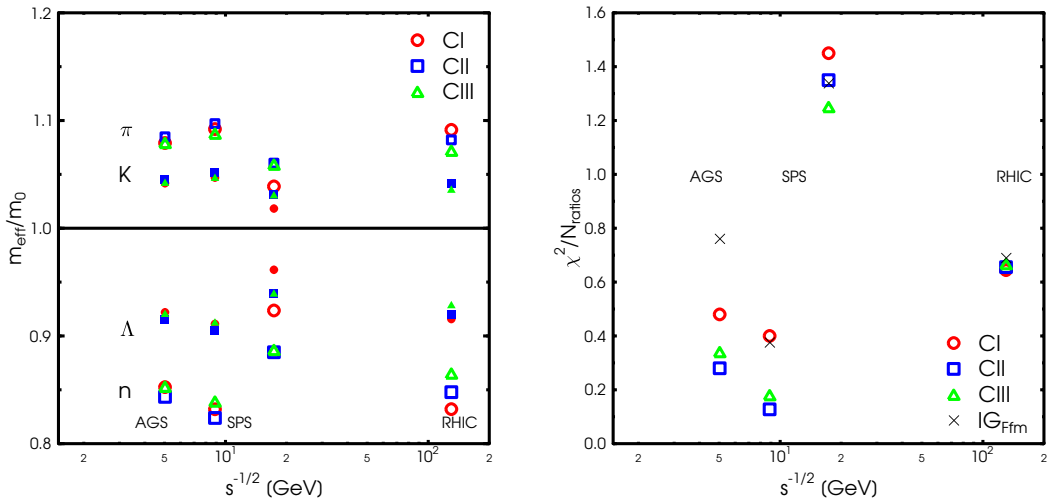

Figure 7.6: Effective masses of N, Λ, π, K (left) and χ^2 value (right) as a function of $\sqrt{s}$ for CI, CII and CIII.

shows the resulting χ^2 values for the different collision systems and energies. It can be seen that all three scenarios give a reasonable description of the data at all energies. If the "quality" of the fit is measured by the χ^2 value, all three parametrizations are equally "successful" in describing the data. The differences in the χ^2 values are too small to discriminate between the different scenarios.

–VIII–

In-medium vector meson properties

8.1 Motivation

The medium modifications of the vector mesons (ρ and ω) in hot and dense matter have recently been a topic of great interest in the strong interaction physics research, both experimentally [Mas95, Aga95, Aga98, Por97, Mor98, Str99] and theoretically [Bro91, Rap97, Rap00, Hat92, Hat95, Jin95b, Mal01, Kli97, Ern98]. One of the explanations of the experimental observation of enhanced dilepton production [Mas95, Aga95, Aga98, Por97] in the low invariant mass regime could be a reduction of the vector meson masses in the medium. It was first suggested by Brown and Rho that the vector meson masses drop in the medium according to a simple (BR) scaling law [Bro91], given as $m_V^*/m_V = f_\pi^*/f_\pi$. f_π is the pion decay constant and the asterisk refers to in-medium quantities. There have also been QCD sum rule approaches extensively used in the literature [Hat92, Hat95, Jin95b, Mal01, Kli97] for consideration of the in-medium vector meson properties. In the framework of Quantum Hadrodynamics (QHD) [Ser86] as a description of the hadronic matter, it is seen that the dropping of the vector meson masses has its dominant contribution arising from the vacuum polarisation effects in the baryon sector [Shi94, Hat96, Jea94, Sai98, Ala99]. This drop is not observed in the mean-field approximation. The vector meson properties [Mis02b] and their

effects on the low mass dilepton spectra [Mis02c] have been investigated recently including the quantum correction effects from the baryon as well as the scalar meson sectors in the Walecka model [Mis97, Mis01, Mis02a]. As has been shown in section 4.3, in the chiral model in mean-field approximation the vector meson masses do not show any significant drop, similar to results in the Walecka model. The effect of the Dirac sea is now taken into account by summing over baryonic tadpole diagrams in the relativistic Hartree approximation (RHA). It is seen that an appreciable decrease of the vector meson masses arises from the nucleon Dirac sea. This shows the importance of taking into account these contributions.

8.2 Relativistic Hartree approximation

So far, only the mean-field approximation of the chiral $SU(3)_L \times SU(3)_R$ model has been considered. Now the question arises, how higher order effects may influence the obtained results. Therefore, the strong coupling field theory described by the Lagrangian (3.1) is used to calculate the corrections to the mean-field approximation. This is of special interest since some observables, like the energy per particle, result from the cancellation of large components. We follow the same procedure as outlined for the original σ-ω models in [Wal74, Ser86] leading to the so called quantum hadrodynamics (QHD). By using the quantum hadrodynamics approach for the chiral model, a consistent framework for calculating corrections to the mean-field results is provided.

8.2.1 Observables

As shown in [Ser86] observable quantities can be calculated using the interacting propagators of the particles. For the fields of interest, i.e., baryons, scalar, and vector mesons these interacting propagators are defined as [Ser86]

$$\begin{aligned} \mathrm{i}G_{\alpha\beta}(x'-x) &= \langle\Psi|T\left[\psi_{H\alpha}(x')\bar{\psi}_{H\beta}(x)\right]|\Psi\rangle \\ \mathrm{i}\Delta(x'-x) &= \langle\Psi|T\left[\phi_H(x')\bar{\phi}_H(x)\right]|\Psi\rangle \\ \mathrm{i}D_{\mu\nu}(x'-x) &= \langle\Psi|T\left[V_{H\mu}(x')\bar{V}_{H\nu}(x)\right]|\Psi\rangle, \end{aligned} \tag{8.1}$$

where $|\Psi\rangle$ is the interacting ground state and $\psi_{H\alpha}$, ϕ_H and $V_{H\mu}$ denote the baryon, scalar meson, and vector meson Heisenberg fields, respectively. Then for example the expectation value of a bilinear product of Heisenberg-picture fermion operators is given by

$$\langle\Psi|\bar{\psi}(x)\Gamma\psi(x)|\Psi\rangle = -\lim_{\vec{y}\to\vec{x}}\lim_{y^0\to x^{0+}}\langle\Psi|T\left[\psi_\alpha(x)\bar{\psi}_\beta(y)\right]|\Psi\rangle\Gamma_{\beta\alpha} \tag{8.2}$$

$$= -i\lim_{\vec{y}\to\vec{x}}\lim_{y^0\to x^{0+}} Tr\left[\Gamma G(x,y)\right], \tag{8.3}$$

where the trace is over the indices of the matrix, $G(x,y)$ denotes the interacting baryon propagator, and the limit $y^0 \to x^{0+}$ ensures the proper ordering of operators. Similar relations hold for the expectation values for operators constructed from meson fields. From this, the expectation value of different operators may be written in terms of the full propagators of the theory. Since the resulting expressions will generally be divergent, they need to be renormalized to extract finite, physical quantities. For the energy momentum tensor this yields for example [Ser86]

$$T^{\mu\nu} = \langle\Psi|\hat{T}^{\mu\nu}+\delta\hat{T}^{\mu\nu}|\Psi\rangle - \lim_{k_f\to 0}\langle\Psi|\hat{T}^{\mu\nu}+\delta\hat{T}^{\mu\nu}|\Psi\rangle \tag{8.4}$$

$$\equiv \langle\Psi|\hat{T}^{\mu\nu}|\Psi\rangle + \mathrm{CTC} - \mathrm{VEV}, \tag{8.5}$$

where CTC denotes the additional counterterm contribution, resulting from the counterterms $\delta\mathcal{L}$ in the Lagrangian and VEV is the vacuum expectation value of the full energy momentum tensor $\hat{T}^{\mu\nu}+\delta\hat{T}^{\mu\nu}$. In the mean-field approach (section 3.2) the divergent contributions (negative energy sea) have just been neglected to render the observables finite.

8.2.2 Effective interacting baryon propagator

Adopting the Relativistic Hartree Approximation, we go beyond the mean-field approximation, i.e., the effect of the baryonic Dirac sea is included. This is done through summing over baryonic tadpole diagrams using an effective baryon propagator $G_H(p)$, which is obtained through a self-consistent solution of the Schwinger-Dyson (SD) equation

$$G_H(p) = G_0(p) + G_0(p)\Sigma_H G_H(p). \tag{8.6}$$

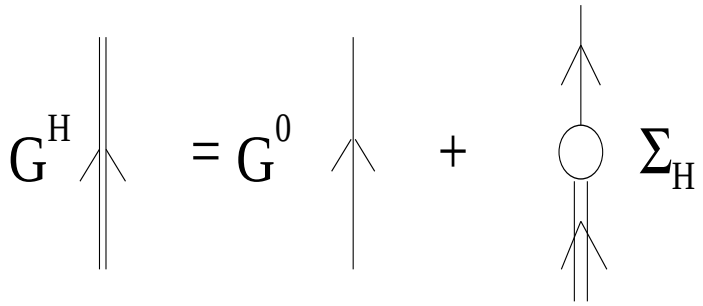

Figure 8.1: Graphical representation of the self-consistent relativistic Hartree equations

Here $G_0(k)$ denotes the free baryon propagator, Σ_H is the modified self-energy due to the summing over the tadpole diagrams and $G_H(k)$ is the effective fermion propagator in the relativistic Hartree approximation. The diagramatical representation of the Schwinger-Dyson equation (8.6) is given in figur 8.1. The self-energy Σ_H contains contributions from both, scalar and vector tadpole diagrams and is given by

$$\Sigma_H = \Sigma_H^s - \gamma^\mu \Sigma_H^{V\mu}, \tag{8.7}$$

where the scalar part of the self-energy reads

$$\Sigma_H^s = i\frac{g_{\sigma NN}^2}{m_\sigma^2}\int \frac{d^4p}{(2\pi)^4}\mathrm{Tr}\left(G_H(p)\right) \tag{8.8}$$

and the vector part is

$$\Sigma_H^{V\mu} = i\frac{g_{\omega NN}^2}{m_\omega^2}\int \frac{d^4p}{(2\pi)^4}\mathrm{Tr}\left(\gamma^\mu G_H(p)\right). \tag{8.9}$$

The couplings $g_{\sigma NN}$ and $g_{\omega NN}$ denote the nucleon-scalar meson and nucleon-vector meson coulings discussed in section 3.1. Similar expression are obtained for the Hyperons [Mis97, Mis01, Mis02a]. The solution of the Schwinger-Dyson equation (8.6) for the interacting fermion propagator gives

$$\begin{aligned} G_H^{-1} &= G_0^{-1} - \Sigma_H \\ &\equiv \gamma_\mu \bar{p}^\mu - M^*. \end{aligned} \tag{8.10}$$

Here, Σ_H is independent of the four-momentum p and represents the average interaction felt by the propagating particle. Thus, the pole structure of the Hartree propagator G_H resembles the noninteracting propagator with shifted mass, $M^* = M + \Sigma_H^s$ and shifted four-momentum $\bar{p}^\mu = p^\mu + \Sigma_H^{V\mu}$. The interacting nucleon propagator in the RHA at finite density is given as

$$\begin{aligned} G_H(p) &= (\gamma_\mu \bar{p}^\mu + M^*) \left[\frac{1}{\bar{p}^2 - M^{*2} + \mathrm{i}\epsilon} + \frac{\mathrm{i}\pi}{E^*(\vec{p})} \delta(\bar{p}^0 - E^*(\vec{p})) \theta(p_F - |\vec{p}|) \right] \\ &\equiv G_H^F(p) + G_H^D(p), \end{aligned} \tag{8.11}$$

with $E^*(\vec{p}) = \sqrt{\vec{p}^2 + M^{*2}}$. We see that in the Hartree approximation the interacting propagator takes a form analogous to the free propagator: G_H^F describes the propagation of virtual positive- and negative-energy quasinucleons, and G_D^H allows for quasinucleon holes inside the Fermi sea, while correcting G_H^F for the Pauli exclusion principle. The name "quasinucleon" refers to a baryon whose energy, mass and Dirac wave function are modified by the nucleon self-energy Σ_H.

8.2.3 Connection to the mean-field approximation

Inserting the interacting nucleon propagator in the expressions for the self energy, (8.8) and (8.9), shows that the contribution of $G_F^H(p)$ diverges. It can be shown by symmetry arguments [Ser86] that resulting from baryon current conservation the vector part $\Sigma_H^{V\mu}$ has no contribution from the nucleon Dirac sea. This is not the case for the scalar part Σ_H^s. The resulting contribution of $G_F^H(p)$ to Σ_H^s is a sum over all occupied states in the negative-energy sea of quasibaryons. Thus, the divergences are of the same origin as those encountered in the derivation of the mean-field Hamiltonian (3.2.2). There the mean-field Hamiltonian was defined by neglecting the divergent contribution δH. The equivalent approximation is obtained by neglecting the contributions from $G_F^H(p)$ (antibaryons) and only taking into account the contributions from G_H^D (filled Fermi sea). Therefore it follows: $G_H \equiv G_H^D$. The replacement of the full interacting nucleon propagator $G_H(p)$ by the contribution of the filled Fermi sea G_H^F, renders the self-energy (8.7)

finite and defines its MFT values:

$$\Sigma^s_{MFT} = \mathrm{i}\frac{g^2_{\sigma NN}}{m^2_\sigma}\int\frac{d^4p}{(2\pi)^4}\mathrm{Tr}\left(G^D_H(p)\right) = -\frac{g^2_{\sigma NN}}{m^2_\sigma}\frac{\gamma}{(2\pi)^3}\int_0^{k_F} d^3p\frac{M^*}{E^*(p)} \quad (8.12)$$

$$\Sigma^{V\mu}_{MFT} = \mathrm{i}\frac{g^2_{\omega NN}}{m^2_\omega}\int\frac{d^4p}{(2\pi)^4}\mathrm{Tr}\left(\gamma^\mu G^D_H(p)\right) = -\delta^{\mu 0}\frac{g^2_{\omega NN}}{m^2_\omega}\rho_B \quad (8.13)$$

8.2.4 Inclusion of vacuum contributions

The vacuum fluctuation corrections are taken into account by using the full effective interacting nucleon propagator G_H, including the Dirac part G^D_H. Thus, in the calculation of the self-energies (8.7) there is a contribution from a sum over all occupied states in the negative-energy sea of nucleons. The resulting self energies read

$$\Sigma^s_H = \frac{g^2_{\sigma NN}}{m^2_\sigma}\left[\mathrm{i}\gamma_N\int\frac{d^4p}{(2\pi)^4}\frac{M^*}{\bar{p}^2 - M^{*2} + \mathrm{i}\epsilon} - \rho_s\right] \quad (8.14)$$

$$\Sigma^{V\mu}_H = \frac{g^2_{\omega NN}}{m^2_\omega}\left[2\mathrm{i}\gamma_N\int\frac{d^4p}{(2\pi)^4}\frac{\bar{p}^\mu}{\bar{p}^2 - M^{*2} + \mathrm{i}\epsilon} - \delta^{\mu 0}\rho_B\right] \quad . \quad (8.15)$$

As was mentioned before, the first term in the vector part of (8.14) vanishes from symmetric integration. I.e., the Dirac sea contributes only to the scalar part of the self-energy, which is given by the first term in Σ^s_H. This divergent integral is rendered finite by dimensional regularization. The counterterms added to extract the finite contributions to the self-energy are [Ser86]

$$\Sigma^s_{CTC} = \sum_{n=0}^{3}\frac{1}{n!}(-1)^n\left(\frac{g^2_{\sigma NN}}{m^2_\sigma}\right)\left(\frac{-\Sigma^s_H}{g_{\sigma NN}}\right)^n\alpha_{n+1}. \quad (8.16)$$

This corresponds to the counterterm

$$\mathcal{L}_{CTC} = \sum_{n=1}^{4}\alpha_n\frac{\sigma^n}{n!} \quad (8.17)$$

in the Lagrangian. The coeffiecients α_i are fixed from a set of renormalization conditions. The first term ensures that the vacuum tadpole vanishes. The second term guarantees that the loop corrections to the scalar meson propagator vanish

on the physical mass shell, i.e., $k^2 = m_\sigma^2$. This implies that the mass of the σ meson is unaltered by the RHA contributions. The last two terms in (8.16) are chosen such that there are no cubic or quartic σ self-interaction contributions arising from vacuum corrections in RHA.

8.2.5 RHA contribution

The addition of the above counter term contributions yields additional terms in the grand canonical potential. These influence the energy, the pressure, and the meson field equations. Here, we use the mass generation C2 with $g_{N\zeta} = 0$ (3.16), i.e., no coupling of the strange condensate to the nucleon[1]. Hence, additional terms will only appear due to summing over baryonic tadpole diagrams arising from the interaction with the scalar field σ, similar to as in the Walecka model. The additional contribution to the energy density is given as

$$\begin{aligned}\Delta\epsilon &= -\frac{\gamma_N}{16\pi^2}\Big(m_N^{*\,4}\ln\Big(\frac{m_N^*}{m_N}\Big) + m_N^3(m_N - m_N^*) - \frac{7}{2}m_N^2(m_N - m_N^*)^2 \\ &\quad + \frac{13}{3}m_N(m_N - m_N^*)^3 - \frac{25}{12}(m_N - m_N^*)^4\Big), \end{aligned} \tag{8.18}$$

where $m_N^* = -g_{N\sigma}\sigma$ and m_N is the nucleon mass in vacuum. This will also modify the pressure and the σ field equation. With inclusion of the relativistic Hartree contributions, the field equation for σ as given by (3.63) gets modified to

$$\begin{aligned}&k_0\chi^2\sigma - 4k_1(\sigma^2 + \zeta^2)\sigma - 2k_2\sigma^3 - 2k_3\chi\sigma\zeta - 2\frac{\delta\chi^4}{3\sigma} \\ &+ m_\pi^2 f_\pi + \frac{\partial m_N^*}{\partial\sigma}(\rho_N^s + \Delta\rho_N^s) = 0, \end{aligned} \tag{8.19}$$

where the additional contribution to the nucleon scalar density is given as

$$\begin{aligned}\Delta\rho_N^s &= -\frac{\gamma_N}{4\pi^2}\left[m_N^{*\,3}\ln\left(\frac{m_N^*}{m_N}\right) + m_N^2(m_N - m_N^*)\right. \\ &\quad \left. - \frac{5}{2}m_N(m_N - m_N^*)^2 + \frac{11}{6}(m_N - m_N^*)^3\right]. \end{aligned} \tag{8.20}$$

[1]This was done, since by neglecting the nucleon-ζ coupling and considering only nonstrange nuclear matter, the strange scalar field ζ does not appear. Thus, the procedure known from the investigation of the Walecka model could directly be applied. The extension to account for the ζ field is in progress.

These necessitate a refitting of some of the parameters. First, one has to account for the change in the energy and the pressure, i.e., $g_{N\omega}$ and χ_0 have to be refitted. Due to the change in χ_0, the parameters k_0, k_2 and k_4 must be adapted to ensure that the vacuum equations for σ, ζ and χ have minima at the vacuum expectation values of the fields. Table 8.1 shows the parameters corresponding to the mean-field and the Hartree approximations.

Parameter	Mean-field		Hartree	
g_4	2.7	0	2.7	0
k_1	1.4	1.4	1.4	1.4
$g_{N\omega}$	12.83	10.52	10.51	9.37
$g_{N\rho}$	4.27	3.51	3.50	3.12
χ_0	402.7	430.1	430.2	446
k_3	-2.64	-2.07	-2.07	-1.73
k_0	2.37	2.07	2.07	1.93
k_2	-5.55	-5.55	-5.55	-5.55
k_4	-0.23	-0.23	-0.23	-0.24
$m_N^*/m_N(\rho_0)$	0.64	0.71	0.73	0.76
m_σ	475.6	560.2	560.4	610.7
K	266.1	359.5	304	377.8
a_4	29.0	27.4	23.9	24.1

Table 8.1: Parameters for the mean-field and the Hartree fit

8.3 Vector meson properties in the medium

8.3.1 In-medium vector meson masses

We now examine how the Dirac sea effects discussed in section 8.2 modify the masses of the vector mesons. Rewriting the expression for the vector interaction of these mesons given in equation (3.19) in terms of the renormalized couplings $g_{N\omega}$ and $g_{N\rho}$ yields

$$\mathcal{L}_{BV}^N = g_{N\omega}\omega_\mu\overline{\psi_N}\gamma_\mu\psi_N + g_{N\rho}\vec{\rho}_\mu\overline{\psi_N}\gamma_\mu\vec{\tau}\psi_N. \tag{8.21}$$

Furthermore, a tensor coupling is introduced:

$$\mathcal{L}_{\text{tensor}} = -\frac{g_{NV}\kappa_V}{2m_N}\left[\bar{\psi}_N\sigma_{\mu\nu}\tau^a\psi_N\partial^\nu V_a^\mu\right], \tag{8.22}$$

where $(g_{NV}, \kappa_V) = (g_{N\omega}, \kappa_\omega)$ or $(g_{N\rho}, \kappa_\rho)$ and $\tau_a = 1$ or $\vec{\tau}$, for $V_a^\mu = \omega^\mu$ or ρ_a^μ, $\vec{\tau}$ being the Pauli matrices. As stated before, the $g_{N\omega}$ coupling is determined from nuclear matter properties and the N-ω tensor coupling is neglected. As shown in section 3.1.2, three $SU(3)$-symmetric baryon-vector meson couplings are possible. Thus, two more coupling constant have to be determined. Here we use two different approches: On the one hand, the parameters are determined by the additional constraints that the strange vector field does not couple to the nucleon and that the d-type coupling vanishes. This fixes the $g_{N\rho}$ vector coupling, while the tensor coupling is undetermined and treated as a free parameter . On the other hand, we only set the N-ϕ coupling to zero and use ρ-N couplings as determined from NN-scattering data.
The vector meson self energy is given as

$$\Pi_V^{\mu\nu}(k) = -\gamma_I g_{NV}^2 \frac{i}{(2\pi)^4}\int d^4p\,\mathrm{Tr}\Big[\Gamma_V^\mu(k)G(p)\Gamma_V^\nu(-k)G(p+k)\Big], \tag{8.23}$$

where $\gamma_I = 2$ is the isospin degeneracy factor for nuclear matter, and, $\Gamma_V^\mu(k) = \gamma^\mu\tau_a - (\kappa_V/2m_N)\sigma^{\mu\nu}\tau_a$ represents the meson-nucleon vertex function. $G(k)$ is the interacting nucleon propagator as given in (8.11). The vector meson self-energy can then be written as the sum of two parts

$$\Pi^{\mu\nu} = \Pi_F^{\mu\nu} + \Pi_D^{\mu\nu}. \tag{8.24}$$

In the above, $\Pi_F^{\mu\nu}$ is the contribution arising from the vacuum fluctuation effects, described by the coupling to the $N\bar{N}$ excitations and $\Pi_D^{\mu\nu}$ is the density dependent contribution to the vector self-energy. For the ω meson, the tensor coupling is generally small as compared to the vector coupling to the nucleons [Hat96]. Thus, this coupling is neglected in the present calculations. The Feynman part of the self-energy, $\Pi_F^{\mu\nu}$, is divergent and needs renormalization. We use dimensional regularization to separate the divergent parts. For the ρ-meson with tensor interactions, a phenomenological subtraction procedure [Shi94, Hat96] is adopted.

After renormalisation, the contributions to the meson self-energies from the Feynman part are given as follows. For the ω meson, one arrives at the expression

$$\Pi_F^{\omega}(k^2) \equiv \frac{1}{3}\mathrm{Re}(\Pi_F^{\mathrm{ren}})_{\mu}^{\mu} = -\frac{g_{N\omega}^2}{\pi^2}k^2\int_0^1 dzz(1-z)\ln\left[\frac{{m_N^*}^2 - k^2z(1-z)}{{m_N}^2 - k^2z(1-z)}\right]. \quad (8.25)$$

and for the ρ meson,

$$\Pi_F^{\rho}(k^2) = -\frac{g_{N\rho}^2}{\pi^2}k^2\Big[I_1 + m_N^*\frac{\kappa_\rho}{2m_N}I_2 + \frac{1}{2}\Big(\frac{\kappa_\rho}{2m_N}\Big)^2(k^2I_1 + {m_N^*}^2 I_2)\Big] \quad (8.26)$$

where,

$$I_1 = \int_0^1 dzz(1-z)\ln\Big[\frac{{m_N^*}^2 - k^2z(1-z)}{{m_N}^2 - k^2z(1-z)}\Big],\quad I_2 = \int_0^1 dz\ln\Big[\frac{{m_N^*}^2 - k^2z(1-z)}{{m_N}^2 - k^2z(1-z)}\Big]. \quad (8.27)$$

The density dependent part for the self energy is given as

$$\Pi^D(k_0, \boldsymbol{k}\to 0) = -\frac{4g_{NV}^2}{\pi^2}\int p^2dp\,F(|\boldsymbol{p}|, m_N^*)\left[f_{FD}(\mu^*, T) + \bar{f}_{FD}(\mu^*, T)\right] \quad (8.28)$$

with

$$\begin{aligned} F(|\boldsymbol{p}|, m_N^*) &= \frac{1}{\epsilon^*(p)(4\epsilon^*(p)^2 - k_0^2)}\Bigg[\frac{2}{3}(2|\boldsymbol{p}|^2 + 3{m_N^*}^2) + k_0^2\Big\{2m_N^*\Big(\frac{\kappa_V}{2m_N}\Big) \\ &\quad + \frac{2}{3}\Big(\frac{\kappa_V}{2m_N}\Big)^2(|\boldsymbol{p}|^2 + 3{m_N^*}^2)\Big\}\Bigg], \end{aligned} \quad (8.29)$$

where $\epsilon^*(p) = (\boldsymbol{p}^2 + {m_N^*}^2)^{1/2}$ is the effective energy for the nucleon. The effective mass of the vector meson is then obtained by solving the equation, with $\Pi = \Pi_F + \Pi_D$,

$$k_0^2 - m_V^2 + \mathrm{Re}\Pi(k_0, \boldsymbol{k} = 0) = 0. \quad (8.30)$$

8.3.2 Meson decay properties

We next proceed to study the vector meson decay widths as modified due to the effect of vacuum polarisation effects through RHA. The decay width for the

process $\rho \to \pi\pi$ is calculated from the imaginary part of the self energy and in the rest frame of the ρ-meson, it becomes

$$\Gamma_\rho(k_0) = \frac{g^2_{\rho\pi\pi}}{48\pi}\frac{(k_0^2 - 4m_\pi^2)^{3/2}}{k_0^2}\left[\Big(1 + f(\frac{k_0}{2})\Big)\Big(1 + f(\frac{k_0}{2})\Big) - f(\frac{k_0}{2})f(\frac{k_0}{2})\right] \quad (8.31)$$

where, $f(x) = [e^{\beta x} - 1]^{-1}$ is the Bose-Einstein distribution function. The first and the second terms in the above equation represent the decay and the formation of the resonance ρ. The medium effects have been shown to play a very important role for the ρ-meson decay width. In the calculation for the ρ decay width, the pion has been treated as free, i.e., any modification of the pion propagator due to effects like delta-nucleon hole excitation [Asa92, Her93, Cha92] have been neglected. The coupling $g_{\rho\pi\pi}$ is fixed from the decay width of ρ meson in vacuum (Γ_ρ=151 MeV) decaying into two pions.

For the nucleon-rho couplings, the vector and tensor couplings as obtained from the N-N forward dispersion relation [Hat96, Ala99, Gre77, Gre80] are used. With the couplings as described above, we consider the modification of ω and ρ meson properties in nuclear matter due to quantum correction effects.

To calculate the decay width for the ω-meson, we consider the following interaction Lagrangian for the ω meson [Sak69, Gel62, Li95]

$$\mathcal{L}_\omega = \frac{g_{\omega\pi\rho}}{m_\pi}\epsilon_{\mu\nu\alpha\beta}\partial^\mu\omega^\nu\partial^\alpha\rho_i^\beta\pi_i + \frac{g_{\omega 3\pi}}{m_\pi^3}\epsilon_{\mu\nu\alpha\beta}\epsilon_{ijk}\omega^\mu\partial^\nu\pi^i\partial^\alpha\pi^j\partial^\beta\pi^k. \quad (8.32)$$

The decay width of the ω-meson in vacuum is dominated by the channel $\omega \to 3\pi$. In the medium, the decay width for $\omega \to 3\pi$ is given as

$$\begin{aligned}\Gamma_{\omega\to 3\pi} &= \frac{(2\pi)^4}{2k_0}\int d^3\tilde{p}_1 d^3\tilde{p}_2 d^3\tilde{p}_3\,\delta^{(4)}(P - p_1 - p_2 - p_3)|M_{fi}|^2 \\ &\quad \Big[(1 + f(E_1))(1 + f(E_2))(1 + f(E_3)) - f(E_1)f(E_2)f(E_3)\Big], \quad (8.33)\end{aligned}$$

where $d^3\tilde{p}_i = \frac{d^3p_i}{(2\pi)^3 2E_i}$, p_i and E_i's denote 4-momenta and energies for the pions, and $f(E_i)$'s are their thermal distributions. The matrix element M_{fi} has contributions from the channels $\omega \to \rho\pi \to 3\pi$ (described by the first term in (8.32)) and the direct decay $\omega \to 3\pi$ resulting from the contact interaction (second term in (8.32)) [Li95, Kli96, Kay84]. For the $\omega\rho\pi$ coupling we take the value $g_{\omega\rho\pi}$ =2 which is compatible with the vacuum decay width $\omega \to \pi\gamma$ [Ala99]. We fix

the point interaction coupling $g_{\omega 3\pi}$ by fitting the partial decay width $\omega \to 3\pi$ in vacuum (7.49 MeV) to be 0.24 [Mis02c]. The contribution arising from the direct decay turns out to be marginal, being of the order of upto 5% of the total decay width for $\omega \to 3\pi$.
With the modifications of the vector meson masses in the hot and dense medium, a new channel becomes accessible, the decay mode $\omega \to \rho\pi$ for $m^*_\omega > m^*_\rho + m_\pi$. This has been taken into account in the present investigation.

8.4 Results and Discussions

We shall now discuss the results of the present investigation: the nucleon properties as modified due to the Dirac sea contributions through the relativistic Hartree approximation and their effects on vector meson properties in the dense hadronic matter. Figure 8.2 shows the equation of state in the mean-field and in the Hartree-approximation with and without quartic self-interaction for the ω field. In both cases we observe that the additional terms resulting from the Hartree approximation lead to a softening of the equation of state at higher densities. However, the compressibilty in the relativistic Hartree approximation is higher than the mean-field value, as shown in table 8.1. Furthermore, the influence of the finite value for the quartic ω coupling, g_4 is clearly visible. In this case the compressibility at nuclear saturation is strongly reduced (table 8.1). Also, the resulting equation of state is much softer in particular at higher densities. The reason for this can be seen from figure 4.10. The vector field ω, which causes the repulsion in the system, rises much more steeply as a function of density for $g_4 = 0$ than for the case of $g_4 = 2.7$, because the quartic self-interaction attenuates the ω field. The effective nucleon mass for the different cases is depicted in figure 8.4. Here the RHA predicts higher nucleon masses than the mean-field case. At higher densities these contributions become increasingly important. This is also reflected in the density dependence of the nonstrange σ field, showing a considerable increase due to the Hartree contributions (figure8.3). In contrast, the strange condensate, ζ, which does not couple to the nucleons, takes only slightly lower values in the MF-case. The in-medium properties of the vector mesons are modified due to the vacuum polarization effects. The nucleon-ω vector coupling, $g_{N\omega}$,

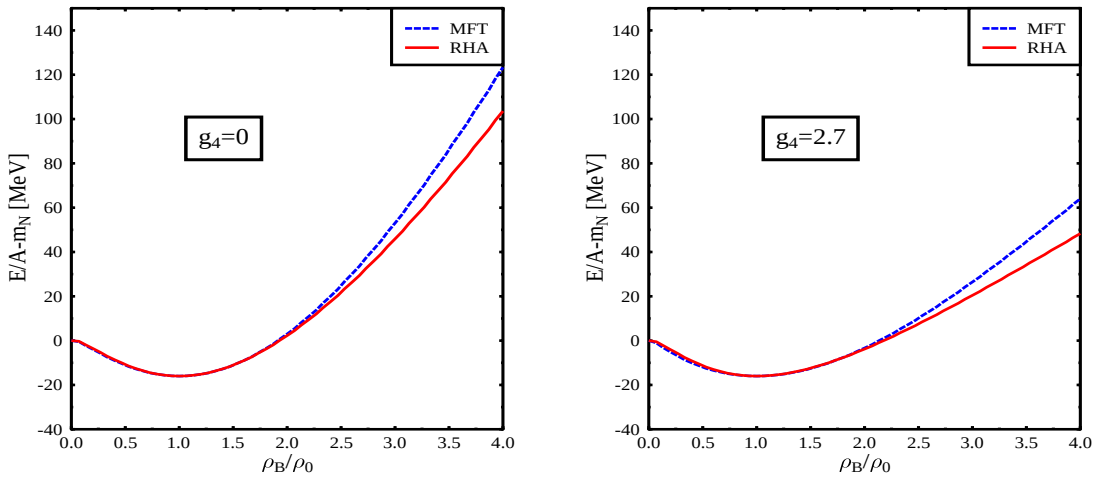

Figure 8.2: Binding energy per particle as a function of density in the mean-field and in the Hartree approximation.

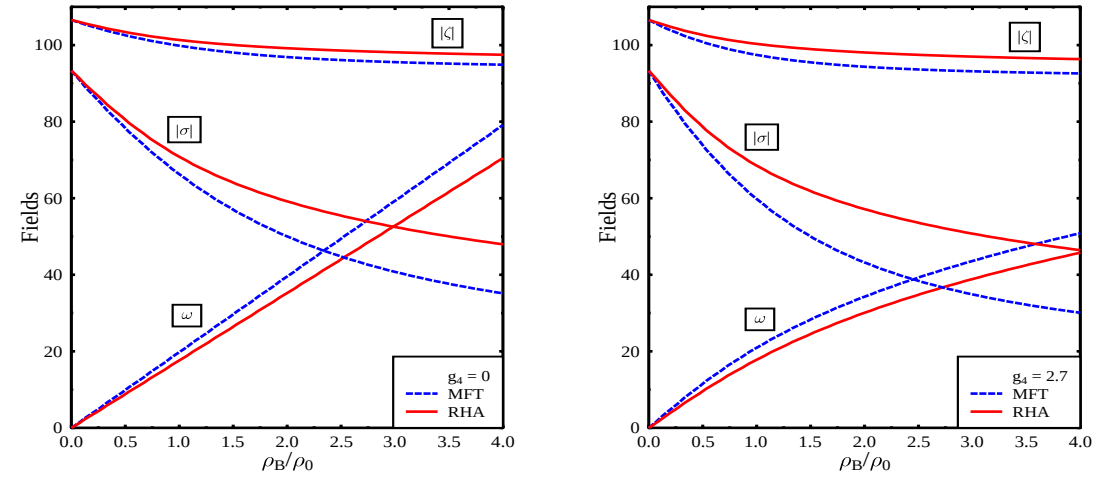

Figure 8.3: Scalar fields σ, ζ and vector field ω as a function of density in the mean-field and in the Hartree-Approximation.

is calculated from the nuclear matter saturation properties. As already stated, the N-ω tensor coupling is neglected. Figure 8.5 shows the resulting modification

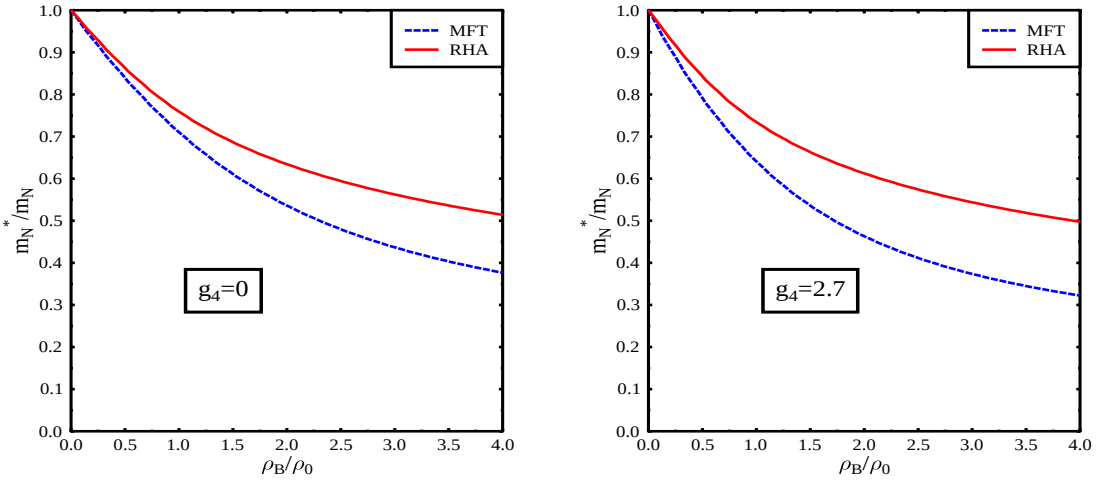

Figure 8.4: Effective nucleon mass as a function of density in the mean-field and in the Hartree approximation.

of the ω–meson mass in the Hartree approximation as compared to the mean-field case. For $g_4 = 0$, the ω mass has no density dependence, because of the frozen glueball approximation. In contrast, a strong reduction due to the Dirac sea polarization is found for densities up to around normal nuclear matter density. At higher densities, the Fermi polarization part of the ω-self-energy starts to become important, leading to an increase in the mass. A similar behaviour has been observed in the Walecka model [Shi94, Hat96, Jea94, Sai98]. The quartic term in the ω field considerably enhances the ω mass with increasing density. Thus, the mass rises monotonically in the mean-field case. For the Hartree approximation a decrease of the ω mass for small densities can still be found. But at higher densities the contribution from the quartic term becomes more important and leads to an increase of the in-medium mass.

In figure 8.6, we illustrate the medium modification for the ρ meson mass with the vector and tensor couplings to the nucleons being fixed from the NN forward dispersion relation [Hat96, Ala99, Gre77, Gre80]. The values for these couplings are given as $g^2_{N\rho}/4\pi$=0.55 and κ_ρ=6.1. We notice that the decrease in the ρ meson with increasing density is much sharper than that of the ω meson. Such

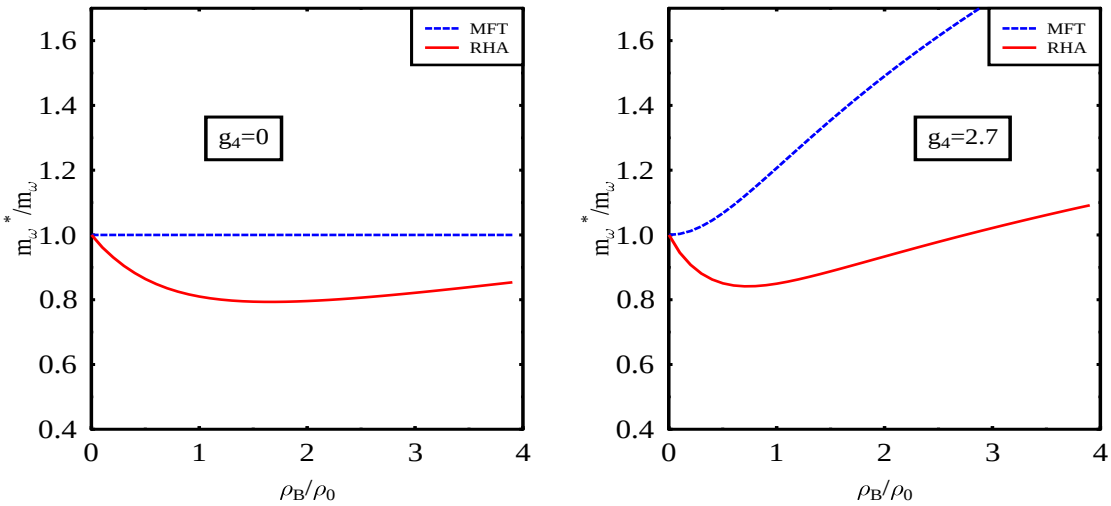

Figure 8.5: Effective ω meson mass in the mean-field approximation and including the Hartree contributions. Left: no quartic vector meson interaction. Right: including ω^4 interaction. There is a significant drop of the vector meson mass due to the Dirac sea effect, which is not seen in the mean-field approximation.

a behaviour of the ρ meson undergoing a much larger medium modification was also observed earlier [Ala99] within the relativistic Hartree approximation in the Walecka model. This indicates that the tensor coupling, which is negligible for the ω meson, plays a significant role for the ρ meson. The in-medium decay width for $\rho \to \pi\pi$, Γ^*_ρ reflects the behaviour of the in-medium ρ mass. This is because in the present work only the case $T = 0$ is considered, and so there is no Bose-enhancement effect. Therefore, in the absence of the quartic vector meson interaction, the significant drop of the mass of the ρ meson in the medium leads to a decrease of the ρ decay width. This is shown in figure 8.7. Since the quartic self-interaction yields an increase in the mass at higher densities, it leads to an increase of the ρ decay width.

In the previous calculations, the ρ-N coupling strengths were used as determined from the NN forward scattering data [Gre77, Gre80]. Now we consider the mass modification for the ρ meson, with the nucleon ρ coupling, $g_{N\rho}$, as determined from the symmetry relations (table 8.1). The symmetry energy coefficient a_{sym}

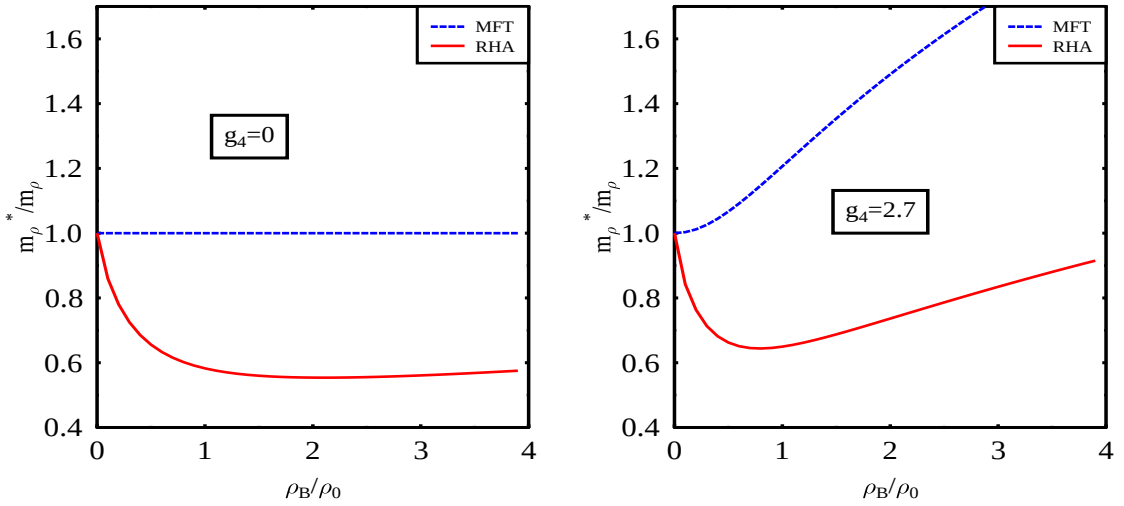

Figure 8.6: Effective ρ meson mass without and with the Hartree contributions, with the nucleon-rho vector and tensor couplings, as fitted from the NN scattering data ($g_{N\rho}$=2.63, κ_ρ = 6.1). The Hartree approximation gives rise to the decrease of the ρ mass in the medium.

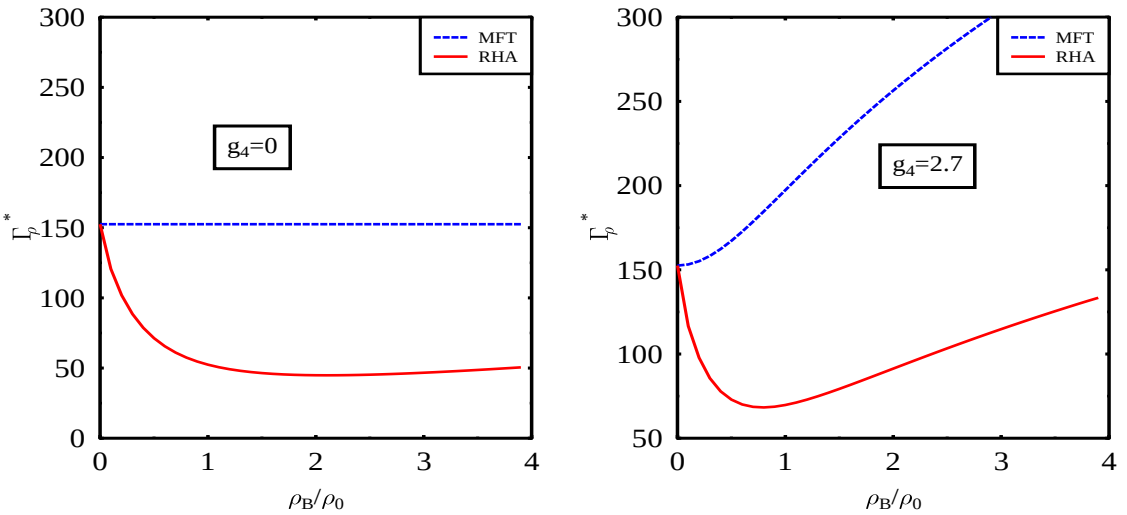

Figure 8.7: Decay width of ρ meson in the absence and presence of the Dirac sea effect with couplings fitted from NN scattering data.

is given as [Gle92, Kuo96]

$$a_{sym} = \frac{1}{2}\left[\frac{\partial^2}{\partial t^2}\left(\frac{\epsilon}{\rho}\right)\right]_{t=0}, \tag{8.34}$$

where $t = \frac{\rho_n - \rho_p}{\rho_0}$. The resulting values of the symmetry energy for the different cases are shown in table 8.1. They are compatible with the experiment. We take the tensor coupling as a parameter in our calculations since this coupling cannot be fixed from infinite nuclear matter properties. However, it influences the properties of finite nuclei. The resulting in-medium mass of the ρ meson is plotted in figure 8.8 as a function of baryon density ρ_B/ρ_0. It is observed that the ρ meson mass has a strong dependence on the tensor coupling. In the Hartree approximation the ρ-nucleon vector coupling does not differ too much in the two cases, i.e., depending on whether it is obtained fromm NN scattering data or from the symmetry relations. Thus, we find a similar behaviour for the ρ mass, if in the latter case we choose $\kappa_\rho = 6$, i.e., close to the value from scattering data. Figure 8.9 shows the decay width for the ρ meson when we take the $N\rho$

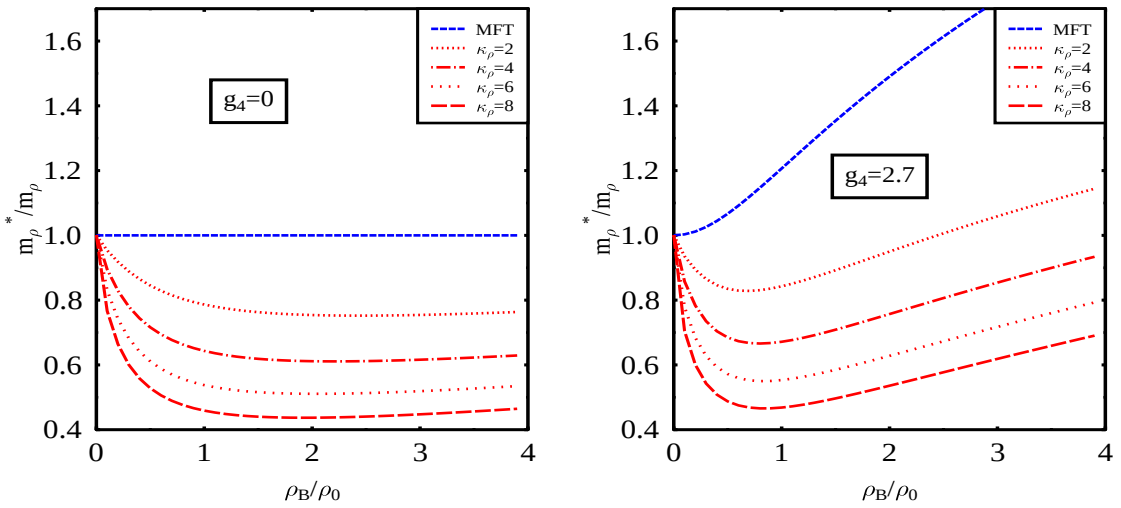

Figure 8.8: Effective ρ meson mass without and with the Hartree contributions, with the nucleon-rho vector coupling, $g_{N\rho}$, as from the chiral model, which is compatible with the symmetry energy. Since we do not know the medium dependent tensor coupling, κ_ρ, it is taken as a parameter. The Hartree approximation gives rise to the decrease of the ρ mass in the medium, which is seen to be quite sensitive to the nucleon-ρ tensor coupling.

vector coupling as determined from symmetry relations and the tensor coupling taken as a parameter. The decay width of the ω meson is plotted as a function

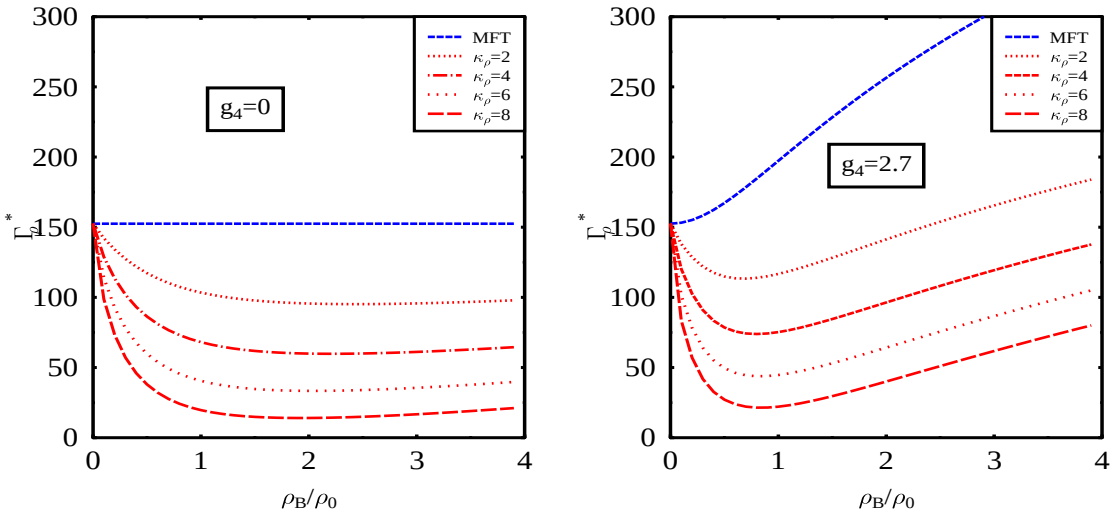

Figure 8.9: Decay width of ρ meson in the absence and presence of the Dirac sea effect with the nucleon-rho vector coupling, $g_{\rho N}$, as from the chiral model, which is compatible with the symmetry energy. The tensor coupling, κ_ρ is taken as a parameter.

of density in figure 8.10. In the vacuum the process $\omega \to 3\pi$ is the dominant decay mode. However, in the medium the channel $\omega \to \rho\pi$ also opens up, since the ρ-meson has a stronger drop in the medium as compared to the ω meson mass. The mean-field approximation, does not have a contribution from the latter decay channel, whereas the inclusion of relativistic Hartree approximation permits both processes in the medium. In the presence of the quartic vector meson interaction, the channel $\omega \to \rho\pi$, which opens up at around $0.3\rho_0$, no longer remains kinematically accessible at higher densities. This is due to the increased importance of ω^4 contributions to the vector meson masses at high densities.

The strong enhancement of the ω meson mass in the presence of a quartic self interaction term for the ω field, makes also the decay channel $\omega \to N\bar{N}$ kinematically accessible in the mean-field approximation. In the present investigation the vector meson properties are considered at rest. Vector mesons with a finite three momentum can also have additional decay channels to particle hole pairs. These

decay modes, e.g, have significant contributions, to the Δ decay width [Kim97]. Additional channels that open up in the mean-field approximation in the presence of a quartic term for ω, however, have not been taken into consideration in the present work. Here the emphasis is on the effect due to the relativistic Hartree approximation on the in-medium vector meson properties. Figure 8.11

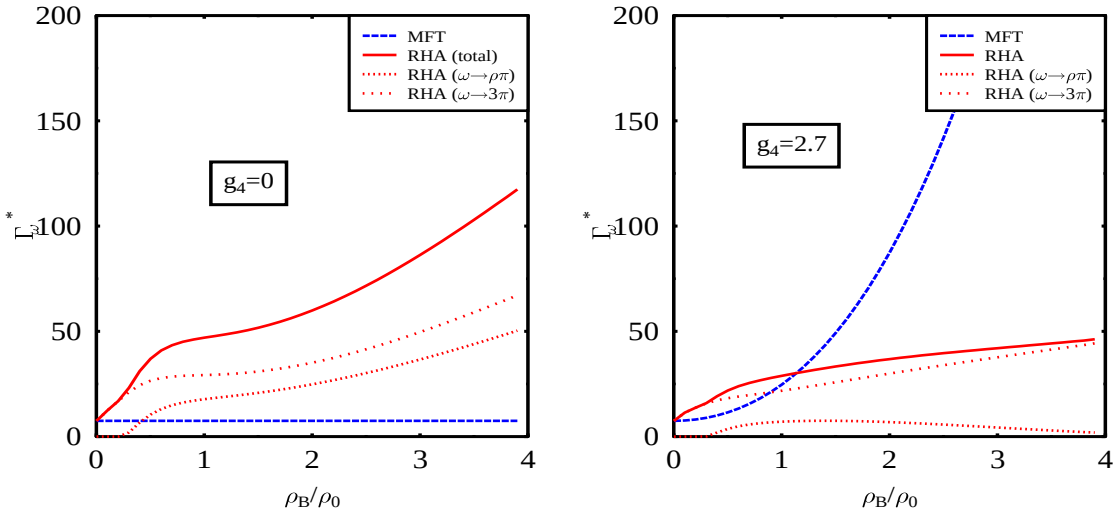

Figure 8.10: Effective decay width of ω meson without and with the Hartree contributions. The decay width has contributions from $\omega \to 3\pi$ as well as $\omega \to \rho\pi$. The latter becomes accessible due to stronger medium modification of the ρ meson mass as compared to the ω mass. The MFT has no contribution from the process $\omega \to \rho\pi$.

illustrates the decay width of the ω-meson when the medium dependence of the ρN vector coupling is taken into account and the tensor coupling is taken as a parameter. The strong dependence of the ρ meson properties on the tensor coupling are reflected in the ω decay width through the channel $\omega \to \rho\pi$.
The in-medium behaviour of the vector meson properties is essential for the understanding of dilepton spectra. These are currently measured at CERN by Na45 and Na49 and future measurements are planned at RHIC by the PHENIX collaboration and at the new GSI facility. In order to be applicable to these investigations, the approach considered here is extended to finite temperature at the moment.

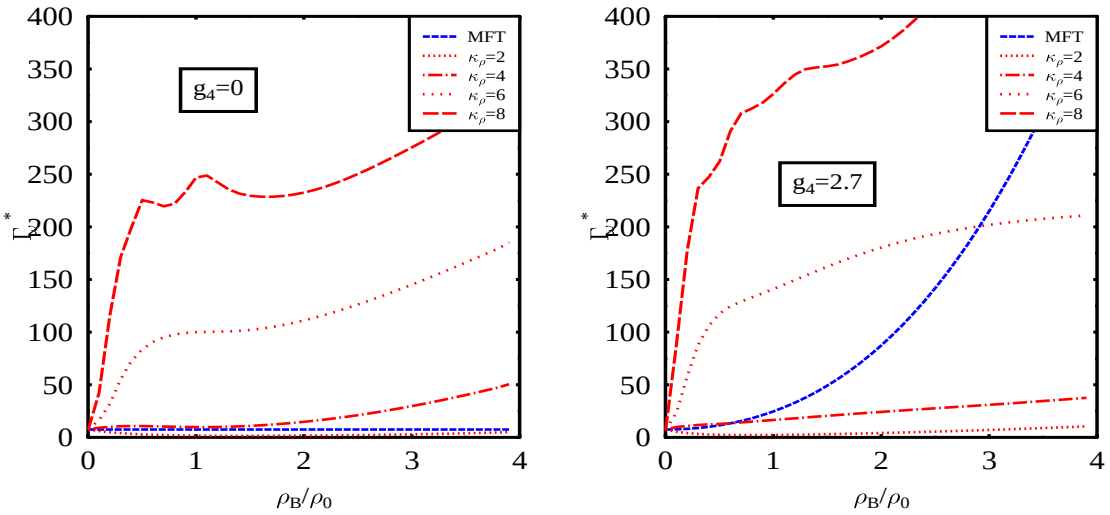

Figure 8.11: Decay width of ω meson in the absence and presence of the Dirac sea effect. For the channel $\omega \to \rho\pi$, the ρ meson properties are determined with the nucleon-ρ vector coupling, $g_{N\rho}$, as from the chiral model, which is compatible with the symmetry energy and, the tensor coupling, κ_ρ is taken as a parameter.

–IX–

Summary and Outlook

In this work the properties of hot and dense hadronic matter were studied in a chiral $SU(3)_L \times SU(3)_R$ model. It was shown before [Pap98a, Pap99] that this model succesfully describes finite nuclei and nuclear matter saturation properties. In [Zsc97] the model was extended to describe also hot symmetric nuclear matter. The aim of this work was threefold: First, the idealized system of hot and dense hadronic matter was systematically studied to get a clear and preferably comprehensive picture of the predicted properties for strongly interacting matter in the chiral $SU(3)$ model. Second, the model was applied to describe physical systems composed of excited hadronic matter, like e.g. neutron stars or systems where excited hadronic matter is produced, like e.g. in relativistic heavy ion collisions [Stö86]. Only by comparing the predicted properties of strongly interacting matter which result from the chiral model to experimental data, the model could be checked, and new insights on the equation of state of hadronic matter were obtained. Third, the approximation scheme used in the main part of this work was modified by adopting the relativistic Hartree approximation, allowing for a theoretical check of the reliability and stability of the predictions. The main outcome of this work is a much more improved understanding of the connection between predicted properties of hadronic matter and the resulting implications for stellar objects or relativistic heavy ion collisions. In addition, as will be discussed below, it should now be possible to deduce an equation of state which simultaneously reproduces the properties of saturated nuclear matter, finite nuclei, neutron stars, and the phase structure as obtained from QCD lattice

calculations [Fod02]. Such an EoS is extremely important for the understanding of many astrophysical processes and of relativistic heavy ion collisions. The main results of this work shall now be presented in more detail. Then the resulting conclusions and the appearing new projects will be discussed.

In the investigation of hot and dense hadronic matter it turned out that the predicted phase diagram strongly depends on the couplings of the baryon resonances which represent a large number of additional degrees of freedom. For cold nuclear matter the inclusion of the baryon decuplet may give rise to a first order phase transition, depending on the coupling to the vector fields. For hot matter with vanishing chemical potential the strength of the coupling of the resonances changes the phase structure from a crossover (no coupling) to a first order phase transition (strong coupling). The strength of this transition and up to which values of the baryon chemical potential it occurs depends on the induced mass generation, i.e., on the coupling to the scalar fields. Three examplary equations of state, denoted by CI, CII, and CIII were extracted. They all give a reasonable description of nuclear matter and finite nuclei. However, the predicted properties for the hot and dense hadronic matter, in particular the type of the phase change at low or vanishing chemical potential, is very different in the three cases. Thus, only from the succesful description of finite nuclei and nuclear matter saturation properties the properties of excited nuclear matter cannot be pinned down. This necessitates the investigation of experimentally observable objects like neutron stars or relativistic heavy ion collisions.

The investigation of the composition and structure of neutron star matter showed that the chiral $SU(3)_L \times SU(3)_R$ model is able to satisfactorily describe the properties of these objects. The resulting predictions were compared with that of a Walecka-type model. It turns out that the two models with similar values of effective nucleon mass, incompressibility, and symmetry energy at the normal nuclear density yield widely different maximum neutron star masses and radii. When the hyperon degrees of freedom are included, the maximum masses and the corresponding radii in the two models are found to be rather similar. However, softness of the nucleonic contribution in the chiral model precludes the hyperons $\Sigma^0, \Sigma^+, \Xi^0$ leading to much smaller hyperon abundances in these stars. In addition, the influence of the baryon resonances was studied. It was found that the neutron star properties yield far stronger constraints on the vector coupling of

the resonances than the symmetric nuclear matter case. To obtain a maximum neutron star mass which is above the observed minimal limit, the ratio of the Δ-ω to the N-ω coupling can only be slightly decreased from unity. Otherwise the predicted equation of state is too soft and the maximum neutron star mass is below the minimal limit.

The space-time evolution of ultra-realtivistic heavy ion collisions at SPS and RHIC energies was studied within a hydrodynamic simulation using the various equations of state obtained from the chiral $SU(3) \times SU(3)$ model. Thereby the influence of different orders of the chiral phase transition and the underlying EoS could be discussed. It turned out that a smooth crossover (CI) or at least the case with a small latent heat (CII) are closest to data. However, all calculations overestimated the lifetime of the system. Since in addition dissipative effects are expected to prolong the lifetime of the pion source even more, it appears very likely that a quasi-adiabatic first order phase transition with large latent heat, for which a hydrodynamic description should be adequate, can not describe the pion HBT data from CERN-SPS and from BNL-RHIC. This observation may be viewed as an experimental confirmation of the predictions from lattice QCD [Bro90, Iwa96, Lae96], which do not show a large latent heat. However, since the quantitative agreement with data was not satisfactorily in all cases, the applied ideal-fluid approach with longitudinal scaling flow is questioned. Here especially the supercooling effects and rapid spinodal decomposition should be accounted for, making a nonequilibrium approach necessary.

Particle ratios as calculated in the chiral $SU(3)$ σ-ω model were compared with measurements in relativistic heavy ion collisions from AGS to RHIC. It turned out that all the different phase transition scenarios studied as well as the noninteracting ideal gas give an equally well description of the data. Thus, in this approach a fit of temperature and chemical potential to the measured particle ratios can not discriminate between different phase transition scenarios. However, the deduced temperature freeze-out values strongly depend on the underlying model. It turns out that the stronger the latent heat the lower the deduced temperature. All the very different scenarios in the chiral model predict similar effective hadron masses at the assumed freeze-out. The in-medium effects are predicted to be in a range up to 15% in all cases and for all the energies. In addition, the freeze-out always takes place below the chiral transition of the corresponding model. Hence

a direct freeze-out from the restored phase is excluded.

The masses of the vector mesons were found to exhibit a significant reduction due to vacuum polarisation effects arising from the Dirac sea in nuclear matter. In particular, it turned out that the Dirac sea contribution dominates over those from the Fermi sea. This shows the importance of the vacuum polarisation effects for the vector meson properties. These modified vector meson properties in a medium play an important role in the dilepton emission rates in relativistic heavy ion collisions. This is reflected by the shift and broadening of the peaks in the low invariant mass regime in the dilepton spectra. Therefore it will be important to investigate how the dilepton rates are modified by the in-medium vector meson properties in the hot and dense hadronic matter. This necessitates the extension of the current work to finite temperatures [Bal03].

As already stated above, the results in this work paved the way for composing an equation of state which satisfactoriliy describes nuclear matter saturation, finite nuclei, neutron stars and the phase structure obtained from QCD lattice results. The key mechanism is the adjustment of the scalar and vector couplings of the baryon resonances. E.g., an explicit symmetry breaking in the mass terms for the Δ-baryons will weaken the phase transition at $\mu = 0$. If this term is increased more and more, the first order phase transition will transform into a crossover. A similar behaviour will be obtained by a coupling of the Δ baryons to the gluon condensate. Furthermore, the results of chapter 4.3 show that the decrease of the vector coupling of the baryon resonances leads to a first order phase transition at high densities. Thus, by modifying these parameters, the phase structure of the model can be adapted to the results of the QCD lattice calculations. If the vector coupling of the baryon resonances is only moderately decreased, the results for nuclear matter and finite nuclei will not be influenced. The properties of neutron stars should also be reproduced succesfully. Thus, all known features of the hadronic matter phase diagram are reproduced in a single approach, which then should be tested, adjusted and improved by considering astrophysical applications and relativistic heavy ion physics. This work is in progress.

From the results stated above many new projects result or are supported. These are theoretical modifications or applications to physical systems not yet studied, in order to further improve the reliability and theoretical conception of the approach:

- The hydrodynamic model used in chapter 6.2 should be amended towards a nonequilibrium approach. This work is in progress [Pae03b, Pae03a].
- The properties of hot and dense hadronic matter in the Hartree approximation should systematically be studied. For example, the hadron properties strongly influence the dilepton production or the measured particle ratios. In addition, the properties of finite nuclei should be studied in this approach.
- The inclusion of the vector mesons as gauge-bosons should be investigated.
- The chiral model predicitons should be implemented in the microscopic transport model UrQMD. This has already been done on a basic level by parametrizing the equation of state of the chiral model and including it as nonrelativistic potentials.
- The EoS as obtained in the chiral model should be included in three dimensional hydrodynamical calculations. Then for example, the resulting p_T spectra could be studied and compared to experiments.
- In the description of supernova explosions the equation of state of excited hadronic matter plays an important role. Thus, here the model can also be applied.
- Correlations among kaons, protons, and nonidentical particles can be analysed. The excitation functions of source sizes and lifetimes and also so-called "azimuthally sensitive" HBT-analysis could be useful to obtain a complete picture of the phase transition via the structure of the pion source in space-time.

Finally, the nature of the chiral symmetry restoration, the properties of hot and dense hadronic matter or the properties of hadrons in the medium will be better understood by analyzing forthcoming experimental data from RHIC, from the new facility at GSI as well as from additional astrophysical observations. With these data emerging and with the projects mentioned above a deeper understanding of the structure and properties of strongly interacting matter will be obtained.

–Appendix A–

Hadron Multiplets

The baryon and meson fields are expanded in a basis of Gell-Mann matrices [Sak69]:

Pseudoscalar mesons:

The expansion for the pseudoscalar mesons reads:

$$\frac{1}{2}\sum_{a=0}^{8}(\overline{q}_R\lambda_a\gamma_5 q_L)\lambda_a \equiv \frac{1}{\sqrt{2}}\sum_{a=0}^{8}\mathrm{i}\pi_a\lambda_a = \mathrm{i}\Pi \qquad , \tag{A.1}$$

and gives the pseudoscalar meson matrix

$$\Pi = \begin{pmatrix} \frac{\pi^0}{\sqrt{2}} + \frac{\eta_8}{\sqrt{6}} + \frac{\eta_0}{\sqrt{3}} & \pi^+ & K^+ \\ \pi^- & -\frac{\pi^0}{\sqrt{2}} + \frac{\eta_8}{\sqrt{6}} + \frac{\eta_0}{\sqrt{3}} & K_0 \\ K^- & \overline{K}^0 & -\frac{2}{\sqrt{6}}\eta_8 + \frac{\eta_0}{\sqrt{3}} \end{pmatrix} \quad . \tag{A.2}$$

Vector mesons:

We define

$$V_\mu = \frac{1}{\sqrt{2}}\sum_{i=0}^{8} v_\mu^i\lambda_i \qquad , \tag{A.3}$$

and obtain the vector meson matrix:

$$V = \begin{pmatrix} \frac{\rho^0}{\sqrt{2}} + \frac{v^8}{\sqrt{6}} + \frac{v^0}{\sqrt{3}} & \rho^+ & K^{*+} \\ \rho^- & -\frac{\rho^0}{\sqrt{2}} + \frac{v^8}{\sqrt{6}} + \frac{v^0}{\sqrt{3}} & K^{*0} \\ K^{*-} & \overline{K}^{*0} & -\frac{2}{\sqrt{6}}v^8 + \frac{v^0}{\sqrt{3}} \end{pmatrix} \quad . \tag{A.4}$$

Baryons

The expansion of the baryon octet reads: $\Psi = \frac{1}{\sqrt{2}} \sum_{k=0}^{8} \psi_k \lambda_k$, and yields the baryon matrix:

$$\Psi = \begin{pmatrix} \frac{\Sigma^0}{\sqrt{2}} + \frac{\Lambda^0}{\sqrt{6}} & \Sigma^+ & p \\ \Sigma^- & -\frac{\Sigma^0}{\sqrt{2}} + \frac{\Lambda^0}{\sqrt{6}} & n \\ \Xi^- & \Xi^0 & -2\frac{\Lambda^0}{\sqrt{6}} \end{pmatrix} \quad . \tag{A.5}$$

The corresponding matrix of the anti-baryons is the given as:

$$\overline{\Psi} = \begin{pmatrix} \frac{\overline{\Sigma}^0}{\sqrt{2}} + \frac{\overline{\Lambda}^0}{\sqrt{6}} & \overline{\Sigma}^- & \overline{\Xi}^- \\ \overline{\Sigma}^+ & -\frac{\overline{\Sigma}^0}{\sqrt{2}} + \frac{\overline{\Lambda}^0}{\sqrt{6}} & \overline{\Xi}^0 \\ \overline{p} & \overline{n} & -2\frac{\overline{\Lambda}^0}{\sqrt{6}} \end{pmatrix} \quad . \tag{A.6}$$

–Appendix B–

Nonlinear realization

As already discussed in section 2, nonlinear realizations of chiral symmetry were introduced to generate a a pseudovector π-N coupling in accordance with scattering data and gives a scheme for the introduction of heavy degrees of freedom in the chiral symmetric model. The main idea is to transform the heavy particles in a different representation, such that they transform equally under left and right chiral transformations. This can be achieved by coupling the heavy particles nonlinearly to the pseudoscalar mesons. Resulting advantages are (see also [Pap98a]) :

- The pseudoscalar mesons exhibit a pseudovector coupling to the baryons, what is in agreement with the experimental finding of a vanishing π-N-scattering length.
- Chiral invariance for the heavy particles is ensured, if their coupling is invariant under local $SU_V(3)$-transformations. Thus, SU(3) couplings are possible between the baryon and meson octets.
- Baryon masses can be fitted to experimental data without explicit symmetry breaking terms
- A connection to the phenomenological succesful Walecka model exists [Pap99].

- The masses of the pseudoscalar mesons do not become imaginary at higher densities.

General considerations

The idea of a nonlinear realization of chiral symmetry was introduced by Weinberg [Wei67] for the $SU_L(2) \times SU_R(2)$ case an extended to arbitrary compact groups by Coleman,Callan,Wess und Zumino [Col69, Cal69]. In the following we present the main ideas of this approach:
G be a compact symmetry group of the theory, which is spontaneously broken to its subgroup H. The generators of the subgroup H are denoted as t_i, and x_a are all remaining generators of G, in a basis of totally anti-symmetric structure constants. As shown in [Wei96], such a basis always exists. Thus, t_i and x_a span the Lie-Algebra of G. Since H is a subgroup of G, t_i represent a sub-algebra:

$$[t_i, t_j] = i \sum_k C_{ijk} t_k, \tag{B.1}$$

where C_{ijk} are the structure constants of G. Since no x_a appear on the r.h.s. of equation (B.1), all C_{ija} must be identical to zero. Due to the asymmetry of the structure constants follows

$$[t_i, x_a] = i \sum_b C_{iab} x_b \ . \tag{B.2}$$

For the commutator of the x_a one makes the general ansatz

$$[x_a, x_b] = i \sum_i C_{abi} t_i + i \sum_c C_{abc} x_c. \tag{B.3}$$

Each set of generators exhibiting commutator relations of the form (B.1)-(B.3) is called a cartan decomposition of the Lie algebra. One example is the chiral $SU_L(N) \times SU_R(N)$, with vanishing C_{abc}. Since t_i and x_i span the Lie algebra, every finite element of G can be written as:

$$g = \exp\left[i \sum \xi_a x_a\right] \exp\left[i \sum \theta_i t_i\right] \equiv U(\xi_a) V(\theta_i). \tag{B.4}$$

Multiplying an element $g \in G$ with $U(\xi_a) = \exp\left[i \sum \xi_a x_a\right]$, again gives an element of G such that

$$g \exp\left[i \sum \xi_a x_a\right] = \exp\left[i \sum \xi'_a x_a\right] \exp\left[i \sum \theta'_i t_i\right]. \tag{B.5}$$

If

$$\phi \to D(h)\phi \tag{B.6}$$

is a linear representation of the subgroup H, then the transformation

$$g : \xi \to \xi', \phi \to D\left(e^{\left[i\sum\theta'_i t_i\right]}\right)\phi \tag{B.7}$$

is a nonlinear realization of G. Successive execution of this transformation shows that the group structure is indeed realized in it. If

$$g_1 \exp\left[i\sum\xi'_a x_a\right] = \exp\left[i\sum\xi''_a x_a\right]\exp\left[i\sum\theta''_i t_i\right], \tag{B.8}$$

it follows that

$$g_1 g_0 \exp\left[i\sum\xi_a x_a\right] = \exp\left[i\sum\xi''_a x_a\right]\exp\left[i\sum\theta'''_i t_i\right], \tag{B.9}$$

with

$$\exp\left[i\sum\theta'''_i t_i\right] = \exp\left[i\sum\theta''_i t_i\right]\exp\left[i\sum\theta'_i t_i\right]. \tag{B.10}$$

Since D is a representation,

$$D\left(\exp\left[i\sum\theta'''_i t_i\right]\right) = D\left(\exp\left[i\sum\theta''_i t_i\right]\right)D\left(\exp\left[i\sum\theta'_i t_i\right]\right), \tag{B.11}$$

holds. If one now considers a field ψ, transforming according to a linear representation $D(g)$ of the broken group G,

$$\psi' = D(g)\,\psi, \tag{B.12}$$

the fields ϕ, which transform according to (B.7) are obtained by defining

$$\phi = D(\exp\left[-i\sum\xi_a x_a\right])\,\psi. \tag{B.13}$$

This can be seen as follows:

$$\begin{aligned}
\phi' &= D\left(\exp\left[-i\sum\xi'_a x_a\right]\right)\,\psi' \\
&= D\left(\exp\left[-i\sum\xi'_a x_a\right]\,g\right)\,\psi \\
&= D\left(\exp\left[-i\sum\xi'_a x_a\right]\,g\exp\left[i\sum\xi_a x_a\right]\right)\,\phi \\
&= D\left(exp\left[i\sum\theta'_i t_i\right]\right)\phi = D\left(V(\theta_i)\right)\,\phi.
\end{aligned} \tag{B.14}$$

Here equation (B.5) was used. With the help of definition (B.13), a transition from the fields transforming according to the broken group G, to new fields, transforming according to the unbroken group H, is obtained.

Nonlinear $SU(3)_L \times SU(3)_R$ Modell

The above formalism is applied to the $SU(3)_L \times SU(3)_R$ case. The generators Q^i and Q^{5a} are identified with the generators of G

$$t_i = Q^i \quad x_a = Q^{5a}. \tag{B.15}$$

Furthermore, as in [Wei67, Col69], the parameters ξ_a are identified with the pseudoscalar fields $\pi_a(x)$, since the quantum number are identical. In addition, by this choice, the pseudoscalar fields become the parameters of the chiral transformation and thus disappear from the chiral invariants (see section B). Inserting $g = L$ in (B.5) gives

$$U(\pi_a'(x)) = LU(\pi_a(x))h^\dagger, \tag{B.16}$$

where h denotes the elements of $SU_V(3)$. The transformation $U(\pi_a(x))$ is a function of the pseudoscalar fields and thus is local. Applying the parity transformation on (B.16) yields

$$PU(\pi_a(x))P^{-1} = \gamma_0 \exp\left[i\sum \pi_a(x)Q^{5a}\right]\gamma_0 = \exp\left[-i\sum \pi_a(x)Q^{5a}\right] = U(-\pi_a(x)). \tag{B.17}$$

thus,

$$U(-\pi_a'(x)) = RU(-\pi_a(x))h^\dagger, \tag{B.18}$$

follows. Hermitian conjugation finally yields

$$U(\pi_a'(x)) = hU(\pi_a(x))R^\dagger. \tag{B.19}$$

Thus, the important transformation properties of U can be summarized as follows:

$$U(\pi_a'(x)) = LU(\pi_a(x))h^\dagger = hU(\pi_a(x))R^\dagger \tag{B.20}$$

$$U^\dagger(\pi_a'(x)) = hU^\dagger(\pi_a(x))L^\dagger = RU^\dagger(\pi_a(x))h^\dagger. \tag{B.21}$$

Relation (B.13) can be used to obtain a connection between the fields q_L and q_R, which transform according to the full $SU(3)_L \times SU(3)_R$ group and the "new" quark fields $\tilde{q_L}$ and $\tilde{q_R}$, which transform according to $SU_V(3)$[1]:

$$\tilde{q_L} = U^\dagger q_L \tag{B.22}$$

$$\tilde{q_R} = U q_R. \tag{B.23}$$

[1]The dependence of U on π_a is omitted in the following to make the expressions clearer

In analogy to (B.14), the transformation of the new quark fields is given as

$$\tilde{q_L}' = U^{\dagger\prime} q_L' = U^{\dagger\prime} L q_L = h U^\dagger L^\dagger L q_L = h \tilde{q_L}$$
$$\tilde{q_R}' = U' q_R' = U' R q_R = h U R^\dagger R q_R = h \tilde{q_R}. \tag{B.24}$$
$$\tag{B.25}$$

Thus, the quark fields transforming according to the full $SU(3)_L \times SU(3)_R$ can be replaced by the new fields, transforming according to the $SU(3)_V$ subgroup. The parameters of thie local transformation $U(\pi_a(x)) = \exp[-i\pi_a(x)Q^{5a}]$ are the pseudoscalar mesons $\pi_a(x)$. With the transformation properties of the new quark fields, the transformation properties of the hadrons are givem as well. The old meson fields Σ and Π are related to the new fields X,Y and π_a by

$$M = \Sigma + i\Pi = U(X + iY)U \quad . \tag{B.26}$$

Hereby, X represents the scalar nonet and Y the pseudoscalar singlet. For the baryons, the old octet Ψ is replaced by the ney baryon octet B

$$\Psi_L = U B_L U^\dagger \qquad \Psi_R = U^\dagger B_R U \quad . \tag{B.27}$$

Thus, the "new" baryons and mesons transform as

$$\begin{aligned} B_L' &= h U^\dagger L^\dagger \cdot L \Psi_L L^\dagger \cdot L U h^\dagger = h B_L h^\dagger \\ B_R' &= h U R^\dagger \cdot R \Psi_R R^\dagger \cdot R U^\dagger h^\dagger = h B_R h^\dagger \\ X' &= \frac{1}{2}(h U^\dagger L^\dagger \cdot L M R^\dagger \cdot R U^\dagger h^\dagger + h U R^\dagger \cdot R M^\dagger L^\dagger \cdot L U h^\dagger) = h X h^\dagger. \end{aligned} \tag{B.28}$$

As can be seen, the new fields transform according to the vector transfromation and the pseudoscalar mesons only appear as "rotation angle" of the symmetry transformation. Thus, the Goldstone bosons do not appear in chiral invariants without derivatives. To guarantee the correct normalization, i.e.

$$\frac{1}{2} Sp\, D_\mu M D^\mu M^\dagger = \frac{1}{2}\left(D_\mu \vec{\pi}^2\right) + \frac{1}{2}\left(D_\mu K^\dagger\right)\frac{1}{2}\left(D^\mu K\right) + ..., \tag{B.29}$$

the pseudoscalar matrix must be renormalized [Bar69]:

$$\Pi = \begin{pmatrix} \frac{1}{\sqrt{2}}\left(\pi^0 + \frac{\eta^8}{\sqrt{1+2\,r^2}}\right) & \pi^+ & 2\,\frac{K^+}{r+1} \\ \pi^- & \frac{1}{\sqrt{2}}\left(-\pi^0 + \frac{\eta^8}{\sqrt{1+2\,r^2}}\right) & 2\,\frac{K^0}{r+1} \\ 2\,\frac{K^-}{r+1} & 2\,\frac{\overline{K}^0}{r+1} & -\frac{\eta^8\sqrt{2}}{\sqrt{1+2\,r^2}} \end{pmatrix} \tag{B.30}$$

with

$$r = \sqrt{2}\frac{\zeta_0}{\sigma_0} \qquad ; P = \frac{1}{\sqrt{2}\sigma_0}\Pi \qquad U = \exp[iP]. \tag{B.31}$$

–Appendix C–

Chiral invariants for the scalar potential

The nonlinear realization of chiral symmetry offers many possibilities to form chiral invariants since the couplings of scalar mesons with each other are only governed by $SU(3)_V$-symmetry. But as will be shown, only three kinds of independent invariants exist, namely

$$I_1 = \mathrm{Tr}X, \quad I_2 = \mathrm{Tr}X^2, \quad I_3 = \det X. \tag{C.1}$$

All other invariants, $\mathrm{Tr}X^n$, with $n \geq 3$, can be expressed as a function of the four invariants shown in (3.33). This can be shown from the characteristic equation of an arbitrary 3×3 matrix X,

$$(X - x_1)(X - x_2)(X - x_3) = 0, \tag{C.2}$$

where x_i are the eigenvalues of X. By writing the coefficients of the powers of X in terms of invariants one obtains

$$X^3 - I_1 X^2 - \frac{1}{2}\left[I_2 - (I_1)^2\right] X - I_3 = 0. \tag{C.3}$$

Hence, one obtains the invariant $\mathrm{Tr}X^3$ as a function of the base (3.33),

$$I_{3m} \equiv \mathrm{Tr}X^3 = I_1 I_2 + \frac{1}{2}\left[I_2 - (I_1)^2\right] I_1 + I_3. \tag{C.4}$$

By multiplying Equation (C.3) with, e.g., X and taking the trace, the invariant for $n = 4$ can be written in terms of Equation (3.33):

$$I_4 \equiv \mathrm{Tr}X^4 = I_1 I_{3m} + \frac{1}{2}\left[I_2 - (I_1)^2\right] I_2 + I_3 I_1. \tag{C.5}$$

A similar expression can be found for all other n. Alternatively, instead of $I_3 = \det X$ the invariant $I_{3m} = \mathrm{Tr}X^3$, can be chosen as an element of the basis. Then, I_3 can be rewritten in terms of the new basis I_1, I_2, and I_{3m} as

$$I_3 = \frac{1}{3} I_{3m} - \frac{1}{2} I_1 I_2 + \frac{1}{6}(I_1)^3. \tag{C.6}$$

–Appendix D–

Scale invariance

Scale transformations or dilatations are space-time transformations of the form

$$x' = \lambda x. \tag{D.1}$$

Space- and time-coordinates are scaled euqually, such that the velocity of light is unaffected. Often, the parametrization $\lambda = e^{\tau}$ is used, since the exponential function represents a one-to-one mapping and shows the desired behaviour $e^{\tau} \simeq 1+\tau$ for infinitesimal transformations. Now, the question arises, how an arbitrary field $\phi(x)$ transforms under (D.1). One assumes that the field $\phi'(x')$ at the point $x' = \lambda x$ is lineraly connected to the field $\phi(x)$. Then, the general transformation reads

$$\phi'(x) = f(\lambda)\phi(\lambda x). \tag{D.2}$$

The initially unknown function $f(\lambda)$ has to be determined. For $\lambda = 1$ the field is unaffected and thus $f(1) = 1$. Furthermore physical arguments suggest

$$f(\lambda_1\lambda_2) = f(\lambda_1)f(\lambda_2), \tag{D.3}$$

with λ_1 and λ_2 denoting two different scale transformations. The successive execution of scale transformation corresponds according to (D.1) to the multiplication of the scale parameters. To determine the function f(λ), equation (D.3) is differentiated with respect to λ_1 and then one sets $\lambda_1 = 1$ and $\lambda_2 = \lambda$. This gives

$$\lambda \frac{df(\lambda)}{d\lambda} = f(\lambda)\frac{df(1)}{d\lambda}\,. \tag{D.4}$$

This differential equation can be solved by using the ansatz

$$f(\lambda) = \lambda^d. \tag{D.5}$$

Here the derivative at $\lambda = 1$ is denoted as d. Thus, the general transformation (D.2) takes the form

$$\phi'(x) = e^{\tau d}\phi(e^{\tau}x), \tag{D.6}$$

if λ is parametrized by the exponential funcion. The meaning of the variable d can be understood from the transformation-law (D.1). If a space-time variable has the dimension [length^p], then it transforms as

$$[g] = [\text{length}^p] \Longrightarrow g' = \lambda^p g. \tag{D.7}$$

Thus, the variable d denotes the dimension of the fields. The set of all transformations with fixed matrix d and arbitrary real parameter τ constitute a group. The infinitesimal transformation can be written as[1]

$$\delta\phi = (d + x^\mu\partial_\mu)\phi. \tag{D.9}$$

From equation (D.9) follows that the dimension of a product of fields and their derivatives is equal to the sum of the factors of the product.
For a wide class of field theories, including the renormalizable field theories, these transformations represent symmetries, if $d = 1$ is assigned to the Bose fields and $d = \frac{3}{2}$ to the fermions, respectively. These numbers are the conventional dimensions of these fields and are obtained directly from the Lagrange density. This is because the Lagrange density always is of dimension [energy^4], the integral $S = \int L dt$ has the physical interpretation of an action and $L = \int \mathcal{L} d^3x$. Thus, infinitesimal transformation for the different fields and the Lagrange density read

$$\begin{aligned} \delta\psi &= (\frac{3}{2} + x^\mu\partial_\mu)\psi \\ \delta\phi &= (1 + x^\mu\partial_\mu)\phi \\ \delta\mathcal{L} &= (4 + x^\mu\partial_\mu)\mathcal{L}. \end{aligned} \tag{D.10}$$

[1]The infinitesimal variation $\delta\phi$ is the linear element of the Taylor-expansion around $\lambda = 1$:

$$\delta\phi = \left.\frac{\partial\phi'}{\partial\lambda}\right|_{\lambda=1} = (d + x^\mu\partial_\mu)\phi\delta\lambda\,. \tag{D.8}$$

Since the transformation shall be valid for arbitrary λ, scale invariance is ensured, if the term in the brackets vanishes. Therefore $\delta\lambda$ is omitted in (D.9)

A theory is invariant under scale transformations, if the change in the Lagrange density, induced by (D.9), gives a total divergence.

$$\delta\mathcal{L} = 4\mathcal{L} + x^\mu \partial_\mu \mathcal{L} = \partial_\mu (x^\mu \mathcal{L})\,, \tag{D.11}$$

since total divergence can be transformed in a surface integral which vanishes for a sufficiently large volume. Thus, a handy criterium for the existence of scale invariance can be deduced from the general form of the variation of $\mathcal{L}$ in (D.11) and only considering the potential V[2]. Then, one obtains

$$\begin{aligned}
\partial_\mu(x^\mu V) - \delta V &= 4V + x^\mu \partial_\mu V - \sum_i \frac{\partial V}{\partial \phi_i}\delta\phi_i \qquad (D.12)\\
&= 4V + x^\mu \partial_\mu V - \sum_i \frac{\partial V}{\partial \phi_i}(d_i + x^\mu\partial_\mu)\phi_i \\
&= 4V + x^\mu \partial_\mu V - \sum_i \frac{\partial V}{\partial \phi_i} d_i \phi_i - x_\lambda \underbrace{\sum_i \frac{\partial V}{\partial \phi_i}\partial^\lambda \phi_i}_{\partial^\lambda V} \\
&= 4V - \sum_i \frac{\partial V}{\partial \phi_i} d_i \phi_i = \begin{cases} 0 & : \text{ scale invariance} \\ \text{else} & : \ scale - breaking\,. \end{cases}
\end{aligned}$$

Equation (D.12) is a generating functional, from which all consequences of the scale invariance of V_0 on the masses, couplings etc. can be derived by differentiation with respect to the fields. Examples for scale invariant terms in the Lagrange density are

$$i\overline{\psi}\gamma_\mu\partial^\mu\psi, \qquad \frac{1}{2}\partial_\mu\phi\partial^\mu\phi, \qquad g\overline{\psi}\psi\phi \quad . \tag{D.13}$$

The form (D.11) shows that the Lagrangian contains only terms where the fields and the corresponding derivatives together have dimension four. If a dimensional quantity appears in the Lagrange density, the scale invariance is broken. To restore the symmetry, the term can be multiplied by an appropriate power of a scalar singlet, the dilaton. This renders the couplings dimensionless. Furthermore, a kinetic term for the dilaton must be added to the Lagrange density. If for example a mass term is multiplied by χ^2, the corresponding scale invariant term reads $m^2\phi^2\chi^2$.

[2]Here the kinetic term is assumed to be scale invariant. However, the criterium can analoguesly be written down for derivative terms

–Appendix E–

Thermal mesons

Already at relatively small temperatures the thermal production of mesons, in particular of the light pions, has to be accounted for. Therefore, the thermal contributions of the mesons has to be included in order to obtain a reasonable description of excited hadronic matter. This modifies the Hamilton operator of the system, which then may be written as

$$\mathcal{H}' = \mathcal{H} + \int d^3\vec{k} \sum_M E_M^* \mathcal{N}_M, \tag{E.1}$$

where $\mathcal{H}$ denotes the Hamilton operator without thermal mesons and $\mathcal{N}_M$ represents the mesonic number operator for meson species m. The sum runs over all included meson species. The single-particle energies of the mesons read

$$E_M^* = \sqrt{\vec{k}^2 + m_M^{*2}}, \tag{E.2}$$

with the effective meson masses m_M^{*2}. Inserting the extended Hamilton operator (E.1) in the partition function (3.60) gives the grand canonical potential. Evaluating the trace over the single-particle states yields

$$\begin{aligned} \frac{\Omega'}{V} &= -\mathcal{L}_{vec} - \mathcal{L}_0 - \mathcal{L}_{SB} - \mathcal{V}_{vac} \\ &- T \sum_{\vec{k},\lambda,i} \left[\ln\left(1 + e^{-\frac{1}{T}[E_i^* - \mu_i^*]}\right) + \ln\left(1 + e^{-\frac{1}{T}[E_i^* + \mu_i^*]}\right) \right] \\ &+ T \sum_{\vec{k},M} \ln\left(1 - e^{-\frac{1}{T}[E_M^* - \mu_M^*]}\right). \end{aligned} \tag{E.3}$$

The chemical potentials of the mesons are given by the sum of the chemical potentials of the corresponding constituent (anti)-quarks. The particle number of meson species M is obtained from the grand canonical potential by

$$\langle N_M \rangle = -\left(\frac{\partial \Omega}{\partial \mu_M}\right)_{T,V} \tag{E.4}$$

giving the mesonic distribution function

$$n_M(\vec{k}) = \frac{1}{e^{\frac{1}{T}[E_M^* - \mu_M^*]} - 1}. \tag{E.5}$$

These extensions also influence the field equations and the thermodynamical variables. The field equations including the mesonic contributions read

$$\frac{\partial(\Omega'/V)}{\partial \sigma} = \frac{\partial(\Omega/V)}{\partial \sigma} + \sum_M \int d^3\vec{k}\, \frac{m_M^*}{E_M^*} \frac{\partial m_M^*}{\partial \sigma}\, n_M(\vec{k}) \tag{E.6}$$

$$\frac{\partial(\Omega'/V)}{\partial \zeta} = \frac{\partial(\Omega/V)}{\partial \zeta} + \sum_M \int d^3\vec{k}\, \frac{m_M^*}{E_M^*} \frac{\partial m_M^*}{\partial \zeta}\, n_M(\vec{k}) \tag{E.7}$$

$$\frac{\partial(\Omega'/V)}{\partial \omega} = \frac{\partial(\Omega/V)}{\partial \omega} + \sum_M \int d^3\vec{k}\, \frac{m_M^*}{E_M^*} \frac{\partial m_M^*}{\partial \omega}\, n_M(\vec{k}) \tag{E.8}$$

$$\frac{\partial(\Omega'/V)}{\partial \phi} = \frac{\partial(\Omega/V)}{\partial \phi} + \sum_M \int d^3\vec{k}\, \frac{m_M^*}{E_M^*} \frac{\partial m_M^*}{\partial \phi}\, n_M(\vec{k}), \tag{E.9}$$

where Ω' and Ω denote the grandcanonical potential including and without the thermal mesons, respectively. The modified thermodynamical quantities read

$$p' = p + \frac{1}{3} \sum_M \frac{\gamma_M}{(2\pi)^3} \int d^3\vec{k}\, \frac{\vec{k}^2}{E_M^{*2}}\, n_M(\vec{k}) \tag{E.10}$$

$$\epsilon' = \epsilon + \frac{1}{3} \sum_M \frac{\gamma_M}{(2\pi)^3} \int d^3\vec{k}\, E_M^{*2}\, n_M(\vec{k}), \tag{E.11}$$

where p, ϵ denote pressure and energy without the meson contributions.

References

[Adl68] S. Adler und R. Dashen, *Current algebra and applications to particle physics*, Benjamin, New York, 1968.

[Adl69] S. L. Adler, Phys. Rev. **177** (1969), 2426–2438.

[Adl01] C. Adler et al., Phys. Rev. Lett. **87** (2001), 082301.

[Afa02a] S. V. Afanasev et al., Nucl. Phys. **A698** (2002), 104–111.

[Afa02b] S. V. Afanasiev et al., Phys. Rev. **C66** (2002), 054902.

[Afa02c] S. V. Afanasiev et al., J. Phys. **G28** (2002), 1761–1768.

[Afa02d] S. V. Afanasiev et al., Phys. Lett. **B538** (2002), 275–281.

[Aga95] G. Agakichiev et al., PRL **75** (1995), 1272.

[Aga98] G. Agakichiev et al., Phys. Lett. B **422** (1998), 405.

[Ala99] J. Alam, S. Sarkar, P. Roy, B. Dutta-Roy und B. Sinha, Phys. Rev. **C59** (1999), 905–913.

[Alf73] V. D. Alfaro, S. Fubini, G. Furlan und C. Rosetti, *Currents in hadron physics*, North-Holland Publishing Company, Amsterdam, 1973.

[Ana83] M. R. Anastasio, L. S. Celenza, W. S. Pong und C. M. Shakin, Phys. Rept. **100** (1983), 327–401.

[And99] C. Anderlik et al., Phys. Rev. **C59** (1999), 3309–3316.

[Ard99] D. Ardouin et al., Phys. Lett. **B446** (1999), 191–196.

[Asa92] M. Asakawa, C. M. Ko, P. Levai und X. J. Qiu, Phys. Rev. **C46** (1992), 1159–1162.

[Bac99] J. Bachler et al., Nucl. Phys. **A661** (1999), 45–54.

[Bal03] K. Balazs, Dissertation, J. W. Goethe–Universität, Frankfurt am Main, 2003, in preparation.

[Bar69] W. A. Bardeen und B. W. Lee, Phys. Rev. **177** (1969), 2389.

[Bar82] J. Bartel, P. Quentin, M. Brack, C. Guet und H. Hakansson, Nucl. Phys. A **386** (1982), 79.

[Bas99a] S. A. Bass et al., Phys. Rev. **C60** (1999), 021902.

[Bas99b] S. A. Bass, M. Gyulassy, H. Stöcker und W. Greiner, J. Phys. **G25** (1999), R1–R57.

[Bas00] S. A. Bass und A. Dumitru, Phys. Rev. **C61** (2000), 064909.

[Bas01] S. A. Bass, P. Danielewicz, S. Pratt und A. Dumitru, J. Phys. **G27** (2001), 635–644.

[Bay71] G. Baym, C. Pethick und P. Sutherland, Astrophys. J. **170** (1971), 299–317.

[Bay83] G. Baym, B. L. Friman, J. P. Blaizot, M. Soyeur und W. Czyz, Nucl. Phys. **A407** (1983), 541–570.

[Bay98] G. Baym, Acta Phys. Polon. **B29** (1998), 1839–1884.

[Bec97] F. Becattini und U. W. Heinz, Z. Phys. **C76** (1997), 269–286.

[Bec98] F. Becattini, M. Gazdzicki und J. Sollfrank, Nucl. Phys. **A638** (1998), 403–406.

[Bec01] F. Becattini, J. Cleymans, A. Keranen, E. Suhonen und K. Redlich, Phys. Rev. **C64** (2001), 024901.

[Ber88] G. Bertsch, M. Gong und M. Tohyama, Phys. Rev. **C37** (1988), 1896–1900.

[Ber89] G. F. Bertsch, Nucl. Phys. **A498** (1989), 173c–180c.

[Bet36] H. A. Bethe und R. F. Bacher, Rev. Mod. Phys. **8** (1936), 82.

[Bet55] H. Bethe und F. de Hoffmann, *Mesons and fields, vol. ii*, Row, Peterson and Co., Illinois, 1955.

[Bir96] M. C. Birse, Z. Phys. A **355** (1996), 231.

[Bjo64] J. D. Bjorken und S. D. Drell, *Relativistic quantum mechanics*, Mc Graw-Hill Book Company, New York, 1964.

[Bjo83] J. D. Bjorken, Phys. Rev. **D27** (1983), 140–151.

[Bla52] J. Blatt und V. Weisskopf, *Theoretical nuclear physics*, Wiley, Ney York, 1952.

[Bla76] J. P. Blaizot, D. Gogny und B. Grammaticos, Nucl. Phys. **A265** (1976), 315.

[Bla80] J. P. Blaizot, Phys. Rept. **64** (1980), 171.

[bnl03] *The physics of rhic*, http://www.bnl.gov/rhic/QGP.htm, 2003.

[Bog77] J. Boguta und A. R. Bodmer, Nucl. Phys. A **292** (1977), 413.

[Bog83a] J. Boguta, Phys. Lett. **B128** (1983), 19–23.

[Bog83b] J. Boguta, Phys. Lett. B **120** (1983), 34.

[Bog83c] J. Boguta und H. Stöcker, Phys. Lett. B **120** (1983), 289.

[Bog89] J. Boguta und J. Kunz, Nucl. Phys. **A501** (1989), 637–652.

[Bol93a] J. Bolz, U. Ornik, M. Plumer, B. R. Schlei und R. M. Weiner, Phys. Lett. **B300** (1993), 404–409.

[Bol93b] J. Bolz, U. Ornik, M. Plumer, B. R. Schlei und R. M. Weiner, Phys. Rev. **D47** (1993), 3860–3870.

[Bor96] B. Borasoy und U. G. Meissner, Int. J. Mod. Phys. A **11** (1996), 5183.

[Bra64] B. Brandow, Dissertation, Cornell University, 1964.

[Bra96] P. Braun-Munzinger, J. Stachel, J. P. Wessels und N. Xu, Phys. Lett. B **365** (1996), 1.

[Bra98] P. Braun-Munzinger und J. Stachel, Nucl. Phys. **A638** (1998), 3.

[Bra99] P. Braun-Munzinger, J. Heppe und J. Stachel, Phys. Lett. B **465** (1999), 15.

[Bra00] J. Brachmann et al., Phys. Rev. **C61** (2000), 024909.

[Bra01] P. Braun-Munzinger, D. Magestro, K. Redlich und J. Stachel, Phys. Lett. **B518** (2001), 41–46.

[Bra03] P. Braun-Munzinger, K. Redlich und J. Stachel.

[Bre37] G. Breit, Phys. Rev. **120** (1937), 248.

[Bre38] G. Breit und J. Stehn, Phys. Rev. **53** (1938), 459.

[Bro90] F. R. Brown et al., Phys. Rev. Lett. **65** (1990), 2491–2494.

[Bro91] G. E. Brown und M. Rho, Phys. Rev. Lett. **66** (1991), 2720–2723.

[Bro96] R. Brockmann und R. Machleidt, nucl-th/9612004 (1996).

[Brü54] K. Brückner, C. Levinson und H. Mahmoud, Phys. Rev. **95** (1954), 217.

[Bug96] K. A. Bugaev, Nucl. Phys. **A606** (1996), 559–567.

[Cal69] C. G. Callan, S. Coleman, J. Wess und B. Zumino, Phys. Rev. **177** (1969), 2247.

[Cal78] J. Callan, Curtis G., R. F. Dashen und D. J. Gross, Phys. Rev. **D17** (1978), 2717.

[Cel86] L. Celenza und C. Shakin, *Relativistic nuclear physics*, World Scientific, Philadelphia, 1986.

[Cha73] M. S. Chanowitz und J. R. Ellis, Phys. Rev. **D7** (1973), 2490.

[Cha92] G. Chanfray und P. Schuck, Nucl. Phys. **A545** (1992), 271c–276c.

[Cha95] S. Chapman, P. Scotto und U. W. Heinz, Phys. Rev. Lett. **74** (1995), 4400–4403.

[Che94] T. P. Cheng und L. F. Li, *Gauge theory of elementary particle physics*, Oxford University Press, New York, 1994.

[Cho74] A. Chodos, R. L. Jaffe, K. Johnson, C. B. Thorn und V. F. Weisskopf, Phys. Rev. **D9** (1974), 3471–3495.

[Cho01] A. Chodos, F. Cooper, W. Mao und A. Singh, Phys. Rev. **D63** (2001), 096010.

[Cla73] B. C. Clark, R. L. Mercer, D. G. Ravenhall und A. M. Saperstein, Phys. Rev. **C7** (1973), 466–471.

[Cla82] B. C. Clark, S. Hama und R. L. Mercer, In *Bloomington 1982, Proceedings, The Interaction Between Medium Energy Nucleons In Nuclei*, 260-287.

[Cle98] J. Cleymans und K. Redlich, Phys. Rev. Lett. **81** (1998), 5284–5286.

[Cle99] J. Cleymans und K. Redlich, Phys. Rev. **C60** (1999), 054908.

[Coe70] F. Coester, S. Cohen, B. Day und C. Vincent, Phys. Rev. C **1** (1970), 769.

[Col69] S. Coleman, Phys. Rev. **177** (1969), 2239.

[Col77] J. C. Collins und D. E. Soper, Phys. Rev. **D16** (1977), 2219.

[Col85] S. Coleman, *Aspects of symmetry*, Cambridge University Press, Cambridge, 1985.

[con03] *The contemporary physics education project*, http://www.cpepweb.org, 2003.

[Cre72] R. J. Crewther, Phys. Rev. Lett. **28** (1972), 1421.

[Cse86] L. P. Csernai und J. I. Kapusta, Phys. Rept. **131** (1986), 223–318.

[Cso94] T. Csorgo und L. P. Csernai, Phys. Lett. **B333** (1994), 494–499.

[Cso96] T. Csorgo, B. Lorstad und J. Zimanyi, Z. Phys. **C71** (1996), 491–497.

[Cso02] T. Csorgo, Heavy Ion Phys. **15** (2002), 1–80.

[Das69] R. F. Dashen und M. Weinstein, Phys. Rev. **183** (1969), 1261–1291.

[DeT89] C. DeTar und T. Kunihiro, Phys. Rev. **D39** (1989), 2805.

[Don89] J. F. Donoghue, Ann. Rev. Nucl. Part. Sci. **39** (1989), 1–17.

[Don92] J. Donoghue, E. Golowich und B. Holstein, *Dynamics of the starndard model*, Cambridge University Press, Cambridge, 1992.

[Dre90] R. Dreizler und E. Gross, *Density functional theory*, Springer, Berlin, 1990.

[Due56] H. Duerr, Phys. Rev. **103** (1956), 469.

[Dum95] A. Dumitru et al., Phys. Rev. **C51** (1995), 2166–2170.

[Dum99] A. Dumitru und D. H. Rischke, Phys. Rev. **C59** (1999), 354–363.

[Dum01] A. Dumitru und R. D. Pisarski, Phys. Lett. **B504** (2001), 282–290.

[Eng94] L. Engvik, M. Hjorth-Jensen, E. Osnes, G. Bao und E. Ostgaard, Phys. Rev. Lett. **73** (1994), 2650–2653.

[Erk74] K. Erkelenz, Phys. Rept. **13** (1974), 191–258.

[Ern98] C. Ernst, S. A. Bass, M. Belkacem, H. Stöcker und W. Greiner, Phys. Rev. **C58** (1998), 447–456.

[Fer50] E. Fermi, Prog. Theor. Phys. **5** (1950), 570–583.

[Flo02] W. Florkowski, W. Broniowski und M. Michalec, Acta Phys. Polon. **B33** (2002), 761–769.

[Fod02] Z. Fodor und S. Katz, hep-lat/0204029 (2002).

[Fom95] V. N. Fomenko, L. N. Savushkin, S. Marcos, R. Niembro und M. L. Quelle, J. Phys. **G21** (1995), 53–62.

[Fom97] V. N. Fomenko, L. N. Savushkin, S. Marcos und P. Ring, Phys. Atom. Nucl. **60** (1997), 1967–1978.

[Fra59] W. Frazer und J. Fulco, PRL **2** (1959), 365.

[Fra60] W. Frazer und J. Fulco, Phys. Rev. **117** (1960), 1609.

[Fri02] V. Friese, Nucl. Phys. **A698** (2002), 487–490.

[Fuj79] K. Fujikawa, Phys. Rev. Lett. **42** (1979), 1195.

[Fur87] R. J. Furnstahl, C. E. Price und G. E. Walker, Phys. Rev. C **36** (1987), 2590.

[Fur90] R. J. Furnstahl und B. D. Serot, Phys. Rev. C **41** (1990), 262.

[Fur93] R. J. Furnstahl und B. D. Serot, Phys. Rev. C **47** (1993), 2338.

[Fur95] R. J. Furnstahl, H. B. Tang und B. D. Serot, Phys. Rev. C **52** (1995), 1368.

[Fur96a] R. J. Furnstahl, B. D. Serot und H. B. Tang, Nucl. Phys. A **598** (1996), 539.

[Fur96b] R. J. Furnstahl, B. D. Serot und H.-B. Tang, Nucl. Phys. **A598** (1996), 539–582.

[Fur00a] R. J. Furnstahl und B. D. Serot, Nucl. Phys. **A673** (2000), 298–310.

[Fur00b] R. J. Furnstahl und B. D. Serot, Nucl. Phys. **A671** (2000), 447–460.

[Fur00c] R. J. Furnstahl und B. D. Serot, Comments Nucl. Part. Phys. **2** (2000), A23–A45.

[Fur00d] R. J. Furnstahl, J. V. Steele und N. Tirfessa, Nucl. Phys. **A671** (2000), 396–415.

[Gam90] Y. K. Gambhir, P. Ring und A. Thimet, Annals Phys. **198** (1990), 132–179.

[Gar48] E. Gardner und C. M. G. Lattes, Science **107** (1948), 270.

[Gas69] S. Gasiorowicz und D. Geffen, Rev. Mod. Phys. **41** (1969), 531.

[Gas82] J. Gasser und H. Leutwyler, Phys. Rept. **87** (1982), 77–169.

[Gas84] J. Gasser und H. Leutwyler, Ann. Phys. **158** (1984), 142.

[Gas85] J. Gasser und H. Leutwyler, Nucl. Phys. **B250** (1985), 465.

[Gei93] K. Geiger und J. I. Kapusta, Phys. Rev. **D47** (1993), 4905–4919.

[Gel60] M. Gell-Mann und M. Levy, Nuovo Cimento **16** (1960), 705.

[Gel62] M. Gell-Mann, D. Sharp und W. G. Wagner, Phys. Rev. Lett. **8** (1962), 261.

[Ger95] L. Gerland et al., nucl-th/9512032 (1995).

[Gle92] N. K. Glendenning, Phys. Rev. **D46** (1992), 1274–1287.

[Gle96] N. Glendenning, *Compact stars*, Springer, Berlin, 1996.

[Gol57] J. Goldstone, Proc. R. Soc. **A239** (1957), 267.

[Gol60] G. Goldhaber, S. Goldhaber, W.-Y. Lee und A. Pais, Phys. Rev. **120** (1960), 300–312.

[Gol61] J. Goldstone, Nuovo Cimento **19** (1961), 154.

[Got86] K. Gottfried und V. Weisskopf, *Concepts of particle physics, vol. ii*, Oxford University Press, New York, 1986.

[Gra89] P. Grange, A. Lejeune, M. Martzolff und J. F. Mathiot, Phys. Rev. **C40** (1989), 1040–1060.

[Gre67] H. S. Green, Rev. Mod. Phys. **39** (1967), 495.

[Gre77] W. Grein, Nucl. Phys. **B131** (1977), 255.

[Gre80] W. Grein und P. Kroll, Nucl. Phys. **A338** (1980), 332.

[Gre87] C. Greiner, P. Koch und H. Stöcker, Phys. Rev. Lett. **58** (1987), 1825–1828.

[Gre88] C. Greiner, D.-H. Rischke, H. Stöcker und P. Koch, Phys. Rev. **D38** (1988), 2797–2807.

[Gre91] C. Greiner und H. Stöcker, Phys. Rev. **D44** (1991), 3517–3529.

[Gre93] W. Greiner, L. Neise und H. Stöcker, *Thermodynamik und statistische mechanik*, Verlag Harri Deutsch, Thun, Frankfurt am Main, 1993.

[Gre01] C. Greiner und S. Leupold, J. Phys. **G27** (2001), L95–L102.

[Gre02a] C. Greiner, Nucl. Phys. **A698** (2002), 591–594.

[Gre02b] C. Greiner, J. Phys. **G28** (2002), 1631–1648.

[Gro73a] D. J. Gross und F. Wilczek, Phys. Rev. **D8** (1973), 3633–3652.

[Gro73b] D. J. Gross und F. Wilczek, Phys. Rev. Lett. **30** (1973), 1343–1346.

[Gro99] D. J. Gross, Nucl. Phys. Proc. Suppl. **74** (1999), 426–446.

[gsi03] *The gsi future project*, http://www-new.gsi.de, 2003.

[Gyu79] M. Gyulassy, S. K. Kauffmann und L. W. Wilson, Phys. Rev. **C20** (1979), 2267–2292.

[Gyu89] M. Gyulassy und S. S. Padula, Phys. Lett. **B217** (1989), 181–185.

[Hag94] K. Haglin und S. Pratt, Phys. Lett. **B328** (1994), 255–258.

[Hah86] D. Hahn und H. Stöcker, Nucl. Phys. **A452** (1986), 723.

[Ham88] Y. Hama und S. S. Padula, Phys. Rev. **D37** (1988), 3237.

[Han56] R. Hanbury Brown und R. Q. Twiss, Nature **178** (1956), 1046–1048.

[Han01] M. Hanauske, L. M. Satarov, I. N. Mishustin, H. Stöcker und W. Greiner, Phys. Rev. **D64** (2001), 043005.

[Hat92] T. Hatsuda und S. H. Lee, Phys. Rev. **C46** (1992), 34–38.

[Hat95] T. Hatsuda, S. H. Lee und H. Shiomi, Phys. Rev. **C52** (1995), 3364–3372.

[Hat96] T. Hatsuda, H. Shiomi und H. Kuwabara, Prog. Theor. Phys. **95** (1996), 1009–1028.

[Hei94] E. K. Heide, S. Rudaz und P. J. Ellis, Nucl. Phys. A **571** (1994), 713.

[Hei99] U. W. Heinz und B. V. Jacak, Ann. Rev. Nucl. Part. Sci. **49** (1999), 529–579.

[Her93] M. Herrmann, B. L. Friman und W. Norenberg, Nucl. Phys. **A560** (1993), 411–436.

[Hol81] K. Holinde, Phys. Rept. **68** (1981), 121–188.

[Hol86] G. Holzwarth und B. Schwesinger, Rept. Prog. Phys. **49** (1986), 825.

[Hor81] C. J. Horowitz und B. D. Serot, Nucl. Phys. **A368** (1981), 503.

[Hul57] L. Hulthen und M. Sugawara, Encycl. Phys. **39** (1957), 1.

[Itz80] C. Itzykson und J. Zuber, *Quantum field theory*, McGraw-Hill, New York, 1980.

[Iwa96] Y. Iwasaki, K. Kanaya, S. Kaya, S. Sakai und T. Yoshie, Z. Phys. **C71** (1996), 343–346.

[Jac83] A. D. Jackson, M. Rho und E. Krotscheck, Nucl. Phys. **A407** (1983), 495.

[Jea94] H. C. Jean, J. Piekarewicz und A. G. Williams, Phys. Rev. **C49** (1994), 1981–1988.

[Jin95a] X. Jin, Phys. Rev. C **51** (1995), 2260.

[Jin95b] X. Jin und D. B. Leinweber, Phys. Rev. **C52** (1995), 3344–3352.

[Joh55] M. Johnson und E. Teller, Phys. Rep. **98** (1955), 783.

[Kaj82] K. Kajantie und L. D. McLerran, Phys. Lett. **B119** (1982), 203.

[Kaj83a] K. Kajantie und L. D. McLerran, Nucl. Phys. **B214** (1983), 261.

[Kaj83b] K. Kajantie, R. Raitio und P. V. Ruuskanen, Nucl. Phys. **B222** (1983), 152.

[Kap95] D. B. Kaplan, nucl-th/9506035 (1995).

[Kay84] O. Kaymakcalan, S. Rajeev und J. Schechter, Phys. Rev. **D30** (1984), 594.

[Ker74] A. K. Kerman und L. D. Miller, *Field theory methods for finite nuclear systems and the possibility of density isomerism*, Proceedings of the Second Relativistic Heavy Ion Summer Study (LBL), Berkeley, 1974.

[Kim97] H.-C. Kim, S. Schramm und S. H. Lee, Phys. Rev. **C56** (1997), 1582–1587.

[Kli96] F. Klingl, N. Kaiser und W. Weise, Z. Phys. A **356** (1996), 193.

[Kli97] F. Klingl, N. Kaiser und W. Weise, Nucl. Phys. **A624** (1997), 527–563.

[Kop74] G. I. Kopylov, Phys. Lett. **B50** (1974), 472–474.

[Kos98] D. Kosov, C. Fuchs, B. Martemyanov und A. Faessler, PL **B 421** (1998), 37–40.

[Kun86] J. Kunz, D. Masak, U. Post und J. Boguta, Phys. Lett. **B169** (1986), 133–138.

[Kun87] J. Kunz, D. Masak und U. Post, Phys. Lett. **B186** (1987), 124–128.

[Kuo96] H. Kuono et al., Phys. Rev. **C53** (1996), 2542–2545.

[Lae96] E. Laermann, Nucl. Phys. **A610** (1996), 1c–12c.

[Lan53] L. D. Landau, Izv. Akad. Nauk SSSR Ser. Fiz. **17** (1953), 51–64.

[Lan59] L. Landau und E. Lifshitz, *Fluid mechanics*, Pergamon Press, New York, 1959.

[Lat47a] C. M. G. Lattes, H. Muirhead, G. P. S. Occhialini und C. F. Powell, Nature **159** (1947), 694–697.

[Lat47b] C. M. G. Lattes, G. P. S. Occhialini und C. F. Powell, Nature **160** (1947), 453–456.

[Lee74] T. D. Lee und G. C. Wick, Phys. Rev. **D9** (1974), 2291.

[Lej00] A. Lejeune, U. Lombardo und W. Zuo, Phys. Lett. **B477** (2000), 45.

[Let93] J. Letessier, A. Tounsi, U. W. Heinz, J. Sollfrank und J. Rafelski, Phys. Rev. Lett. **70** (1993), 3530–3533.

[Let00] J. Letessier und J. Rafelski, Int. J. Mod. Phys. **E9** (2000), 107–147.

[Li95] B.-A. Li und C. M. Ko, Phys. Rev. **C52** (1995), 2037–2063.

[Mac86] R. Machleidt, Relativistic Dynamics and Quark-Nuclear Physics (1986), 71.

[Mac89] R. Machleidt, ANP **19** (1989), 189–376.

[Mag99] V. K. Magas et al., Heavy Ion Phys. **9** (1999), 193–216.

[Mak88] A. N. Makhlin und Y. M. Sinyukov, Z. Phys. **C39** (1988), 69.

[Mal01] S. Mallik und A. Nyffeler, Phys. Rev. **C63** (2001), 065204.

[Mas95] M. Masera, Nucl. Phys. **A590** (1995), 93c–102c.

[Mat82] T. Matsui und B. D. Serot, Ann. Phys. **144** (1982), 107.

[Mei86] U. Meissner und I. Zahed, Adv. Nucl. Phys. **17** (1986).

[Mic01] M. Michalec, Dissertation, Institute of Nuclear Physics, Crakow, 2001.

[Mig67] A. Migdal, *Theory of finite fermi systems and applications to atomic nuclei*, Wiley, New York, 1967.

[Mil72] L. Miller und A. Green, Phys. Rev. C **5** (1972), 241.

[Mis97] A. Mishra, P. K. Panda, S. Schramm, J. Reinhardt und W. Greiner, Phys. Rev. **C56** (1997), 1380–1388.

[Mis01] A. Mishra, P. K. Panda und W. Greiner, J. Phys. **G27** (2001), 1561–1576.

[Mis02a] A. Mishra, P. K. Panda und W. Greiner, J. Phys. **G28** (2002), 67–83.

[Mis02b] A. Mishra, J. C. Parikh und W. Greiner, J. Phys. **G28** (2002), 151–168.

[Mis02c] A. Mishra, J. Reinhardt, H. Stöcker und W. Greiner, Phys. Rev. **C66** (2002), 064902.

[Mit68] P. K. Mitter und L. J. Swank, Nucl. Phys. B **8** (1968), 205.

[Mor51] M. Moravcsik, *The two-nucleon interaction*, Clarendon Press, Oxford, 1951.

[Mor72] M. Moravcsik, Rep. Prog. Phys. **32** (1972), 587.

[Mor98] D. P. Morrison et al., Nucl. Phys. **A638** (1998), 565–570.

[Mor00] K. Morita, S. Muroya, H. Nakamura und C. Nonaka, Phys. Rev. **C61** (2000), 034904.

[Mos89] U. Mosel, *Fields, symmetries, and quarks*, Mc Graw-Hill, Hamburg, 1989.

[Mur02] A. Muronga, Phys. Rev. Lett. **88** (2002), 062302.

[Nam57] Y. Nambu, Phys. Rev. **106** (1957), 1366.

[Neg70] J. Negele, Phys. Rev. C **1** (1970), 1260.

[Neg73] J. W. Negele und D. Vautherin, Nucl. Phys. **A207** (1973), 298–320.

[Noe18] E. Noether, Nachr. Kgl. Geo. Wiss Gottinger **235** (1918).

[Now96] M. A. Nowak, M. Rho und I. Zahed, Singapore, Singapore: World Scientific (1996) 528 p.

[Nym76a] E. M. Nyman und M. Rho, Nucl. Phys. **A268** (1976), 408–444.

[Nym76b] E. M. Nyman und M. Rho, Phys. Lett. **B60** (1976), 134.

[Opp39] J. Oppenheimer und G. Volkoff, Phys. Rev. **55** (1939), 374.

[Pae03a] K. Paech, Dissertation, J. W. Goethe–Universität, Frankfurt am Main, 2003, in preparation.

[Pae03b] K. Paech, H. Stöcker und A. Dumitru, nucl-th/0302013 (2003).

[Pal99] S. Pal, M. Hanauske, I. Zakout, H. Stöcker und W. Greiner, Phys. Rev. **C60** (1999), 015802.

[Pap98a] P. Papazoglou, *Einheitliche Beschreibung von Hadronen und Kernen in einem chiralen $SU(3)$-Modell*, Dissertation, J. W. Goethe–Universität, Frankfurt am Main, 1998.

[Pap98b] P. Papazoglou, S. Schramm, J. Schaffner-Bielich, H. Stöcker und W. Greiner, Phys. Rev. C **57** (1998), 2576.

[Pap99] P. Papazoglou, D. Zschiesche, S. Schramm, J. Schaffner-Bielich, H. Stöcker und W. Greiner, Phys. Rev. C **59** (1999), 411.

[Pau46] W. Pauli, *The meson theory of nuclear forces*, Interscience, New York, 1946.

[Phi59] R. Phillips, Rep. Prog. Phys. **22** (1959), 562.

[phy85] Physics Today **37** (1985), 20.

[Pic91] A. Pich und E. de Rafael, Nucl. Phys. **B367** (1991), 313–333.

[Pis84] R. D. Pisarski und F. Wilczek, Phys. Rev. **D29** (1984), 338–341.

[Pol58] J. C. Polkinghorne, Nuovo Cimento **8** (1958), 179.

[Pol73] H. D. Politzer, Phys. Rev. Lett. **30** (1973), 1346–1349.

[Por97] R. J. Porter et al., Phys. Rev. Lett. **79** (1997), 1229–1232.

[Pra84] S. Pratt, Phys. Rev. Lett. **53** (1984), 1219–1221.

[Pra86] S. Pratt, Phys. Rev. **D33** (1986), 1314–1327.

[Pra93] M. Prakash, M. Prakash, R. Venugopalan und G. Welke, Phys. Rept. **227** (1993), 321–366.

[Pra94] S. Pratt, Phys. Rev. **C49** (1994), 2722–2728.

[Pra97] M. Prakash et al., Phys. Rept. **280** (1997), 1–77.

[Pud97] B. S. Pudliner, V. R. Pandharipande, J. Carlson, S. C. Pieper und R. B. Wiringa, Phys. Rev. **C56** (1997), 1720–1750.

[Raf01] J. Rafelski, J. Letessier und G. Torrieri, Phys. Rev. **C64** (2001), 054907.

[Rap97] R. Rapp, G. Chanfray und J. Wambach, Nucl. Phys. **A617** (1997), 472–495.

[Rap00] R. Rapp und J. Wambach, Adv. Nucl. Phys. **25** (2000), 1.

[Rap01] R. Rapp und E. V. Shuryak, Phys. Rev. Lett. **86** (2001), 2980–2983.

[Rei68] J. Reid, Roderick V., Ann. Phys. **50** (1968), 411–448.

[Rei86] P. G. Reinhard, M. Rufa, J. Maruhn, W. Greiner und J. Friedrich, Z. Phys. **A323** (1986), 13–25.

[Rei89] P. G. Reinhard, Rept. Prog. Phys. **52** (1989), 439.

[Rin80] P. Ring und P. Schuck, *The nuclear many-body problem*, Springer, New York, 1980.

[Ris95] D. H. Rischke, S. Bernard und J. A. Maruhn, Nucl. Phys. **A595** (1995), 346–382.

[Ris96a] D. H. Rischke und M. Gyulassy, Nucl. Phys. **A597** (1996), 701–726.

[Ris96b] D. H. Rischke und M. Gyulassy, Nucl. Phys. **A608** (1996), 479–512.

[Ros45] L. Rosenfeld, Nature **145** (1945), 141.

[Ros48] L. Rosenfeld, *Nuclear forces*, North-Holland, Amsterdam, 1948.

[Sai98] K. Saito, K. Tsushima, A. W. Thomas und A. G. Williams, Phys. Lett. **B433** (1998), 243–249.

[Sak60a] J. Sakurai, Ann. Phys. **11** (1960), 1.

[Sak60b] J. Sakurai, Phys. Rev. **119** (1960), 1784.

[Sak60c] J. Sakurai, Nuovo Cimento **16** (1960), 388.

[Sak69] J. J. Sakurai, *Currents and mesons*, University of Chicago Press, Chicago, 1969.

[Sar85] S. Sarkar und S. K. Chowdhury, Phys. Lett. **B153** (1985), 358–362.

[Sca01a] O. Scavenius, A. Dumitru, E. S. Fraga, J. T. Lenaghan und A. D. Jackson, Phys. Rev. **D63** (2001), 116003.

[Sca01b] O. Scavenius, A. Dumitru und A. D. Jackson, Phys. Rev. Lett. **87** (2001), 182302.

[Sca02] O. Scavenius, A. Dumitru und J. T. Lenaghan, Phys. Rev. **C66** (2002), 034903.

[Sch51] L. Schiff, Phys. Rep. **84** (1951), 1, 10.

[Sch57] J. Schwinger, Ann. Phys. (N.Y.) **2** (1957), 407.

[Sch67] J. S. Schwinger, Phys. Lett. **B24** (1967), 473–476.

[Sch69] J. Schechter, Y. Ueda und G. Venturi, Phys. Rev. **177** (1969), 2311.

[Sch71] J. Schechter und Y. Ueda, Phys. Rev. D **3** (1971), 168.

[Sch80] J. Schechter, Phys. Rev. D **21** (1980), 3393.

[Sch92] B. R. Schlei, U. Ornik, M. Plumer und R. M. Weiner, Phys. Lett. **B293** (1992), 275–281.

[Sch93] T. Schoenfeld, H. Stoecker, W. Greiner und H. Sorge, Mod. Phys. Lett. **A8** (1993), 2631–2641.

[Sch94] J. Schaffner, C. B. Dover, A. Gal, C. Greiner, D. J. Millener und H. Stöcker, Ann. Phys. (N.Y.) **235** (1994), 35–76.

[Sch95] R. N. Schmid, E. Engel und R. M. Dreizler, Phys. Rev. **C52** (1995), 164–169.

[Sch96a] J. Schaffner und I. N. Mishustin, Phys. Rev. **C53** (1996), 1416–1429.

[Sch96b] B. R. Schlei, U. Ornik, M. Plumer, D. Strottman und R. M. Weiner, Phys. Lett. **B376** (1996), 212–219.

[Sch02] S. Schramm, Phys. Rev. **C66** (2002), 064310.

[Sch03] S. Schramm und D. Zschiesche, J. Phys. **G29** (2003), 531–542.

[Seg77] E. Segre, *Nuclei and particles*, Benjamin, London, 1977.

[Ser86] B. D. Serot und J. D. Walecka, Adv. Nucl. Phys. **16** (1986).

[Ser92] B. D. Serot, Rept. Prog. Phys. **55** (1992), 1855–1946.

[Ser97] B. D. Serot und J. D. Walecka, Int. J. Mod. Phys. E **6** (1997), 515.

[Sha74] A. de Shalit und H. Feshbach, *Theoretical nuclear physics, vol i*, Wiley, New York, 1974.

[Sha93] M. M. Sharma, M. A. Nagarajan und P. Ring, Phys. Lett. **B312** (1993), 377–381.

[Shi91] M. A. Shifman, Phys. Rept. **209** (1991), 341–378.

[Shi94] H. Shiomi und T. Hatsuda, Phys. Lett. **B334** (1994), 281–286.

[Shu73] E. V. Shuryak, Phys. Lett. **B44** (1973), 387–389.

[Sky59] T. H. R. Skyrme, Nucl. Phys. **9** (1959), 615.

[Sof97] S. Soff et al., J. Phys. **G23** (1997), 2095–2105.

[Sof01] S. Soff, S. A. Bass und A. Dumitru, Phys. Rev. Lett. **86** (2001), 3981–3984.

[Spi98] C. Spieles, H. Stöcker und C. Greiner, Eur. Phys. J. **C2** (1998), 351–358.

[Ste00] J. V. Steele und R. J. Furnstahl, Nucl. Phys. **A663** (2000), 999–1002.

[Stö78] H. Stöcker, W. Greiner und W. Scheid, Z. Phys. A **286** (1978), 121.

[Stö82] H. Stöcker et al., Phys. Rev. C **25** (1982), 1873.

[Stö86] H. Stöcker und W. Greiner, Phys. Rept. **137** (1986), 277–392.

[Stö94] H. Stöcker et al., Nucl. Phys. A **566** (1994), 15C.

[Sto99a] R. Stock, Phys. Lett. **B456** (1999), 277–282.

[Sto99b] R. Stock, Nucl. Phys. **A661** (1999), 282–299.

[Str99] J. Stroth et al., Advances in Nuclear Dynamics **5** (1999), 311.

[Sub86] P. R. Subramanian, H. Stöcker und W. Greiner, Phys. Lett. **B173** (1986), 468–472.

[Sug94] Y. Sugahara und H. Toki, Nucl. Phys. A **579** (1994), 557–572.

[Sup56] Prog. Theor. Phys. Suppl **3** (1956).

[Sup67] Prog. Theor. Phys. Suppl **39** (1967).

[Tak51] M. Taketani, S. Nakamura und M. Sasaki, Proc. Theor. Phys. **6** (1951), 581.

[Tea03] D. Teaney, nucl-th/0301099 (2003).

[t'H76] G. t'Hooft, Phys. Rev. **D14** (1976), 3432–3450.

[t'H80] G. t'Hooft et al., New York, USA: Plenum (1980) 438 P. (Nato Advanced Study Institutes Series: Series B, Physics, 59).

[The83] J. Theis, G. Graebner, G. Buchwald, J. A. Maruhn, W. Greiner, H. Stöcker und J. Polonyi, Phys. Rev. D **28** (1983), 2286.

[Tho84] A. Thomas, Adv. Nucl. Phys. **13** (1984).

[Tol39] R. Tolman, Phys. Rev. **55** (1939), 364.

[urq] *Urqmd collaboration*, http://www.th.physik.uni-frankfurt.de/ urqmd/.

[Vaf84] C. Vafa und E. Witten, Nucl. Phys. B **234** (1984), 173.

[Van98] S. E. Vance, M. Gyulassy und X. N. Wang, Nucl. Phys. **A638** (1998), 395c–398c.

[Ven94] R. Venugopalan, M. Prakash, M. Kataja und P. V. Ruuskanen, Nucl. Phys. **A566** (1994), 473c–476c.

[Vog91] U. Vogl und W. Weise, Prog. Part. Nucl. Phys. **27** (1991), 195–272.

[Wal74] J. D. Walecka, Ann. Phys. (N.Y.) **83** (1974), 49.

[Wal87] B. M. Waldhauser, J. Theis, J. A. Maruhn, H. Stöcker und W. Greiner, Phys. Rev. **C36** (1987), 1019.

[Wal95] J. D. Walecka, *Theoretical nuclear and subnuclear physics*, Oxford University Press, New York, 1995.

[Web99] F. Weber, *Pulsars as astrophysical laboratories for nuclear and particle physics*, IoP, Bristol, 1999.

[Wei35] C. F. von Weizsäcker, Z. Phys. **96** (1935), 431.

[Wei67] S. Weinberg, Phys. Rev. Lett. **18** (1967), 188–191.

[Wei68] S. Weinberg, Phys. Rev. Lett. **166** (1968), 1568.

[Wei73] S. Weinberg, Phys. Rev. **D8** (1973), 605–625.

[Wei79] S. Weinberg, Physica **A96** (1979), 327.

[Wei83] D. Weingarten, Phys. Rev. Lett. **51** (1983), 1830.

[Wei84] J. Weisberg und J. Taylor, Phys. Rev. Lett. **52** (1984), 1348.

[Wei96] S. Weinberg, *The quantum theory of fields, volume 2*, Cambridge University Press, Cambridge, 1996.

[Wei00] R. M. Weiner, *Introduction to bose-einstein correlations and subatomic interferometry*, Wiley, Chichester, UK, 2000.

[Wel92] H. A. Weldon, Z. Phys. **C54** (1992), 431–438.

[Wen49] G. Wenzel, *Quantum theory of fields*, Interscience, New York, 1949.

[Wes76] G. D. Westfall et al., Phys. Rev. Lett. **37** (1976), 1202–1205.

[Wie99] U. A. Wiedemann und U. W. Heinz, Phys. Rept. **319** (1999), 145–230.

[Wil63] R. Wilson, *The nucleon-nucleon interaction*, Interscience, New York, 1963.

[Wir95] R. B. Wiringa, V. G. J. Stoks und R. Schiavilla, Phys. Rev. **C51** (1995), 38–51.

[Xu02] N. Xu und M. Kaneta, Nucl. Phys. **A698** (2002), 306–313.

[You77] D. Youngblood, C. Rozsa, J. Moss, D. Brown und J. Bronson, Phys. Rev. Lett. **39** (1977), 1188.

[Yuk35] H. Yukawa, Proc. Phys. Math. Soc. Jpn **17** (1935), 48.

[Zah86] I. Zahed und G. E. Brown, Phys. Rept. **142** (1986), 1–102.

[Zsc97] D. Zschiesche, *Beschreibung von Heißer, Dichter und Seltsamer Hadronischer Materie in einem chiralen $SU(3)_L \times SU(3)_R$ σ-Modell*, Diplomarbeit, J. W. Goethe–Universität, Frankfurt am Main, 1997.

[Zsc00a] D. Zschiesche, P. Papazoglou, C. Beckmann, S. Schramm, J. Schaffner-Bielich, H. Stöcker und W. Greiner, Nucl. Phys. **A663** (2000), 737–740.

[Zsc00b] D. Zschiesche, P. Papazoglou, S. Schramm, C. Beckmann, J. Schaffner-Bielich, H. Stöcker und W. Greiner, Springer Tracts in Modern Physics **163** (2000), 129.

[Zsc01a] D. Zschiesche, L. Gerland, S. Schramm, J. Schaffner-Bielich, H. Stöcker und W. Greiner, Nucl. Phys. **A681** (2001), 34–40.

[Zsc01b] D. Zschiesche, P. Papazoglou, S. Schramm, J. Schaffner-Bielich, H. Stöcker und W. Greiner, Phys. Rev. **C63** (2001), 025211.

[Zsc02a] D. Zschiesche, S. Schramm, J. Schaffner-Bielich, H. Stöcker und W. Greiner, Phys. Lett. **B547** (2002), 7–14.

[Zsc02b] D. Zschiesche, S. Schramm, H. Stöcker und W. Greiner, Phys. Rev. **C65** (2002), 064902.

[Zsc03] D. Zschiesche, G. Zeeb, K. Paech, S. Schramm und H. Stöcker, submitted to J. Phys G.

Danksagung

Vor allen anderen möchte ich mich herzlich bei meiner Freundin Sophia, meiner Familie, meinen Freunden und bei Kim für ihre großartige Unterstützung sowie ihre Geduld und Nachsicht bedanken.
Mein ganz besonderer Dank gilt Prof. Dr. Horst Stöcker, der diese Arbeit durch meine Anstellung am Institut für Theoretische Physik ermöglicht hat. Zudem danke ich ihm für die vielen Ideen, Vorschläge und kritischen Kommentare, die gewährte wissenschaftliche Freiheit und die ganz besondere Arbeitsatmosphäre.
Meinen ausdrücklichen Dank richte ich an PD. Dr. habil. Stefan Schramm für seine Unterstützung und ständige Bereitschaft, mir bei der Klärung der verschiedensten Fragestellungen zu helfen. Alle Teile dieser Arbeit sind in enger Zusammenarbeit mit ihm entstanden.
Nachdrücklich danken möchte ich Prof. Dr. Adrian Dumitru für die von ihm inspirierte, hervorragende Zusammenarbeit, die vielen Korrekturvorschläge und Anmerkungen zu dieser Arbeit sowie die persönliche Unterstützung.
Ich danke Prof. Dr. Dr. h. c. mult. Walter Greiner für die Aufnahme an das Institut für Theoretische Physik, sein stetes Interesse an meiner Arbeit und die Ausbildung in Theoretischer Physik.
Ich danke Prof. Dr. Jürgen Schaffner-Bielich für seine ständige Bereitschaft, mit mir physikalische Fragestellungen zu diskutieren, die Ideen für neue Projekte sowie sein reges Interesse an meiner Arbeit.
Ich danke Dr. Amruta Mishra für die konzentrierte und produktive Zusammenarbeit und die konstruktive Kritik.
Ich danke Dr. Ludwig Neise, Prof. Dr. Igor Mishustin und Prof. Dr. Leonid Satarov für ihr stetes Interesse an meiner Arbeit und die vielen konstruktiven Diskussionen.

Ich danke Prof. Dr. Steffen Bass, Prof. Dr. Christoph Hartnack und Prof. Dr. Dirk Rischke für ihr Interesse an meiner Arbeit.
Ich danke meinen (ehemaligen) Zimmergenossen Christian Beckmann, Dr. Lars Gerland, Dirk Röder und Dr. Anto Sulaksono für die angenehme, erbauliche und produktive Gemeinschaft.
Ich danke Manuel Reiter und Dr. Henning Weber für die geduldige und kompetente Hilfe bei allen Computerfragen.
Ich danke Kerstin Paech und Gebhard Zeeb für die gute und produktive Zusammenarbeit sowie für die Unterstützung und Hilfe in den verschiedensten Belangen.
Ich danke allen Mitgliedern des Instituts für Theoretische Physik für die hervorragende Gemeinschaft, für die wertvollen Ideen und Anregungen sowie für jegliche Art von Hilfe, die mir während der Erstellung dieser Arbeit zuteil wurde. Insbesondere möchte ich danken: Kristof Balazs, Dr. Marcus Bleicher, Dr. Jörg Brachmann, Dr. Uli Eichmann, Matthias Hanauske, Uli Harbach, Dr. Markus Hofmann, Dr. Stefan Hofmann, Sabine Hossenfelder, Wolfram Krause, Dr. Panajotis Papazoglou, Jörg Ruppert, Stefan Scherer, Dr. Sven Soff und Dr. Henning Weber.
Ich danke Daniela Radulescu für ihre kompetente Unterstützung und Hilfe in administrativen Belangen.
Ich danke der GEANT4 Kollaboration am CERN sowie dem BCPL in Bergen für die Möglichkeit zu Forschungsaufenthalten.
Ich danke dem Center for Scientific Computing an der Johann Wolfgang Goethe-Universität Frankfurt für die Bereitstellung von Rechenzeit.

Lebenslauf

Name : Detlef Zschiesche
Geburtstag: 12.11.71
Geburtsort: Bad Homburg v.d.H.

Bildungsweg:

- 1978-1982
  Besuch der Erich Kästner-Schule in Rodheim v.d.H
- 1982-1991
  Besuch des Augustiner Gymnasiums Friedberg (Hessen)
- Mai 1991
  Abitur
- Okt.1991
  Beginn des Physikstudiums an der Johann Wolfgang Goethe-Universität Frankfurt am Main
- Juli 1993
  Vordiplom Physik
- September 1994 bis April 1995
  Auslandssemester an der University of Leeds/England
- Mai 1995
  Eintritt in das Institut für Theoretische Physik der Johann Wolfgang Goethe-Universität Frankfurt
- 12. Februar 1998
  Diplom in Physik
- Seit März 1998
  Wissentschaftlicher Mitarbeiter am Institut für Theoretische Physik der Johann Wolfgang Goethe-Universität Frankfurt am Main

- Oktober 1998
  Beginn des Promotionsstudiums am Institut für Theoretische Physik. Thema der Dissertation: Excited hadronic matter in a chiral $SU(3)_L \times SU(3)_R$ model.

- November 1998
  Verleihung des Philipp Siedler Wissenschaftspreises des Physikalischen Vereins der Johann Wolfgang Goethe-Universität Frankfurt

Akademische Lehrer

Prof. Dr. Aßmus
Prof. Dr. Bethge
Prof. Dr. Fink
Prof. Dr. Elze
Prof. Dr. Dumitru
Prof. Dr. Geisel
Prof. Dr. Dr. h. c. mult. Greiner
Prof. Dr. Görnitz
Prof. Dr. de Groote
Prof. Dr. Hirst
Prof. Dr. Kersting
Prof. Dr. Klein
Prof. Dr. Kummer
Prof. Dr. Kulze
Prof. Dr. Maruhn
Prof. Dr. Dr. h. c. Martienssen
Prof. Dr. Mohler
Dr. Neise
AOR Dr. Reinhardt
Prof. Dr. Rischke
Dr. Ritter
Prof. Dr. Schaarschmidt
Prof. Dr. Schäfer
HD Dr. habil. Schaffner-Bielich
Prof. Dr. Schmidt–Böcking
PD Dr. habil. Schramm
Prof. Dr. Siemsen
Prof. Dr. Soff
PD Dr. habil. Schwarz
Prof. Dr. Stock
Prof. Dr. Stöcker